PHOTOCHEMICAL AND PHOTOPHYSICAL STUDIES OF SYNTHETIC DERIVATIVES OF THE GREEN FLUORESCENT PROTEIN CHROMOPHORE

A Dissertation
Presented to
The Academic Faculty

by

Jian Dong

In Partial Fulfillment
of the Requirements for the Degree
Doctor of Philosophy in the
School of Chemistry & Biochemistry

Georgia Institute of Technology
August 2008

PHOTOCHEMICAL AND PHOTOPHYSICAL STUDIES OF SYNTHETIC DERIVATIVES OF THE GREEN FLUORESCENT PROTEIN CHROMOPHORE

Approved by:

Dr. Laren M. Tolbert, Advisor
School of Chemistry & Biochemistry
Georgia Institute of Technology

Dr. Uwe H. F. Bunz
School of Chemistry & Biochemistry
Georgia Institute of Technology

Dr. Andreas S. Bommarius
School of Chemistry & Biomolecular Engineering
Georgia Institute of Technology

Dr. Donald F. Doyle
School of Chemistry & Biochemistry
Georgia Institute of Technology

Dr. Bridgette Barry
School of Chemistry & Biochemistry
Georgia Institute of Technology

Date Approved: July 1st, 2008

ACKNOWLEDGEMENTS

This dissertation arose in part out of years of research that has been done since I came to Tolbert's group. During that time, I have worked with a great number of people whose contribution in assorted ways to the research and the making of the disseration desereved special mention. It is a pleasure to convey my gratitude to them all in my humble acknowledgment.

First of all, I would like to record my gratitude to my research advisor, Dr. Laren M. Tolbert, for his supervision, advice, and guidance from the very early stage of this research as well as offering me tremendous support with his extraordinary experience throught out my work. In addition, he provided me timely and instructive comments and evaluation even when he was out of the country, allowing me to complete this project on schedule.

Many thanks go in particular to Dr. Kyril M. Solntsev for his supervision and crucial contribution, which made him a backbone of this research and so to this dissertation. I truly learned much from him in the numberous discussions about science and life.

It is a pleasure to pay tribute also to those who provided me various helps during my work. To Dr. Kenneth Hardcastle and Rui Cao at X-ray Crystallography Center of Emory Univeristy, I would like to thank them for their crystal structure analysis. I would also acknowledge Dr. Mohan Srinivasarao and Matija Crne for the microscopy measurements, Dr. Robert A. Braga for the Infrared instrument, Dr. Robert M. Dickson for TCSPC system, Dr. Christine K. Payne for the discussion of cell incubation, Dr.

Joseph R. Carlise for HPLC seperation, Lex Nunnery for DSC analysis, and Dr. Simon Jones for XRD measurement.

I would also like to thank my committee for taking the time to review my work, offer suggestions and serve at my defense.

For the sake of completeness, data accumulate in other laboratories by collaborators is included. This includes transient IR spectra in *Chapter 4* and transient absorption UV-Vis Spectra in *Chapters 6* and *7*. I gratefully acknowledge Professors Erik T. J. Nibbering, Clemens Burda, and Olivier Poizat for these data.

Collective and individual acknowledgments are also owned to my past and present colleagues, Dr. Janusz Kowalik, Dr. Nguyen Vu, Dr. Lorreta Crowe, Dr. Yu Li, Dr. Chien-Kuo Ku, Jason Bell, Jay Xu, Juan Vargas, Michael Salvitti, Robert Whetsell, Anthony Baldridge, Russell Vegh, E-A Gould, Fardokht Abulwerdi, Dr. Jonas Jarvholm, Dr. Christina Bauer, and Dr. Luke Roberson for giving me such a pleasant time when working together with them.

My parents, parents-in-law, sister, and my wonderful wife, Cynthia, deserve special mention for their inseparable support and encouragement. Mom and Dad, you are great parents and friends. Mei, I could not ask for a better sister and friend. And Cynthia, my wife, words fail me to express my appreciation to you. If I could write down everything I ever wanted in a wife and best friend, I would not have believed I could meet somenone better! To all of you, thanks for always being there for me.

Finally, I would like to thank everybody who was important to the successful realization of this dissertation, as well as expressing my apology that I could not mention everyone's name.

TABLE OF CONTENTS

LIST OF TABLES

LIST OF FIGURES

LIST OF SYMBOLS AND ABBREVIATIONS

GFP	Green Fluorescent Protein
HBI	hydroxybenzylidenimidazolinone
IR	Infrared
p	para
m	meta
ESPT	excited-state pront transfer
*wt*GFP	wild-type GFP
DsRed	red fluorescent protein
Ser	Serine
Tyr	Tyrosine
Gly	Glycine
EGFP	enhanced GFP
YFP	yellow fluorescent protein
EBFP	enhanced blue fluorescent protein
ECFP	enhanced cyan fluorescent protein
Φ_f	fluorescence quantum yield
IC	internal conversion
Glu/E	Glutamic acid
Thr	Threonine
NAC	nonadiabatic crossing
HT	hula twist
HOBDI	hydroxybenzylidenedimethyl-imidiazolone
AH	proton-containing molecule

k^*_{pt}/ k^*_{-pt}	rates for forward and back excited-state proton transfer
k_f(')	rates of acid (base) fluorescence
k_{nr}(')	rates of acid (base) nonradiative decay
k_q(')	rate of acid (base) quenching by protons
ArOH	hydroxyarene
τ	fluorescence lifetime
$1/\tau$	the rate constant for exponential decay
S_0	Electronic singlet ground state
S_1, S_2,…S_n	Electronic singlet excited state (1, 2, …n)
A	Absorbance
c	concentration of the absorber
ε	extinction coefficient
l	pathlength of the light through the sample
k_{ic}	rate of internal conversion
k_{isc}	rate of intersystem crossing
UV-Vis	Ultra-Violet/Visible Spectroscopy
RA	Right Angle
FF	Front Face
TCSPC	Time-Correlated Single Photo Counting
MCP	MicroChannel Plate
PMT	PhotoMultiplier
CFD	Constant Fraction Discriminator
TAC	time-to-amplitude-converter
AMP	Amplifier
IRF	Instrument Response Function

IPA	optical parametric amplifier
SHG	second harmonic generator
CCD	charge coupled device
TLC	Thin Layer Chromatography
NMR	Nuclear Magnetic Resonance Spectrascopy
THF	tetrahedrofuran
ACN	acetonitrile
TFE	trifluoroethanol
DMF(A)	*N, N*-dimethylformamide
DMSO	dimethyl sulfoxide
λ_{max}	wavelength maximum
EEM	excitation-emission matrix
ICT	intramolecular charge transfer
μ_{eg}	electronic transition dipole moment
ΔA_{iso}	anisotropy difference absorbance response
D	dichroic ratio
$\Delta A_{//}$/ $\Delta A_{\perp}$	parallel/perpendicular difference absorbance response
DABCO	1,4-diaza[2.2.2]bicyclooctane
ppm	parts per million
δ	chemical shift (ppm)
d	doublet
t	triplet
m	multiplet
s	siglet
mp	melting pointing

nm	nanometer
σ	substituent constant
ρ	reaction constant
DMAP	4-(dimethylamino)pyridine
HOMO	highest occupied molecular orbital
LUMO	lowest unoccupied molecular orbital

SUMMARY

Green Fluorescent Protein (GFP) is widely used as a biological marker in molecular biology, medicine, and cell biology because of its superb fluorescence properties. The chromophore of GFP, responsible for the fluorescence, is *p*-hydroxybenzylidenimidazolinone (**HBI**). The GFP crystal structure shows that the chromophore is always located in the middle part of a central helix inside an 11-stranded *β*-barrel, which plays an important pole for the intense fluorescence of GFP and its mutants. However, the denatured GFP and the isolated chromophore are poorly fluorescent outside of their protein shells. The question naturally arises, "Is a *β*-barrel necessary?" We have synthesized dimethyl derivatives of the GFP chromophore (*p*-**HOBDI**) and several of its derivatives, and their photochemistry and photophysics were investigated using various steady-state and time-resolved techniques as follows.

We first consider the effect of the *β*-barrel on the optical properties of the GFP chromophore (*p*-**HOBDI**) experimentally by selective variation of the protonation state of chromophores and different solvents. Each of these forms shows a complex solvatochromic behavior and is governed by both polar and acid/base properties of the solvents. In contrast to their solution behavior, some *O*-alkyl GFP chromophore (alkoxy-**BDI**) derivatives exhibit large fluorescent enhancement in the solid state. The color of the crystalline **BDI** is tuned by substituent-mediated crystal packing, showing the potential applications in optoelectronic devices.

Using femtosecond polarization-sensitive infrared (IR) spectrosceopy of the C=O stretching mode of the **HOBDI**, we have then discovered a near complete twisting around

the ethylenic bridge between the phenolate and imidazolidinone groups upon electronic excitation. *Cis/trans* isomerization induced by the rotation around the bridge is thought to be responsible for the behavior of blinking in fluorescent protein; however, the mechanism of the thermal reverse isomerization is more problematic. Thus we synthesized **BDI** derivatives with decreasing *para*-donating ability, HO, CH_3O, CH_3, H, and Cl, and used a Hammett plot for the rate study. With a positive ρ value, we conceived, for the first time, a novel nucleophilic addition/elimination mechanism.

Finally, the GFP chromophore falls into the general category of hydroxyarene photoacids, which exhibit high excited-state acidities but neutral ground states. A hydroxyl substituent at the *meta* position shows enhanced charge transfer and greater acidity in the excited state. As a result, we have demonstrated that the fast quenching of the excited state by internal conversion to the ground state is much slower in *meta*- than in *para*-**HOBDI** derivatives. This allows studies of this ultrafast intermolecular ESPT that competes with isomerization. The photoinduced dynamics of the *meta* isomer of GFP chromophore was further investigated using femtosecond transient absorption and fluorescence upconversion spectroscopies.

CHAPTER 1

INTRODUCTION

Background

Green Fluorescent Protein (GFP) was first discovered by Osamu Shimomura as a chemiluminescent protein from *Aequorea victoria* jellyfish.[1] In *A. victoria*, GFP is a companion protein to aequorin and fluorescence occurs when aequorin binds with calcium ions, inducing a blue glow. The blue emission is absorbed by GFP, which in turn gives off the green light.[2] However, the potential of GFP becoming a significant tracer and reporter molecule for molecular biologists was not realized until Douglas Prasher cloned the gene and reported the nucleotide sequence of wild-type GFP (*wt*GFP) in 1992.[3] It was demonstrated by Martin Chalfie[4] and Frerick Tsuji[5] that expression of the gene in other organisms creates fluorescence. A major breakthrough in GFP applications came when Sergey Lukyanov found some GFP-like proteins in corals, including first red fluorescent protein (DsRed).[6] His findings resulted in the discovery of many new GFP-like proteins in non-bioluminescent and non-fluorescent marine organisms. Remarkably, GFP was fluorescent at room temperature, without the exogenous cofactors specific to the jellyfish. To date, the GFP gene is frequently used as a reporter of expression or biosensors in cell and molecular biology. It can also be introduced as a marker into organisms, such as bacteria, yeast and other fungal cells, plant, fly, and mammalian cells.[7]

The Remington group first reported the crystal structure of the S65T mutant GFP in 1996.[8] One month later, the Phillips group reported the *wt*GFP structure.[9] GFP comprises 238 amino acid residues; and the chromophore of this protein is a *p*-hydroxybenzylidene-imidazolidinone (**HBI**) derivative formed by an autocatalytic,

posttranslational cyclization and oxidation of the Ser-65, Tyr-66, and Gly-67 residues.[10-12] The GFP crystal structure shows that the chromophore is located in the middle part of a central helix inside a unique 11-stranded β-barrel (*Figure 1.1*).[8,9] The tightly packed β-barrel shell maintains the mature chromophore formation of the Ser65-Tyr66-Gly67 tripeptide and protects the fluorophore from quenching by the surrounding microenvironments. The study of the crystal structure provides critical background on chromophore formation and neighboring residue interactions, helps the understanding of how GFP works and results in the development of new techniques and mutants of GFP.

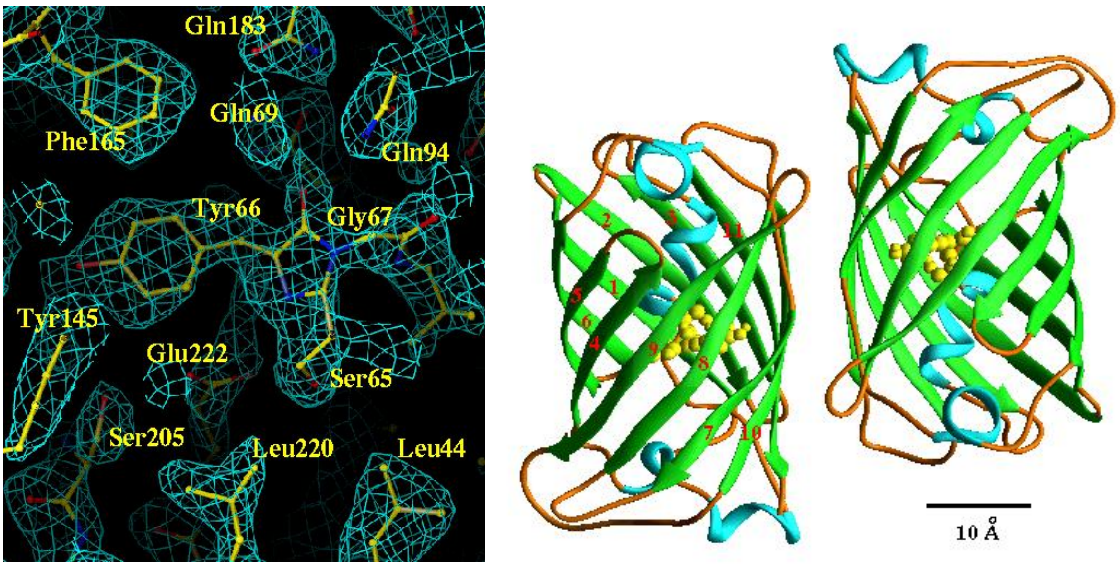

Figure 1.1. Model of the fluorophore (left) and the overall shape of the *wt*GFP (right)[9]

The first single point mutation (S65T) improvement was made by Roger Tsien in 1995.[13] This mutation dramatically improved the spectral characteristics of GFP and increased fluorescence and photostability. The addition of the 37 folding efficiency (F64L) point mutant yielded enhanced GFP (EGFP). A series of mutations that allow GFP to rapidly fold and mature were reported.[14] Many other color mutants have been made as well, in particular blue fluorescent protein (EBFP), cyan fluorescent protein (ECFP) and yellow fluorescent protein derivatives (YFP).[15] With the compatible spectral characteristics, these GFP derivatives have more potential for widespread usage.

Photochemistry and Photophysics Literature Review

The wild-type GFP has a major absorption at 398 nm and a minor absorption at 475 nm with a shoulder on the red edge.[16,17] Early in the study of the photophysics of GFP[18,19] it was determined that the 398 nm absorption is associated with the neutral, protonated form of the chromophore (HO_y, N, O_x, species **A**, See *Figure 1.2*), whereas the absorption at 475 nm is associated with the anionic, de-protonated form (^-O_y, N, O_x, species **B**),[20,21] and the red shoulder at 475 nm is attributed to a zwitterionic species (^-O_y, HN^+, O_x, species **I**).[17] Furthermore, the long Stokes shift associated with emission at 508 nm after 398 nm results from a process known as excited-state proton transfer (ESPT) in which the proton is lost before emission.[22] The 508 nm emission is fairly close to the peak from the irradiation of 475 nm, which produces an emission with a maximum at 503 nm.[23] In other words, excitation of either species **A** (neutral) or species **B** (anionic) results in similar excitation spectra. This is apparently due to the fact that the phenolic oxygen of Tyr66 is more acidic in the excited state than in the ground state, and ESPT occurs, resulting in a common anionic excited state.[18,23,24] Comparing with the above experimental observations, four different protonation states over the pH range from -3.2 to 9.4 are identified by a computational analysis of the denatured GFP chromophore. The anionic form is at pH > 9.4, an equilibrium between the neutral and the zwitterionic form between 1.1 and 9.4, and the cationic form (HO_y, HN^+, O_x) between -3.2 and 1.1.[25]

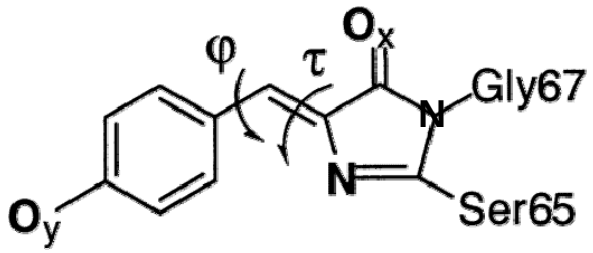

Figure 1.2. *p*-hydroxybenzylideneimidazolidinone (**HBI**) structure of the chromophore.[21]

Wild-type GFP has a fluorescence quantum yield (Φ_f) of 0.8,[26] but neither denatured GFP, nor synthetic model compounds fluoresce. The quantum yield of the

isolated chromophore in solution is only 10^{-4}.[20] The denatured GFP and the model chromophore do however become highly fluorescent at 77 k. Steady-state and time-resolved absorption and fluorescence reveal that inhibition of vibration or rotation around the exo-methylene double bond of the chromophore prevents reduction in the fluorescence rate due to fast internal conversion.[27,28] Quantum mechanical calculations suggested the loss of fluorescence is a result of fast internal conversion from the perpendicular excited-state structure of the protonated chromophore and that this perpendicular orientation is sterically prohibited in most GFPs.[29] The internal conversion distorts the conplanarity of the chromophore and increases the nonradiative decay rate of the excited-state molecule.[30,31] Molecular mechanics and dynamics simulations have shown the protein environment of GFP allows the chromophore some rotational freedom, particularly by a hula-twist and in the φ dihedral angle (see *Figure 1.2*). The excited state, responsible for fluorescence, may be twisted relative to the ground state, but *cis-trans* photoisomerization cannot occur by a 180 ºC rotation of the τ dihedral angle. However, some fluorescence and ultrafast ground-state recovery studies are not consistent with the theory that fast internal conversion occurs through large-scale torsonal rotation in the excited state.[32]

On the basis of the calculations and experimental observations, three-state[33,34,35] and four-state[18,28,31] photoisomerization model mechanisms had been proposed. In the three-state photoisomerization model (See *Figure 1.3* a and b), the neutral form (**A**) of the chromophore converts to the anionic species (**B**) through the intermediate state (**I**). As shown in *Figure 1.3*b, the blue emission from **A*** at 460 nm is observed only on the picosecond time scale, and its decay kinetics match the rise kinetics of the green emission from **I*** at 508 nm.[35] Going from the neutral to the anion form, the Tyr66 phenolic proton is shuttled through an extensive hydrogen-bonding network to the carboxylate oxygen of Glu222. The change from forms **A** to **I** is only a protonation change, while the change from **I** to **B** is a conformational change involving Thr203. The mechanism shown in

Figure 1.3 has been partially validated by the results of the absorption and Stark spectra of the wild type, the S65T and Y66H/Y145F GFP mutants.[36] The results show that the excitation of species **A** involves a small charge displacement in electronic spectra, while excitation of species **B** involves a significant change from ground state. In going from state **A** to state **B**, the protein has to undergo structural changes because the intermediate state (**I**) is structurally similar to both the ground and excited state of species **A** and electronically similar to the ground and excited state of species **B**. The X-ray structure of S65T shows that there is no hydrogen-bonding interaction between the side chain of Thr203 and the phenolic oxygen of the chromophore at low pH, while the side chain dihedral rotates by 100º to form a hydrogen bond in the high pH structure.[37] Three new photoproducts are found by low-temperature optical investigation, one corresponding to **A*** (489 nm) and two to **I*** (502 and 510 nm).[38]

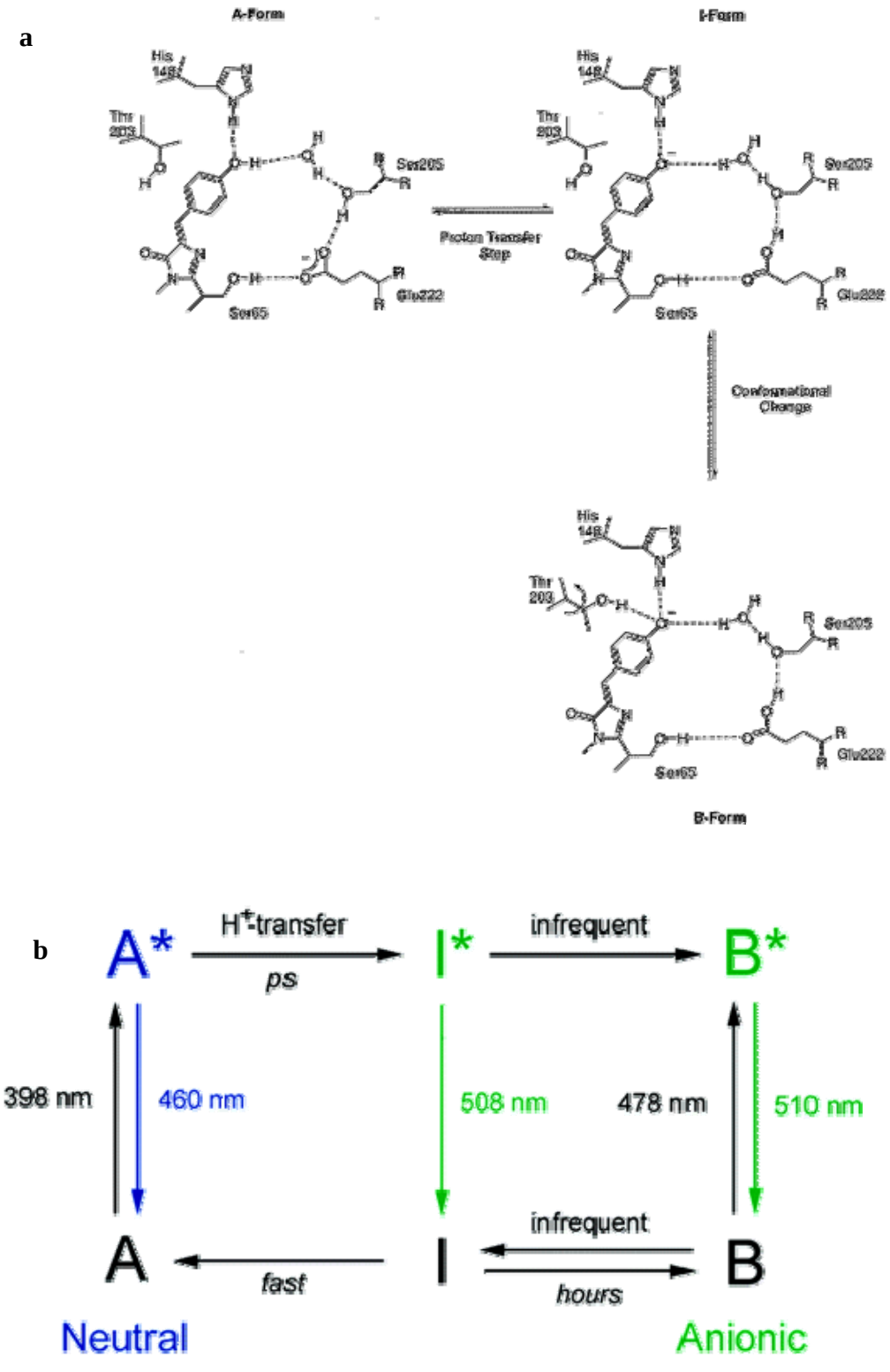

Figure 1.3. Proposed mechanism for the photoisomerization of *wt*GFP. [21,35]

The four-state photoisomerization model is an extension of the three-state model, which has been used to explain the short- and long-lived "dark" states and the relaxed excited-state decay channels in GFP based on quantum mechanical calculations.[39] As shown in *Figure 1.4*, a *cis-trans* photoisomerization and a zwitterionic form, **Z**, have been added to the three-state model. Radiationless decay through nonadiabatic crossing (NAC) is the preferred decay channel for the zwitterionic form. The isomerization could occur around the τ and φ dihedral angles as well as by a concerted hula-twist of both the τ and φ dihedral angles.[39] The excited states of the neutral (**A***), intermediate (**I***), and anionic (**B***) species undergo minimal radiationless decay through **NAC**. Time-resolved spectroscopy studies have validated parts of the mechanism shown in *Figure 1.4*, determining the fluorescence lifetimes of the **I** and **B** species and showing that the irreversible photochromomicity observed between species **A*** and **B***.[40]

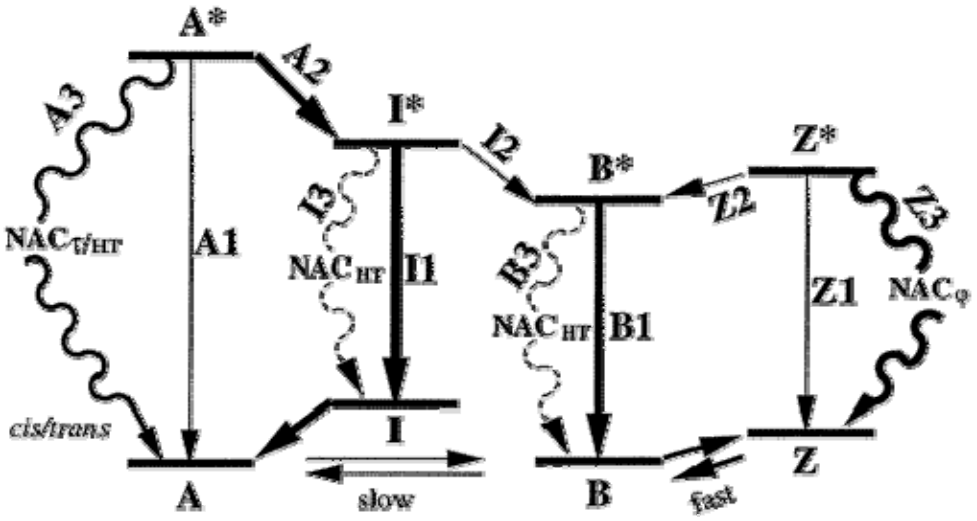

Figure 1.4. Model for the photophysical behavior of GFP (four-state mechanism). [31]

These theoretical and experimental analyses have shown the apparent brightness of GFP mutants depend on the local protein environment of the chromophore and internal conversion leads to reduction of Φ_f.[28,31,41,42] Jung et al. recently reported that fluorescence quantum yields Φ_f of up to 100% are possible with an appropriate chromophore environment.[43] However, these results contradict the common observation using

ultrasensitive fluorescence microscopy that GFP and its derivatives are not as bright as would be expected.[44] Indeed, when GFP molecules are observed individually they display on/off blinking and switching behavior.[44-48] The on/off blinking occurred on time scales of hundreds of ms. After some cycles of blinking, GFP mutants undergo a transition to a long-lived (>1 h) dark state (the "off" state). The dark state is different than the off-blinking behavior. The blinking has been shown to photoinduced,[44] and it has been suggested that a reversible transition between the emitting anionic form and a dark intermediate state of an unidentified species is responsible for this behavior. Instead, two dark states have been observed for the E222Q mutants. One of the dark states has been identified as the neutral form of the chromophore (species **A** in *Figure 1.3*), and the other is presumably a triplet state.[49,50] Habuchi et al. proposes that transition from a protonated off-state to the deprotonated on-state proceeds via ESPT after irradiation, and the rate constant of on- to off-state switching depends linearly on the intensity of the irradiation.[51,52] However, Andresen et al. propose that the basis of switching is the reversible isomerization of the hydroxyphenyl ring of Tyr64.[53] This is thought be a universal mechanism behind photoswitching.[53-55]

Motivation and Overview

Motivation

Although various GFP and its derivatives have been used in cell biology and other biological disciplines, the majority of users pay less attention to the mechanistic details. The crystal structure reveals that the unique 11 β-sheet barrel-like structure apparently plays a critical role for the superb fluorescence properties of *wt*GFP comparing with its synthetic model chromophore. The question naturally arises, "Is a β-barrel necessary?" How does the β-barrel affect on the optical properties of the GFP chromophore?

Both three-state and four-state photoisomerization mechanisms and charge distribution shown in *Figure 1.3* and *1.4* provide general framework for understanding the photochemistry and photophysics of *wt*GFP and synthetic GFP chromophore, however, a number of details and their general applicability remain open questions. In addition, the majority of the mechanisms are based on molecular, quantum mechanical and electrostatic calculations, and only parts of them have been confirmed by experimental spectroscopic data. Moreover, as the investigations go further, numerous inconsistencies have emerged in both the experimental and theoretical results, including the role of twisting of the internal bond, perhaps invoking a "hula twist" leading to efficient internal conversion(IC).

The prototropic behavior of GFP chromophore is responsible for its green fluorescence. This chromophore falls into the general category of hydroxyarene photoacids with which our group has significant experience. These involve high excited-state acidities but neutral ground states. In the case of the GFP hydroxyarene, the imidazolinone ring acts as an electron-withdrawing substituent, increasing the excited-state acidities. In general, the effect of such substitutions in the excited state is the reverse of the ground-state "*para/meta*" formalism, as noted by Lewis in the case of hydroxybiphenyls. Since *para*-**HOBDI** exhibits weak fluorescence, by analogy with the hydroxybiphenyls, it is worth examining *meta*-**HOBDI**.

Similar to synthetic the GFP chromophore *p*-hydroxybenzylidenedimethyl-imidiazolone (**HOBDI**), various **HOBDI** derivatives hardly fluoresce in solutions. It is surprising that some *O*-alkyl substituted **BDI** shows fluorescent in their solid state. Thus exploring their photophysical and photochemical behaviors is an attractive topic.

Overview

Chapter 2 reports that the solvatochromic behavior of *p*-**HOBDI** and its derivatives is governed by both polar and acid/base properties of the solvent. The

magnitudes and directions of the solvatochromic shifts strongly depend on the protonation state of the solute. (Copyright 2006 by American Chemical Society.)

Chapter 3 reports the enhanced fluorescence in solid state *O*-alkyl **BDI** derivatives. The color of the crystalline **BDI** is tuned by substituent-mediated crystal packing.

Chapter 4 uses femtosecond polarization-sensitive infrared (IR) spectroscopy of the C=O stretching mode of the **HOBDI** to discover a near complete twisting around the ethylenic bridge between the phenolate and imidazolidinone groups upon electronic excitation, hinting at a decisive role of this motion in the efficient internal conversion process. (The major part of this chapter is joint work with Prof. Erik T. J. Nibbering, copyright 2005 by American Chemical Society.)

Chapter 5 proposes an addition/elimination mechanism in the thermal reverse ground-state isomerization of GFP chromophore. This discovery solves the inconsistentcy between experimental observation and calculated isomerization barrier. We are able to isolate both the *Z* and *E* isomers of GFP chromophore and, for the first time, obtain their ir and absorption spectra.

Chapter 6 reveals the excited-state *para*/*meta* effects in **HOBDI** derivatives. Substitution on the *meta* position shows enhanced charge transfer and excellent acidity in the exited state by examining the corresponding frontier molecular orbits. In this case, the *para* isomer undergoes rapid *cis/trans* isomerization and sluggish proton transfer, while the *meta* isomer exhibits the reverse behavior. The synthetic *meta*-**HOBDI** leads to carry out a major study of its photophysics in the next chapter. (Copyright 2007 by American Chemical Society)

Chapter 7 investigates the photoinduced dynamics of the *meta* isomer of GFP chromophore using femtosecond transient absorption and fluorescence upconversion experiments. Fast quenching of the excited S_1 state by internal conversion (IC) to the ground state was observed. In the *para* compounds, IC, presumably promoted by the

internal twisting, arises in < 1 ps. A similar process takes place in the *meta* compounds, which undergo ultrafast intermolecular excited-state proton transfer that competes with isomerization. (The major part of this chapter is joint work with Prof. Olivier Poizat,)

Terminology and Methodology

Excited-State Proton Transfer

Since excited-state proton transfer plays a critical pole in the emission spectra of *wt*GFP and it is also a major phenomenon in photochemistry, an introduction is appropriate.

Proton transfer reactions in the ground-state are one of the simplest and most important processes in chemistry. Excited-state proton transfer (ESPT) is much less studied, but it is very important in understanding the fundamental of photochemistry. Certain molecules undergo a dramatic change in their acidity upon electronic excitation. The phenomenon has first been discovered by Förster and Weller,[56,57] and several reviews have been written on this class of reaction.[58-64] There are two types of reactions: when the acidic and basic moieties exist closely within the same molecule, it is called intramolecular ESPT, otherwise, the reaction is intermolecular, which is either bimolecular or pseudo-unimolecular, such as in the case of ESPT to solvent.

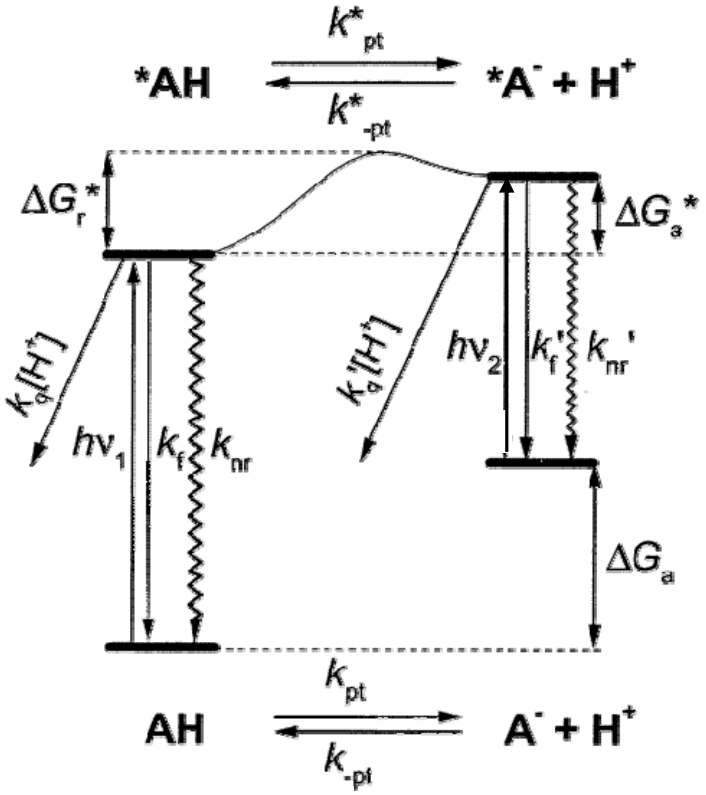

Figure 1.5. Proton transfer and decay processes in photoacids. [63]

Generally, for any proton-containing molecule (AH), if the absorption or emission spectrum of the conjugate base is characterized by a bathochromic shift relative to that of the conjugate acid, its excited state (*AH) is predicted to be a stronger acid than the ground state.[63] This thermodynamic cycle is known as the "Förster cycle" described by the Föster equation[65] shown in *Figure 1.5* and described by the following equation:

$$pK_a^* = pK_a - (h\nu_1 - h\nu_2)/2.3RT$$

$\Delta G_a^*/2.3RT$ is the ground (excited)-state acidity constant and $h\nu_{1(2)}$ is the energy of the 0-0 electronic transition for the conjugate acid (base). In this figure, k^*_{pt} and k^*_{-pt} are the rates for forward and back excited-state proton transfer, respectively, k_f(') and k_{nr}(') are rates of acid (base) fluorescence and nonradiative decay, and k_q(') is the rate of acid (base) quenching by protons. The peak fluorescence frequencies of the acid and base forms, together with the ground-state pK_a, could allow one to calculate pK_a^* via this Först equation. Such a determination may be inaccurate, because the solvent relaxes around the

*AH after excitation, and around the $^{*}A^{-}$ after proton dissociation, which the Förster equation does not take into account.[63]

Many hydroxyarenes (ArOH) exhibit proton transfer competitive with excited-state decay, of which the GFP chromophore is an example. The hydroxyarenes have fluorescent conjugate bases with nonbonding oxygen-centered molecular orbitals and excited states with charge distribution at the distal oxygen site. This reduces the basicity of the excited-state anion and, converesly, increases the acidity of the conjugate acid.

Besides fluorescence and ESPT, hydroxyarenes undergo a number of processes, shown in *Figure 1.5*. These include various nonradiative processes characteristic of hydroxyarenes such as proton-induced quenching and homolytic OH bond cleavage to produce radicals. These numerous consecutive processes occur from subfemtosecond to submicrosecond time scales. Specifically, they include electronic redistribution upon excitation (subfemtosecond), hydrogen-bond rearrangements near the OH group (femtosecond), proton dissociation followed by proton solvation and mobility (picosecond), geminate recombination of the dissociated proton with the conjugate photobase, quenching and excited-state decay (nanosecond).[64] Again, the presence of competing processes and incomplete excited-state equilibria may lead to erroneous results in the determination of pK_a^{*} and complicated factors involved in transient measurements.

Fluorescence and photophysics

Fluorescent spectroscopy is used intensely in the photophysics behavior of synthetic GFP chromophore and its derivatives. A quick review of several basic concepts is as follows:

Fluorescence is the property of some atoms and molecules to absorb at a particular wavelength and to subsequently emit light of longer wavelength after a brief interval, termed the fluorescence lifetime τ, where $1/\tau$ is the rate constant for exponential

decay. The fluorescence process consists three important events: excitation of a molecule by an incoming photon in femtoseconds (10^{-15} seconds), vibrational relaxation of excited state to the lowest energy level in picoseconds (~10^{-12} seconds), and emission of a longer wavelength photon and return to the ground state in nanoseconds (~10^{-9} seconds).[66] This phenomenon forms the basis for the expansive fields of steady state and time-resolved fluorescence spectroscopy.

Fluorescence is generally studied with highly conjugated polycyclic aromatic molecules, which are known as fluorescent chromophores, fluorophores, or simply dyes. For any particular molecule, several different electronic states exist (S_0, S_1, and S_2 in *Figure 1.6*).[66] Each electronic state is further subdivided into a number of vibrational and rotational energy levels associated with the atomic nuclei and bonding orbitals. All of these various energy levels are classically presented by a Jablonski energy diagram (see *Figure 1.6*).

The ground state of a large majority of fluorescent molecules is an electronic singlet in which all electrons are spin-paired. The ground state is also called S_0. When ground-state fluorophores absorb light (ultraviolet or visible), they are usually vertically excited to higher vibrational levels of the first (S_1), second (S_2) or higher (S_n) singlet energy state. As referred to in the Franck-Condon principle, transitions from the ground to the excited state occur in such a short timeframe (femtoseconds) that the internuclear distance associated with the bonding orbitals does not have sufficient time to change, and thus the transitions are represented as vertical lines. These different transitions in molecules give rise to an absorption spectrum containing multiple peaks. The capacity of absorption of a molecule can be determined by Beer-Lambert Law, which states that the absorbance is the product of the concentration of the absorber, c, its extinction coefficient, ε, and the pathlength of the light through the sample, l.

$$A = lc\varepsilon$$

Once the molecule is in an excited state, several processes occur with varying

probabilities, but the most likely is relaxation to the lowest vibrational energy levels of the first excited state (S_1=0, *Figure 1.6*). This process is known as internal conversion or vibrational relaxation and generally occurs in a picosecond or less.

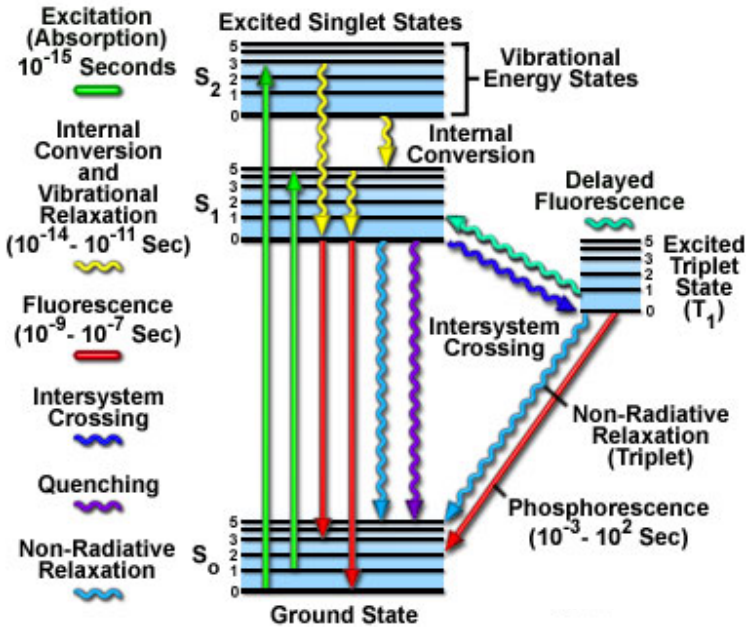

Figure 1.6. Jablonski energy diagram.[66]

The excited molecule exists in the lowest excited singlet state (S_1) for periods on the order of nanoseconds before finally relaxing to the ground state. If the relaxation is accompanied by emission of a photon, the process is formally known as fluorescence. The different closely-spaced vibrational energy levels of the ground state, produce a wide range of photon energies during emission. As a result, fluorescence is normally observed as emission intensity over a band of wavelengths. For many of the common fluorophores, the vibrational energy level spacing is similar for the ground and excited states, which results in a fluorescence spectrum that strongly resembles the mirror image of the absorption spectrum. This concept, known as the Mirror Image Rule, is illustrated in *Figure 1.7*.[66] Another phenomenon known as Stokes Shift is because the molecules relaxes to a new geometry in the excited state, causing the energy associated with

fluorescence emission transitions to be typically less that that of absorption, the resulting emitted photos have less energy and are shifted to longer wavelengths.[67,68]

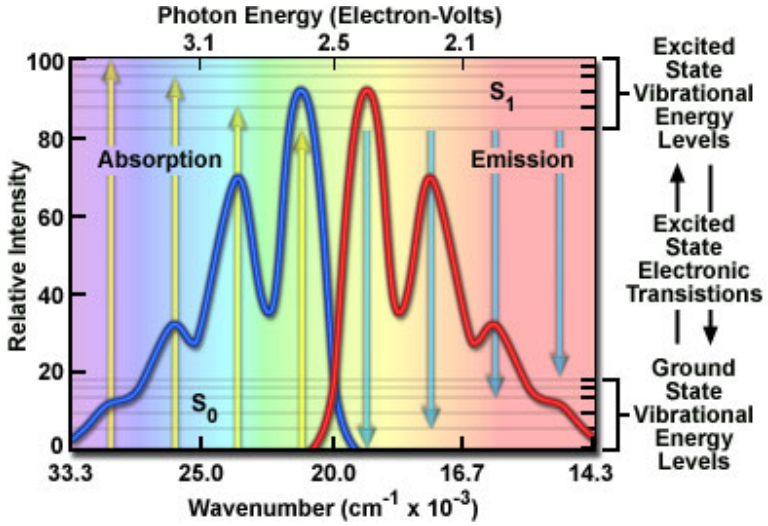

Figure 1.7. Electronic absorption and emission bands.[66]

However, several other relaxation pathways that have varying degrees of probability compete with the fluorescence emission process. The excited-state energy can be dissipated non-radiatively as heat (the cyan wavy arrow in *Figure 1.6*), quenching (the purples wavy arrow in *Figure 1.6*), or intersystem crossing (the blue wavy arrow in *Figure 1.6*) to the lowest excited triplet state resulting phosphorescence or delayed fluorescence. Furthermore, due to long excited-state lifetime, these fluorophore molecules are particularly sensitive to photochemical reactions, including charge (electron or hole) transfer, proton transfer (intra- or intermolecular), *cis-trans* isomerization of double bonds, twisted intramolecular charge transfer, photooxidations, photoadditions, etc.[69]

Indentifying a method to measure the efficiency of the fluorescence is therefore necessary. The concept is known as the fluorescence quantum yield, Φ_f, which is defined as the ratio of number of photos emitted to the number of photons absorbed or equivalently, the ratio of the number of emitted photons to the number of excited

molecueles initially created by photoexcitation. The maximum fluorescence quantum yield is 1.0 (100 %). This occurs when every photon absorbed is re-emitted and no energy is lost in other decay pathways.[67,68] The quantum yield of *wt*GFP is 0.8,[26] which is a good example of a highly fluorescent species. The quantum yield of fluorescence is related to the first-order radiative and non-radiative rate constant by

$$\Phi_f = \frac{k_f}{(k_f + k_{ic} + k_{isc})} = \frac{k_f}{k_f + k_{nr}}$$

where k_f is the rate of fluorescence, k_{ic} is the rate of internal conversion, k_{isc} is the rate of intersystem crossing, and k_{nr} is the rate of total non-radiative decay. Based on the Kasha-Vavilov rule,[68] which states because of rapid relaxation from higher electronic and vibrational levels to the lowest vibrational level of S_1, quantum yield of fluorescence is generally independent of excitation wavelength, thus the most practical method for measuring Φ_f is to compare a well characterized standard sample with known quantum yield.[70]

Fluorescence spectroscopy is one of the most widely used spectroscopic techniques in the fields of biochemistry and molecular biophysics. Because of its acute sensitivity to changes in the structural and dynamic properties of molecules, fluorescence spectroscopic studies can be carried out at many levels ranging from steady-state emission intensity to quite sophisticated time-resolved studies.

Steady-State Spectroscopy

Steady-state absorption and fluorescence spectra are measured in order to characterize new GFP chromophore derivatives, study their solvatochromism behavior and trace the possibility of excited-state proton transfer.

Absorption measurements

Absorption spectra were recorded on a Perkin-Elmer Lambda 19 UV/vis/NIR spectrophotometer, which has 1.0 nm resolution or better.

Fluorescence measurements

Fluorescence spectra were measured using a spectrofluorometer (SPEX Fluorolog 1680 0.22m double spectrometer and 1681 0.22m spectrometer). Fluorescence was collected in Right Angle (RA) geometry for solution and Front Face (FF) geometry for film sample. The entrance/exit slits of the monochromators were adjusted to the proper fluorescence intensity of each sample. The emission data was corrected to the emission of a NIST tungsten lamp.

Time-Resolved Spectroscopic Measurements

Time-resolved fluorescence measurements were carried out in our laboratory and in the laboratories of our collaborators. The fluorescence decay kinetics can be observed on the picosecond (Time-Correlated Single Photon Counting) to femtosecond (fluorescence upconversion) time scales. We also used femtosecond pump-probe transient absorption spectroscopy to study the kinetics of photoinduced processes in synthetic GFP chromophores.

Time-Correlated Single Photon Counting

Time-Correlated Single Photon Counting (TCSPC) is used to detect single photons of a periodical light signal. TCSPC makes use of the fact that for low-level, high- repetition rate signals that the light intensity is usually low enough that the probability to detect more than one photon in one signal period is negligible. Therefore,

based on the measurement of the detection times of the individual photons and the reconstruction of the waveform from the individual time measurements, this technique yields a histogram depicting the time dependence of the fluorescence of the sample.[71-73]

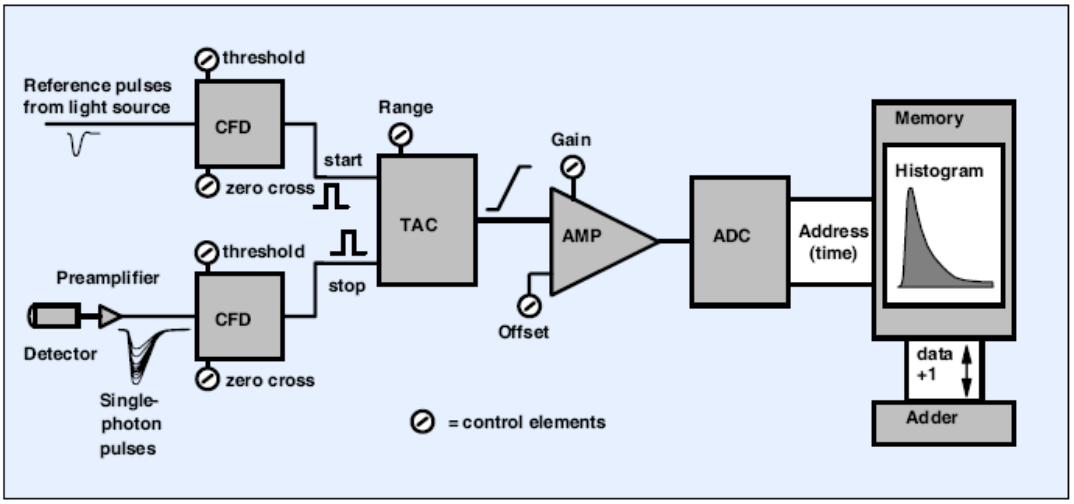

Figure 1.8. Architecture of a classic TCSPC device.[73]

The architecture of a classic TCSPC device is shown in *Figure 1.8*. In the experiment, two picosecond excitation pulses dye lasers (LDH-P-C-375 and LDH-P-C470) with different wavelength (372 nm and 467 nm) are used as excitation light sources. The signal of the detector, a high speed MicroChannel Plate PhotoMultiplier Tube(MCP-PMT, Hammamatsu R3809U-50) is cooled to -20 ^{o}C to reduce noise, and delivers pulses for individual photons of the repetitive light signal. The pulses are detected by a Constant Fraction Discriminator (CFD). The CFD triggers at a constant fraction of the pulse amplitude, thus avoiding pulse-height induced timing jitter. A second CFD is used to obtain a timing reference pulse from the light source. The reference signal is usually generated by a photodiode. The essential part is a time-to-amplitude-converter (TAC) which transforms the arrival time between a start and a stop pulse from output pulses of the CFDs into a voltage. The TAC output voltage is sent

through a "Biased Amplifier', AMP. The amplifier has a variable gain and a variable offset. It is used to select a smaller time window within the full-scale conversion range of the TAC. Subsequently, the amplified TAC signal is fed to the Analog-to Digital Converter, ADC. The output of the ADC is used as an address word for the measurement data memory. Finally, a multichannel analyzer software (EDINBURGH INSTRUMENTS F900) displays and saves the results on a PC. The Instrument Response Function (IRF) of the TCSPC setup is typically in the range of 20 ps to 30 ps and does not depend on the excitation source.

Fluorescence Up-conversion measurement

The up-conversion instrument is used to study dynamics of the photo-induced emission in femto-picosecond time domain. The instrument optical scheme is shown as *Figure 1.9*.[74] A FOG-100 fluorescence up-conversion system from CDP Systems (Moscow, Russia) pumped by a Clark MXR CPA 2000 amplified laser system followed by a TOPAS optical parametric amplifier (OPA) from Light Conversion (Lithuania) is used for the fluorescence lifetime measurements. The FOG-100 has been adapted to match the femtosecond amplifier system operating at 1 kHz pulse repetition rate with laser output at 780 nm and 150 fs pulse width or for the tunable excitation wavelengths from the OPA. The time-resolution of the system is analyzed by the rise time of zinc porphyrin fluorescence and by cross correlation of the pump and gate pulse. Both methods reveal a 180-200 fs time resolution, depending on the day-to-day compression of the amplified laser pulses. The providing excitation is 390 nm after double of the 780 nm Ti-Sapphire laser pulses using second harmonic generator (SHG) from 780 nm laser pulses.

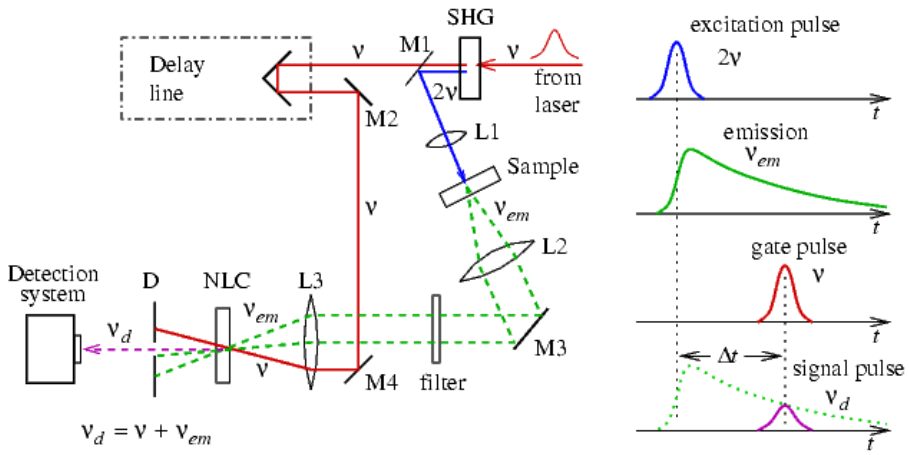

Figure 1.9. Optical scheme of the up-conversion instrument. [74]

Femtosecond Transient Absorption

The absorption pump-probe system is designed to measure time resolved spectra at single shot or averaging hundreds of shots. Typically the spectra are measured in a range of delay times to provide both the spectrum and time dependences of the transient absorption. After the measurements the data are analyzed using global fitting routines to gain information on the lifetimes and spectra of transient states.

Transient absorption measurement are performed using a Ti:Sapphire oscillator/ regenerative amplifier system which has already been described.[75] Briefly, the setup involves 1 kHz Ti:Sappire laser system based upon a Coherent (MIRA 900D) oscillator and a BM Industries (ALPHA 1000) regenerative amplifier. Pump excitation at 380 nm is obtained by frequency doubling the Ti:Sapphire fundamental tuned at 760 nm (0.3 mm BBO crystal). The pump pulse (~90 fs) power is limited to 2-6 μJ per pulse (0.2-0.6 mJ/cm^2). A white light continuum probe pulse is generated at 760 nm in a CaF_2 plate. The pump-probe polarization configuration is set at the magic angle to avoid rotational

depolarization effects on the measured fluorescence.[76] The probe pulse is delayed in time relative to the pump pulse using an optical delay line (Microcontrol Model MT160-250PP driven by an ITL09 controller, precision ± 1 μm). The overall time resolution (full-width at half maximum, fwhm, of the pump-probe intensity cross correlation) is estimated to be about 250 fs from the two-photon (pump + probe) absorption signal in pure hexane. The time dispersion of the continuum light over the 400-700 nm region of analysis is about 300 fs. The transmitted light is analyzed by a CCD optical multichannel analyzer (Princeton Instrument LN/CCD-1340/400-EB detector with ST-138 controller). Sample solutions (0.25-1.0 mM) circulate in a flow cell with 2 mm optical path length. Data are accumulated over 3 min (~ 180000 pump-probe sequences). The characteristic times related to the spectral changes are obtained from exponential fit of the observed kinetics and convolution with the instrument response function.[77]

References

[1] Shimomura O.; Johnson F. H.; Saiga Y. J. *Cell. Comp. Physiol*. **1962**, *59*, 223-239.

[2] Morise H.; Shimomura O.; Johnson F.; Winant J. *Biochemistry*, **1974**, *13*, 2656-2662.

[3] Prasher D.; Eckenrode V.; Ward W.; Prendergast F.; Cornier M. *Gene*, **1992**, *111*, 229-233.

[4] Chalfie M.; Tu Y.; Euskirchen G.; Ward W.; Prasher D. *Science*, **1994**, *263*, 802-805.

[5] Inouye S.; Tsuji F. *FEBS Lett*, **1994**, *341*, 277-280.

[6] Matz M. V.; Fradkov A. F.; Labas Y. A.; Savitsky A. P.; Zaraisky A. G.; Markelov M. L.; Lukyanov S. A. *Nat Biotechnol* **1999**, *17*, 969-973.

[7] "Green Fluorescent Protein", *http://www.conncoll.edu/ccacad/zimmer/GFP-ww/lukyanov.html,* 2008 (accessed March 2008).

[8] Ormo, M.; Cubitt A.; Kallio K.; Gross L.; Tsien R.; Remington S. *Science*, **1996**, *273,* 1392-1395.

[9] Yang F.; Moss L.; Phillips G. *Nat Biotechnol*, **1996**, *14*, 1246-1251.

[10] Shimomura, O. *FEBS Lett.* **1979**, *104*, 220-222.

[11] Cody, C. W.; Prasher, D. C.; Westler, W.M.; Prendergast, F. G.; Ward, W. W. *Biochemistry,* **1993**, *32*, 1212-1218.

[12] Romoser, V. A.; Hinkle, P. M.; Persechini, A. *J. Biol. Chem*. **1997**, *272*, 13270-13274.

[13] Heim R.; Cubitt A.; Tsien R. *Nature*, **1995**, *373*, 663-664.

[14] Pedelacq, J.; Cabantous, S.; Tran, T.; Terwilliger, T. ; Waldo, G. ; *Nat. Biotechnol,* **2006**, *24*, 79-88.

[15] "Green Fluorescent Protein", *http://en.wikipedia.org/wiki/Green_fluorescent_protein #_note-0*, 2008 (accessed March 2008).

[16] Ward, W. W.; Bokman, S. H. *Biochemistry*, **1982**, *21*, 4535-4540.

[17] Creemers, T. M. H.; Lock, A.J.; Subramaniam, V.; Jovin, T. M.; Volker, S. *Nat. Struct. Biol.* **1999**, *6*, 557-560.

[18] Chattoraj M.; King B. A.; Bublitz G. U. Boxer S. G. *Proc. Natl. Acad. Sci. USA*, **1996**, *93*, 8362-8376.

[19] Brejc, K et al. *Proc. Natl. Acad. Sci. USA***, 1997**, *94*, 2306-2311.

[20] Niwa, H.; Inouye, S.; Hirano, T.; Matsuno, T. ; Kojima, M. ; Kubota, M.; Ohashi, M.; Tsuji, F. I. *Proc. Natl Acad. Sci. U.S.A.* **1996**, 13617-13622.

[21] Zimmer, M. *Chem. Rev***. 2002**, 759-781.

[22] van Thor, J. J.; Gensch T.; Hellingwerf, K. J.; Johnson L. N. *Nat. Struct Biol,* **2002***, 9*, 37-41.

[23] Heim, R.; Prasher, D. C.; Tsien, R. Y. *Proc. Natl. Acad. Sci. U.S.A.* **1994**, *91*, 12501-12504.

[24] Lossau, H.; Kummer, A.; Heinecke, R.; Poellinger-Dammer, F.;Kompa, C.; Bieser, G.; Jonsson, T.; Silva, C. M.; Yang, M. M.;Youvan, D. C.; Michel-Beyerle, M. E. *Chem. Phys.* **1996**, *213*,1-16.

[25] Yazal, J. E.; Pendergast, F. G.; Shaw, D. E.; Pang, Y.-P. *J. Am.Chem. Soc.* **2000**, *122*, 11411-11416.

[26] Shimomura, O. *Biol. Bull*. **1995**, *189*, 1-5.

[27] Phillips, G. N. J. *Curr. Opin. Struct. Biol.* **1997**, **7**, 821-827.

[28] Kummer, A. D.; Kompa, Lossau, H.: Poellinger-Dammer, F.; Michel-Beyerle, M. –E.; Silva, C. M.; Bylina, E. J.; Coleman, W. J.; Yang, M. M.; Youvan, D. C. *Chem. Phys* **1998**, *237*, 183-193.

[29] Voityuk, A. A.; Michel-Beyerle, M.-E.; Roesch, N. *Chem. Phys.Lett.* **1998**, *296*, 269-276.

[30] Voityuk, A. A.; Michel-Beyerle, M. E.; Rosch, N. In NBS Special Publicaton: Standard Reference Materials. **1980**, Washington, DC. 260-264.

[31] Weber, W.; Helms, V.; McCammon, J. A.; Langhoff, P. W. *Proc. Natl. Acad. Sci*. **1999**, *96*, 6177-6182.

[32] Chen, M. C.; Lambert, C. R.; Urgitis, J. D.; Zimmer, M. *Chem.Phys.* **2001**, *270*, 157-164.

[33] Brejc, K.; Sixma, T. K.; Kitts, P. A.; Kain, S. R.; Tsien, R. Y.;Ormoe, M.; Remington, S. J. *Proc. Natl. Acad. Sci*. **1997**, *94*,2306-2311.

[34] Wachter, R. M.; King, B. A.; Heim, R.; Kallio, K.; Tsien, R. Y.; Boxer, S. G.; Remington, S. J. *Biochemistry*, **1997**, *36*, 9759-9765.

[35] Shi, X.; Abbyad, P. Shu, X.; Kallio, K.; Kanchanawong, P.; Childs, W.; Remington, S. J.; Boxer, S. G. *Biochemistry*, **2007**, *46*, 12014-12025.

[36] Bublitz, G.; King, B.; Boxer, S. *J. Am. Chem. Soc.* **1998**, *120*, 9370-9371.

[37] Elsliger, M. A.; Wachter, R. M.; Hanson, G. T.; Kallio, K.; Remington, S. J. *Biochemistry* **1999**, *38*, 5296-5301.

[38] Seebacher, C.; Deeg, F.; Brauchle, C.; Wiehler, J.; Steipe, B. *J. Phys. Chem.* **1999**, *103*, 7728-7732.

[39] Weber, W.; Helms, V.; McCammon, J.; Langhoff, P. *Proc. Natl. Acad. Sci. U.S.A.* **1999**, *96*, 6177-6182.

[40] Striker, G.; Subramaniam, V.; Seidel, C. A. M.; Volkmer, A. *J. Phys. Chem. B* **1999**, *103*, 8612-8617.

[41] Kummer A. J.; Wiehler H.; Rehaber H.; Kompa C.; Steipe B.; Michel-Beyerle M. E. *J. Phys. Chem B* **2000,** *104,* 4791-4798.

[42] Martin M. F.; Negri F.; Olivucci M. *J. Am Chem. Soc*. **2004,** *126*, 5452-5464.

[43] Jung G.; Wiehler J.; Zumbusch A. *Biophys. J.* **2005,** *88*, 1932-1947.

[44] Garcia-Parajo M. F.; Segers-Nolten G. M. J.; veerman J-A.; Greve J.; van Hulst N. F.; *Proc. Natl. Acad. Sci USA* **2000**, *97*, 7237-7242.

[45] Dickson, R. M.; Cubitt, A. B.; Tsien, R. Y.; Moerner, W. E. *Nature* **1997**, *388*, 355-358.

[46] Peterman, E. J. G.; Brasselet, S.; Moerner, W. E. *J. Phys. Chem. A* **1999**, *103*, 10553-10560.

[47] Pierce, D. W.; HomBooher, N.; Vale, R. D. *Nature* **1997**, *388*, 338-338.

[48] Pierce, D. W.; Vale, R. D. *Methods Cell. Biol.* **1998**, *58*, 49-73.

[49] Jung, G.; Zumbusch, A.; Brauchle, C. *J. Phys. Chem.* **2000**, *104*, 3149-3156.

[50] Jung, G.; Brauchle, C.; Zumbusch, A. *J. Chem. Phys.* **2001**, *114*, 3149-3156.

[51] Habuchi S.; et al. *J. Am. Chem. Soc* **2005,** *127*, 8977-8984.

[52] Habuchi S.; et al. *Photochem Photobiol Sci.* **2006**, 567-576.

[53] Andrsen M. et al. *Proc Natl Acad sci USA* **2005**, *102*, 13070-13074.

[54] Henderson J. N.; Ai H. W.; Campbell R. E.; Remington S. J. *Proc Natl Acad Sci USA* **2007**, *104*, 6672-6677.

[55] Stiel A. C. et al. *Biochem J.* **2007**, *402*, 35-42.

[56] Forster, T. Z. *Elektrochem*. **1950***, 54*, 531.

[57] Weller, A. *Prog. React. Kinet*. **196**1, *1*, 187.

[58] Förster, T. *Pure Appl. Chem.* **1970**, *24*, 443.

[59] Ireland, J. F.; Wyatt, P. A. H. *Ad*V. *Phys. Org. Chem.* **1976**, *12*, 131.

[60] Shizuka, H. *Acc. Chem. Res.* **1985**, *18*, 141.

[61] Gutman, M.; Nachliel, E. *Biochim. Biophys. Acta* **1990**, *1015*, 391.

[62] Arnaut, L. G.; Formosinho, S. J. *J. Photochem. Photobiol. A* **1993**, *75*, 1.

[63] Tolbert, L. M.; Solntsev, K. M. *Acc. Chem. Res.* **2002**, *35*, 19.

[64] Agmon, N. *J. Phys. Chem. A* **2005**, *109*, 13-35.

[65] Weller, A. Z. *Elektrochem*. **1952**, *93*, 571-584.

[66] Herman, B.; Lakowicz, J. R.; Murphy, D. B.; Fellers, T. J. Davidson, M. W. "Fluorescence Excitation and Emission Fundamentals" *http://www.olympusfluoview.com/theory/fluoroexciteemit.html* (accessed April 2008).

[67] Wayne, C. E.; Wayne, R. P. *Photochemistry,* Oxford University Press: **1996**; 92p.

[68] Jameson, D. "Absorption, Excitation and Emission Spectra, Quantum Yield, Polarization/Anisotropy", *http://www.fluorescence-foundation.org/2005_course.htm,* **2005**, (accessed April 2008).

[69] "Molecular electronic structure and photophysics" *http://www.monos.leidenuniv.nl/smo/index.html?basics/photophysics.htm* (accessed April 2008).

[70] Williams, A. T. R.; Winfield S. A.; Miller, J. N. *Analyst*, **1983**, *108*, 1067.

[71] Becker, W.; "Advanced time-correlated single-photon counting techniques", Springer, Berlin, Heidelberg, New York, 2005.

[72] O'Connor, D. V.; Phillips, D. *Time-correlated single photon counting*, Academic Press, London, 1984.

[73] Becker, W. "*The Bh TCSPC Handbook*", Becker & Hickl GmbH, 2nd Edition, 2006.

[74] "Ultrafast Spectroscopy System", *http://kemia.me.tut.fi/instruments/femto.html*, (accessed April 2008)

[75] Bunitnx, G.; Naskrecki, R.; Poizat, O. *J. Phys. Chem*. **1996,** *100*, 19380.

[76] O'Connor, D. V.; Phillips, D. "*Time-correlated single photon counting*." Academic Press, London, 1984.

[77] Solntsev, K. M.; Poizat, O.; Dong, J.; Rehault, J.; Lou, Y.; Burda, C.; Tolbert, L. M.; *J. Phys. Chem. B.* **2008**, *112*, 2700-2711.

CHAPTER 2

SOLVATOCHROMISM OF THE GREEN FLUORESCENCE PROTEIN CHROMPHORE AND ITS DERIVATIVES

Introduction

Solvatochromism is the ability of a chemical substance to change color due to the changes in solvent polar and acid/base properties. Negative solvatochromism corresponds to hypsochromic shift; positive solvatochromism corresponds to bathochromic shift with, for example, increasing solvent polarity. The difference in dipole moment of the molecule between its ground state and excited state results the sign of the solvatochromism. Since polarities of the ground and excited state of a chromophore are different, a change in the solvent polarity will lead to differential stabilization of the ground and excited state, and thus, a change in the energy gap between these electronic states. Consequently, variations in the position, intensity, and shape of the absorption spectra can be direct measurement of the specific interactions between the solute and solvent molecules.[2]

Green fluorescent protein (GFP) and its mutants have revolutionized molecular biology.[3] Despite the effort toward expanding the class of GFP through gene shuffling techniques, successful examples invariably incorporate the β -barrel to isolate the chromophore. The β-barrel, presumably by restricting the conformational space of the chromophore, reduces the rate of radiationless decay, leading to ca. 10^4 higher fluorescence quantum yields. At the same time, the β -barrel can apparently tolerate a high degree of disorder within the protein, as judged by analysis of the numerous crystal structures, as well as a variety of π systems. The β -barrel obviously plays an enormous

role in the photophysics of GFP; its most obvious effect is to solvate both the chromophore and its conjugate base.

Due to the Franck-Condon principle, the excited state solvent shell is not in equilibrium with the excited state solute molecule. In fact, charge-transfer transitions of ground state ion-pairs give the largest changes in absorption spectra, and thus, the most useful for measuring solvent property. In this work we consider the effect of the β -barrel on the optical properties (absorption spectra) of the GFP chromophore (*p*-hydroxybenzylideneimidazolone, *p*-**HOBDI**) experimentally by selective variation of the protonation state of the latter and its microenviroment.

Experimental

General Experimental

4-Hydroxybenzaldehyde (99 %), p-anisaldehyde (99+ %), *N*-acetylglycine (99 %), and methyl trifluoromethanesulfonate (96 %) were purchased from Acros. Sodium acetate (99.7 %) and potassium carbonate (99.94 %) were purchased from Fisher. Methylamine (33 % wt. solution in absolute ethanol) was purchased from Aldrich. The progression of reactions was monitored by thin-layer-chromatography using Analtech UNIPLATE TLC plates (Silica Gel GF) with visualization by illumination with ultraviolet light. NMR spectra were recorded on a Varian Mercury spectrometer (300 MHz). Mass spectral analysis was provided by the Georgia Tech Mass Spectrometry facility. Elemental analyses were conducted at Atlantic Microlab. Ultraviolet-visible (UV-Vis) spectra were obtained on a Perkin-Elmer Lambda 19 spectrophotometer.

Synthesis

4-Methoxybenzylidene-2-methyloxazalone. *N*-Acetylglycine (2.0 g), sodium acetate (1.23 g), *p*-anisaldehyde (1.9 g), and acetic anhydride (4.2 ml) were heated at 80 °C with stirring for 2 h. Heated ethanol (20 ml) was added slowly and the mixture was allowed to

stand at room temperature for 4 h. The separated crystalline solid was filtered off, washed with ice-cold alcohol, then with hot water to obtain 1.4g (44%) of yellow oxazalone; 1H NMR ($CDCl_3$), δ, ppm: 2.40 (s, 3H, CH_3); 3.88 (s, 3H, O-CH_3); 6.98 (d, 2H, Ar-H); 7.12 (s, 1H, H on bridging carbon); 8.08 (d, 2H, Ar-H).

4-Methoxybenzylidene-1,2-dimethylimidazolinone (*p*-MeOBDI).

1.0 g of 4-(4- Methoxybenzylidene)-2-methyl-oxazalone was added to 0.4 g of potassium carbonate in a 25 ml round-bottom flash to which 0.75 g methylamine (33% wt. solution in absolute ethanol) and 8.0 ml ethanol were then added. The reaction mixture was refluxed for 4 h. After cooling, the mixture was neutralized with 10% HCl, and stayed at 0 ^oC for a further 4 h. The separated substance was filtered off, washed with ice-cold alcohol, then with hot water to obtain 0.76g (84%) of dark orange imidazolinone. mp 128-129 °C. 1H NMR ($CDCl_3$), δ, ppm: 2.37 (s, 3H, CH_3); 3.18 (s, 3H, N-CH_3); 3.85 (s, 3H, O-CH_3); 6.95 (d, 2H, Ar-H); 7.08 (s, 1H, H on bridging carbon); 8.12 (d, 2H, Ar-H). Molecular weight: EI-MS M+ calculated for [$C_{13}H_{14}N_2O_2$] = 230.26, found = 230.1.

4-Hydroxybenzylinene-1,2,3-trimethylimidazolinium (*p*-HOBDIMe+).

200 mg of 4-(4-Hydroxybenzylidene)-1,2-dimethyl-imidazolinone (*p*-**HOBDI**) was dissolved in 10 ml dry 1,4-dioxane to which 5 drops of methyl trifluoromethanesulfonate were then added. The mixture was stirring at room temperature for 1 h. The separated substance was filtered off, washed with ice-cold alcohol to obtain 185 mg of deep yellow imidazolinium. Decomposed above 175 °C. 1H NMR spectrum (D_2O), δ, ppm: 2.63 (s, 3H, CH_3); 3.28 (s, 3H, N-CH_3); 3.58 (s, 3H, N-CH_3); 6.91 (d, 2H, Ar-H); 7.49 (s, 1H, H on bridging carbon); 8.14 (d, 2H, Ar-H). Molecular weight: EI-MS M+ calculated for [$C_{13}H_{15}N_2O_2^+$] = 231.27, found = 231.1.

Results and Discussion

It is known that a careful pH titration indicates three forms of *p*-**HOBDI**: a (presumably nitrogen-) protonated cationic form C below pH = 2, the neutral form N, and

the anionic form A above pH = 10.[4] The absorbance spectrum of wild-type GFP demonstrates the presence of the two forms of the chromophore with absorbance bands at 398 (A_p band) and 477 nm (B_p band, *Figure 2.1*), their ratio very weakly depending on pH. For comparison we present the absorption spectra of *wt*GFP at pH 7 at "*p*-**HOBDI** C" graph as a black dash-dotted line. It has been noted that the high-energy *wt*GFP absorbance band corresponds to the absorbance of the *p*-**HOBDI** cation in water (*Figure 2.1*). Nevertheless, most of the current literature assigns band A_p to the absorbance of the neutral species, not the cation, because no evidence of the latter was found in the Raman and resonance Raman spectra of *wt*GFP and its S65T mutant,[5] and the imidazolone nitrogen atom is not sufficiently basic to be protonated in the protein. As a reference point, the analogous spectra of *p*-**HOBDI** at different pH were used.[6,7] Despite this observation, the possibility of cationic involvement in the absorbance spectra of the *wt*GFP cannot be excluded.[8,9]

Only scattered experimental treatments of solvatochromism in *p*-**HOBDI** and its derivatives are known.[4,10-12] A very weak solvent dependence of the N form absorption was reported,[10] while the absorbance of the C form exhibited a blue shift with polarity increase.[11] The hypsochromic shift of the A form was correlated with either solvent polarity[10] or acidity[4,12] increase. At the same time, it was found that mutations influence the position of the absorption bands of the chromophore to a much greater extent than simple solvent variations.[13] In all cases, no *quantitative* analysis was made. To more clearly understand the role of the solvent and protein in mediating the photophysics, and to correlate the absorbance bands of the chromophore in bulk solvents and in protein, we have undertaken a careful evaluation of the solvent effects on the various acid/base forms of *p*-**HOBDI** and its new derivatives, *O*- and *N*-methylated analogues. The selective blocking of the acid-base groups in the chromophore may give insight into the relative contribution of the various protonated form of the chromophore to the ground-state behavior of the protein.

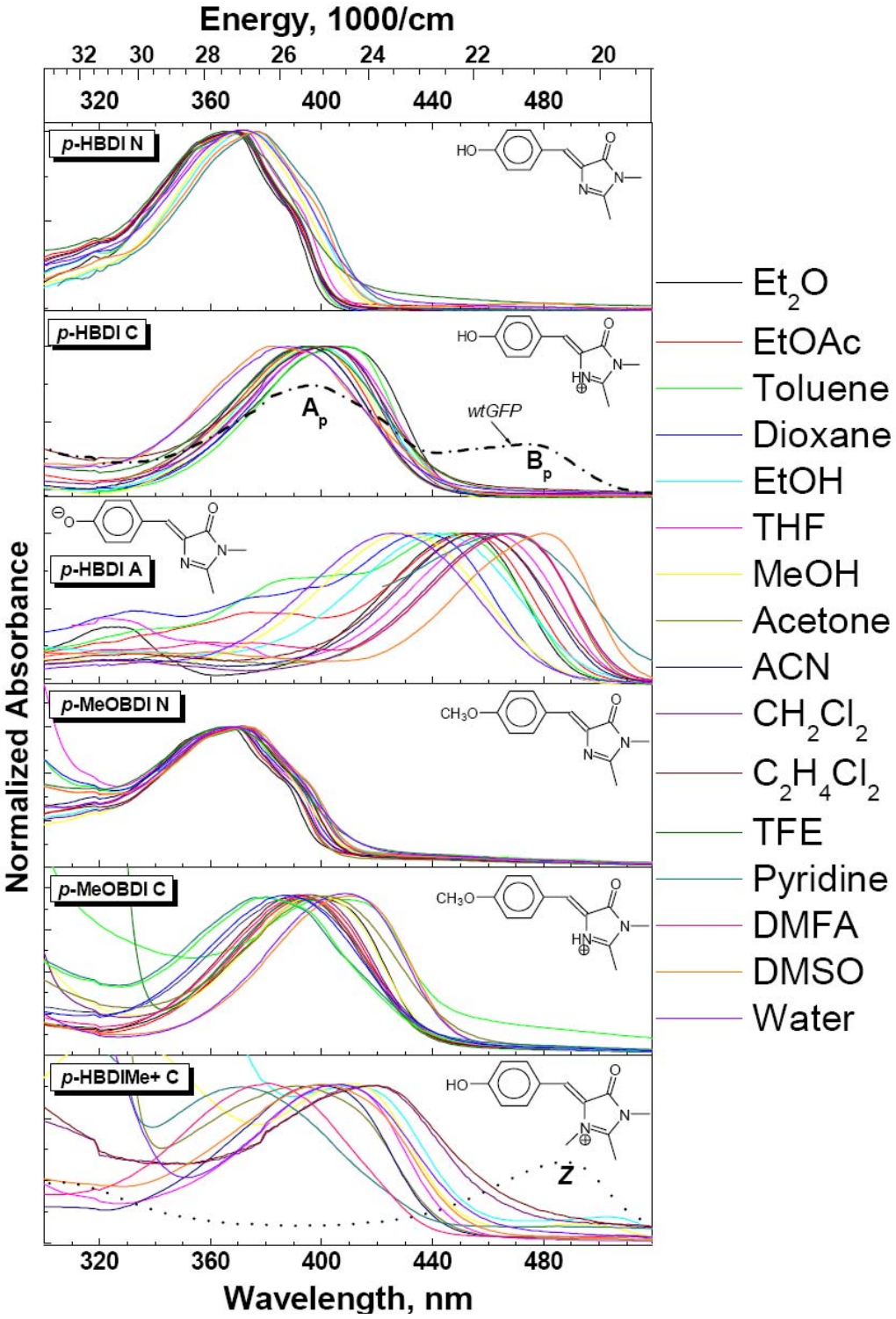

Figure 2.1. Absorption spectra of different protonation states of *p*-**HOBDI**, *p*-**MeOBDI**, and *p*-**HOBDIMe**$^+$ in various solvents. Absorbance of *p*-**HOBDIMe**$^+$ in water at pH 7.6 is presented at the bottom graph as black dotted line, the absorption peak at 486 nm is due to the zwitterion (Z) absorption. The intensity of the latter is scaled to fit the graph.

The GFP chromophore *p*-**HOBDI** was synthesized according to ref 14. Its *O*-methylated derivative, *p*-**MeOBDI**, was synthesized by a slightly modified procedure sing *p*-methoxybenzaldehyde. The *N*-methylated derivative, *p*-**HOBDIMe**$^+$, was synthesized by methylation of *p*-**HOBDI** with methyl trifluoromethanesulfonate. Similar to *p*-**HOBDI**, both new compounds had negligible fluorescence in bulk solvents at room temperature.

The C forms of *p*-**HOBDI** and *p*-**MeOBDI** were generated by adding trifluoromethanesulfonic acid to their neutral solutions, while the A forms of *p*-**HOBDI** were formed by adding KOH/crown ether complex. In aqueous solutions, the pH was controlled to ensure complete (de)protonation. The basicity of the imidazole nitrogen increased slightly upon methylation of the hydroxy group in *p*-**HOBDI**, while the acidity of the hydroxy group increased by more than 2 p*K*a units upon methylation of the imidazole nitrogen (*Table 2.1*, *Figure 2.2*). Titration of *p*-**HOBDIMe**$^+$ in the region pH = 4-7.4 demonstrated a clear equilibrium between C and its conjugate base (Figure 2.2), the zwitterion Z that absorbs at 486 nm in water (*Figure 2.1*). This is the first experimental observation of the ground-state GFP chromophore zwitterion that allows the investigation of the long-debated *p*-**HOBDI** tautomer.[8,10,15,16] In solutions with pH > 8.0, the Z form decomposed rapidly, probably by hydrolysis of the imidazolone ring. For the same reason, we could not detect absorbance of the Z in nonaqueous solvents in the presence of base; however, trace amounts of Z were observed in several neutral solvents.

compound	ν_0	p	a	b	R^a	$pK_a{}^b$
p-HBDI N	28.3	−0.71	−0.17	−0.7	0.94	8.53
p-HBDI C	24.5	1.2	0	0.5	0.90	2.36
p-HBDI A	22.9	−1.4	1.7	0.53	0.89	
p-MeOBDI N	27.9	−0.6	0	−0.18	0.87	
p-MeOBDI C	24.0	0.8	0	1.8	0.95	2.76
p-HBDIMe + C	23.0	2.2	−1.3	1.9	0.92	6.4

[a] Correlation coefficient. [b] Measured in MeOH/H_2O 1:1 v/v.

Table 2.1. Solvatochromic parameters (in 10^3/cm) used in multivariable regression fits of absorption data for neutral, cationic, and anionic forms of various chromophores according to Eq1.

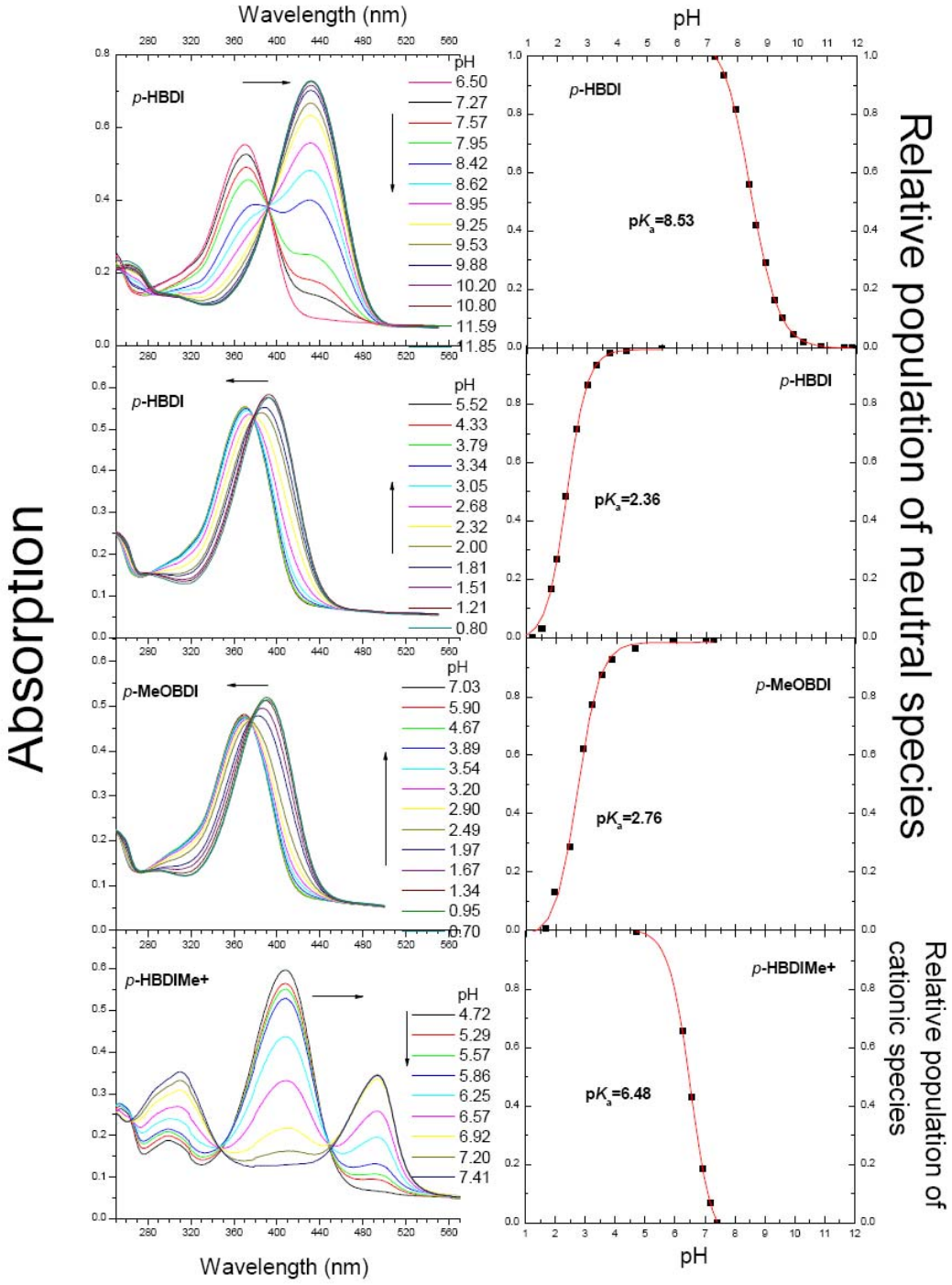

Figure 2.2. Left column: Absorption spectra of *p*-**HOBDI** and its derivatives at various pH in 1/1 vol. MeOH/H_2O mixtures. Right column: pH-titration curves corresponding to each graph on the left.

For further understanding the solvatochromic effect of p-**HOBDIMe**$^{+}$, a carefully hydrolysis testing experiment was performed. As shown in *Figure 2.3*, the absorption spectrum of this compound in water at pH 6.25 consisted of absorption bands at 400 nm and 490 nm, belonging to the cationic C and zwitterionic Z form, correspondingly. Step 1: Upon pH increase to 7.5, the cationic form converted into the zwitterionic Z completely. Step 2: However, upon following pH increase the intensity of Z band decreased, and the new absorption band at 350 nm appeared. Step 3: This band did not belong to parent p-**HOBDIMe**+ since the initial spectra was not restored after re-acidification to pH 3. Only a weak band at 400 nm was observed.

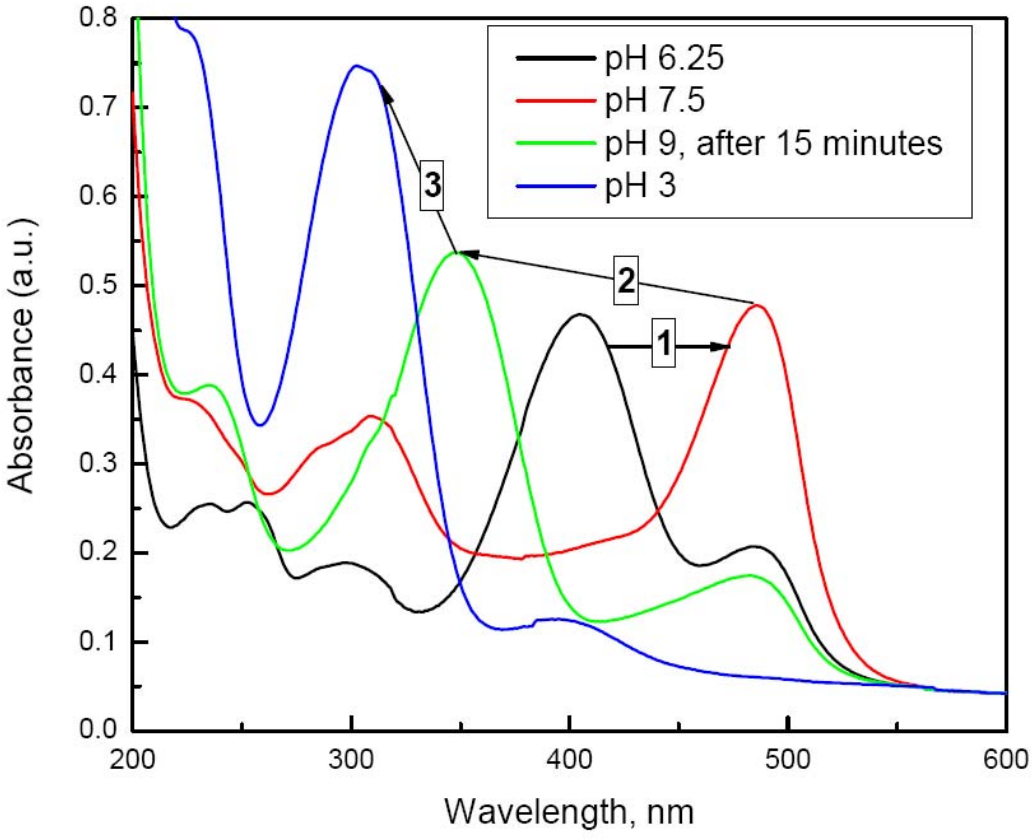

Figure 2.3 Hydrolysis of *p*-**HOBDIMe**$^{+}$ in basic conditions.

Each of these forms showed a complex solvatochromic behavior (see *Figure 2.1*). The absorption maxima of the N forms of the molecules had the weakest solvent dependence, while those of C and especially A forms varied over a very broad range. To analyze the solvatochromic behavior of the N, C, and A forms of the chromophores, we used the Kamlet-Taft multivariant approach,[17] which correlates the spectral shift *v* of the solute with the solvent parameters that are responsible for its acidic (α), basic (*β*), and polar solvating (*π**) properties:

$$v(1000/cm) = v_0 + p\pi^* + a\alpha + b\beta \qquad \text{Eq. 1}$$

We[18] and others[19] have successfully used this approach for various hydroxyaromatic compounds. It allows a straightforward separation of selective (H-bonding) and nonselective (dipole-dipole interaction) solvation. Here we report that the solvatochromic behavior of *p*-**HOBDI** and its derivatives is governed by *both* polar and acid/base properties of the solvents. The details refer to *Table 2.2*, solvent parameters *π**, α, and *β* were taken from Ref 17. We added 18-crown-6 into some solvents in which an anion could not produced by adding KOH. The absorption of *p*-**MeOBDI** had a very little solvent dependence of this peak, and the regression analysis had a poor correlation coefficient. For this column we used the data from Gaussian fit of the 30% top portion of the absorption spectra. It resulted in much better correlation coefficient (See *Table 2.1*), and surprisingly gave the similar solvatochromic parameters. The bottom lines in italic are the experimental data in nm (λ_{max}), while the top lines are the data in wavenumbers obtained by $10^7/\lambda_{max}$, and used for further calculations. *Figure 2.4* indicated the results of multiparameter regression fit according to Eq. 1.

#	Solvent[a]	π^*	β	α	*p*-HBDI			*p*-MeOBDI		*p*-HBDIMe+
					neutral	cation	anion[b]	neutral[c]	Cation	cation
1	Et_2O	0.24	0.47	0	27696[d] *361.0*	24926 *401.2*	22412* *446.2**	27708 *360.9*	25063 *399.0*	
2	EtOAc	0.45	0.45	0	27678 *361.3*	25502 *392.1*	22290* *448.6**	27629 *361.9*	25317 *395.0*	
3	Toluene	0.49	0.11	0	27649 *361.7*	24992 *400.1*	22491 *444.6*	27324 *366.0*	24509 *408.0*	
4	Dioxane	0.49	0.37	0	27603 *362.3*	25170 *397.3*	23109 *432.7*	27454 *364.2*	25125 *398.0*	
5	EtOH	0.54	0.77	0.83	27178 *367.9*	25427 *393.3*	22781 *439.0*	27278 *366.6*	25641 *390.0*	24201 *413.2*
6	THF	0.55	0.55	0	27397 *365.0*	25175 *397.2*	21940* *455.8**	27503 *363.6*	25316 *395.0*	24759 *403.9*
7	MeOH	0.60	0.62	0.93	27232 *367.2*	25465 *392.7*	23364 *428.0*	27398 *365.0*	25575 *391.0*	24390 *410.0*
8	Acetone	0.62	0.48	0.08	27595 *362.4*	25627 *390.2*	21598* *463.0**	27599 *362.3*	25381 *394.0*	25893 *386.2*
9	ACN	0.66	0.31	0.19	27696 *361.1*	25591 *390.8*	22130* *451.9**	27565 *362.8*	25445 *393.0*	25044 *399.3*
10	CH_2Cl_2	0.73	0	0.3	27794 *359.8*	25306 *395.2*	21674* *461.4**	27366 *365.4*	24331 *411.0*	24143 *414.2*
11	$C_2H_4Cl_2$	0.73	0	0	27670 *361.4*	25296 *395.3*	22097* *452.6**	27356 *365.6*	24450 *409.0*	24254 *412.3*
12	TFE	0.73	0	1.51	27539 *363.1*	25401 *393.7*		27497 *363.7*	24876 *402.0*	
13	Pyridine	0.87	0.64	0	26832 *372.7*		20724 *482.5*	27214 *367.5*		26205 *381.6*
14	DMF	0.88	0.69	0	27166 *368.1*	26461 *377.9*	21662 *461.6*	27265 *366.8*		26532 *376.9*
15	DMSO	1.00	0.76	0	26997 *370.4*	26080 *383.4*	21214 *471.4*	27141 *368.4*	26178 382.0	26274 *380.6*
16	water	1.09	0.4	1.17	26855 *372.4*	25842 *387.0*	23479 *425.9*	27196 *367.7*	25773 *388.0*	24631 *406.0*

Table 2.2. Absorption maxima of synthetic GFP chromophores in various solvents.
a Solvent parameters were taken from Ref 17.
b. In presence of 18-crown-6/KOH complex.
c. Gaussian fit of the spectra.
d. Bottom lines in nm unites; Top lines in wavenumber unites.

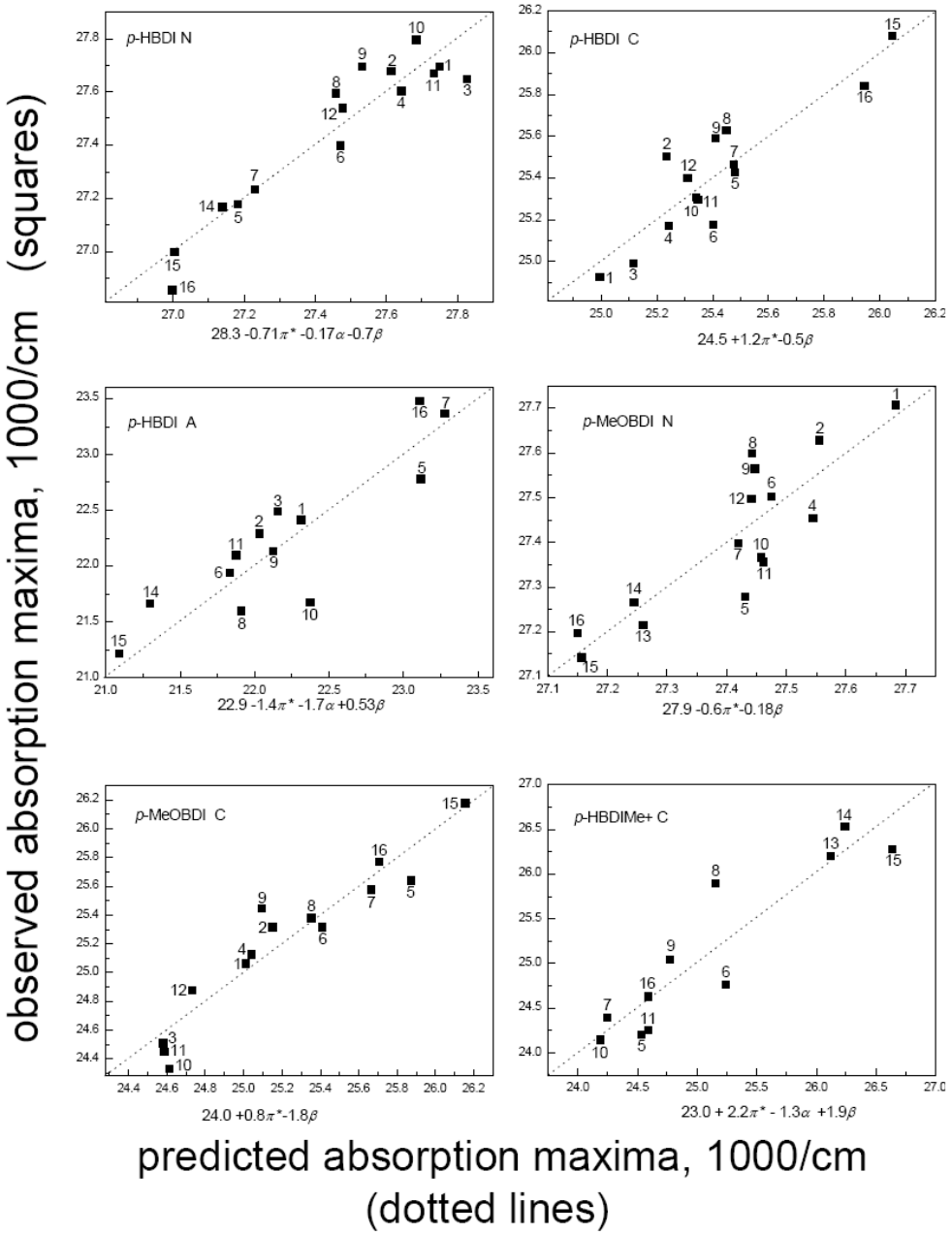

Figure 2.4. Results of multiparameter regression fit according to Eq. 1. Experimental data (squares) were approximated by the linear combination of π*, α, and β solvents parameters (dotted lines and equations at the bottom of each graph). Each point is labeled corresponding to solvent numbering in *Table 2.2*. The correlation coefficients for each fit are listed in *Table 2.1*.

The magnitudes and directions of the solvatochromic shifts strongly depend on the protonation state of the solute (*Table 2.1*). For N forms of *p*-**HOBDI** and *p*-**MeOBDI**, an increase in all solvent parameters induced a bathochromic shift. As with the naphthols,[18] the presence of a hydroxy group in *p*-**HOBDI** makes the solvent basicity (selective solvation) as important as the polar solvation factor. The *p*-**HOBDI** cationic form blue-shifts as solvent polarity and basicity are increased, while for the anionic form the polarity and acidity of the solvent work in opposite directions! The magnitude of the *solute* parameters *p* can be related to the relative dipole moments of the molecules, while proton susceptibility parameters *a* and *b* reflect the relative proton basicity and acidity of the chromophore. Our analysis clearly demonstrates an increase in dipole moment of the chromophores upon ionization and shows their amphoteric behavior. *p*-**HOBDIMe**$^+$ C shows the same absorption pattern for the *p*-**HOBDI** C, validating the protonation site in *p*-**HOBDI**.

We note, however, that at no polarity/acidity extreme did the absorption of the *p*-**HOBDI** neutral correspond to those in the protein. We are tempted to conclude that the *wt*GFP absorption was misassigned and the A_p band corresponds to the cation, leaving the 477 nm absorption to the zwitterion.[9] However, as we have discovered, the red-shifted absorbance maximum of the Z form does not match this value in any solvent, while the *p*-**HOBDI** A absorption in some basic solvents fits the 477 nm *wt*GFP absorption quite well (*Figure 2.1*). Thus, there is no reason to discount the common assignment of A_p as the neutral form. To explain the existing discrepancy between the experimental data on neutral species absorption in *p*-**HOBDI** and red-shifted *wt*GFP, a combination of mainly structural factors (small breakdown of planarity), with a small contribution from polarization effects of the environment,[20,21] must be taken into account. Equally important could be the presence in GFP and all its fluorescent mutants of the obligatory positively charged Arg96. Calculations indicate[21] that Arg96 red-shifts the absorption spectrum of the chromophore by ca. 40 nm, presumably by lowering the

energy of the charge-transfer excited state. Nevertheless, this is the first experimental verification of this rationale.

The complex solvatochromic behavior of the GFP chromophore and its derivatives requires both polar and acid/basic properties of the environment to be taken into account. However, no solvent effect serves to "turn on" the fluorescence, which remains subject to stereoelectronic effects. This stark contrast between solution and protein-constrained behavior suggests that there is something truly unusual about this chromophore, which is the subject of continued investigation in many laboratories.

Conclusions

The solvatochromic behavior of the green fluorescence protein (GFP) chromophore (*p*-hydroxybenzylideneimidazolone, *p*-**HOBDI**) and its derivatives (*p*-methoxybenzylideneimidazolone, *p*-**MeOBDI**, and *N*-methyl-*p*-hydroxybenzylideneim-idazolonium iodide, *p*-**HOBDIMe**$^{+}$) was studied using UV-vis-absorption spectroscopy in a wide array of solvents. The relative contribution of specific (polarity) vs nonspecific (hydrogen-bonding) solvation to the absorbance spectra was studied. (See *Figure 2.5*) On the basis of these data, we discuss the nature of the absorption peak of the protonated and deprotonated forms of the wild-type GFP.

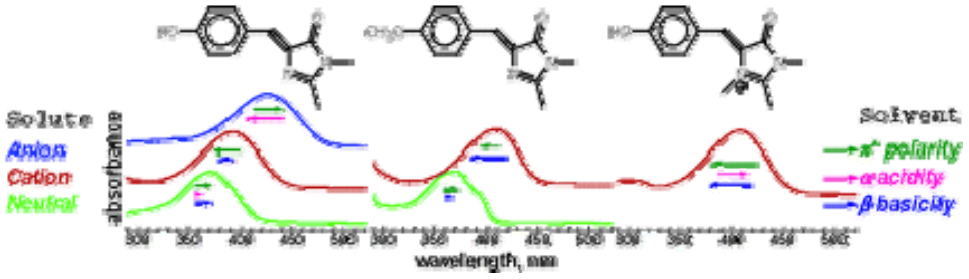

Figure 2.5 Table of contents for *Chapter 2*.

References

[1] Dong, J.; Solntsev, K. M.; Tolbert, L. M. *J. Am. Chem. Soc*. **2006**, *128*, 12038-12039.

[2] "Solvatochromism", *http://en.wikipedia.org/wiki/Solvatochromism*, (accessed April 2008).

[3] Zimmer, M. *Chem. Rev*, **2002**, *102*, 759-781.

[4] Bell, A. F.; He, X.; Wachter, R. M.; Tonge, P. T. *Biochemistry* **2000**, *39*, 4423-4431.

[5] Bell, A. F.; Stoner-Ma, D.; Wachter, R. M.; Tonge, P. J. *J. Am. Chem. Soc*. **2003**, *125*, 6919-6926.

[6] He, X.; Bell, A. F.; Tonge, P. T. *J. Phys. Chem. B* **2002**, *106*, 6056-6066.

[7] Schellenberg, P.; Johnson, E.; Esposito, A. P.; Reid, P. J.; Parson, W. W. *J. Phys. Chem. B* **2001**, *105*, 5316-5322.

[8] El Yazal, J.; Prendergast, F. G.; Shaw, D. E.; Pang, Y.-P. *J. Am. Chem. Soc*. **2000**, *122*, 11411-11415

[9] Voityuk, A. A.; Michel-Beyerle, M.-E.; Rösch, N. *Chem. Phys*. **1998**, *231*, 13-25.

[10] Niwa, H., Inouye, S., Hirano, T., Matsuno, T., Kojima, S., Kubota, M., Ohashi, M., Tsuji, F. I. *Proc. Natl. Acad. Sci. U.S.A.* **1996**, *93*, 13617-13622.

[11] Voityuk, A. A.; Kummer, A. D.; Michel-Beyerle, M.-E.; Rösch, N. *Chem. Phys*. **2001**, *269*, 83-91

[12] Yampolsky, I. V.; Remington, S. J.; Martynov, V. I.; Potapov, V. K.; Lukyanov, S.; Lukyanov, K. A. *Biochemistry* **2005**, *44*, 5788-5793.

[13] Jung, G.; Wiehler, J.; zumbusch, A. *Biophys. J.* **2005**, *88*, 1932-1947.

[14] Kojima, S.; Ohkawa, H.; Hirano, Tl; Maki, S.; Niwa, H.; Ohashi, M.; Inouye, S.; Tsuji, F. I. *Tetrahedron Lett.* **1998,** *39*, 5239-5242.

[15] Weber, W.; Helms, V.; McCammon, J. A.; Langhoff, P. W. *Proc. Natl. Acad. Sci. U. S. A.* **1999**, *96*, 6177-6182.

[16] Scharnagl, C.; Raupp-Kossmann, R. A. *J. Phys. Chem. B* **2004,** *108*, 477-489.

[17] Kamlet, M. J.; Abboud, J.-L. M.; Abraham, M. H.; Taft, R. W. *J. Org. Chem.* **1983**, *48*, 2877-2887.

[18] (a) Solntsev, K. M.; Huppert, D.; Tolbert, L. M.; Agmon, N. *J. Am. Chem. Soc.* **1998**, *120*, 7981-7982. (b) Solntsev, K. M.; Huppert, D.; Agmon, N. *J. Phys. Chem. A* **1998**, *102*, 9599-9606.

[19] (a) Mijin, D. Z.; Uscumlic, G. S.; Perisic-Janjic, N. U.; Valentic, N. V. *Chem. Phys. Lett.* **2006**, *418*, 223-229. (b) Reta, M.; Cattana, R.; Silber, J. J. *J. Solut. Chem*. **2001**, 30, 237-252. (c) Magnes, B.-Z.; Pines, D.; Strashnikova, N.; Pines, E. *Solid State Ion.* **2004**, *168*, 225-233.

[20] Marques, M. A. L.; López, X.; Varsano, D.; Castro, A.; Rubio, A. *Phys. Rev. Lett.* **2003**, *90*, 258101.

[21] Laino, T.; Nifosi, R.; Tozzini, V. *Chem. Phys*. **2004**, *298*, 17-28.

CHAPTER 3

SOLID STATE FLUORESCENCE STUDY OF *O*- ALKYL GFP CHROMOPHORE DERIVATIVES -COLOR TUNING OF CRYSTALLINE BDI EMISSION BY SUBSTITUENT-MEDIATED CRYSTAL PACKING

Introduction

The Green Fluorescent Protein (GFP) is used widely as a biological marker in molecular biology, medicine, and cell biology.[1-3] The chromophore of this protein, a *p*-hydroxybenzylidenimidazolinone (*p*-**HBI**) derivative, is embedded in the middle of an internal α-helix directed along a rigid β-barrel axis, with some degree of rotational freedom.[4] The chromophore is covalently bound to the protein backbone and further constrained via an extended hydrogen-bond network involving the phenolic hydroxyl and carbonyl groups. A number of ultrafast fluorescence experiments and simulation analysis have shown the fundamental photophysical processes of GFP and its mutants are facile excited-state proton transfer from the neutral excited chromophore to form the fluorescent anionic state, and the new anionic excited state is accommodated by an However, the denatured protein, isolated fragments of protein containing the chromophore, and synthetic model compounds, as discussed in *Chapter 2*, are all essentially nonfluorescent in fluid solution at room temperature.[5-7] This is presumably due to the free rotation around the exo-methylene double bond in the excited-state of the model compound, which allows nonadiabatic crossing (NAC) to occur, resulting in fluorescence quenching through internal conversion.[8] Fluorescence can, however, be achieved by cooling the solution, which imposes steric barriers to rotation at 77K.

Experiments have also shown that the radiationless decay mechanism exhibits a weak viscosity dependence, [9-11] suggesting that a volume conserving motion, for example, hula-twist (HT) might be involved in the fluorescence quenching.[8,12] Therefore, it is believed that the β-barrel plays a critical role in shielding the chromophore from external quenchers, providing steric hindrance that prevents the cis/trans isomerization pathway, and allowing the superb fluorescence properties of GFP and its mutants.

Previous studies showed that the protein cavity surrounding the chromophore in GFP or GFP-like protein is not complementary with a planar chromophore in the ground state.[12] The chromophore in wild-type GFP is planar because of its highly conjugated π system. The GFP protein matrix does, conversely, exert some strain away from planarity. This force from planarity should have an effect on the fluorescence of the chromophore, however, the photophysical mechanism remains unclear. Recently, Yamada et al.[13] also reported the protein prevents the chromophore from adopting a completely planar structure in photoactive yellow protein (PYP). Based on their calculations, they proposed that the efficiency of photoisomerization in PYP is due to the asymmetric protein chromophore interaction that can serve as the initial accelerant for the light-induced photocycle.

Compared to that in solution, some fluorophore molecules can be restricted in their motions and adopt planar conformation as aggregates in the solid state, which result in more effective conjugation between the electron donor and acceptor groups of the molecules. This effective conjugation may further induce the red-shift of the emission maximum and enhance the fluorescence quantum yields.[14] However, organic fluorophores with high solid-state fluorescence are less common. Many organic chromophores are highly emissive in dilute solutions but become weakly luminescent or non-luminescent in their solid states. The formation of molecular aggregates by strong intermolecular π-π interactions[15-17] or intermolecular hydrogen bonding[12] in the solid state generally results in reduction of luminescence efficiency. In view of the fact that

most GFP chromophore derivatives are nonfluorescent in solution, it is interesting to examine their intermolecular interactions in bulk materials that lead to the formation of aggregates, significantly alter the photophysical and photochemical properties of these molecules, resulting in large changes in their spectral characteristics and luminescence efficiency. Moreover, the optical and photophysical properties of these organic π-conjugated molecules in the solid state, defined largely by their molecular packing which in turn is controlled by various noncovalent forces, have been used as key elements in optoelectronic devices.[18,19] Understanding the nature of these forces and controlling them for the design of functional materials is of significant importance, especially with reference to tuning their application in devices such as light-emitting diodes,[20] photovoltaics,[21] and field effect transistors.[22,23]

Here we describe the synthesis and fluorescence properties of several isoelectronic *O*-alkyl GFP chromophore (alkoxybenzylideneimidazolinone) derivatives in solution and in the solid state. The role of the molecular packing in controlling the solid-state fluorescence of these derivatives is elucidated by studying their X-ray crystal structures.

Experimental Section

General Experimental

1-Bromohexane (99+ %), 1-bromododecane (98 %), potassium carbonate (99.94 %) and 2-butanone (99+ %) were purchased from Fisher. *N,N*-Dimethyl-formamide (DMF) (extra dry, water < 50 ppm) was purchased from Acros. The progression of reactions was monitored by thin-layer-chromatography using Analtech UNIPLATE TLC plates (Silica Gel GF) with visualization by illumination with ultraviolet light. ^{1}H NMR spectra were recorder on a Varian Mercury spectrometer (300 MHz). Mass spectral analysis was provided by the Georgia Tech Mass Spectrometry facility.

Ultraviolet-visible (UV-Vis) spectra were recorded on a Perkin Elmer Lambda19 spectrophotometer. Measurements of solid-state photoluminescence were carried out using the front face emission scan mode on a SPEX Fluorolog 1680/1681 spectro-fluorimeter. The entrance/exit slits of the monochromators were adjusted to the proper fluorescence intensity of each sample. The emission data were corrected using the method described in Ref. 24. Two types of solid-state samples were prepared. One was crystalline powder, by using double-sided cellophane tape to hold the vacuum-dried samples in place.[25] The other was thin film, by heating the samples placed between two glass cover slips above their respective melting points to make good film and cooling to room temperature.[18] Fluorescence lifetimes were measured using an Edinburgh Instruments time-correlated single photon counting (TCSPC) system. In this measurement, two picosecond excitation pulses diode lasers (LDH-P-C-375 and LDH-P-C470) with different wavelengths (372 nm and 467 nm) were used as excitation light sources. The detection system consisted of a high speed MicroChannel Plate PhotoMultiplier Tube (MCP-PMT, Hamamatsu R3809U-50) and TCSPC electronics (details refer to *Chapter 1*). Single crystal analyses were provided by Emory X-ray Crystallography Center. For crystal structure visualization, MERCURY 1.4.2 was used.

Synthesis

The synthesis and characterization of GFP chromophore (*p*-hydroxybenzylidene-dimethylimidazolone, *p*-**HOBDI**) and its *O*-methylated derivative, *p*-**MeOBDI** (**MEOBDI**) have been reported earlier.[26,27] *p*-hexyloxy **BDI** (**C6OBDI**) and p-dodecyloxy **BDI** (**C12OBDI**) were synthesized in a similar manner by the reaction of *p*-**HOBDI** with the corresponding alkyl bromide under basic conditions.[28,29]

4-(4-Hexyloxybenzylindene)-1,2-dimethylimidazolinone (C6OBDI).

p-**HOBDI** (100 mg, 0.46 mmol), 1-bromohexane (65 μL, 0.46 mmol, d = 1.17), and potassium carbonate (69 mg, 0.50 mmol) were dissolved in butanone (5 ml) and heated under reflux overnight. The solution was cooled to room temperature, poured into water (10 mL) and stirred for 2 h. The organic layer was separated and dried over anhydrous magnesium sulfate. Filtration and subsequent removal of the solvent *in vacuo* yielded a yellow solid, which was purified by recrystallization from ethyl acetate. The yield of yellow crystal was 104 mg (75%); mp 114 °C. ^{1}H NMR ($CDCl_3$), δ, ppm: 0.91 (t, 3H, CH_3); 1.33 (m, 4H, $2CH_2$); 1.45 (quintet, 2H, CH_2); 1.78 (quintet, 2H, CH_2); 2.36 (s, 3H, CH_3); 3.17 (s, 3H, N-CH_3); 3.99 (t, 2H, O-CH_2); 6.91 (d, 2H, Ar-H); 7.07 (s, 1H, H on bridging C); 8.07 (d, 2H, Ar-H). Molecular weight: EI-MS M+ calculated for [$C_{18}H_{24}N_2O_2$] = 300.4, found = 300.2.

4-(4-Dodecyloxybenzylindene)-1,2-dimethylimidazolinone (C12OBDI). p-**HOBDI** (77 mg, 0.36 mmol), 1-bromohexane (104 μL, 0.43 mmol, d = 1.038), and potassium carbonate (50 mg, 0.36 mmol) were dissolved in *N,N*-dimethyl-formamide (DMF) (2 mL) and heated at 100 °C with stirring overnight. After cooling to ambient temperature, the DMF was removed by rotary evaporation under reduced pressure. The residue was redissolved in chloroform (5 mL) and washed with water (3 × 5 mL). The organic layer was separated and dried over anhydrous magnesium sulfate. Filtration and subsequent removal of the solvent *in vacuo* to yield the crude product, which was purified by column chromatography on silica gel using chloroform/ethyl acetate (3:1) as eluent to afford the desired product. The yield of yellow powder was 126 mg (91%), mp 86-87 °C. ^{1}H NMR ($CDCl_3$), δ, ppm: 0.88 (t, 3H, CH_3); 1.26 (m, 16H, $8CH_2$); 1.45 (m, 2H, CH_2); 1.78 (quintet, 2H, CH_2); 2.37 (s, 3H, CH_3); 3.18 (s, 3H, N-CH_3); 4.00 (t, 2H, O-CH_2); 6.92 (d, 2H, Ar-H); 7.08 (s, 1H, H on bridging C); 8.08 (d, 2H, Ar-H). Molecular weight: EI-MS M+ calculated for [$C_{24}H_{36}N_2O_2$] = 384.5, found = 384.3.

Results

Photophysical Properties in Solution.

The absorption spectra of all neutral alkoxy-BDI (**ROBDI**) derivatives were measured in various solvents. As in previous measurements of **MeOBDI**,[27] the absorption maxima of all these derivatives were almost identical. The λ_{max} observed for their neutral forms were around 370 nm and had weak solvent dependence reported earlier. The steady-state emissions of these molecules were extremely weak in various solvents at room temperature as expected.[30] These emission peaks were obscured by Raman scattering, and must be considered with caution. The λ_{max} observed for these derivatives (~ 450nm) were consistent with the previous reported values.[27,31] Similarly to **HOBDI**, all of these **ROBDI** derivatives showed essentially nonfluorescent in fluid solution at room temperature. (See *Figure 3.1*)

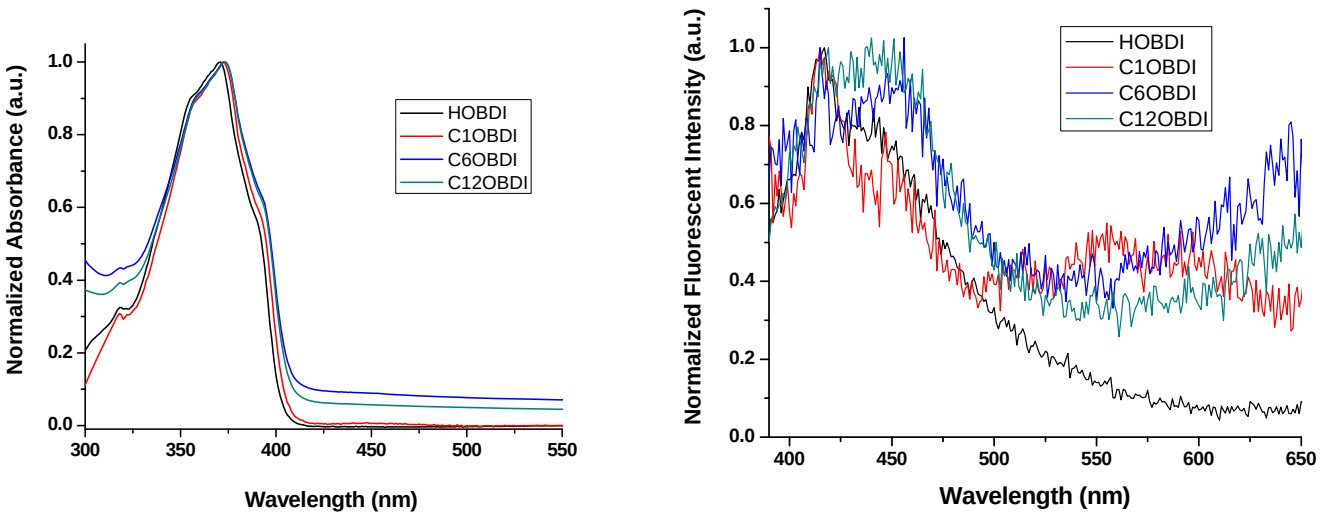

Figure 3.1. Normalized absorbance (left) and emission (right) spectra of **HOBDI** and **ROBDI** in solution (Toluene).

Solid-State Luminescence.

In contrast to solutions, crystals of **C6OBDI** and **C12OBDI** exhibited strong greenish-yellow and blue fluorescence emission, respectively, whereas **MeOBDI** exhibited relatively weak yellowish-organe fluorescence emission (See *Figure 3.2* top). The crystal of **HOBDI**, however, still remained nonfluorescent. In order to investigate the difference in the solid-state photophyiscal properties among these **ROBDI** derivatives, we measured the fluorescence excitation and emission spectra of the crystals and thin films. For each compound the emission spectra in their powdered crystalline state and thin films formed from their melts were almost identical (except for **MeOBDI**). Considering the difficulty of reproducibility of the fluorescence intensity in loading powdered crystalline samples,[24,32] thin films of these **ROBDI** derivatives were used in the measurements. A thin film form was not available for **HOBDI**, because it decomposed over 200 °C. The fluorescence spectra of these **ROBDI** derivatives were much broader and their emission intensities are significantly higher compared to those in solution. As shown in *Figure 3.2*, the fluorescence intensity of **HOBDI** was still low and shows a very weak emission peak at about 465 nm. Comparing to **HOBDI**, more than 10-fold fluorescence enhancement were observed in **C12OBDI** and **MEOBDI** samples. The emission maximum of **C12OBDI** thin film sample was also at ~ 465 nm, with a peak position similar to that of the solid-state **HOBDI** sample; however, the spectrum of **MEOBDI** was red-shifted to λ_{max} 560 nm. The **C6OBDI** sample showed the broadest and highest fluorescence intensity. Besides the excitation peak at around 465nm, it apparently possessed another broad band centered at 550 nm.

The optical properties of **MeOBDI** samples were significantly dependent upon their different solid states (*Figure 3.3*). The emission spectra of its crystal showed two structured bands with one sharp peak at 450 nm and the other broad band centered at about 550 nm. The emission spectra of thin films formed by heating above its melting point and suddenly cooling it to room temperature showed a structured band centered at

about 600 nm. However, the thin film form was less stable thermally, and a blue-shift in its emission maximum was observed after 2 days at room temperature. The difference in fluorescence of two different solid states could be attributed by the formation of a thermodynamically unstable aggregation form upon melting and cooling. In addition, we noticed the fluorescence of crystalline **MeOBDI**, as well as **C6OBDI** (see *Figure 3.4*) and **C12OBDI**, was lost when melting above its melting point, but its fluorescence quickly returned after cooling. The loss/restoration of the fluorescence upon melting/cooling is reversible.

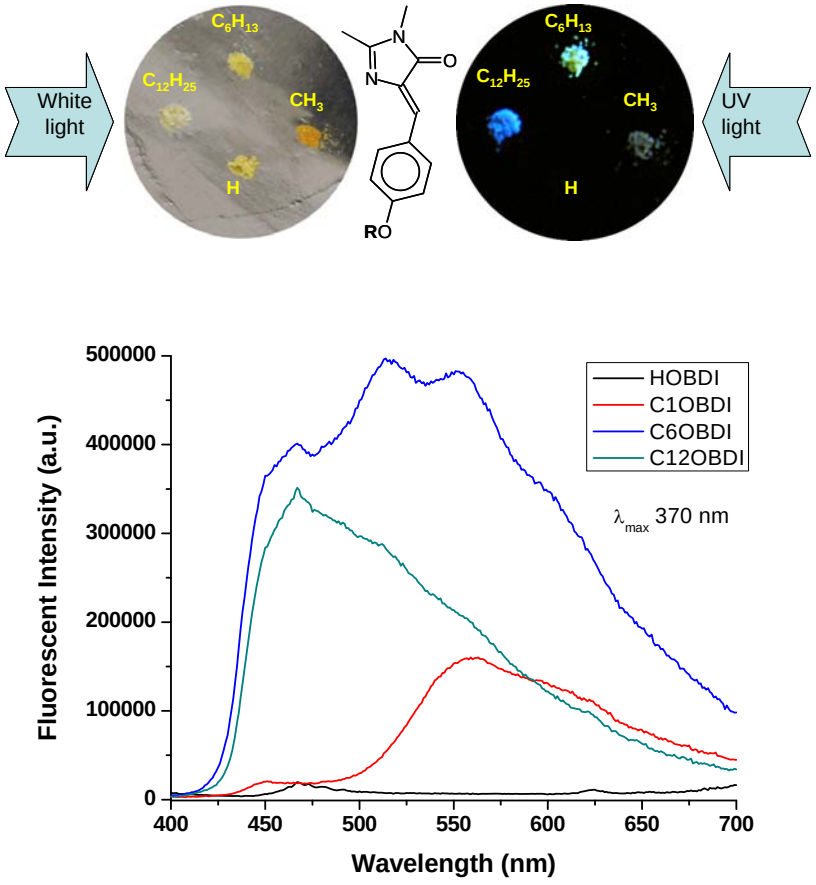

Figure 3.2. Top: **ROBDI** crystal image obtained under white light and UV light. Bottom:Solid-state fluorescence spectra of **HOBDI** (crystal), **MeOBDI** (thin film), **C6OBDI** (thin film), and **C12OBDI** (thin film). λ_{max} = 370 nm. (Fluorescent intensities are relative for reference purpose.)

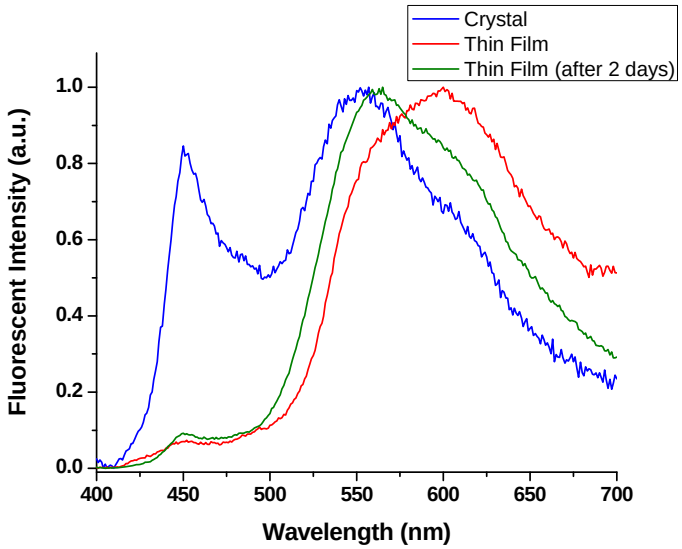

Figure 3.3. Normalized solid-state fluorescence spectra of **MeOBDI**. λ_{max} = 370 nm.

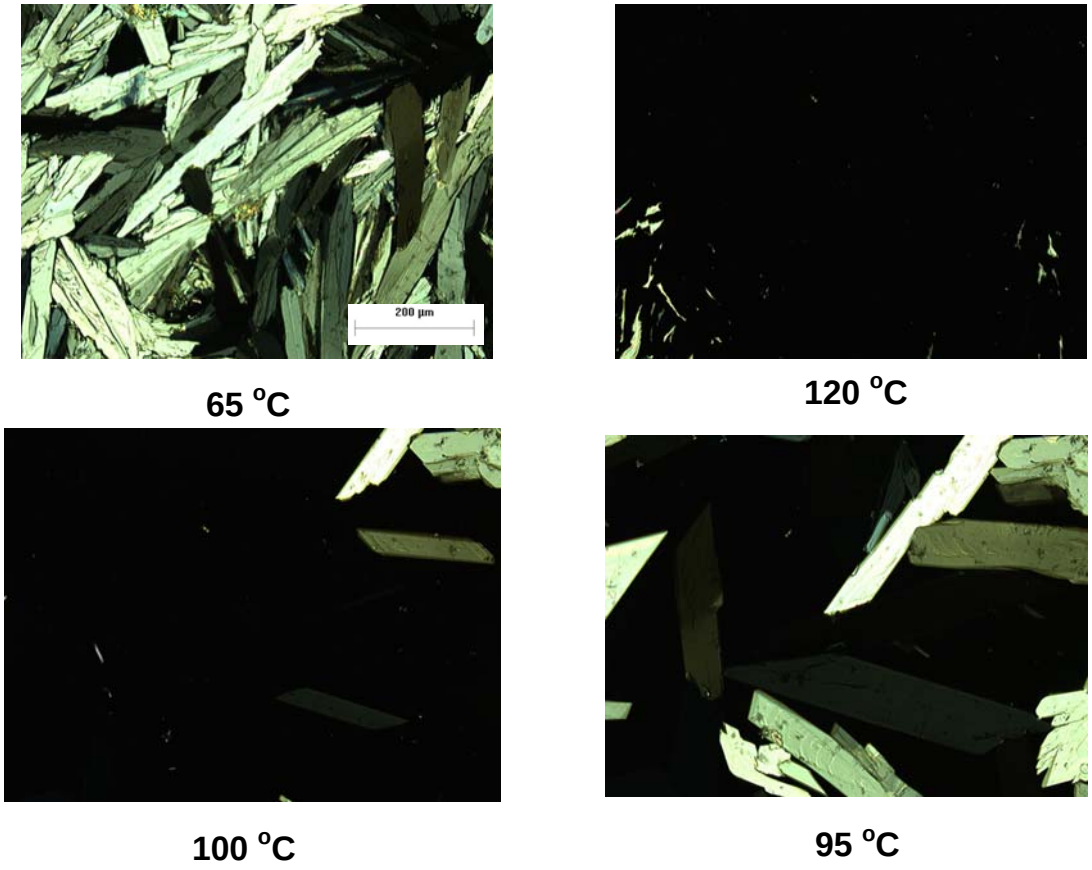

Figure 3.4. Polarized light optical microscopy image in the heating (top) and cooling (bottom) cycle of **C6OBDI** (mp = 114 °C) at selected temperatures.

For a more detailed study of the photophysical properties of these **ROBDI** derivatives in solid-phase, we investigated their excitation-emission matrix (EEM) spectroscopy. EEM spectroscopy has recently been developed and is known as an effective investigation method for complete spectroscopic characterization of multifluorophoric system in the literature.[33-35] We collected the emission spectra at room temperature, shifting the excitation wavelength by 5 nm after every acquisition in a spectra interval extending from 250 nm to 550 nm. In *Figures 3.5*, all the emission spectra of the **HOBDI** amd **ROBDI** samples are converted to contour plots, which allow the observation of every emission band and its correlation to the appropriate excitation wavelength. The contour plot of **MeOBDI** is the simplest, showing only one symmetric peak at E_x/E_m of ~ 470 nm/~ 550 nm. The intensive E_x/E_m peak of the **C12OBDI** solid-state sample is shifted to ~ 470 nm/~ 520 nm, however, the spectrum is asymmetric and apparently possesses another short-wavelength E_x/E_m peak at ca. 425 nm/470 nm. Apparently, the excitation/emission maximum of **C12OBDI** is highly blue-shifted compared to **MeOBDI**. Two visible-emitting centers in **C6OBDI** are more clearly distinguished. One emission center is at around 450-500 nm, and the other is at about 550 nm. Their corresponding excitation peaks are ~ 425 nm and ~ 470 nm respectively. The EEM spectra of **HOBDI** are much more interesting, whose emission spectra show fine structures in the region of 460-500 nm when excited at shorter wavelength, while its emission maximum unexceptionally shifts to ~520 nm under the excitation of longer wavelength. The straight lines corresponds to instrument artifacts;[36] for example, the second harmonic of the excitation lamp is observed in the corner of the 3-D graph, while in the empty zone of the opposite corner, no acquisition is performed due to excitation light scattering. In addition, the light scattering, as well as refraction from crystal or film morphology and geometrical effects observed on microspectrophotometer devices, may slightly alter the fluorescence spectra.

Lifetime measurements used in fluorescence spectroscopy, for instance, time-correlated single-photon counting (TCSPC), are expected to be less dependent on morphology and concentration than steady-state, thus providing an easier comparison of crystalline samples. Furthermore, lifetime measurements may allow the deconvolution of contribution from different fluorophores. Fluorescence lifetimes obtained from measurements of the solid-state of materials are often complex and multiexponential decay profiles are observed, and this could be attributed to the presence of molecules in different states of aggregation in solid state.[37] In addition, due to the complexity of the excitation spectra in the solid-state **ROBDI** derivatives, it is feasible to use pulsed diode lasers with two different wavelengths (372 nm and 467 nm) as excitation sources in the TCSPC system. Upon 372 nm excitation, all compounds clearly domenstrate an existence of two major decaying species at around 450 nm and 570 nm. The emission spectra excited at 467 nm of all **ROBDI** demenstrate only one component at 570 nm observed in the previous case. *Table 3.1* shows the fluorescence lifetimes measured from powered crystalline forms of **ROBDI** derivatives. The fluorescence lifetimes of **ROBDI** observed at 450 nm excitation indicate a biexponential decay and the amplitude of 0.1 ns component increases from **C6OBDI** to **C12OBDI**. Alternatively, the lifetimes at 570 nm indicate a triexponential decay, and the value of the longest time component increases in the order of C1-C6-C12.

Table 3.1 Fluorescence lifetime of the solid-state **ROBDI** derivatives.

compound	detected λ (nm)	τ_1 (ns)	F_1 %	τ_2 (ns)	F_2 %	τ_3 (ns)	F_3 %
MeOBDI	450	0.014	99	0.72	1	-	-
	570	0.044	52	0.54	30	1.6	18
C6OBDI	450	0.09	51	0.33	49	-	-
	570	0.017	14	1.1	60	2.4	26
C12OBDI	450	0.11	75	0.35	25	-	-
	570	0.21	12	1.1	60	3.2	28

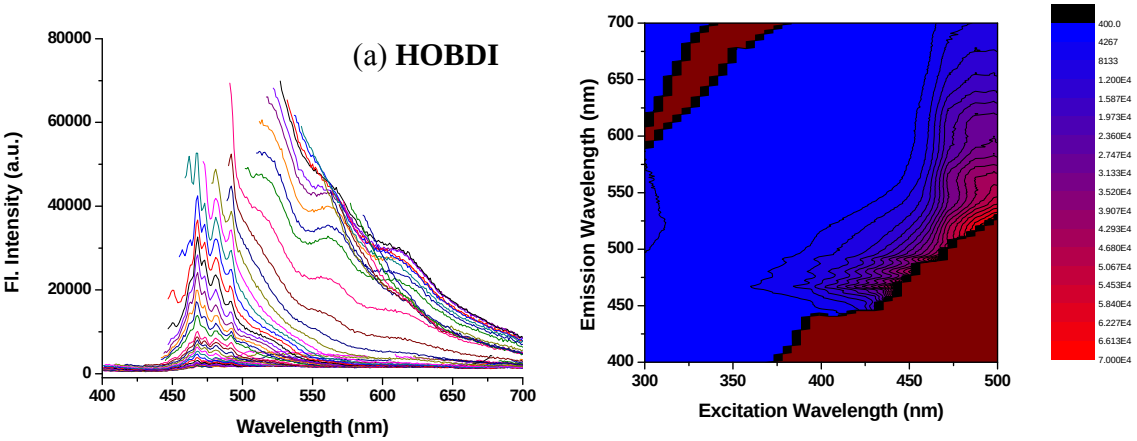
(a) HOBDI
Fl. Intensity (a.u.)
Wavelength (nm)
Emission Wavelength (nm)
Excitation Wavelength (nm)

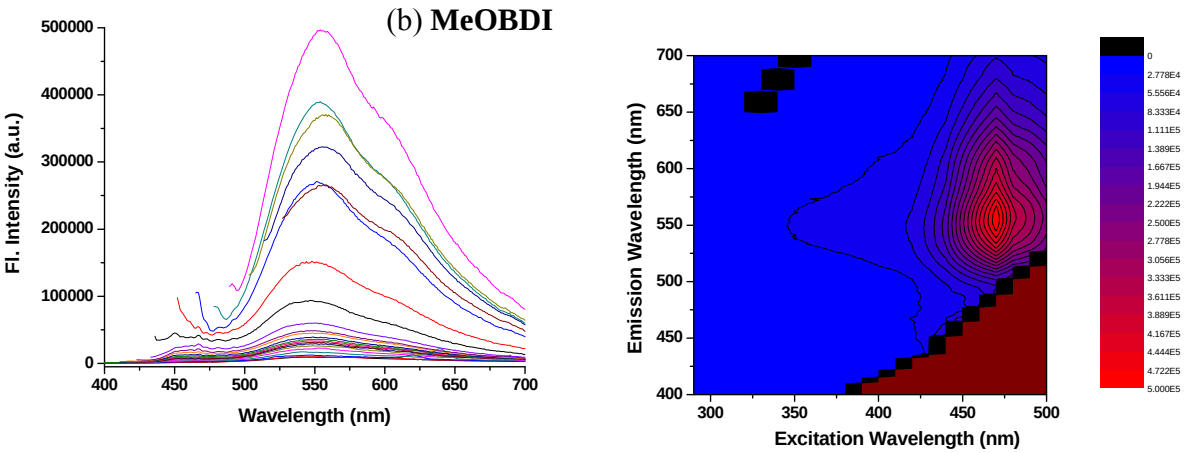
(b) MeOBDI
Fl. Intensity (a.u.)
Wavelength (nm)
Emission Wavelength (nm)
Excitation Wavelength (nm)

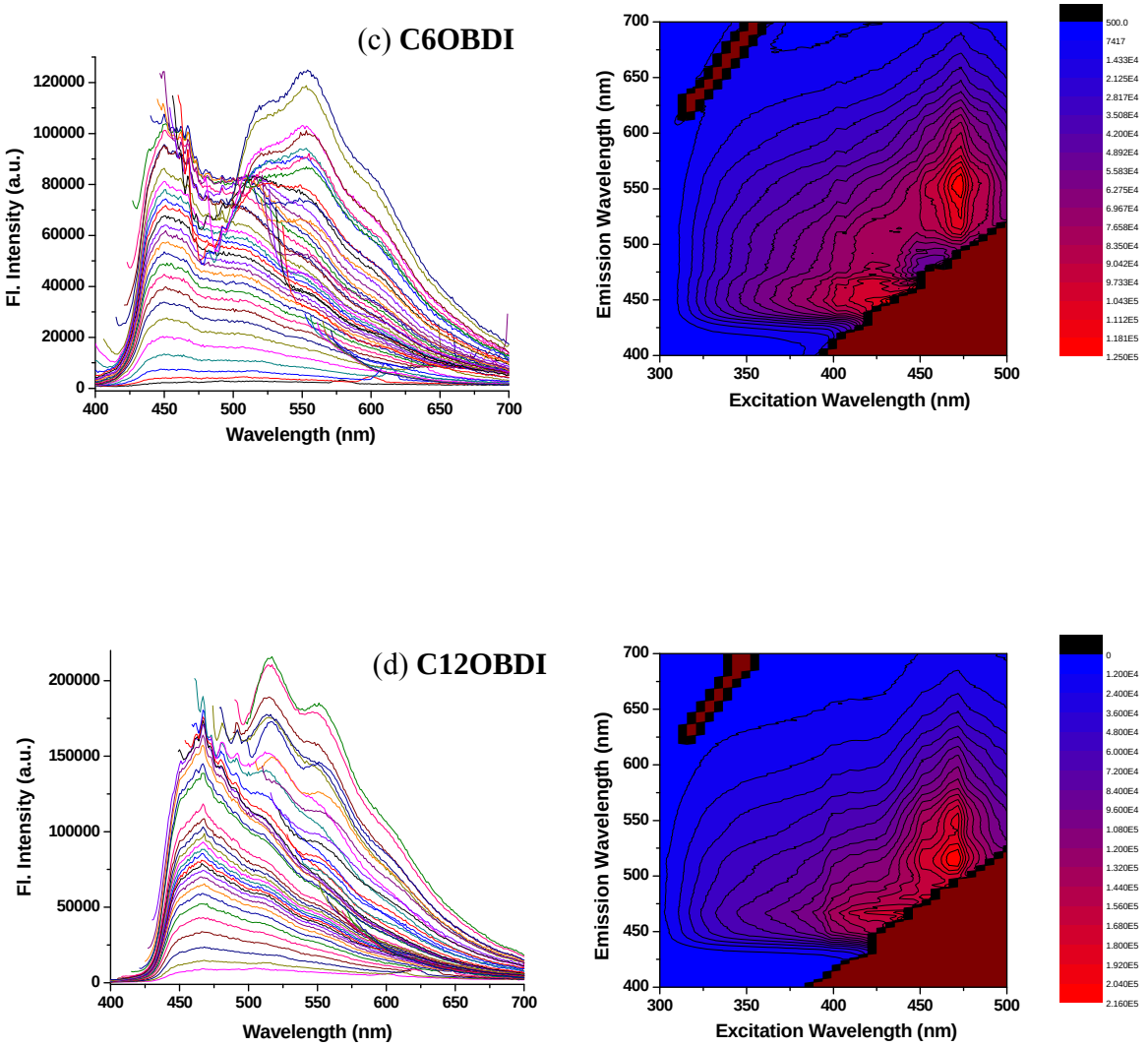

Figure 3.5. Emission spectra of solid-state (a) **HOBDI**, (b) **MeOBDI**, (c) **C6OBDI**, and (d) **C12OBDI** shifting the excitation wavelength of 5 nm after every acquisition in a spectral interval of 250-500 nm, (left). 3-D representation of all the spectra shown in left, (right).

Crystal Structure.

Single crystals of the **HOBDI** and **ROBDI** derivatives, **MeOBDI**, **C6OBDI**, and **C12OBDI** grow at room temperature in dichloromethane, or ethyl acetate solvents. Their crystal data are summarized in *Table 3.2*.

Table 3.2. Summary of crystallographic data for **HOBDI** and **ROBDI.**

	HOBDI	**MeOBDI**	**C6OBDI**	**C12OBDI**
empirical formula	C_{12} H_{12} N_2 O_2	C_{13} H_{14} N_2 O_2	C_{18} H_{24} N_2 O_2	C_{24} H_{36} N_2 O_2
formula weight	216.24	230.26	300.39	384.55
crystal system	monoclinic	monoclinic	triclinic	triclinic
space group	P2(1)/n	P2(1)/n	P-1	P-1
Z	8	4	2	2
a, Å	7.6165(3)	11.4832(4)	7.4623(5)	7.4678(3)
b, Å	16.5619(7)	7.7162(3)	10.0972(6)	10.2078(7)
c, Å	16.8917(t)	13.3246(5)	11.7537(8)	15.4909(7)
α, deg	90	90	88.216(3)	85.971(3)
β, deg	92.805(1)	102.553(2)	79.002(2)	85.619(4)
γ, deg	90	90	71.188(2)	71.602(4)
V, A^3	2128.23(15)	1152.43(7)	822.48(9)	1115.91(10)
d_{calc}, Mg/cm^3	1.350	1.327	1.213	1.144
μ, mm^{-1}	0.767	0.740	0.629	0.562
total reflections	7768	7792	5807	5685
unique reflections	3176	1863	2247	3090
R_{int}	0.0130	0.0246	0.0173	0.0244
final *R* indices *R*1, w*R*2	0.0338, 0.0899	0.0361, 0.0997	0.0353, 0.1029	0.0449, 0.1261
R indices (all data) *R*1, w*R*2	0.0349, 0.0908	0.0384, 0.1015	0.0396, 0.1077	0.0557, 0.1349

HOBDI has eight molecules per unit cell (*Figure 3.6*) with the molecules arranged into two nonequivalent stacks with their dipoles pointing in opposite directions in a herringbone fashion.[38] A part of the X-ray structure of **HOBDI** containing four monomer molecules is shown in *Figure 3.7*a. The figure also includes two major alignments of the molecules, namely, (1) AB (alternate stack), (2) AA'(neighboring stack), which are separately shown in *Figure 3.7*b, and c. An intermolecular hydrogen bond between the hydroxyl proton and the carbonyl oxygen (O-H···O distance is 2.673 Å) is observed in AB couples of **HOBDI**. In addition, the imidazoline and phenyl moieties

in AA' and BB' couples are overlapped with the distances of 3.590 Å and 3.546 Å. The intermolecular hydrogen bonding[39] and the intermolecular π- π interaction[16,17,40] in solid state have been reported as general factors in fluorescence quenching.

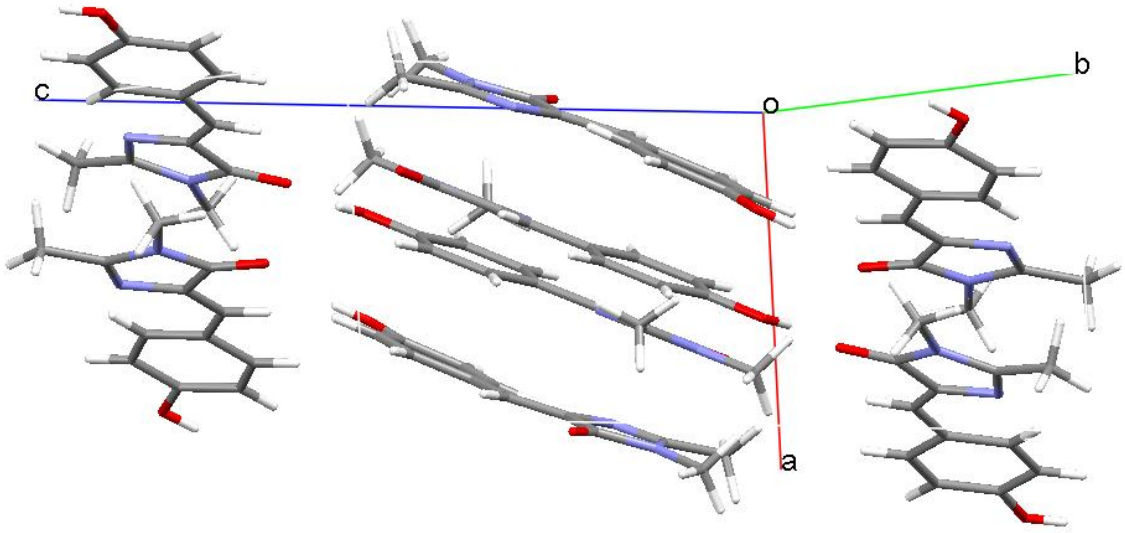

Figure 3.6. Crystal structure of **HOBDI** showing a unit cell.

One unit cell of **MeOBDI** contains four molecules. The structure of **MeOBDI** is similar to **HOBDI**, but the angle between two mean plains of alternate molecules increases from 31.9° to 50.4° (See *Figure 3.8* a). Since hydroxyl proton is substituted by methyl group in **MeOBDI**, the possibility of inter- or intramolecular hydrogen bond is eliminated. Moreover, this herringbone configuration is stabilized by aromatic C-H ··· O (2.651 Å) and aromatic C-H ··· N (2.845 Å) interaction[23] as shown in *Figure 3.8* b. In the case of AA', aromatic C-H ··· O, aromatic C-H ··· π, and π ··· π interaction from the phenyl rings of both A and A' are seen, and the overlapping of the parallel layers is partially reduced comparing to **HOBDI**.

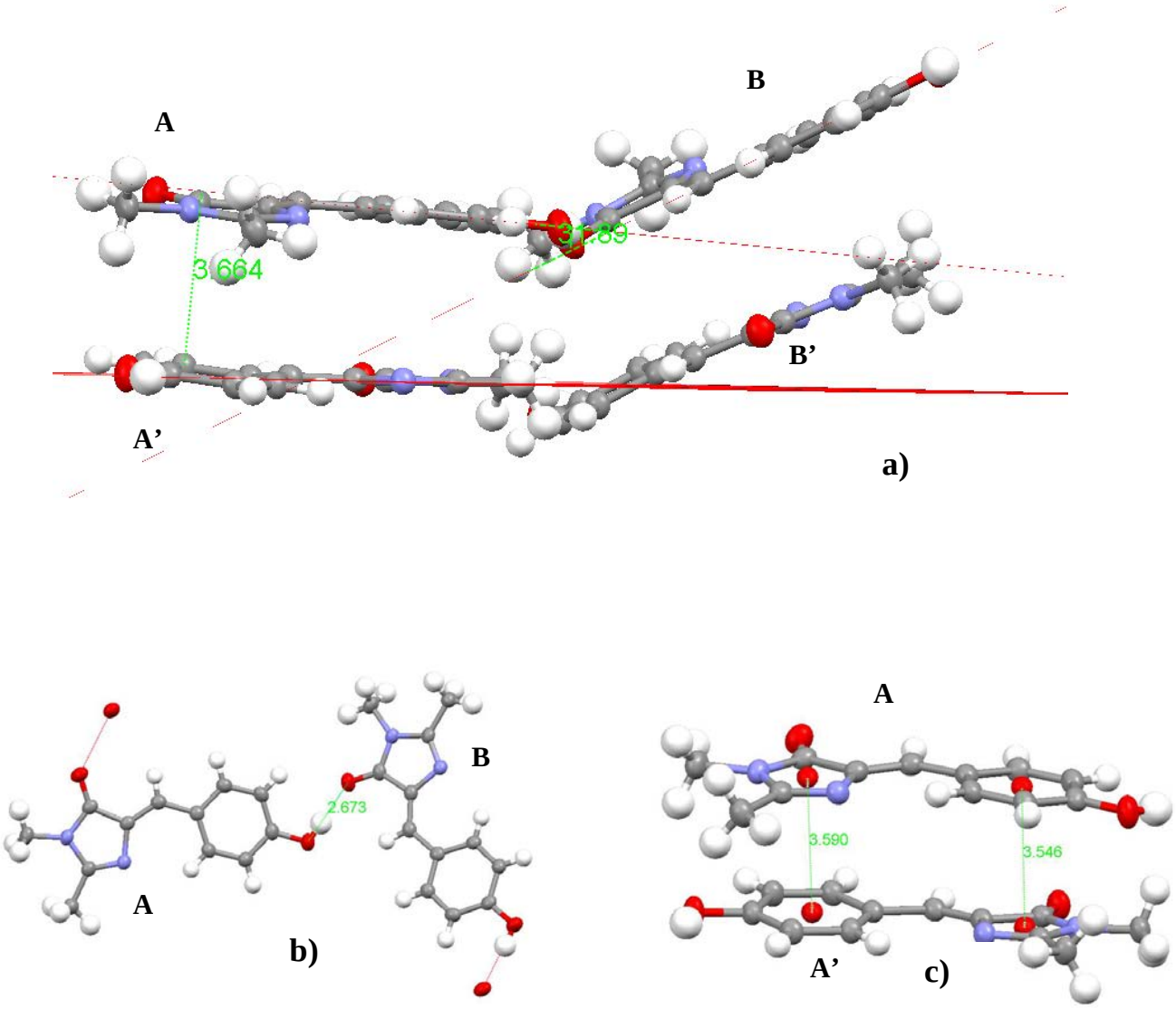

Figure 3.7. (a) A tetramer unit of **HOBDI** taken from the X-ray structure. (b-c) Dimer units showing the AB and AA' interaction. All distances are in angstrom units.

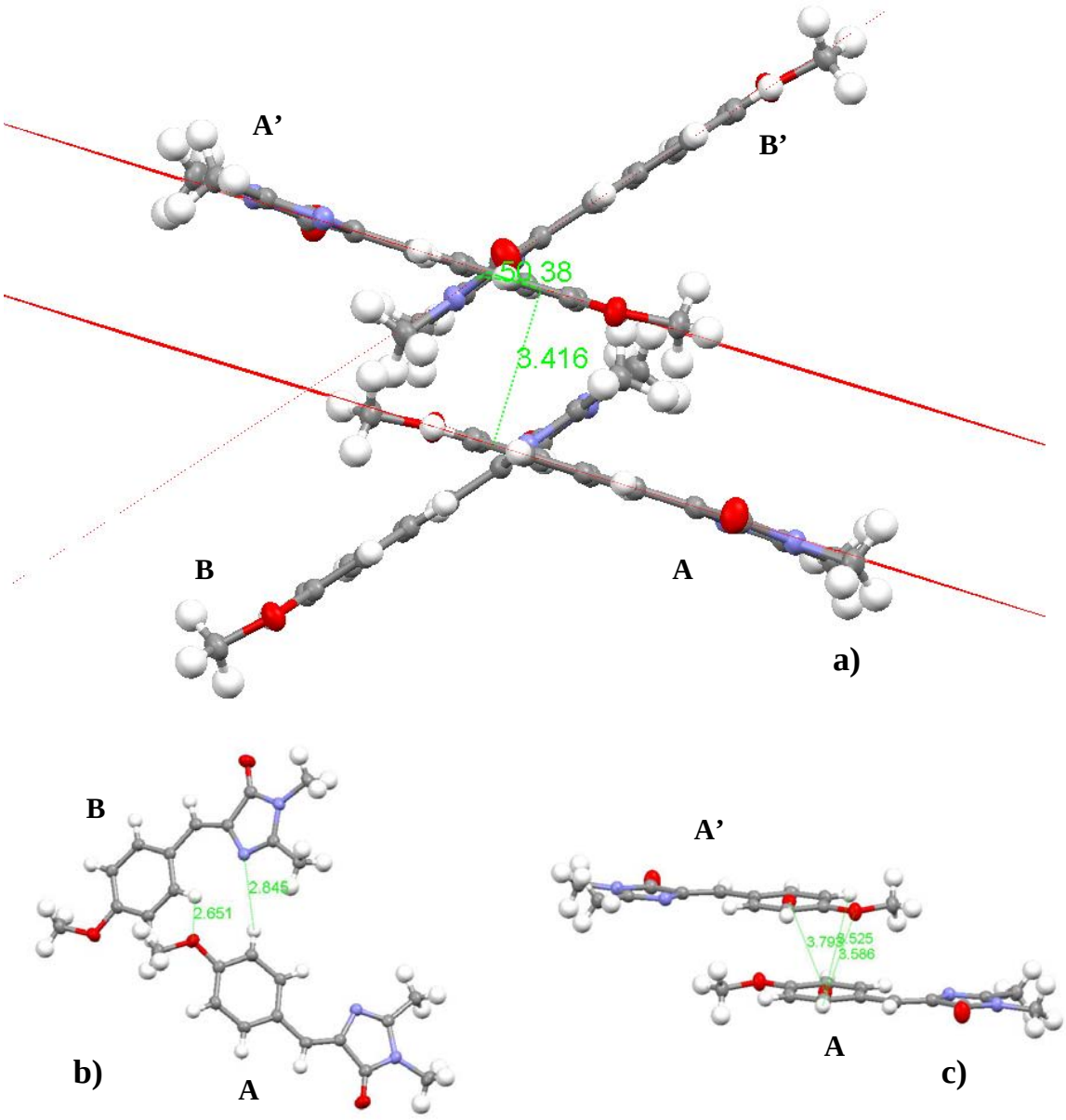

Figure 3.8. (a) A tetramer unit of **MeOBDI** taken from the X-ray structure. (b-c) Dimer units showing the AB and AA' interaction. All distances are in angstrom units.

The structure of **C6OBDI** is significantly different from those of **HOBDI** and **MeOBDI** (see *Figure 3.9*). It has only two molecules in one unit cell. The relative alignment of A and B is the most deviated as they are aligned antiparallel to each other while in both **HOBDI** and **MeOBDI** they are arranged in an angular fashion with respect to each other. Two strong intermolecular aromatic C- H ··· O (2.677 Å) interactions (electronically) are responsible for the planar AB alignment, whereas, the AA' unit is characterized by the presence of both aliphatic C-H ··· O and aliphatic C-H ··· π interactions. Such C-H ··· O hydrogen bonding stabilized planarization of crystal structures has been reported for various molecules.[23,41] The only aggregation interaction can be contributed from between aromatic C-H and imidazoline moiety with distance of 3.298 Å in neighboring molecules. However, since A and A' are translated along both the long and short axis relative to each other, the π-overlap between them is also minimized.

The structure of **C12OBDI** is very similar to that of **C6OBDI** as it shows AB, AA' type dimer units with aromatic C-H···O, aliphatic C-H···O and aliphatic C-H···π interactions (*Figure 3.10*). Compared to **C6OBDI**, the A and B units of **C12OBDI** make a stronger interaction for the coplanar alignment while the aromatic planes of the shifted antiparallel units A and A' in **C12OBDI** are located at a larger distance compared to **C6OBDI** (see *Figure 3.9* b, c and *Figure 3.10* b, c), which could be attributed more to the formation of planarization and less to aggregation.

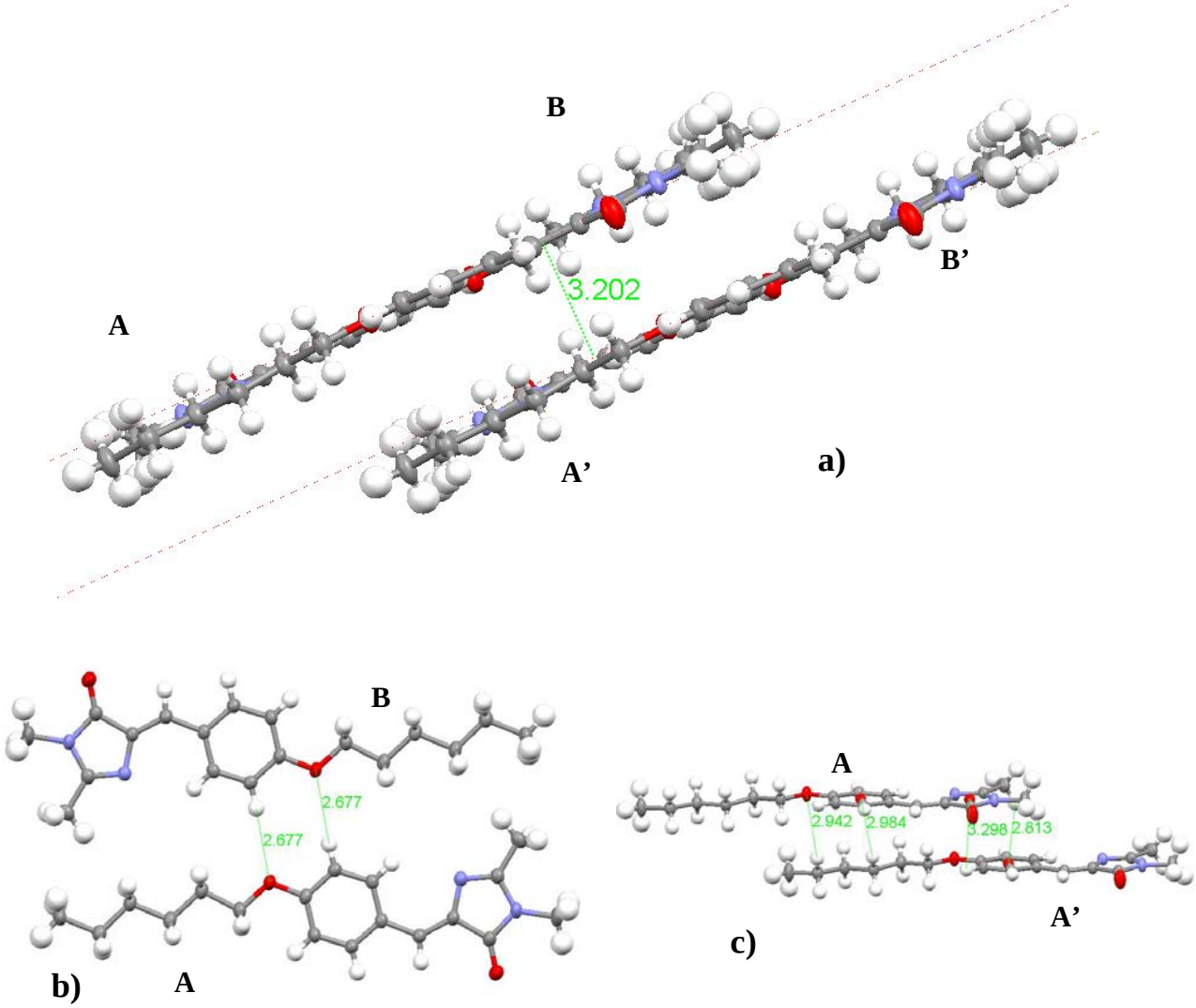

Figure 3.9. (a) A tetramer unit of **C6OBDI** taken from the X-ray structure. (b-c) Dimer units showing the AB and AA' interaction. All distances are in angstrom units.

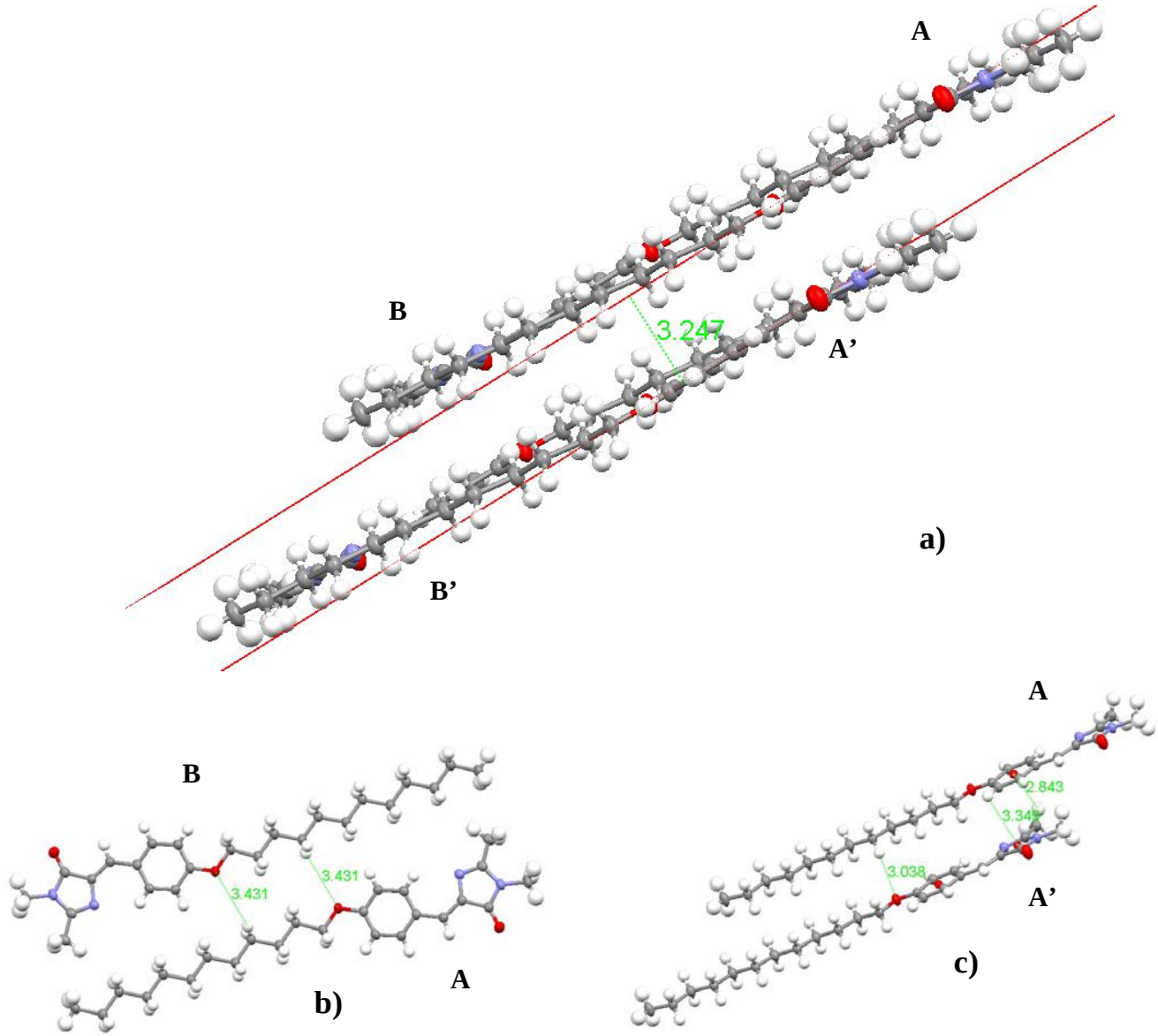

Figure 3.10. (a) A tetramer unit of **C12OBDI** taken from the X-ray structure. (b-c) Dimer units showing the AB and AA' interaction. All distances are in angstrom units.

Discussion

The protein-free synthetic **HOBDI** and its derivatives are nonfluorescent in solutions at room temperature, and their fluorescence quenching are presumably because of nonadiabatic crossing transition induced by the free rotation around the exo-methylene double bond in the exited-state of the model compound.[8] While in their solid states, the formation of aggregates from intermolecular interaction significantly alters the photophysical and photochemical properties of the molecules, resulting in large changes in their spectral characteristics and luminescence efficiency.[42-44] In the present study, the solid-state luminescence properties of **ROBDI** derivates are characterized by large enhancement in emission yields compared to that observed in solution, which may be attributed to planarization of the molecules resulting in more effective conjugation between the electron donor and acceptor groups of the molecules.

Consistent with previous reports, [23,45] the solid-state fluorescence spectra of the derivative possessing a shorter alkoxy group (**MeOBDI**) is significantly broader and red-shifted compared to that of the derivative with longer alkoxy chains (**C12OBDI**), while solid-state intensive emission band of **C6OBDI** is in the between and apparently possesses all peaks from both solid-state derivatives. The red-shifted emission observed in the solid state is clearly different from solution, because the absorption and emission spectra are almost independent of the length of the alkoxy substituent in latter case. Solid-state EEM spectra of **MeOBDI** clearly show a totally different E_x/E_m peak than that in solution. The significant red shift in the emission spectra could due to electronic coupling resulting from aggregation of molecules[23,42,44,45] or planarization of the backbones with increased conjugation length.[46,47] A recent study[23] on the dependence of the emission spectra upon dilution with an inert material have shown that the formation of red-shifted band is due to the formation of aggregates and is not merely due to planarization. Moreover, the fluorescence spectrum of the thin films of **MeOBDI** formed by rapid cooling is more red-shifted, broader and unstructured, indicating strong

intermolecular vibronic coupling. Similar reports[18] suggest the existence of the alternate molecular packing changing from a herringbone type arrangement in powdered crystalline state to a brickstone type arrangement in thin film form. In the brickstone arrangement, the material would result in a significant enhancement of the overlap of the π orbitals of the molecules from alternate stacks, leading to significant increase in electronic coupling between these molecules and red-shifted emission.

In the case of **C6OBDI** and **C12OBDI**, besides aggregate peaks, their EEM spectra show an additional E_x/E_m peak at ~ 425 nm/~ 475 nm, and only a small red-shift of ~25 nm of emission maxima is observed between the solid and solution states. For these molecules, since the additional peak is different with where aggregation is observed in the solid state, the small red-shift may be attributed to planarization and rigidization of the molecules in the solid state, and exhibiting monomer-like fluorescence.[23,48]

Since fluorescence emission of the thin films of **ROBDI** samples match closely with that the corresponding crystals, it indicates that the molecular packing responsible for the luminescent properties is the same in both cases. The crystal packing of **HOBDI** and **ROBDI** derivatives shows that the molecules are stacked in a cofacial manner, and the dipole moments of the neighboring stacks (AA' and BB') point in opposite directions in **HOBDI** and **MeOBDI** while same directions in **C6OBDI** and **C12OBDI**. The crystal packing of **HOBDI** indicates the electronic interaction is maximum for AA', BB' couples; in addition, the effect of an intermolecular hydrogen bond leads to the solid-state fluorescence of **HOBDI** being totally quenched. In contrast to **HOBDI**, within each neighboring stack, the molecules of **MeOBDI** are slightly translated (slipped) along the long axis and partially minimize the π-overlap between them, resulting the highly red-shifted emission band and relatively intensive fluorescence. Alternately, since the chromophore in GFP or GFP-like protein is not complementary with a planar chromophore in the ground state[49] but free rotating chromophore of protein is highly twisted based on calculation,[8] it is interesting to see if the fluorescence quenching in

solid-state **HOBDI** is induced by twisting of the exo-methylene double bond in chromophore, resulting efficient IC decay at conical intersection.[50,51] However, based on the observation of the ground-state single crystal structures of **HOBDI** and **ROBDI** derivatives, though they are not complementary with planar structures, the torsional angles around the double bond in all four samples are less than 2°, which are close to that of chromophore in GFP and GFP-like proteins.[8,48]

The molecular packing in the single crystal of longer alkoxy chain derivatives **C6OBDI** and **C12OBDI**, which unlike **MeOBDI** exhibits yellowish-orange fluorescence, is very different. As in the other cases, the molecules of alternate stacks (AB couples) arrange in a herringbone fashion. The AB couples in **C6OBDI** and **C12OBDI** are antiparallel molecules which are close enough to electronically interact with each other (See *Figures 3.9* and *3.10*). From the crystal structure, it becomes evident that in these arrangements, the overlap between the **C6OBDI** and **C12OBDI** chromophore part of these structures is minimal because of the interdigitated arrangement. Instead, the main overlap occurs between the neighboring stacks (AA' and BB' couples). The crystal packing of **C6OBDI** and **C12OBDI** shows A and A' (or B and B') are translated along both the long and short axis relative to each other. The molecule number in each unit cell is reduced in **C6OBDI** and **C12OBDI** as well. (See *Table 3.2*) As a result of these factors, electronic interacting between the two molecules is minimized and excitonic coupling does not occur. The interaction of the neighbor molecules in **C12OBDI** is relatively weaker compared to **C6OBDI**, therefore it indicates monomer-like blue fluorescence. Conversely, analysis of the weak interactions in the crystal structure of **C6OBDI** represents that it exhibits both the monomer and red-shifted aggregate emission.

Conclusion

In contrast to their behavior in solution, some *O*-alkyl GFP chromophore (**ROBDI**) derivatives exhibit large fluorescent enhancement in solid state. Our studies

provide clear evidence for exciton splitting in the solid state resulting in red-shifted emission for the derivatives. The role of the alkyl chain length in controlling the nature of the molecular packing and consequently their fluorescence properties has been elucidated. In alkoxy-**BDI** derivatives, increasing the length of the alkyl chain results in a visual change in fluorescence from yellow to blue. On the basis of the analysis of the molecular packing in the single crystals, this difference is attributed to fluorescence arising from aggregates in the molecule possessing a short alkyl chain (methyl) to monomer fluorescence in the long alkyl chains (hexyl and docecyl) containing derivatives. The color of crystalline **BDI** is tuned by substituent-mediated crystal packing, showing their potential applications in optoelectronic devices.

References

[1] Zimmer, M. *Chem. Rev*. **2002,** *102*, 759-781.

[2] Tsien, R. Y. *Annu. Rev. Biochem***. 1998**, *67*, 509-544.

[3] *Green Fluorescent Protein: Properties, Applications, and Protocols*; 2nd ed.; Chalfie, M., Kain, S. R., Eds.; Wiley-Intersciences; Hoboken, NJ, **2005**.

[4] Chen, M. C.; Lambert, C. R.; Urgitis, J. D.; Zimmer, M. *Chem. Phys*. **2001**, *270*, 157.

[5] Niwa, H.; Ionuye, S.; Horano, T.; Matsuno, T.; Kojima, S.; Kubota, M.; Ohashi, M.; Tsuji, F. I. *Proc. Natl. Acad. Sci. USA* **1996**, *93*, 13617.

[6] Kojima, S.; Ohkawa, H.; Hirano, T.; Maki, S.; Niwa, H.; Ohashi, M.; Inouye, S.; Tsuji, F. I.; *Tetrahedron Lett.* **1998**, *39*, 5239.

[7] Litvinenko, K. L.; Webber, N. M.; Meech, S. R. *J. Phys. Chem. A* **2003**, *107*, 2616-2623.

[8] Maddalo, S. L.; Zimmer, M.; *Photochemistry and Photobiology*, **2006**, *82*, 367-372.

[9] Mandal, D.; Tahara, T.; Webber, N. M.; Meech, S. R. *Chem. Phys. Lett.* **2002**, *358*, 495-501.

[10] Mandal, D.; Tahara, T.; Meech, S. R. *J. Phys. Chem. B* **2004**, *108*, 1102-1108.

[11] Litvinenko, K. L.; Webber, N. M.; Meech, S. R. *J. Phys. Chem. A* **2003**, *107*, 2616-2623.

[12] Yoshida, K.; K. Uwada, H. Kumaoka, L. Bu, S. Watanabe, *Chem. Lett.* **2001**, 808.

[13] Yamada, A.; Ishikura, T.; Yamato, T. *Prot. –Struct. Funct. Bioinform.* **2004**, *55*, 1063-1069.

[14] (a) Deans, R.; Kim, J.; Machacek, M. R.; Swager, T. M. *J. Am. Chem. Soc.* **2000**, *122*, 8565. (b) An, B.-K.; Kwon, S.-K.; Jung, S.-D.; Park, S. Y. *J. Am. Chem. Soc.* **2002**, *124*, 14410. (c) Luo, J.; Xie, Z.; Lam, J. W. Y.; Cheng, L.; Chen, H.; Qiu, C.; Kwok, H. S.; Zhan, X.; Liu, Y.; Zhu, D.; Tang, B. Z. *Chem. Commun.* **2001**, 1740. (d) Chen, J.; Xu, B.; Ouyang, X.; Tang, B. Z.; Cao, Y. *J. Phys. Chem. A* **2004**, *108*, 7522. (e) Li, Z. H.; Wong, M. S.; Tao, Y.; Lu, J. *Chem.*s*Eur. J*. **2005**, *11*, 3285.

[15] Dreuw, A.; Plöner, J.; Lorenz, L.; Wachtveitl, J.; Djanhan, J.E.; Br¨uning, J.; Metz, T.; Bolte, M.; Schmidt, M.U. *Angew. Chem. Int. Ed.* **2005**, *44*, 7783.

[16] Ooyama, Y.; Yoshida, K. *New J. Chem.* **2005,** *29*, 1204.

[17] Mizukami, S.; H. Houjou, K. Sugaya, E. Koyama, H. Tokuhisa, T. Sasaki, M. Kanesato, *Chem. Mater.* **2005**, *17*, 50.

[18] Kumar, N. S. S.; Varghese, S.; Rath, N. P.; Das, S. *J. Phys. Chem. C.* **2008**, 112, 8429-8437.

[19] (a) Hudson, A. J.; Weaver, M. S. In *Functional Organic and Polymeric Materials*; Richardson, T. H., Ed.; John Wiley & Sons: New York, **2000**. (b) Kaneko, M. In *Handbook of Organic Molecules and Polymers*; Nalwa, H. S., Ed.; Wiley: New York, **1997**.

[20] (a) Burroughes, J. H.; Bradley, D. D. C.; Brown, A. R.; Marks, R. N.; Mackay, K.; Friend, R. H.; Holmes, P. L.; Holmes, A. B. *Nature* **1990**, *347*, 539. (b) Kraft, A.; Reichert, A. *Tetrahedron* **1999**, *55*, 3923. (c) In *Organic Light Emitting De*V*ices: Synthesis, Properties and Applications*; Mu¨llen, K., Scherf, U., Eds.; Wiley-VCH: Weinheim, Germany, 2006. (d) Yamaguchi, Y.; Ochi, T.; Miyamura, S.; Tanaka, T.; Kobayashi, S.; Wakamiya, T.; Matsubara, Y.; Yoshida, Z.-i. *J. Am. Chem. Soc.* **2006**, *128*, 4504. (e) Armaroli, N.; Accorsi, G.; Holler, M.; Moudam, O.; Nierengarten, J.-F.; Zhou, Z.; Wegh, R. T.; Welter, R. *Ad*V. *Mater*. **2006**, *18*, 1313.

[21] (a) O'Neill, M.; Kelly, S. M. *Ad*V. *Mater.* **2003**, *15*, 1135. (b) Shirota, Y. *J. Mater. Chem.* **2005**, *15*, 75. (c) Strohriegl, P.; Grazulevicius, J. V. *Ad*V. *Mater.* **2002**, *14*, 1439.

[22] (a) Dimitrakopoulos, C. D.; Malenfant, P. R. L. *Ad*V. *Mater.* **2002**, *14*, 99. (b) Garnier, F.; Hajlaoui, R.; Yassar, A.; Srivastava, P. *Science* **1994**, *265*, 1684. (c) Li, X.-C.; Sirringhaus, H.; Garnier, F.; Holmes, A. B.; Moratti, S. C.; Feeder, N.; Clegg, W.; Teat, S. J.; Friend, R. H. *J. Am. Chem. Soc.* **1998**, *120*, 2206. (d) Kelly, S. M.; O'Neill, M. In *Handbook of Ad*V*anced Electronic and Photonic Materials*; Nalwa, H. S., Ed.; Academic Press: San Diego, CA, 2000; Vol. 1, Chapter 1.

[23] Davis, R.; Kummar N. S. S.; Abraham, S.; Suresh, C. H.; Rath, N. P.; Tamaoki, N.; Das, S. *J. Phys. Chem. C* **2008**, *112*, 2137-2146.

[24] Gardecki, J. A.; Maroncelli, M. *Appl. Spectrosc*. **1998**, *52*, 1179-1189.

[25] Sharma, V. K.; Kalonia, D. S. *J. Pharm. Sci*. **2003**, *92*, 890-899.

[26] Kojima, S.; Ohkawa, H.; Hirano, Tl; Maki, S.; Niwa, H.; Ohashi, M.; Inouye, S.; Tsuji, F. I. *Tetrahedron Lett.* **1998,** *39*, 5239-5242.

[27] Dong, J.; Solntsev, K. M.; Tolbert, L. M. *J. Am. Chem. Soc*. **2006**, *128*, 12038-12039.

[28] Cowling, S. J.; Goodby, J. W. *Chem. Commun*. **2006**, *39*, 4107-4109.

[29] Yam, V. W-W.; Yang, Yu.; Zhang, J.; Chu, B. W-K.; Zhu, N. *Organometallics,* **2001**, *20*, 4911-4918.

[30] Solntsev, K. M.; Poizat, O.; Dong, J.; Rehault, J.; Lou, Y.; Burda, C.; Tolbert, L. M. *J. Phys. Chem. B* **2008**, *112*, 2700-2711.

[31] Kummer, A. D.; Kompa, C.; Niwa, H.; Hirano, T.; Kojima, S.; Michel-Beyerle, M. E. *J. Phys. Chem. B* **2002**, *106*, 7554.

[32] Ramachander, R.; Jiang, Y.; Li, C.; Eris, T.; Young, M.; Dimitrova, M.; Narhi, L.; *Analytical Biochemistry*, **2008**, *376*, 173-182.

[33] Weber, G. *Nature,* **1961**, *190*, 27.

[34] Gill, D. M.; Wright, J. C.; McCaughan, L. *Appl. Phys. Lett.* **1994**, *64*, 2483.

[35] Divya, O.; Mishra, A. K. *Anal. Chim. Acta* **2007**, *592*, 82-90.

[36] Marolo, T.; Baldacchini, G.; Kalinov, V. S. ; Montereali, R. M.; *Phys. Stat. Sol* **2005**, *2*, 367-370.

[37] Li, H.; He, L.; Zhong, B.; Li, Y.; Wu, S.; Liu, J.; Yang, G. *ChemPhysChem*. **2004**, *5*, 124.

[38] (a) Koren, A. B.; Curtis, M. D.; Francis, A. H.; Kampf, J. W. *J.Am. Chem. Soc.* **2003**, *125*, 5040. (b) Gierschner, J.; Ehni, M.; Egelhaaf, H.-J.; Medina, B. M.; Beljonne, D.; Benmansour, H.; Bazan, G. C. *J. Chem. Phys.* **2005**, *123*, 144914. (c) Spano, F. C. *J. Chem. Phys.* **2003**, *118*, 981. (d) Nishio, M. *CrystEngComm* **2004**, *6*, 130.

[39] K. Yoshida, K. Uwada, H. Kumaoka, L. Bu, S. Watanabe, *Chem. Lett.* **2001**, 808.

[40] Dreuw, A.; Plöner, J.; Lorenz, L.; Wachtveitl, J.; Djanhan, J.E.; Brüning, J.; Metz, T.; Bolte, M.; Schmidt, M.U. *Angew. Chem. Int. Ed.* **2005**, *44*, 7783.

[41] (a) Desiraju, G. R. *Acc. Chem. Res.* **1996**, *29*, 441. (b) Desiraju, G. R. *Acc. Chem. Res.* **2002**, *35*, 565. (c) Vargas, R.; Garza, J.; Dixon, D. A.; Hay, B. P. *J. Am. Chem. Soc.* **2000**, *122*, 4750. (d) Jeffrey, G. A. *An Introduction to Hydrogen Bonding*; Oxford University Press: Oxford, U.K., 1997.

[42] Cornil, J.; Beljonne, D.; Calbert, J.-P.; Brédas, J.-L. *Ad*v. *Mater.***2001**, *13*, 1053.

[43] Vaday, S.; Geiger, H. C.; Cleary, B.; Perlstein, J.; Whitten, D. G. *J. Phys. Chem. B* **1997**, *101*, 321

[44] (a) Sheikh-Ali, B. M.; Rapta, M.; Jameson, G. B.; Cui, C.; Weiss, R. G. *J. Phys. Chem.* **1994**, *98*, 10412. (b) Sheikh-Ali, B. M.; Weiss, R. G. *J. Am. Chem. Soc.* **1994**, *116*, 6111. (c) Lewis, F. D.; Yang, J.-S.; Stern, C. L. *J. Am. Chem. Soc.* **1996**, *118*, 2772. (d) Lewis, F. D.; Yang, J.-S.; Stern, C. L. *J. Am. Chem. Soc.* **1996**, *118*, 12029.

[45] Davis, R.; Rath, N. P.; Das, S. *Chem. Commun.* **2004**, 74.

[46] Bunz, U. H. F.; Imhof, J. M.; Bly, R. K.; Bangcuyo, C. G.; Rozanski, L.; Bout, D. A. V. *Macromolecules* **2005**, *38*, 5892-5896.

[47] Miteva, T. ; Palmer, L. ; Kloppenburg, L. ; Neher, D.; Bunz, U. H. F. *Macromolecules* **2001**, *33*, 652.

[48] Da Como, E.; Loi, M. A.; Murgia, M.; Zamboni, R.; Muccini, M. *J. Am. Chem. Soc.* **2006**, *128*, 4277.

[49] Yang F.; Moss L.; Phillips G. *Nat Biotechnol*, **1996**, *14*, 1246-1251.

[50] Weber, W.; Helms, V.; McCammon, J. A.; Langhoff, P. W. *Proc. Natl. Acad. Sci. U.S.A.* **1999**, *96*, 6177-6182.

[51] Toniolo, A.; Olsen, S.; Manohar, L.; Martinez, T. J. *Faraday Discuss.* **2004**, *127*, 149-163.

CHAPTER 4

EXCITED-STATE STRUCTURE DETERMINATION OF THE GREEN FLUORESCENT PROTEIN CHROMOPHORE USING ULTRAFAST POLARIZATION-SENSITIVE INFRARED SPECTROSCOPY

Introduction

In order to gain a clear picture of the roles that nearby solvent molecules have in the chemical reaction dynamics, femtosecond UV/vis-mid-infrared pump-probe technique is an ideal method for time-resolved studies of this chemical reaction dynamics. The spatial parameters of the structural dynamics can be resolved for the molecular probe under study as well as for the nearby solvent molecules. It is well known that with time-resolved vibrational spectroscopy one can grasp the dynamics of specific chemical bonds in the case where the probed vibrations can be regarded as local modes. In contrast, by probing electronic states with optical frequencies additional arguments are necessary to determine whether certain chemical bonds are involved in the reaction pathways. [2]

In wild-type green fluorescent protein (GFP), an important photosensor protein used in bioimaging,[3,4] the photochemical dynamics of the chromophore incorporates a Förster cycle, where excitation of the photoacid chromophore is followed by proton transfer to the side groups of the protein pocket[5] through, apparently, an intramolecular charge transfer (ICT) state.[6] As a result, fluorescent emission with high efficiency quantum yield $\Phi_{fl} = 0.8$) occurs from the chromophore in its photobase form. In contrast, the chromophore of GFP, *p*-hydroxybenzylideneimidazolidinone (**HOBDI**, see *Figure*

4.1), shows markedly different behavior, in which the ground state is recovered within picoseconds with high quantum yield ($\Phi_{IC} > 0.999$).[7] Twisting between the phenolate and imidazolidinone moieties of **HOBDI** has been suggested as the underlying mechanism of this ultrafast internal conversion (IC) process.[8] Thus, understanding the microscopic mechanisms that underlie the dynamics and outcome of such photoinduced chemical reactions requires the determination of the molecular structure in the electronic excited state, which involves couplings with electronic ground and product states, thereby affecting the reaction quantum yield. The surrounding solvent may affect both the excited-state structure and the couplings with other states, often leading to pronounced solvent-induced changes in the reaction dynamics.

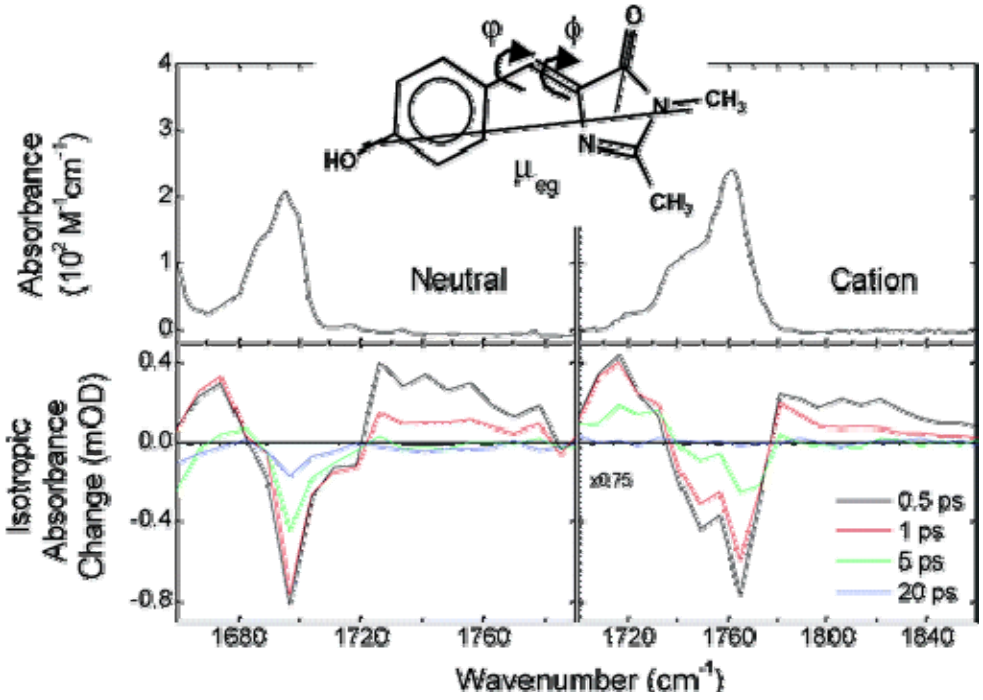

Figure 4.1. Steady-state and transient spectra showing the isotropic response of the C=O stretching bands in neutral and cationic **HOBDI** in CD_3OD. Inset shows the **HOBDI** chromophore with the direction of the electronic transition dipole moment, μ_{eg}, and the twisting angles, ϕ and φ.[1]

We now report on the ultrafast polarization-sensitive infrared (IR) spectroscopy[9] of the excited-state structure of **HOBDI**, from which we can draw conclusions on the importance of twisting motions. Our focus is on the orientation of the transition moment

of the IR-active carbonyl stretching vibration of **HOBDI** relative to that of the electronic transition dipole moment, which indicates that the C=O vibration acts as a "spectator mode" for the relative orientation of the phenolate and imidazolidinone groups, from which we derive an effective near-complete twisting around the ethylenic bridge upon electronic excitation of **HOBDI**. We include the anisotropy of the C=O vibration of **HOBDI** in the S_0 and S_1 states for three charged configurations (anionic, neutral, and cationic form) in the fully deuterated solvents CD_3OD and dimethyl sulfoxide-d_6 (DMSO-d_6).

Experimental

Sample Preparation

The **HOBDI** chromophore was synthesized according to the procedure reported before.[10] We prepared the **HOBDI** sample in perdeuterated methanol or perdeuterated dimethylsulfoxide (Deutero GmbH) solutions between two 1 mm thick BaF_2 plate-windows with a 50 μm teflon spacer. The concentration of **HOBDI** was adjusted to have an optical density in the range of 1.5 to 1.8 OD at the excitation wavelengths. The different ionic states of **HOBDI** were obtained by controlling the pH of the solution. Neutral, anionic and cationic forms were obtained in neutral (pH ~7), basic (pH ~12) and acidic (pH ~2) solutions, respectively. In the UV/vis–mid-IR pump-probe experiments, the sample cell was translated and rotated perpendicularly with respect to the pump and probe laser beams.

Ultrafast UV/vis–mid-IR pump-probe experiments

The UV/vis–mid-IR pump-probe experimental setup has been described in detail previously.[2] Here we present some modifications. We have performed experiments with electronic pump pulses tuned to 400 nm and 440 nm. The 400 nm visible pulses were produced by second-harmonic generation of the fundamental output of the Ti:sapphire

amplified laser system, whereas the 440 nm pulses were generated by sum frequency mixing of the fundamental laser output with the second harmonic of the idler (1000 nm) of an optical parametric amplifier, tuned to 2000 nm.[11] The pump pulse energy on the sample was in the range of 1-2 μJ and the pulse duration around 40 fs. The pump pulses could be variably delayed and were focused on the sample with a concave mirror with a beam diameter of approximately 500 μm.

The mid-infrared pulses were generated using double-pass collinear optical parametric amplification followed by difference frequency mixing of signal and idler.[12] The center frequency was tuned to 1550 cm^{-1} and the output energy was around 400 nJ. Probe and reference pulses were derived using reflections from a BaF_2 wedge, and focused in the sample with off-axis parabolic mirrors (focal diameter 100 mm). The whole pump – probe set-up was purged with nitrogen gas to avoid spectral and temporal reshaping of the MIR pulse by the absorption of water vapor and CO_2 in air.[2]

Probe and reference pulses were dispersed in a polychromator and complete spectra were recorded simultaneously for each shot using a liquid nitrogen cooled 2 × 31 HgCdTe detector array. Normalizing probe and reference signal on a single shot basis provides highly reliable spectra. The polychromator was not tuned during measurements to avoid the repositioning error (± 2 cm^{-1}). Synchronous chopping of the UV-pump pulses was used to eliminate long term drift effects. Experimental curves shown here represent an average of 100–200 delay time traces each taking 100 shots average per delay step.

Spectrally resolved absorbance changes in the mid-IR have been recorded with a spectral resolution of 2-7 cm^{-1} and a temporal resolution in the range of 190-280 fs. Polarization sensitive measurements were performed by rotating the polarization plane of the pump pulse by 90° with a broadband halfwave plate. Anisotropy free signals ΔA_{iso} were derived by $\Delta A_{iso} = (\Delta A_{//} + 2\Delta A_{\perp})/3$. Angles between the dipole moment vector of the electronic transition excited by the UV/vis pump pulse and infrared transition dipole

moments probed were calculated from the dichroic ratio $D = \Delta A_{//} / \Delta A_{\perp}$ and $\vartheta_{exp} = \text{acos}([(2D-1)/(D+2)]^{½})$.

Results and Discussion

Ultrafast UV/vis-mid-IR pump-probe experiments

Femtosecond polarization-sensitive mid-infrared spectroscopy monitors the anisotropy of vibrational transitions, from which e.g. the direction of small ligands bound to the heme iron in myoglobin or hemoglobin have been determined.[9,13,14] A direct correlation between the measured direction of the vibrational transition moment and a chemical bond vector can only be made when the nuclear motions of the vibrational mode are of local nature, otherwise one has to rely on comparison between experimental results and quantum chemical calculations.[14,15] In the case of **HOBDI**, fortunately, extensive studies of the IR and Raman spectra for different isotopomers have led to a definitive assignment of vibrational modes in the electronic ground state.[16,17] In the S_0 state the C=O stretching vibration is located between 1640 and 1750 cm^{-1}, depending on the charge state of **HOBDI** and on the solvent used.

Although polarization-sensitive probing may distinguish between vibrational bands in the S_1-state and red-shifted resonances in the "hot" S_0-state,[11] we have found this to be problematic in the fingerprint region due to the dense number of vibrational transitions (see *Figures. 4.2* and *4.3*). Fortunately, the vibrational bands for the C=O stretching mode in the S_0 and S_1-states are sufficiently isolated to analyse reliably the anisotropy properties. Since we were not able to identify for the anionic form of **HOBDI** a distinct C=O stretching band in the S_1-state, we have analyzed the 1200-1218 cm^{-1} spectral region for estimation of the lifetime of anionic **HOBDI** in CD_3OD, where the

positive signals can safely be assigned to S_1-state decay. Due to solubility limitations we were not able to detect the C=O stretching band of anionic **HOBDI** in DMSO-d_6.

The experimentally found frequency positions and angles for the C=O stretching bands in the S_0 and S_1 states are summarized in *Table 4.1*.

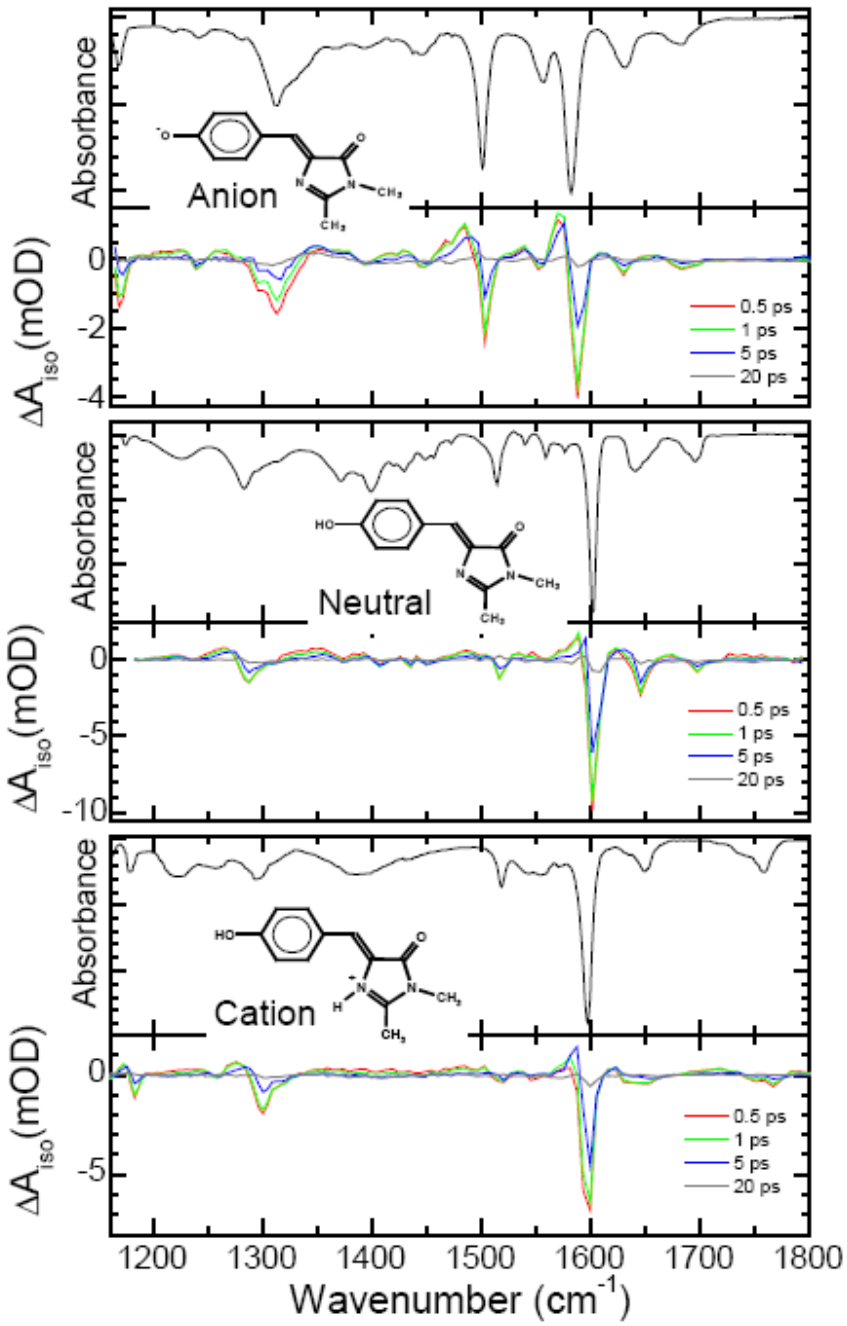

Figure 4.2. Steay-state (inverted scale) and transient spectra showing the isotropic response of the IR-active transtions in the fingerprint region in anionic, neutral and cationic **HOBDI** in CD_3OD. [1]

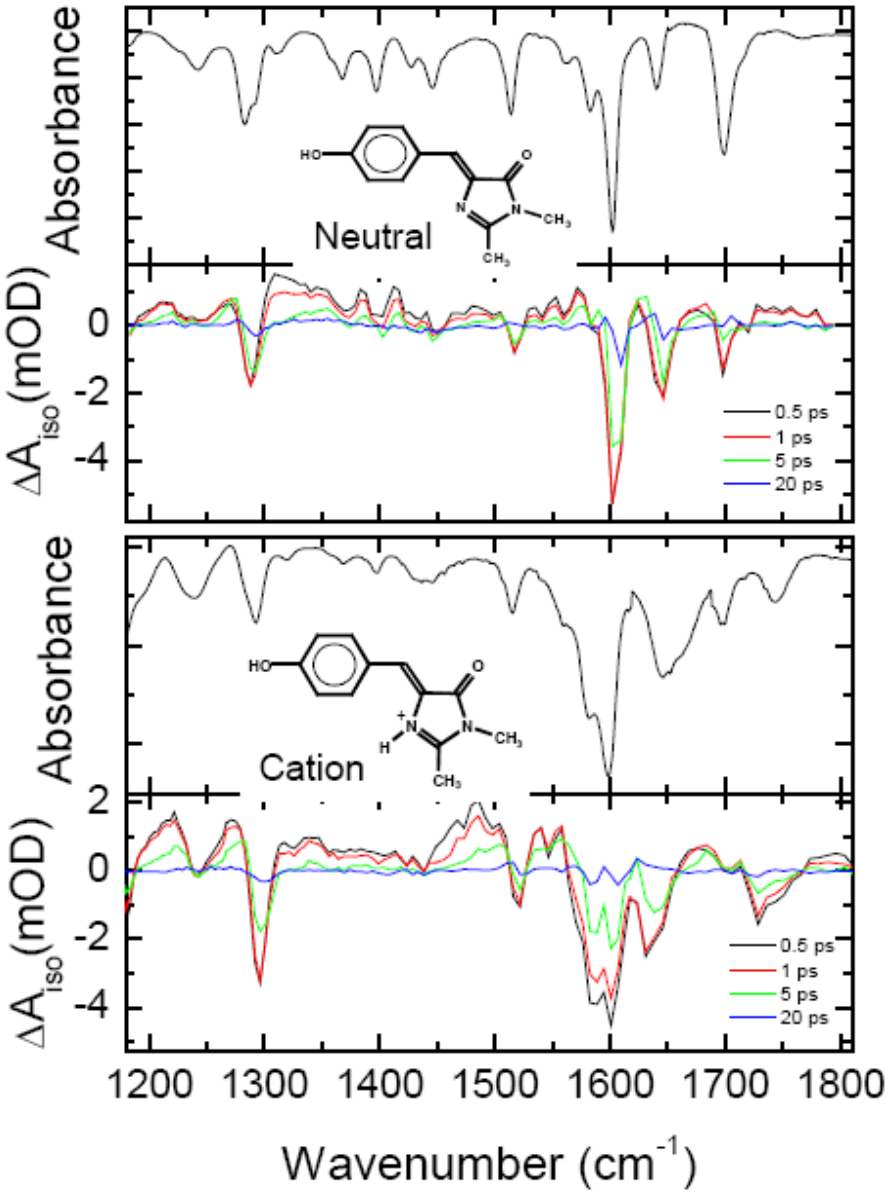

Figure 4.3. Steay-state (inverted scale) and transient spectra showing the isotropic response of the IR-active transtions in the fingerprint region in neutral and cationic **HOBDI** in DMSO-d_6. [1]

Charge State	Solvent	$\nu_{C=O}$ (cm^{-1}) S_0 state	ϑ_{exp} [a] (°) S_0 state	ϑ_{calc} [b] (°) S_0 state	$\Theta_{C=O}$ [c] (°) S_0 state	$\nu_{C=O}$ (cm^{-1}) S_1 state	ϑ_{exp} [d] (°) S_1 state
Anion	CD_3OD	1675-1697	75 (4)	59	73	not observed	not observed
	CD_3OD *	1684-1702	56(10)			not observed	not observed
Neutral	CD_3OD	1690-1704	68(3)	44	72	1733-1779	54(5)
	DMSO-d_6	1696-1706	66(3)			1736-1780	50(5)
Cation	CD_3OD	1740-1773	60(4)	41	74	1783-1840	49(5)
	DMSO-d_6	1721-1751	70(2)			1773-1811	56(8)

Excitation wavelength 400 nnm except *) 450 nm. [a,d]) Derived from the ground state bleach and exited state signals of the imidazoline carbonyl band, respectively. [b,c]) Calculated from the direction of the transition dipole moment of the vibrational modes: νC=O + νC=C + δ(=CH) + δCH(NCH_3) and the imidazolidinone C=O bond vector, respectively, using the B3LYP functional with respect to the direction of μ_{eg} of the $\pi \rightarrow \pi^*$ transition calculated using the TD-DFT method.

Table 4.1. Experimental and calculated values for frequency positions and orientations for the C=O stretching bands of **HOBDI**. [1]

Quantum chemical calculations

We performed density functional theory calculations of vibrational spectra for the **HOBDI** in the three charge states in the electronic ground state using the B3LYP/6-31+G(d,p) method as implemented in Gaussian98 [18]. The B3LYP optimised structures were used in the calculations of electronic transition dipole moments for vertically excited states using the time-dependent density functional theory (TD-DFT) method [19,20]. An active orbital space of 80 molecular orbitals (HOMO-40 to LUMO+40) was chosen. The dipole moment for the first strongly allowed $\pi \rightarrow \pi^*$ electronic transition (μ_{eg}), that is excited in the experiments, is found to be positioned on the chromophore molecular plane in the direction from the amino methyl group to the hydroxyl oxygen (*Figure 4.1*). The angles calculated between the electronic μ_{eg} and vibrational transition dipole moments for the carbonyl vibrational mode, represented as ϑ_{calc}, and those between the carbonyl C=O bond vector and μ_{eg}, represented as $\Theta_{C=O}$ are summarized in *Table 4.1*. Deviations between calculated ϑ_{calc} and experimental ϑ_{exp} values may be caused by site-specific

solvent interactions through hydrogen bonding with the phenolate and carbonyl moieties,[11] and need further investigation.

We visualized the single twist motion by a rotation angle ϕ and the hula twist motion by two concerted and simultaneous torsion angles ϕ and φ. The angles φ and ϕ define the twisting around the single bond next to the phenolic ring and around the double bond next to the imidazolinone ring, respectively (*Figure. 4.1*). For the single twist motion the position of the phenolate is unchanged, whereas for the hula twist motion the center of mass remains constant. In both motions, involving the imidazolinone ring, the C=O bond vector can be considered as "spectator mode". During the torsional motions, the angle $\Theta_{C=O}$ was calculated between the new coordinates of the C=O group and μ_{eg}. The acute angle of $\Theta_{C=O}$ is shown in *Figure. 4.4* as function of the torsion angle(s) φ (and ϕ).

Results and discussion

In *Figure 4.1*, we show the transient difference absorbance response of **HOBDI** in the spectral region of the C=O stretching vibration in CD_3OD. The anisotropy free response, ΔA_{iso} (as defined by $\Delta A_{iso} = [\Delta A_{//} + 2\Delta A_{\perp}]/3$) shows an absorbance decrease (bleach signals) corresponding to transitions of IR-active vibrations in the S_0 state, while an absorbance increase indicates vibrational bands of **HOBDI** in the S_1 state at early pulse delays and red-shifted vibrational transitions in the S_0 state with high internal vibrational excess energy ("hot" ground state). The red-shifts are caused by anharmonic coupling between highly excited, presumably low-frequency, modes and the IR-active fingerprint vibrations probed in the experiment.[21,22] The decay of the C=O band in the S_1 state is equal to the population decay time. In contrast, the bleach decay associated with the C=O stretching vibration in the S_0 state is determined by both the $S_1 \rightarrow S_0$ IC rate and the subsequent cooling process when the excess internal vibrational energy is dissipated

to the solvent. As a result, we observe a faster excited-state C=O stretching band decay than

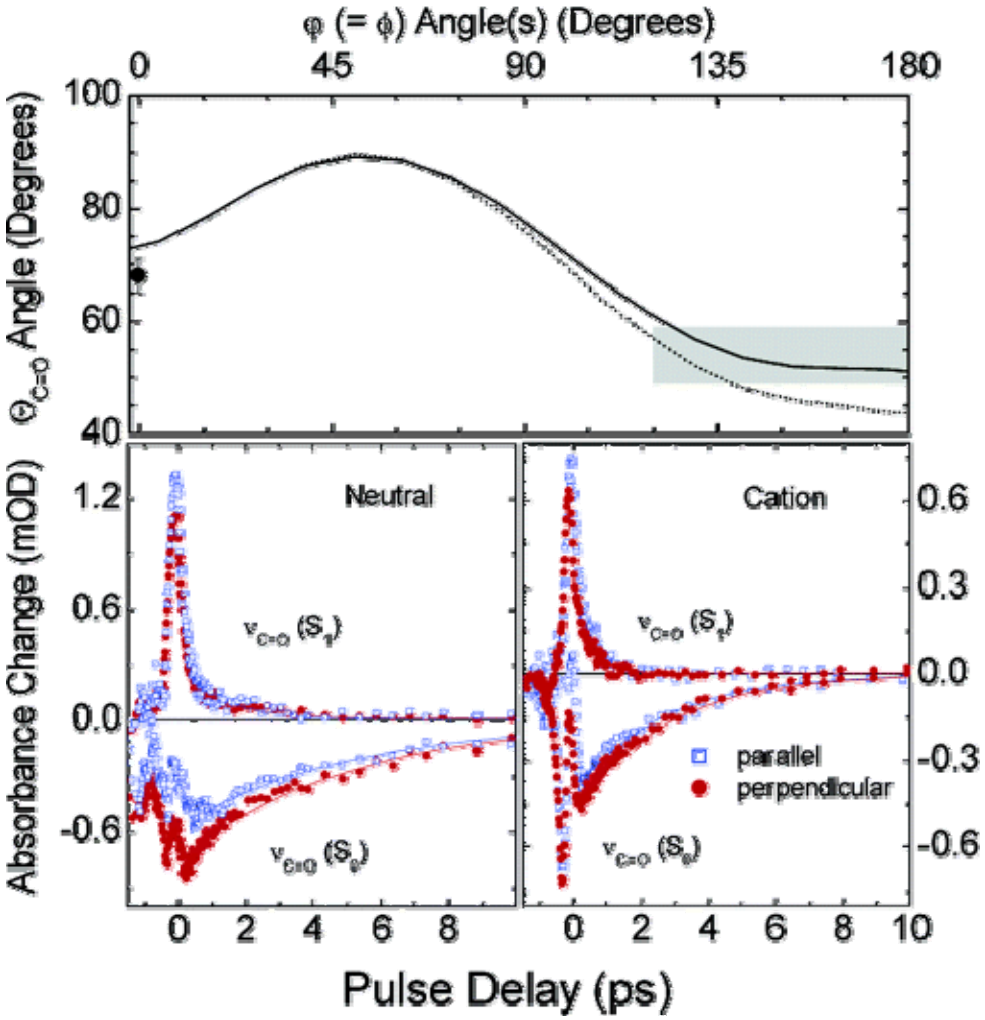

Figure 4.4. Transient polarization-sensitive response of the C=O stretching bands in the S_0 and S_1 states for the neutral and cationic species of **HOBDI** in CD_3OD. Top panel shows the direction of the C=O bond vector, $\vartheta_{C=O}$, with respect to the electronic transition dipole moment, μ_{eg}, as function of the twisting angle for single twist (dashed line) and hula twist (solid line). The observed value for $\vartheta_{C=O}$ in ground-state **HOBDI**, with $\varphi = 0$, is shown as a dot, whereas the gray bar indicates the possible configuration space for $\vartheta_{C=O}$ in the excited state.[1]

a ground-state C=O stretching bleach recovery. *Figure 4.4* shows the decay S_0 state bleach and the S_1 state absorption signals of the C=O stretching mode for parallel and perpendicular polarizations for the neutral and cationic forms of **HOBDI** in CD_3OD.

These measurements provide the anisotropy, $D = \Delta A_{//}/\Delta A_{\perp}$, from which the direction of the C=O stretching transition dipole moment can be derived. In *Table 4.1*, we summarize our findings for the C=O stretching mode.

For the S_0 state, we observe an increase in C=O stretching frequency going from anionic, via neutral, to cationic **HOBDI** in CD_3OD and DMSO-d_6, in accordance with the literature,[17] reflecting an increase in C=O bond strength. Differences in electronic charge distributions are considered to be the cause of this,[17] but also, changes in hydrogen bonding interactions between the C=O and -OH/-O^- groups with the solvent may play a role. Surprisingly, upon electronic excitation, the C=O stretching mode increases its frequency even further with 50 cm^{-1} for the neutral and cationic forms, which belies the presumed intramolecular charge-transfer nature of the excited state. We observe a rather broad band (width of 40-50 cm^{-1}) for the excited-state C=O stretching transition, hinting at significant inhomogeneous broadening. We were not able to identify for the anionic form of **HOBDI** a distinct C=O stretching band in the S_1 state, which may imply much lower cross-sections, or more likely a frequency downshift by significant mixing with aromatic ring vibrations, resulting from mesomeric delocalization of the negative charge on the excited molecule.

Observation of the decay rates of the C=O stretching bands in both S_0 and S_1 states allows for an unequivocal determination of the IC and vibrational cooling rates in one experiment. *Table 4.1* shows the results for **HOBDI** in the different charged states. For neutral and anionic **HOBDI**, we find an IC rate of $(1.2 \pm 0.2\ ps)^{-1}$. Even faster IC rates have been found for cationic **HOBDI** $(0.6 \pm 0.2\ ps)^{-1}$. Similar values have been found with ultrafast fluorescence up-conversion [23] and electronic pump-dump-probe [24] spectroscopy, where, however, the signals are also affected by solvation dynamics. Conversely, the bleach recovery signals of the C=O stretching band are dominated by the slower vibrational cooling rate of about $(6\ ps)^{-1}$ to $(5\ ps)^{-1}$.

From our anisotropy measurements, we derive the angle between the electronic and vibrational transition dipole moments (see *Table 4.1*) to be around 70 in the S_0 state for all charged forms of **HOBDI**. For neutral and cationic **HOBDI** in the S_1 state, we find a lower value of around 52. Comparison with the angle between the electronic transition dipole moment and the C=O bond vector shows perfect correspondence for the hypothesis that the C=O stretching vibration should be considered as a local mode without substantial mixing of other nuclear motional degrees of freedom, even though the chromophores have been calculated to be of planar geometries. On the basis of the fact that the C=O stretching exhibits a frequency up-shift upon electronic excitation, we feel confident that this hypothesis is even more valid in the S_1 state. Thus, using the explicit assumption of the C=O stretching transition moment coinciding with the C=O bond vector, we conclude that a significant reorientation of the C=O group occurs upon the S_0 S_1 excitation, and we further conclude that the ICT state involves little charge migration to the C=O bond.

A structural change in **HOBDI** is likely to proceed by cis/trans isomerization by a single twist or a hula twist[25] of the ethylenic bond. We have considered the orientational changes of the C=O bond vector caused by single and hula twisting motions of the chromophore affecting the relative positions of the phenolate and imidazolidinone moieties (see *Figure 4.4*). We find that our estimated value for the C=O bond vector in the S_1 state can only be explained by a single twist of 120 ± 10 or a hula twist of 150 ± 30. These values are much larger than the twisting angle of 90 found in quantum chemical calculations,[8,26] from which conical intersections at this twisting angle have been assigned as the efficient IC channel. Although, according to our findings, the equilibrium structure of **HOBDI** in the S_1 state is even more displaced along the twisting coordinate upon electronic excitation than in the reported calculations, we conclude that this large displacement [21] makes the twisting coordinate a likely candidate for the efficient coupling between S_1 and S_0, leading to IC. The >90 twist also suggests the

intervention of the *E*-isomer in the photochemistry of *Z*-**HOBDI**, an isomerization reported by Tonge.[27] We note, however, that the rapid reisomerization to the *Z*-isomer even in the ground state suggests that the potential energy curve provides a strong restoring force. A highly twisted species together with the short excited-state lifetime suggests the involvement of an intersection in the deactivation of the S_1 state. Whether additional degrees of freedom play a decisive role in the IC process and other aspects of the photophysics[26,28,29] remains the subject of further studies.

Conclusions

Ultrafast polarization-sensitive infrared (IR) spectroscopy of the C=O stretching mode of the chromophore of the green fluorescent protein reveals a near complete twisting around the ethylenic bridge between the phenolate and imidazolidinone groups upon electronic excitation, hinting at a decisive role of this motion in the efficient internal conversion process.

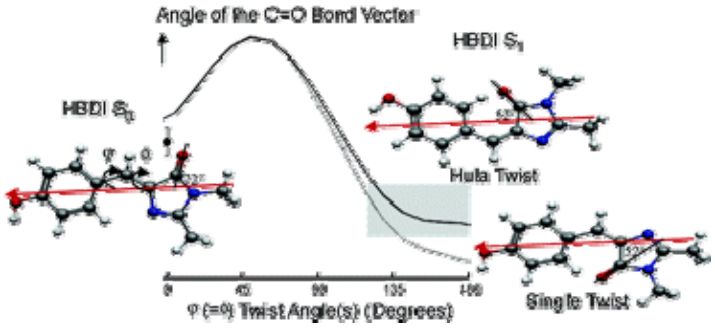

Figure 4.5 Table of contents for *Chapter 4*.

References

[1] Usman, A.; Mohammed, O. F.; Nibbering, E. T. J.; Dong, J.; Solntsev, K. M.; Tolbert, L. M. *J. Am. Chem. Soc.* **2005**, *127*, 11214-11215.

[2] Rini, M.; Kummrow, A.; Dreyer, J.; Nibbering, E. T. J.; Elsaesser, T. Faraday Discuss. **2003**, 122, 27-40.

[3] Tsien, R. Y. *Annu. Rev. Biochem.* **1998**, *67*, 509-544.

[4] Zimmer, M. *Chem. Rev.* **2002**, *102*, 759-781.

[5] Stoner-Ma, D.; Jaye, A. A.; Matousek, P.; Towrie, M.; Meech, S. R.; Tonge, P. J. *J. Am. Chem. Soc.* **2005**, *127*, 2864-2865.

[6] Grabowski, Z. R.; Rotkiewicz, K.; Rettig, W. *Chem. Rev.* **2003**, *103*, 3899-4031.

[7] Webber, N. M.; Litvinenko, K. L.; Meech, S. R. *J. Phys. Chem. B* **2001**, *105*, 8036-8039.

[8] Weber, W.; Helms, V.; McCammon, J. A.; Langhoff, P. W. *Proc. Natl. Acad. Sci. U.S.A.* **1999**, *96*, 6177-6182.

[9] Lim, M.; Jackson, T. A.; Anfinrud, P. A. *Science* **1995**, *269*, 962-966.

[10] Kojima, S.; Ohkawa, H.; Hirano, T.; Maki, S.; Niwa, H.; Ohashi, M.; Inouye, S.; Tsuji, F. I. *Tetrahedron Lett.* **1998**, *39*, 5239-5242.

[11] Usman, A.; Mohammed, O. F.; Heyne, K.; Dreyer, J.; Nibbering, E. T. J. Chem. Phys. Lett. **2005**, *401*, 157-163.

[12] Hamm, P.; Kaindl, R. A.; Stenger, J. *Opt. Lett.*, **2000**, *25*, 1798.

[13] Lim, M.; Jackson, T. A.; Anfinrud, P. A. J. Am. Chem. Soc. **2004**, 126, 7946-7957.

[14] Zemojtel, T.; Rini, M.; Heyne, K.; Dandekar, T.; Nibbering, E. T. J.; Kozlowski, P. M. J. Am. Chem. Soc. **2004**, 126, 1930-1931.

[15] Spiro, T. G.; Kozlowski, P. M. *J. Am. Chem. Soc.* **1998**, *120*, 4524-4525.

[16] Schellenberg, P.; Johnson, E.; Esposito, A. P.; Reid, P. J.; Parson, W. W. *J. Phys. Chem. B* **2001**, *105*, 5316-5322.

[17] He, X.; Bell, A. F.; Tonge, P. J. *J. Phys. Chem. B* **2002**, *106*, 6056-6066.

[18] Frisch, M. J.; Trucks, G. W.; Schlegel, H. B.; Scuseria, G. E.; Robb, M. A.; Cheeseman, J. R.; Zakrzewski, V. G.; Montgomery, J. A.; Stratmann, R. E.; Burant, J. C.; Dapprich, S.; Millam, J. M.; Daniels, A. D.; Kudin, K. N.; Strain, M. C.; Farkas, O.; Tomasi, J.; Barone, V.; Cossi, M.; Cammi, R.; Mennucci, B.; Pomelli, C.; Adamo, C.; Clifford, S.; Ochterski, J.; Petersson, G. A.; Ayala, P. Y.; Cui, Q.; Morokuma, K.; Malick, D. K.; Rabuck, A. D.; Raghavachari, K.; Foresman, J. B.; Cioslowski, J.; Ortiz, J. V.; Stefanov, B. B.; Liu, G.; Liashenko, A.; Piskorz, P.; Komaromi, I.; Gomperts, R.; Martin, R. L.; Fox, D. J.; Keith, T.; Al-Laham, M. A.; Peng, C. Y.; Nanayakkara, A.; Gonzalez, C.; Challacombe, M.; Gill, P. M. W.; G. Johnson, B.; Chen, W.; Wong, M. W.; Andres, J. L.; Head-Gordon, M.; Replogle, E. S.; Pople, J. A. Gaussian 98 (Revision A.2); Gaussian, Inc.: Pittsburgh PA., 1998.

[19] Marques, M. A. L.; Gross, E. K. U. Annu. Rev. Phys. Chem. **2004**, 55, 427-455.

[20]Stratmann, R. E.; Scuseria, G. E.; Frisch, M. J. J. Chem. Phys. **1998**, 109, 8218-8224.

[21] Fidder, H.; Rini, M.; Nibbering, E. T. J. *J. Am. Chem. Soc.* **2004**, *126*, 3789-3794.

[22] Nibbering, E. T. J.; Fidder, H.; Pines, E. *Annu. Rev. Phys. Chem.* **2005**, *56*, 337-367.

[23] Mandal, D.; Tahara, T.; Meech, S. R. *J. Phys. Chem. B* **2004**, *108*, 1102-1108.

[24] Vengris, M.; van Stokkum, I. H. M.; He, X.; Bell, A. F.; Tonge, P. J.; van Grondelle, R.; Larsen, D. S. *J. Phys. Chem. A* **2004**, *108*, 4587-4598.

[25] Liu, R. S. H.; Hammond, G. S. *Proc. Natl. Acad. Sci. U.S.A.* **2000**, *97*, 11153-11158.

[26] Toniolo, A.; Olsen, S.; Manohar, L.; Martinez, T. J. *Faraday Discuss.* **2004**, *127*, 149-163.

[27] He, X.; Bell, A. F.; Tonge, P. J. *FEBS Lett.* **2003**, *549*, 35-38.

[28] Vendrell, O.; Gelabert, R.; Moreno, M.; Lluch, J. M. *Chem. Phys. Lett.* **2004**, *396*, 202-207.

[29] Altoe, P.; Bernardi, F.; Garavelli, M.; Orlandi, G.; Negri, F. *J. Am. Chem. Soc.* **2005**, *127*, 3952-3963.

CHAPTER 5

A SURPRISING MECHANISM OF THERMAL ISOMERIZATION IN FLUORESCENT PROTEIN CHROMOPHORE

Introduction

Fluorescent proteins related to the green fluorescent protein (GFP) are thought to undergo *E/Z* photoisomerization between dark and fluorescent states. The *Z* form ("cis") is the resting fluorescent form, while the *E* ("trans") form is non-fluorescent.

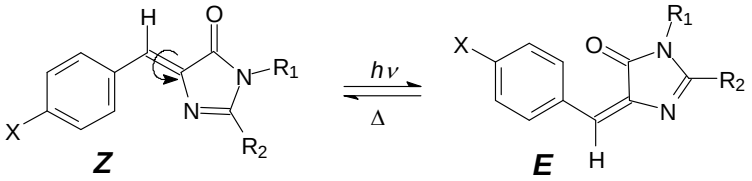

Figure 5.1. Isomerization in the GFP chromophores.

Such proteins are also characterized by "blinking", that is, temporary conversion to a non-fluorescent form, which has been variously attributed to triplet formation,[1] proton transfer,[2] or the aforementioned cis/trans isomerization. Strong support for cis/trans isomerization is provided by the behavior of kindling fluorescent proteins,[3] in which the resting non-fluorescent form has trans stereochemistry. Upon irradiation into the long-wavelength band, the protein is "kindled" to the fluorescent form. That kindling is the result of photoisomerization is given strong support by recent single crystal x-ray determinations of both forms of two kindling proteins, *dronpa* and *mTFP0.7*, which differ in the stereochemistry about the benzylidene bond of the chromophores.[4] A key unresolved issue in the photophysics of the fluorescent proteins is whether the cis/trans isomerization is related to the blinking phenomenon, which, in addition to isomerization, has been ascribed to protonation and triplet formation mentioned earlier. We have

observed that, in solution, the GFP chromophore undergoes a fast relaxation to yield a resting state which shows considerable twisting[5] at the same time that the excited-state is quenched.[6] In the protein, however, the common view is that the protein prohibits twisting about the double bond. Nonetheless, both calculations[7] and the aforementioned kindling behavior require that, in at least some instances, formal isomerization, i.e., decay from the twisted intermediate onto the *trans* hypersurface, must be permitted. Moreover, the quite wide variation in blinking behavior as a function of protein structure—conditions which either facilitate or inhibit such isomerization—suggest that blinking and isomerization are intimately involved.

While the mechanism of photoisomerization has been the subject of several studies[8] and corresponds in unexceptional ways to the mechanisms of other arylidene chromophores, the mechanism of the thermal reverse isomerization is more problematic. The blinking phenomenon requires that isomerization, if involved, be thermally reversible. Tonge has recently measured the rates of thermal isomerization of the representative protein chromophore hydroxybenzylidenedimethylimidazo-lidinone (**HOBDI**, X=OH) and obtained a barrier of 13.1 kcal/mol for the isomerization from an Arrhenius plot.[9] For the reverse isomerization of the disfavored *trans* form, this barrier should be lower, allowing it to compete effectively on a kinetic timescale. Surprisingly, a high level ab initio calculation from Langhoff, et al, produces a barrier of 57 kcal/mol.[10] The latter value is more typical of double-bond isomerization barriers for unexceptional benzylidene molecules such as **HOBDI** and poses a conundrum: how does one resolve the discrepancies between two highly credible determinations?

Experimental

General Experimental

Benzaldehyde (99%), p-tolualdehyde (97%), 4-chlorobenzaldehyde (98.5%) and *N*-acetylglycine (99%) were purchased from Acros. Sodium acetate (99.7%) and potassium carbonate (99.94%) were purchased from Fisher. Methylamine (33% wt. solution in abs. ethanol) were purchased from Aldrich. The progression of reactions was monitored by thin-layer-chromatography using Analtech UNIPLATE TLC plates (Silica Gel GF) with visualization by illumination with ultraviolet light. NMR spectra were recorder on a Varian Mercury spectrometer (300 MHz). Mass spectral analysis was provided by the Georgia Tech Mass Spectrometry facility. Elemental analyses were conducted at Atlantic Microlab. Ultraviolet-visible (UV-Vis) spectra were obtained on a Perkin Elmer Lambda19 spectrophotometer.

Synthesis

The synthesis procedure of the oxazolone compounds was very similar to the previous report.[11] benzaldehyde or its derivative (5.0 g), *N*-acetylglycine (4.6 g), sodium acetate (2.8 g), and acetic anhydride (12 mL) were mixed and heated at 80 °C with stirring for 4 h. Heated ethanol was added slowly and the mixture was allowed to stand at room temperature for 4 h. The separated crystalline solid was filtered, washed with ice-cold alcohol, then with hot water to obtain the oxazalone. The yields for these compounds are over 80%.

4-Benzylindene-2-methyloxazalone: m.p.142-143 ^{o}C. ^{1}H NMR spectrum ($CDCl_3$), δ, ppm: 2.41 (s, 3H, CH_3); 7.15 (s, 1H, H on bridging carbon); 7.44 (m, 3H, Ar-H); 8.08 (d, 2H, Ar-H).

4-(4-Methylbenzylindene)-2-methyleoxazolone: m.p.126-128 ^{o}C. ^{1}H NMR spectrum ($CDCl_3$), δ, ppm: 2.40 (s, 6H, CH_3); 7.13 (s, 1H, H on bridging carbon); 7.26 (d, 2H, Ar-H); 7.98 (d, 2H, Ar-H).

4-(4-Chlorobenzylindene)-2-methyloxazolone: m.p.:139-140 ^{o}C. ^{1}H NMR spectrum ($CDCl_3$), δ, ppm: 2.41 (s, 3H, CH_3); 7.15 (s, 1H, H on bridging carbon); 7.44 (d, 2H, Ar-H); 8.08 (d, 2H, Ar-H).

The procedure to synthesize the 4-(4-hydroxybenzylindene)-1,2-dimethylimidazolinone (**HOBDI**) and 4-(4-methoxybenzylindene)-1,2-dimethyl-imidazolinone (**MeOBDI**) was reported as well.[11] The same procedure was applied to synthesize the remaining imidazolidinone compounds. 2.0 g Oxazolone or its derivative was added 2.1 g potassium carbonate in a round-bottom flask to which 0.96 mL

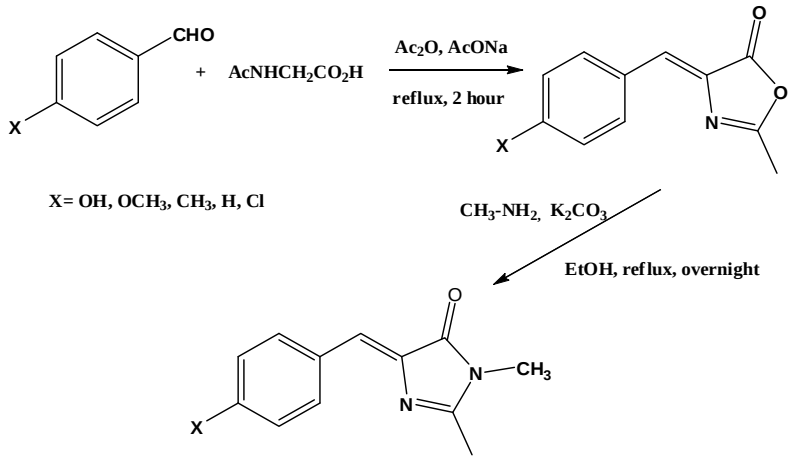

Figure 5.2 Synthsis of X**BDI** derivatives.

methylamine (33% wt. solution in abs. ethanol) and 5-10 mL of ethanol were then added. The reaction mixture was heated at reflux overnight. After cooling, the mixture was neutralized with 10% HCl, and kept at 0ºC for a further 4 h. The resulting solid was either filtered or extracted with hexane, purified by silica gel column to obtain imidazolinone. The yield for **MeOBDI** was 65 %, however, the yields for **HOBDI** and **ClBDI** were only 20% or less.

An alternate procedure was employed to synthesize **HOBDI** and **ClBDI.** Methyl 2-(1-ethoxyethylidene) aminoethanoate was prepared according to Bazureau's report,[12] in 65 % yield. *N*-methyl-benzylideneimine was obtained by mixing 5.0 g benzaldehyde and 4.6 mL methylamine (33% wt. solution in absolute ethanol) for 4 hours. The resulting

imidate (1.0 g) and *N*-methylbenzylideneamine (1.0 g) were mixed and heated at 70 ºC during 6-8 hours with magnetic stirring. After removal of solvent in *vacuo*, gravity column chromatography on silica gel provided the imidazolinone, after elution with chloroform/acetone (15:1), in 70-80% yield, as a yellow solid.

4-Benzylindene-1,2-dimethylimidazolinone (**HOBDI**) m.p. 102-104 ^{o}C. ^{1}H NMR spectrum (CD_3CN), δ, ppm: 2.34 (s, 3H, CH_3); 3.12 (s, 3H, N-CH_3); 6.96 (s, 1H, H on bridging carbon); 7.44 (d, 2H, Ar-H); 8.21 (d, 2H, Ar-H). EI-MS M+ calculated for [$C_{12}H_{12}N_2O$] = 200.23, found = 200.1.

4-(4-Methylbenzylindene-1,2-dimethylimidazolinone (**MeBDI**) m.p. 141-143 ^{o}C. ^{1}H NMR spectrum (CD_3CN), δ, ppm: 2.33 (s, 3H, CH_3); 2.39 (s, 3H, CH_3-Ar), 3.11 (s, 3H, N-CH_3); 6.94 (s, 1H, H on bridging carbon); 7.30 (d, 2H, Ar-H); 8.09 (d, 2H, Ar-H). Molecular weight: EI-MS M+ calculated for [$C_{13}H_{14}N_2O$] = 214.26, found = 214.2

4-(4-Chlorobenzylindene-1,2-dimethylimidazolinone (**ClBDI**) m.p. 154-155 ^{o}C. ^{1}H NMR spectrum (CDCl3), δ, ppm: 2.37 (s, 3H, CH_3); 3.17 (s, 3H, N-CH_3); 7.02 (s, 1H, H on bridging carbon); 7.37 (d, 2H, Ar-H); 8.06 (d, 2H, Ar-H). Molecular weight: EI-MS M+ calculated for [$C_{12}H_{11}N_2OCl$] = 234.68, found = 234.6.

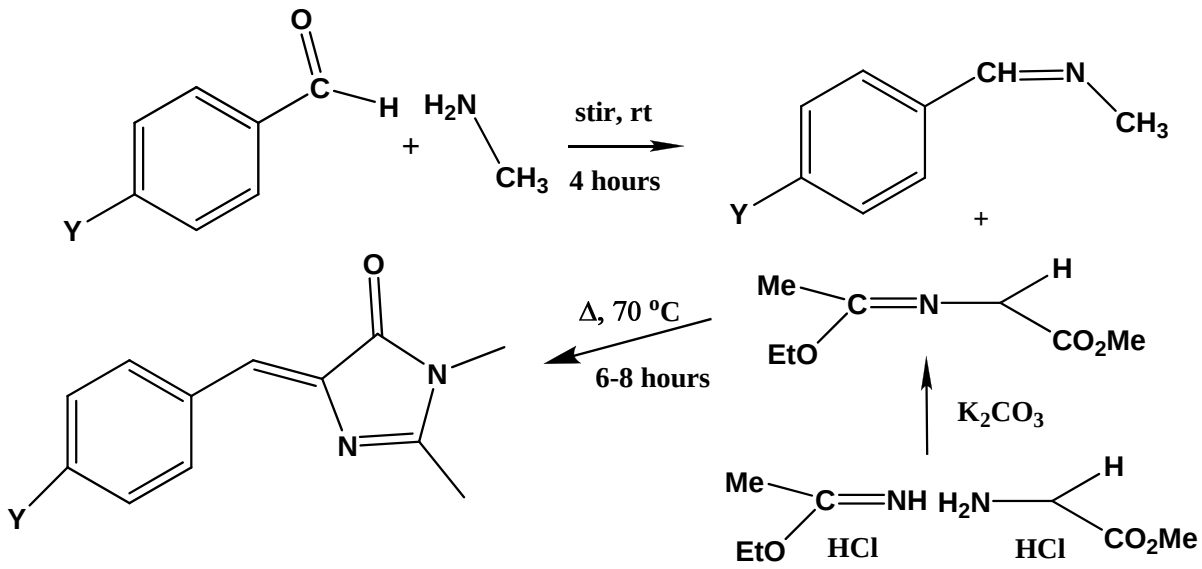

Figure 5.3 Synthsis of X(Y)**BDI** derivatives. (Y=H, Cl).

Irradiations

These **BDI** derivative samples were irradiated with Pyrex-filtered light. ($\lambda > 300$ nm) from a. 450 W Hanovia medium-pressure Hg lamp at room temperature. Their before and after irradiation nmr spectra (CD_3CN) are as followed (*Figure 5.4*).

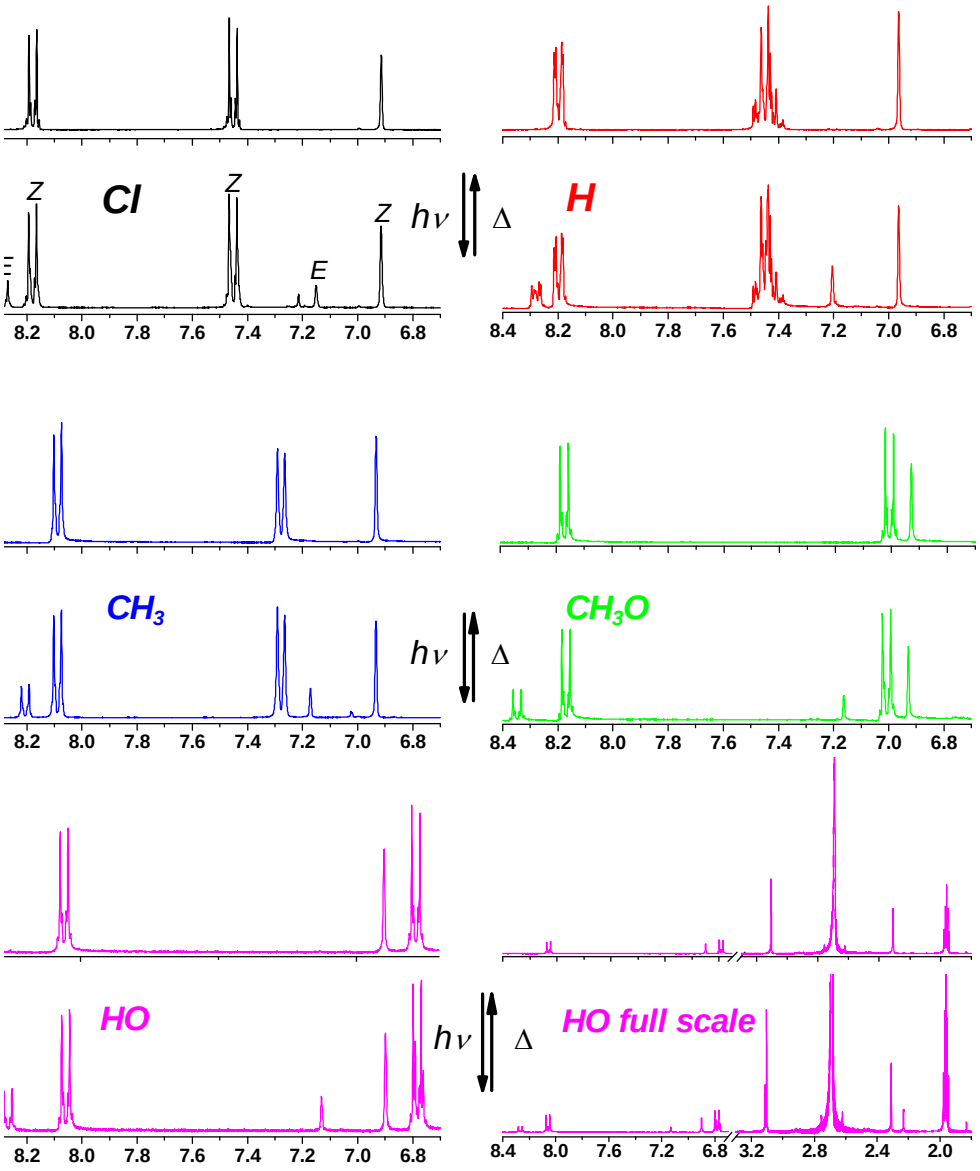

Figure 5.4. ^{1}H NMR spectra of **XBDI** derivatives in CD_3CN in the presence of 0.089 M DABCO before (upper color panels) and after (bottom color panels) irradiation for 3 hrs with >300 nm light of 450 W medium pressure Hg lamp.

Kinetic Analyses

The corresponding **BDI** derivatives and 1,4-diaza[2.2.2]bicyclooctane (DABCO) were dissolved in Acetonitrille-d_3 into a NMR tube. These samples were irradiated at room temperature using a 450 W medium pressure Hg lamp for 3 hours in a Pyrex tube with 300 nm cut off filter. About 25-35% *trans* isomers were achieved in 3 hours. The resulting solutions were kept in dark at a constant temperature, and the percentages of the isomers were recorded every hour.

Results and Discussion

In order to develop further insight into this process, and to exclude possible proton-transfer processes in the isomerizations, we first examined the methyl ether of **HOBDI**, **MeOBDI**. In the process of exploring the optimal solvents for our physical studies, we encountered a suprise. That is, in benzene and acetonitrile, no thermal isomerization occurred, but isomerization was readily observed in methanol and dimethyl sulfoxide. Indeed, we were able to isolate the *trans* isomer of **MeOBDI** by silica gel chromatography and record its nmr, ir, and electronic absorption spectra (see *Figures. 5.4,*

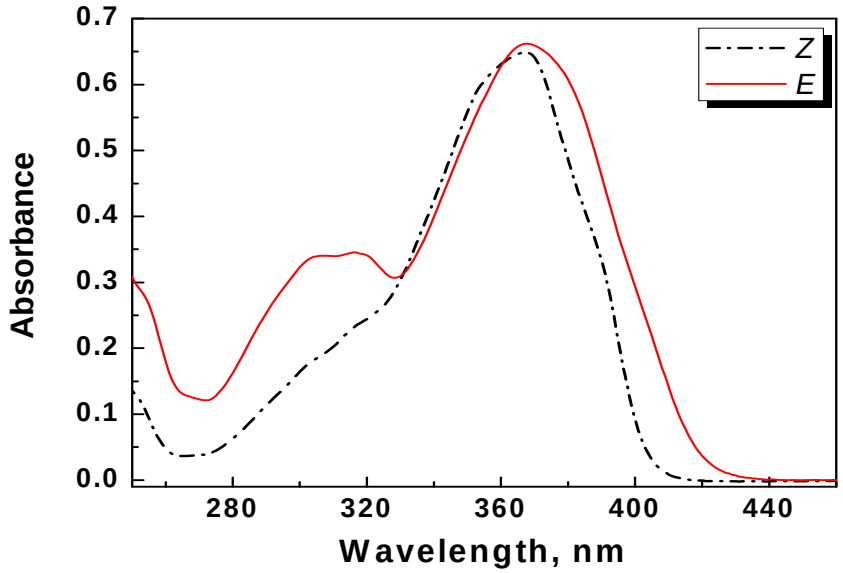

Figure 5.5 Absorption spectra of *E*- and *Z*- isomers of *p*-**MeOBDI** in MeCN.

5.5, and *5.6*). Again, this result is inconsistent with a facile thermal isomerization, and suggests that a more complex process is intervening.

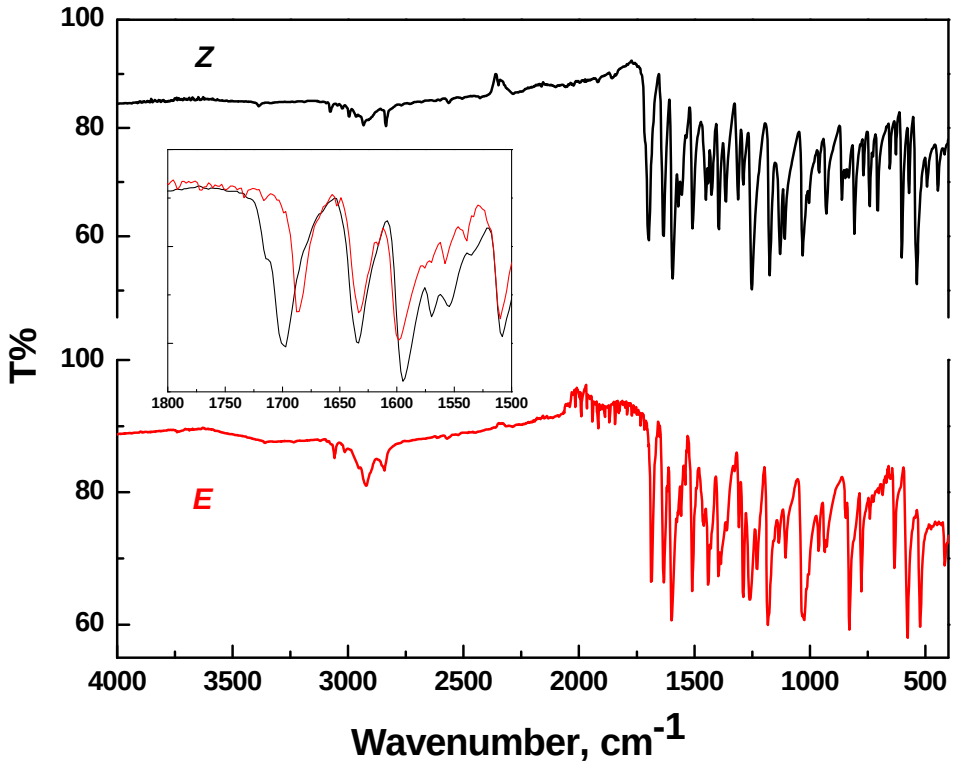

Figure 5.6 IR spectra of *Z* and *E*-**MeOBDI** isomers.

These waters were further muddied by a recent claim[13] that an analogous 4-methylbenzylidene derivative does not isomerize under similar conditions, which was rationalized as the result of a strong "push-pull" transition structure (see Path a in *Figure 5.7*) in which a donating group such as hydroxyl weakens the double bond character. However, such a structure belies the strong electron donation effect of the methyl group, which would be inconsistent with a difference in rates of 3 or more orders of magnitude.

In order to resolve this conundrum, we embarked on the synthesis and rate study of the effect of substituents on the thermal isomerization of *cis*-**XBDI**, using substituents which are either donors or acceptors. We reasoned that use of a classical Hammett plot

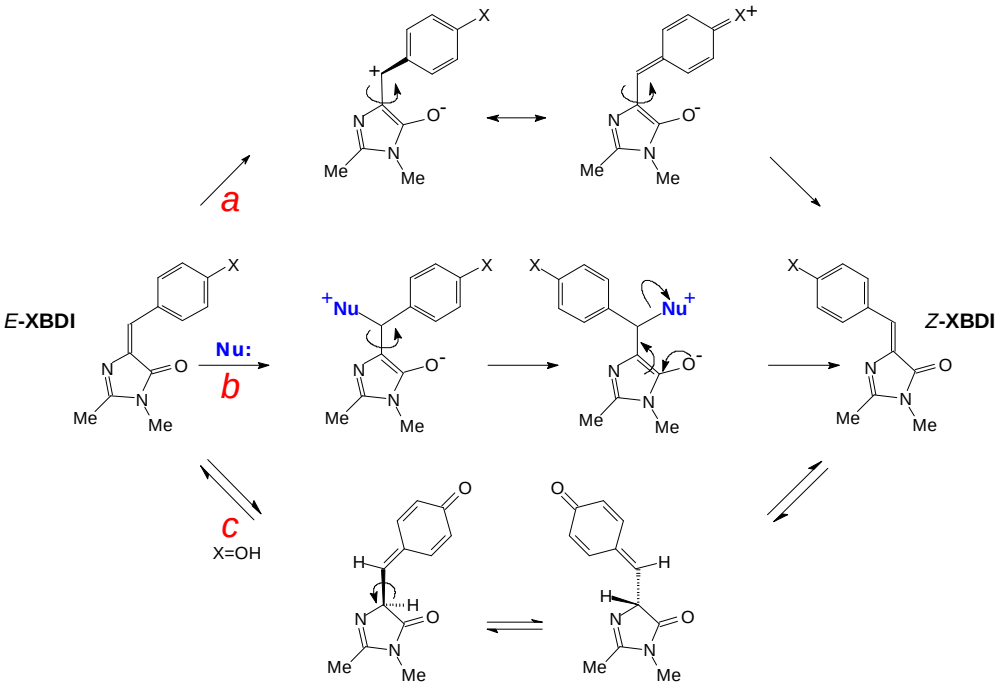

Figure 5.7. Pathways for the ground-state *E*-**XBDI** isomerization. (a) Direct (traditional); (b) Addition/elimination mechanism; (c) Isomerization by tautomerization.

would reveal the nature of the isomerization and confirm or disprove the proposed mechanism. Thus we used or synthesized **BDI** derivatives with decreasing para-donating ability, HO, CH_3O, CH_3, H, and Cl, with the expectation that a Hammett plot would produce a negative ρ value if the "push-pull" zwitterionic nature of the transition state dominates as in Path a in *Figure 5.7*.

In the process we discovered that the reported[13a] CH_3 derivative does not have the assigned structure, an observation we confirmed by single-crystal x-ray diffraction. The nmr of the reported derivative is characterized by a downfield doublet at 7.45 ppm, while every **BDI** derivative we have made has a doublet at 8.0-8.2 ppm for the alpha aryl proton. Since this product was obtained in 15% yield, we conclude that this was a byproduct of the reaction. (*See Figure 5.4*, molecular structure of its derivative as shown in *Figure 5.8* and *Table 5.1*).

In our hands, all five isomers underwent ready photoisomerization in a variety of solvents, including MeOH or DMSO, allowing us to study the thermal reversion by proton nmr spectroscopy (see *Figure 5.4*). In addition, all photoisomers, including **MeBDI**, underwent the reverse reaction at a convenient rate. (See *Figure 5.9*) Ignoring the points for **HOBDI** (see below), the plot of $\log(k_X/k_H)$ gave a positive correlation with σ, with the best results obtained in acetonitrile (see *Figure 5.10* and *Table 5.2* below), a result inconsistent with Falk's mechanistic analysis.

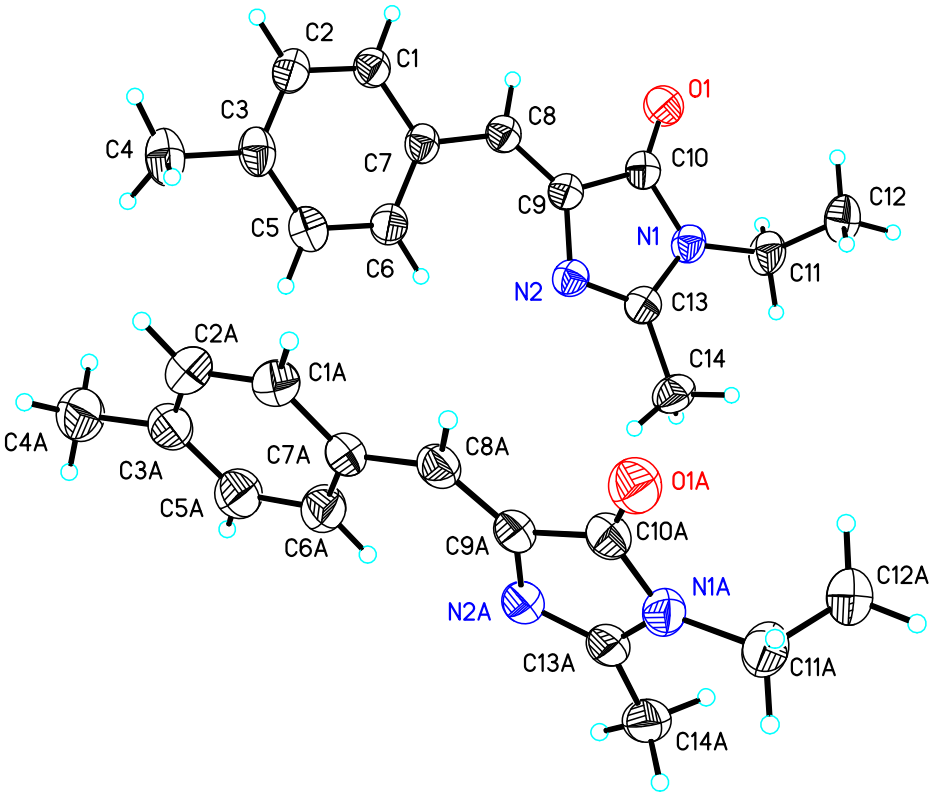

Figure 5.8 Molecular structure of MeBDI derivative 3-Ethyl-2-methyl-5-[1-p-tolyl-meth-(Z)-ylidene]-3,5-dihydro-imidazol-4-one.

Table 5.1 Crystal data and structure refinement for 3-Ethyl-2-methyl-5-[1-p-tolyl-meth-(Z)-ylidene]-3,5-dihydro-imidazol-4-one.

Identification code	AB1	
Empirical formula	C14 H16 N2 O	
Formula weight	228.29	
Temperature	173(2) K	
Wavelength	1.54178 Å	
Crystal system	Triclinic	
Space group	P-1	
Unit cell dimensions	a = 7.4341(5) Å	α= 106.146(5)°.
	b = 11.6805(9) Å	β= 95.634(4)°.
	c = 15.2385(11) Å	γ = 92.276(4)°.
Volume	1261.77(16) $Å^3$	
Z	4	
Density (calculated)	1.202 Mg/m^3	
Absorption coefficient	0.608 mm^{-1}	
F(000)	488	
Crystal size	0.25 x 0.15 x 0.12 mm^3	
Theta range for data collection	3.04 to 66.07°.	
Index ranges	-8<=h<=8, -13<=k<=13, -17<=l<=17	
Reflections collected	8205	
Independent reflections	3817 [R(int) = 0.0149]	
Completeness to theta = 66.07°	86.8 %	
Absorption correction	Semi-empirical from equivalents	
Max. and min. transmission	0.9306 and 0.8628	
Refinement method	Full-matrix least-squares on F^2	
Data / restraints / parameters	3817 / 0 / 314	
Goodness-of-fit on F^2	1.033	
Final R indices [I>2sigma(I)]	R1 = 0.0363, wR2 = 0.1012	
R indices (all data)	R1 = 0.0397, wR2 = 0.1040	
Extinction coefficient	0.0042(5)	
Largest diff. peak and hole	0.182 and -0.149 e.$Å^{-3}$	

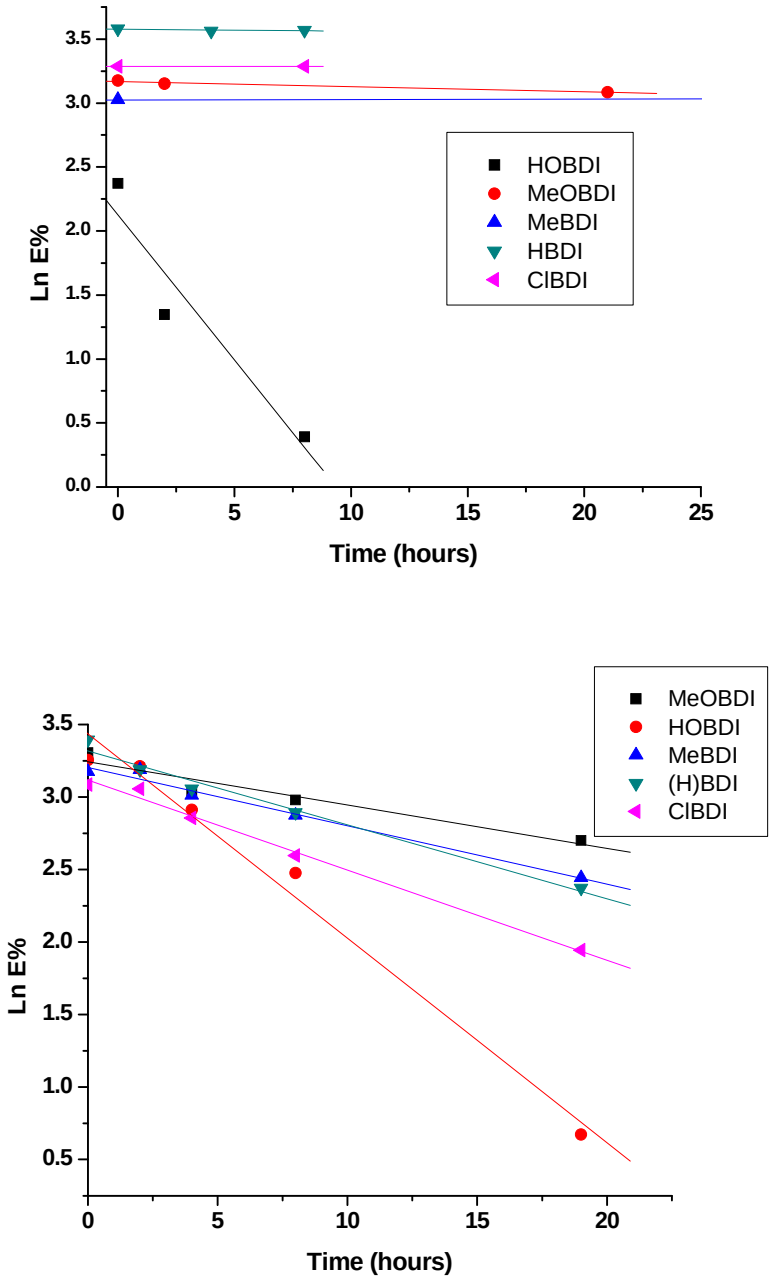

Figure 5.9 XBDI reserved isomerization reaction rates in acetonitrile solvent. Top: No nucleophile was added. Bottom: 0.089 M DABCO was presented.

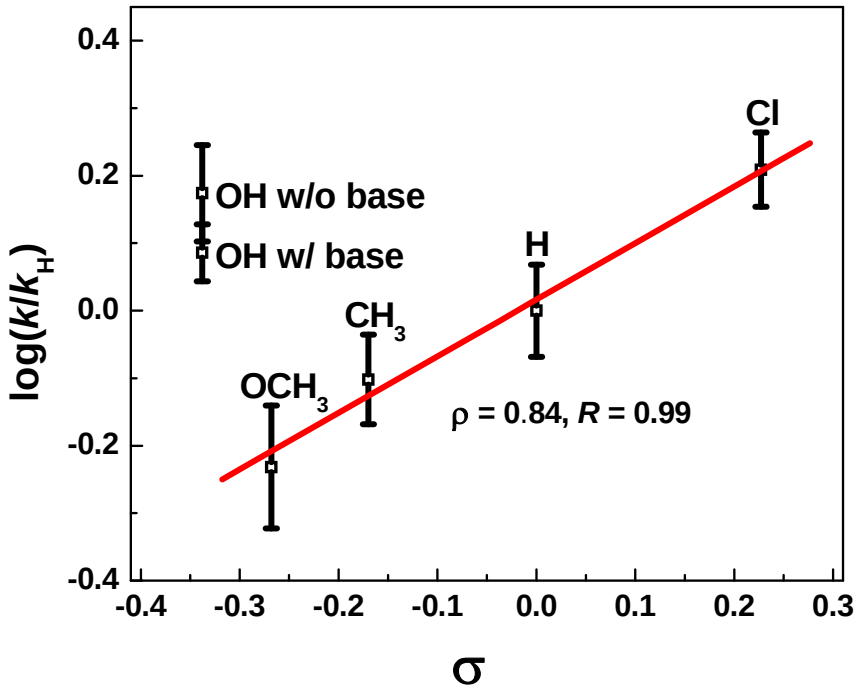

Figure 5.10. Hammett σ-ρ plot for *para E*-**XBDI** thermal isomerization in CD_3CN in the presence of 0.089 M DABCO; $k_H = 1.4\ 10^{-5}\ s^{-1}$.

Table 5.2. Rates of isomerizations of different **XBDI** derivatives in CD_3CN. The concentration of the DABCO in each sample was 0.089 M. See Fig. 5.10 for graphical representation of the data.

Compound	σ	K_{obs}, 10^{-5}/s	$Log(K/K_H)$
HOBDI	**-0.37**	**3.9**	**0.44**
MeOBDI	**-0.268**	**0.83**	**-0.23**
MeBDI	**-0.17**	**1.1**	**-0.10**
(H)BDI	**0**	**1.4**	**0**
ClBDI	**0.227**	**1.7**	**0.21**
HOBDI (no base)	**-0.37**	**6.3**	**0.65**

What, then, is the correct mechanism? The key is provided by the positive ρ and by the observation that thermal isomerization occurs only in nucleophilic solvents such as MeOH or DMSO. This result is reminiscent of that for S_NAr reaction, in which substitution by an electron-releasing group at the ipso position retards the reaction, producing a positive ρ.[14] Thus we conceived instead a similar mechanism, an addition/elimination mechanism (Path b in *Figure 5.7*). In order to test this mechanism, we examined the thermal reversion in a variety of solvents. As a test case, we again used **MeOBDI**, since this molecule is isoelectronic to **HOBDI** without allowing for the possibility of intra- or intermolecular proton transfer involving hydroxyl group. Unlike the results in the nucleophilic solvents water, methanol, or DMSO, we observed no isomerization in the absence of added base in either acetonitrile or benzene. However, both exhibited facile isomerization in the presence of primary amines. In the case of tertiary amines, either 1,4-diaza[2.2.2]bicyclooctane (DABCO) or 4-(dimethylamino)pyridine (DMAP), isomerization was observed only in acetonitrile solvent.

If the proposed mechanism were correct, the rate of isomerization should be rate-limiting in formation of the adduct, which in term should be proportional to the concentration of nucleophile. Again we used DABCO with **MeOBDI** in acetonitrile. As anticipated for the proposed bimolecular mechanism, isomerization was linear with base concentration over one order of magnitude (see *Figure 5.11*). Repeating the Hammett plot with 0.089 M DABCO, we obtained a ρ-value of 0.84, consistent with nucleophilic attack (see *Figure 5.10*). Curiously, **HOBDI** itself isomerized without added base, but the isomerization was inhibited by the presence of added amine.

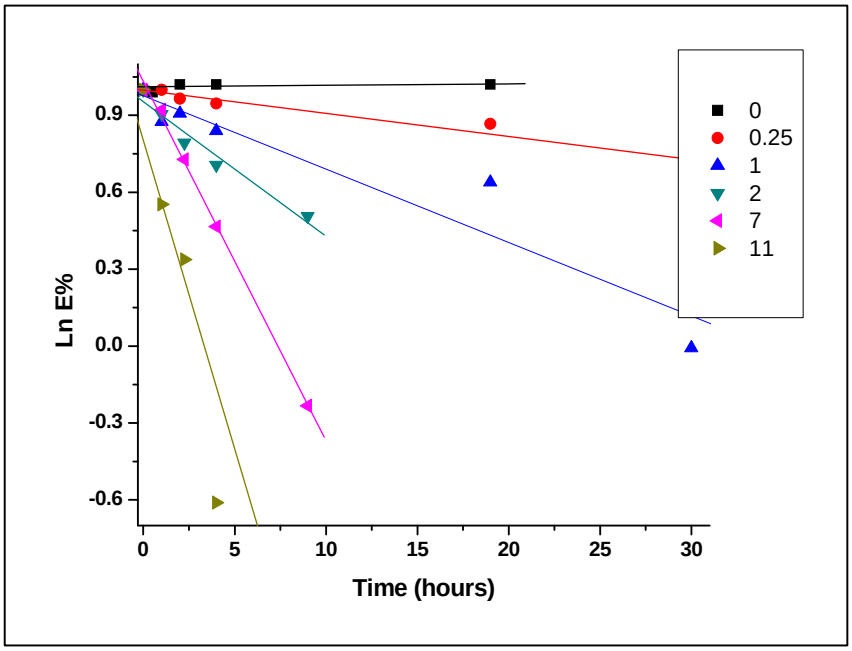

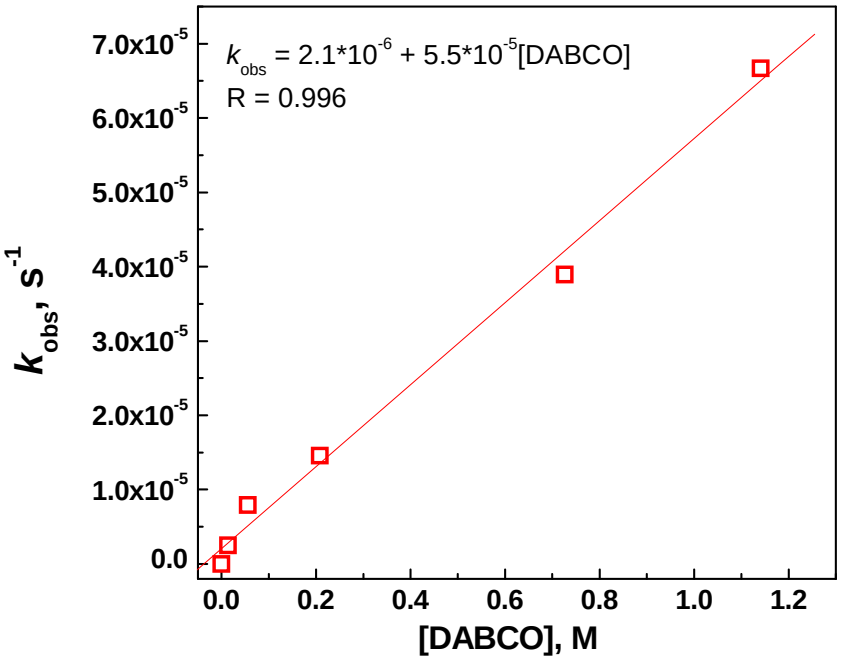

Figure 5.11. Effect of DABCO on **MeOBDI** isomerization. Top: Reaction rates at different (DABCO/**MeOBDI**) molar ratio. Bottom: $K_{obs}(s^{-1})$ vs. [DABCO] (M) plot.

The results we have observed are consistent with the addition/elimination mechanism shown as Path b in *Figure 5.7*. Although this is a plausible mechanism, literature precedents are fairly rare. The isomerization of cinnamate anion has been shown to involve such processes.[15] Such mechanisms have been proposed as possible mechanisms in biological isomerizations,[16] but no examples are reported. A more immediate question is the relevance to the chemistry of fluorescent proteins, particularly to the blinking phenomenon. As noted earlier, if blinking is associated with cis/trans isomerization, blinking "on" requires either reverse photoisomerization or a thermal process, and this work demonstrates that the unassisted process has too high a barrier to compete. Conversely, the addition/elimination mechanism, as a bimolecular diffusional process, is also relatively slow. In a protein, however, such diffusion is irrelevant; rather, the question is whether there is a competent nucleophile to initiate such a mechanism. In the particular case of *mTFP0.7*, fluorescence recovery through reisomerization occurs over a span of minutes.[4a] Is there a nucleophile available for this process? Indeed there is! The crystal structure of *trans-mTFP0.7* is characterized by the presence of a water molecule interposed between a glutamate and the benzylidene carbon

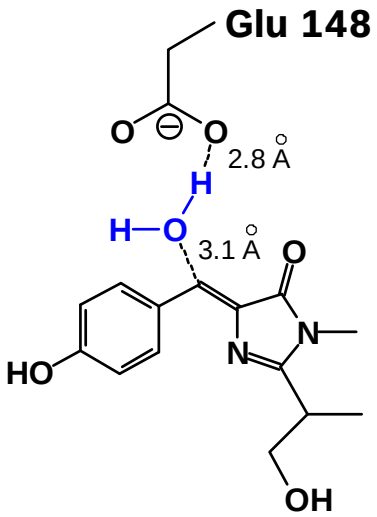

Figure 5.12 Nucleophile in *mTFP0.7*.

of the chromophore such that the glutamate can promote addition of water to the double bond (see *Figure 5.12*).[17]

Finally, we consider the isomerism of **HOBDI** itself. This derivative, the closest analogy to the wtGFP chromophore, undergoes isomerization in the absence of base, although its limited solubility in non-polar solvents precluded studies in benzene. Curiously, the presence of DABCO *depressed* the isomerization rate (see *Fig. 5.10*). On the one hand, if the Falk's mechanism were valid, the methoxy derivative **MeOBDI**, with similar resonance characteristics, should undergo equally facile isomerization. On the other hand, if deprotonation were required, then the base should accelerate the reaction. Furthermore, calculations are not consistent with the deprotonated form of **HOBDI** undergoing faster reaction.[11] Based on O-H deuterated **HOBDI** experimental result (see *Figure 5.13*), we can only propose another possible mechanism in solution, namely, tautomerization to a quinomethane derivative (see Path c in *Figure 5.7*). Whether this mechanism is equally available within the β-barrel is somewhat speculative, although the crystal structure of *mTFP0.7* shows a more favorable disposition for nucleophilic attack via Path b (see *Figure 5.7*).

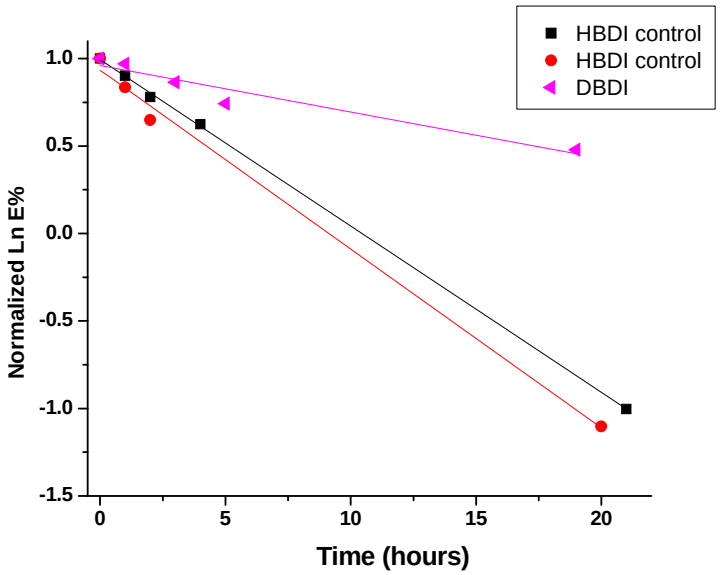

Figure 5.13. Effect of O-H deuterated **HOBDI** (**DOBDI**) isomerization. **DOBDI** was prepared by dissolving **HOBDI** in CH_3OD then evaporated the solvent in vacuum.

Addition/elimination emerges as a compelling mechanism for isomerization of fluorescent protein chromophores. The presence of an internal nucleophile thus becomes an additional point of mutation of such chromophores that may mediate their photophysical properties. Such mutations are currently being explored.

Conclusions

The green fluorescent protein (GFP) and its related mutants undergo both photochemical and thermal isomerizations. Typically, the *Z* form is more stable and undergoes photochemical conversion to the *E* form followed by thermal reversion over a period of seconds or minutes. Although the mechanism of the thermal reversion has been the subject of some investigations, the surprisingly low activation energy for this process has not sparked any controversy. We showed that the chromophore is surprisingly stable in both *E* and *Z* forms, and that the facile thermal reversion is the result of a novel nucleophilic addition/elimination mechanism. This observation may have implication for the intervention of such processes, as well as blinking and kindling, in fluorescent proteins.

References

[1] (a) Habuchi, S.; Ando, R.; Dedecker, P.; Verheijen, W.; Mizuno, H.; Miyawaki, A.; Hofkens, J. *Proc. Natl. Acad. Sci. USA* **2005**, *102*, 9511-9516. (b) Jimenez-Banzo, A.; Nonell, S.; Hofkens, J.; Flors, C. *Biophys. J.* **2008**, *94*, 168-172.

[2] (a) Haupts, U.; Maiti, S.; Schwille, P.; Webb, W. W. *Proc. Natl. Acad. Sci. USA* **1998**, *95*, 13573-13578. (b) Liu, Y.; Kim, H. –R.; Heikal, A. A. *J. Phys. Chem. B* **2006**, *110*, 24138-24146.

[3] (a) Chudakov, D. M.; Feofanov, A. V.; Mudrik, N. N.; Lukyanov, S.; Lukyanov, K. A. *J Biol Chem.* **2003**, *278*, 7215-7219. (b) Quillin, M. L.; Anstrom, D. M.; Shu, X.; O'Leary, S.; Kallio, K.; Chudakov, D. M.; Remington, S. J. *Biochemistry* **2005**, *44*, 5774-5787. (c) Henderson, J. N.; Remington, S. J. *Physiol*. **2006**, *21*, 162-170.

[4] (a) Henderson, J.N.; Ai, H.-W.; Campbell, R. E.; Remington, S. J. *Proc. Natl. Acad. Sci. USA* **2007**, *104***,** 6672-6677. (b) Andresen, M.; Stiel, A. C.; Trowitzsch, S.; Weber, G.; Eggeling, C.; Wahl, M. C.; Hell, S. W.; Jakobs, S. *Proc. Natl. Acad. Sci. USA* **2007**, *104***,** 13005-13009.

[5] Usman, A.; Mohammed, O. F.; Nibbering, E. T. J.; Dong, J.; Solntsev, K. M.; Tolbert, L. M. *J. Am. Chem. Soc.* **2005**, *127*, 11214-11215.

[6] Solntsev, K. M.; Poizat, O.; Dong, J.; Rehault, J.; Lou, Y.; Burda, C.; Tolbert, L. M. *J. Phys. Chem. B* **2008**, *112*, 2700-2711.

[7] Maddalo, S. L.; Zimmer, M. *Photochem. Photobiol*. **2006**, *82*, 367-372.

[8] (a) Toniolo, A.; Olsen, S.; Manohar, L.; Martínez, T. *J. Faraday Discuss*. **2004**, *127*, 149.(b) Martin, M. E.; Negri, F.; Olivucci, M. *J. Am. Chem. Soc.* **2004**, *126*, 5452. (c) Gepshtein, R., Huppert, D.; Agmon, N. *J. Phys. Chem. B* **2006**, *110*, 4434. (d)Altoe, P.; Bernardi, F.; Garavelli, M.; Orlandi, G.; Negri, F. *J. Am. Chem. Soc*. **2005**, *127*, 3952. (e) Yang, J.-S.; Huang, G.J.; Liu, Y.-H.; Peng, S.-M. *Chem. Commun.* **2008**, 1344-1346.

[9] (a) Vengris, M.; van Stokkum, I. H. M.; He, X.; Bell, A. F.; Tonge, P. J.; van Grondelle, R.; Larsen, D. S. *Springer Ser. Chem. Phys.* **2005***, 79*, 610-612. (b) Vengris, M.; van Stokkum, I. H. M.; He, X.; Bell, A. F.; Tonge, P. J.; van Grondelle, R.; Larsen, D. S. *J. Phys. Chem. A* **2004***, 108*, 4587-4598.

[10] Weber, W.; Helms, V.; McCammon, J. A.; Langhoff, P. W. *Proc. Natl. Acad. Sci. USA* **1999**, *96,* 6177-6182

[11] Dong, J.; Solntsev, K. M.; Tolbert, L. M. *J. Am. Chem. Soc*. **2006**, *128*, 12038-12039.

[12] Lerestif, J. M.; Perrocheau, J.; Tonnard, F.; Bazureau, J. P.; Hamelin, J. *Tetrahedron* **1995,** *51*, 6757-6774.

[13] (a) Hager, B.; Schwarzinger, B.; Falk, H. *Monatsh. Chem.* **2006**, *137*, 163-168. See also: (b) Fendler, K.; Hager, B.; Falk, H. *Monatsh. Chem.* **2007**, *138*, 859-862.

[14] Um, L. –H.; Lee, J. –Y.; Fujio, M.; Tsuno, Y. *Org. Biomol. Chem*. **2006**, *4*, 2979-2985.

[15] (a) G. A. Reed, D. R. Dimmel, E. W. Malcolm, *J. Org. Chem.* **1993**, *58*, 6364. (b) B. A. Feit, R. Pazhenchevsky, B. Pazhenchevsky, *J. Org. Chem.* **1976**, *41*, 3246.

[16] *Cis-trans Isomerization in Biochemistry*, C. Dugave, (ed.) Wiley, 2006.

[17] We thank Prof. S. J. Remington for drawing our attention to this fact and providing the figure.

CHAPTER 6

THE META-GREEN FLUORESCENT PROTEIN CHROMOPHORE

Introduction

As discussed in previous chapters, the GFP crystal structure shows the chromophore in the middle part of a central helix created by an 11-stranded *β*-barrel, which plays a critical role for the superb fluorescence properties of GFP and its mutants. Such fluorescent proteins are restricted to the toolbox of natural aromatic amino acids which can replace the *p*-phenol moiety, for example, phenyl alanine, tryptophan, and histidine, and we wondered how replacement of the *p*-phenol with its *m*-equivalent might alter its photophysics.

The dimethyl derivative of the GFP chromophore (*p*-**HOBDI**) and several of its derivatives have been synthesized, and their photochemistry investigated. Released from the protein *β*-barrel *p*-**HOBDI** demonstrated ultrafast (< 1 ps) deactivation in all organic and aqueous solvents at room temperature owning to ultrafast conformational relaxation to a non-fluorescent twisted intermediate. Recently, an *ortho*-isomer of **HOBDI** was synthesized.[2] A ground-state hydrogen bond between hydroxyl group and imidazolone nitrogen in this compound resulted in ultrafast formation of the tautomer (zwitterion) with an increased fluorescence quantum yield.

The prototropic behavior of the the GFP chromophore is responsible for its green fluorescence. This chromophore falls into the general category of hydroxyarene photoacids with which our group has significant experience.[3] Such hydroxyarenes exhibit high excited-state acidities but neutral ground states. In the case of the GFP, the imidazolinone ring is an electron-withdrawing substituent, increasing both the ground

state- the excited-state acidities, but to different extents. We speculated that m-hydroxy substitution would have analogous effects on the photophysics to those noted by Lewis in the case of another hydroxystyryl aromatic, hydroxystilbene.[4]

Experimental

General Experimental

3-Hydroxybenzaldehyde (98.5 %), m-anisaldehyde (97 %) and *N*-acetylglycine (99 %) were purchased from Acros. Sodium acetate (99.7%) and potassium carbonate (99.94%) were purchased from Fisher. Methylamine (33% wt. solution in abs. ethanol) was purchased from Aldrich. The progression of reactions was monitored by thin-layer-chromatography using Analtech UNIPLATE TLC plates (Silica Gel GF) with visualization by illumination with ultraviolet light. NMR spectra were recorder on a Varian Mercury spectrometer (300MHz). Mass spectral analysis was provided by the Georgia Tech Mass Spectrometry facility. Elemental analyses were conducted at Atlantic Microlab. Ultraviolet-visible (UV-Vis) spectra were obtained on a Perkin Elmer Lambda19 spectrophotometer.

Synthesis

4-(3-Acetoxybenzylidene)-2-methyloxazalone

N-Acetylglycine (2.0 g, 17 mmol), sodium acetate (1.23 g,), *p*-anisaldehyde (1.9 g), and acetic anhydride (4.2 mL) were heated at 80 °C with stirring for 2 h. Heated Ethanol (20 ml) was added slowly and the mixture was allowed to stand at room temperature for 4 h. The separated crystalline solid was filtered off, washed with ice-cold alcohol, then with hot water to obtain 1.4g (44%) of yellow oxazalone; ^{1}H NMR spectrum ($CDCl_3$), δ, ppm: 2.40 (s, 3H, CH_3); 3.88 (s, 3H, O-CH_3); 6.98 (d, 2H, Ar-H); 7.12 (s, 1H, H on bridging carbon); 8.08 (d, 2H, Ar-H).

4-(3-Methoxybenzylindene)-2-methyloxazalone

N-Acetylglycine (1.9 g, 16 mmol), sodium acetate (1.23 g, 15 mmol), *m*-anisaldehyde (2.0 g, 15 mmol), and acetic anhydride (4.2 mL, 45 mmol) were heated at 80 °C with stirring for 4 h. Heated ethanol (20 ml) was added slowly and the mixture was allowed to stand at room temperature for 4 h. The separated crystalline solid was filtered off, washed with ice-cold alcohol, then with hot water to obtain 1.8 g (56 %) of yellow oxazalone; ^{1}H NMR spectrum ($CDCl_3$), δ, ppm: 2.40 (s, 3H, CH_3); 3.86 (s, 3H, O-CH_3); 6.99 (d, 1H, Ar-H); 7.11 (s, 1H, H on bridging carbon); 7.35 (t, 1H, Ar-H); 7.58 (d, 1H, Ar-H); 7.75 (s, 1H, Ar-H).

4-(3-Hydroxybenzylindene)-1,2-dimethylimidazolinone(m-HOBDI)

1.0 g (4.6 mmol) of 4-(3- Acetoxybenzylindene)-2-methyl-oxazalone was added to 0.40 g (2.9 mmol) of potassium carbonate in a 25 mL round-bottom flash to which 0.75 g (9.7 mmol) methylamine (33% wt. solution in absolute ethanol) and 8.0 mL ethanol were then added. The reaction mixture was refluxed overnight. After cooling, the mixture was neutralized with 10% HCl, and stayed at 0 ºC for a further 4 h. The separated substance was filtered off, washed with ice-cold alcohol, then with hot water to obtain 0.76g (86%) of dark orange imidazolinone. Decomposed over 180 °C. ^{1}H NMR spectrum (DMSO), δ, ppm: 2.39 (s, 3H, CH_3); 3.1 (s, 3H, N-CH_3); 6.83 (d, 1H, Ar-H); 6.92 (s, 1H, H on bridging carbon); 7.23 (t, 1H, Ar-H); 7.50 (d, 1H, Ar-H), 7.67 (s, 1H, Ar-H). Molecular weight: EI-MS M+ calculated for [$C_{13}H_{14}N_2O_2$] = 216.24, found = 216.1.

4-(3-Methoxybenzylindene)-1,2-dimethylimidazolinone(m-MeOBDI)

0.9 g (4.2 mmol) of 4-(3- Methoxybenzylindene)-2-methyl-oxazalone was added to 0.36 g (2.6 mmol) of potassium carbonate in a 25 mL round-bottom flash to which 0.41 g (10 mmol) methylamine (33% wt. solution in absolute ethanol) and 9.0 mL ethanol were then added. The reaction mixture was refluxed overnight. After cooling, the

mixture was neutralized with 10% HCl, and stayed at 0 ºC for a further 4 h. The separated substance was filtered off, washed with ice-cold alcohol, then with hot water to obtain 0.78g (81%) of dark orange imidazolinone. ^{1}H NMR spectrum ($CDCl_3$), δ, ppm: 2.37 (s, 3H, CH_3); 3.18 (s, 3H, N-CH_3); 3.85 (s, 3H, O-CH_3); 6.93 (d, 1H, Ar-H); 7.07 (s, 1H, H on bridging carbon); 7.32 (t, 1H, Ar-H); 7.64 (d, 1H, Ar-H); 7.80 (s, 1H, Ar-H). Molecular weight: EI-MS M+ calculated for [$C_{13}H_{14}N_2O_2$] = 230.26, found = 230.1.

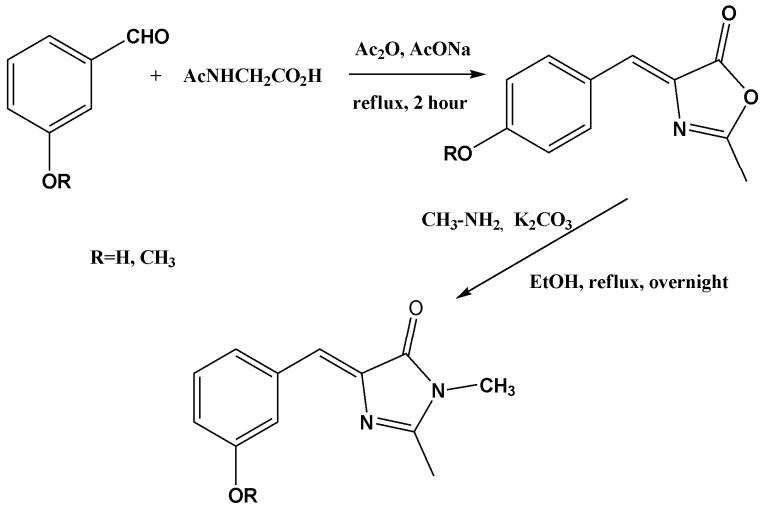

Figure 6.1 Synthesis of m-H(M)**OBDI**.

Determination of p*K*a Values:

Measurements were performed with a combination glass microelectrode (Orion, Thermo Electron Corp, Waltham). The electrode was precalibrated in aqueous buffers at pH 4, 7, and 10. Solution pH measurements were performed in 1/1 v/v methanol-water mixtures. For the determination of the p*K*a's, a series of UV-vis spectra were acquired for which –log[H_3O^+] was varied between 5 and 12. It was demonstrated[5] that the pH can be measured directly in alcohol-water mixtures using glass electrodes precalibrated in aqueous buffers. In this case for 1/1 v/v methanol/water mixtures the observed pH values are about 0.1 pH units higher than the real ones for this mixture. The raw spectral data

were processed via non-linear least squares fit analysis using the SPECFIT software package,[6] providing deconvoluted spectra for each species present as well as the acidity constants for the relevant protonation equilibria.

Determination of p*K*a Values:

The femtosecond transient absorption setup has been already described[7]. Briefly, it involves a 1 kHz Ti-sapphire laser system based upon a Coherent (MIRA 900D) oscillator and a BM Industries (ALPHA 1000) regenerative amplifier. Pump excitation at 380 nm was obtained by frequency doubling the Ti-sapphire fundamental tuned at 760 nm (0.3 mm BBO crystal). The pump pulse (~100 fs) power was limited to 2-6 μJ per pulse (0.2-0.6 mJ/cm^2). A white light continuum probe pulse was generated at 760 nm in a CaF_2 plate. The pump-probe polarization configuration was set at the magic angle. The probe pulse was delayed in time relative to the pump pulse using an optical delay line (Microcontrol Model MT160-250PP driven by an ITL09 controller, precision $\pm$1 μm). The overall time resolution (fwhm of the pump-probe intensity cross-correlation) was estimated to be about 300 fs from the two-photon (pump + probe) absorption signal in pure hexane. The time dispersion of the continuum light over the 400-700 nm region of analysis was about 0.5 ps. The transmitted light was analyzed by a CCD optical multichannel analyzer (Princeton Instrument LN/CCD-1340/400-EB detector + ST-138 controller). Sample solutions (2.5×10^{-4} M) were circulating in a flow cell with 2 mm optical path length. Data were accumulated over 3 min (~180000 pump-probe sequences). The characteristic times related to the spectral changes were obtained from exponential fit of the observed kinetics.

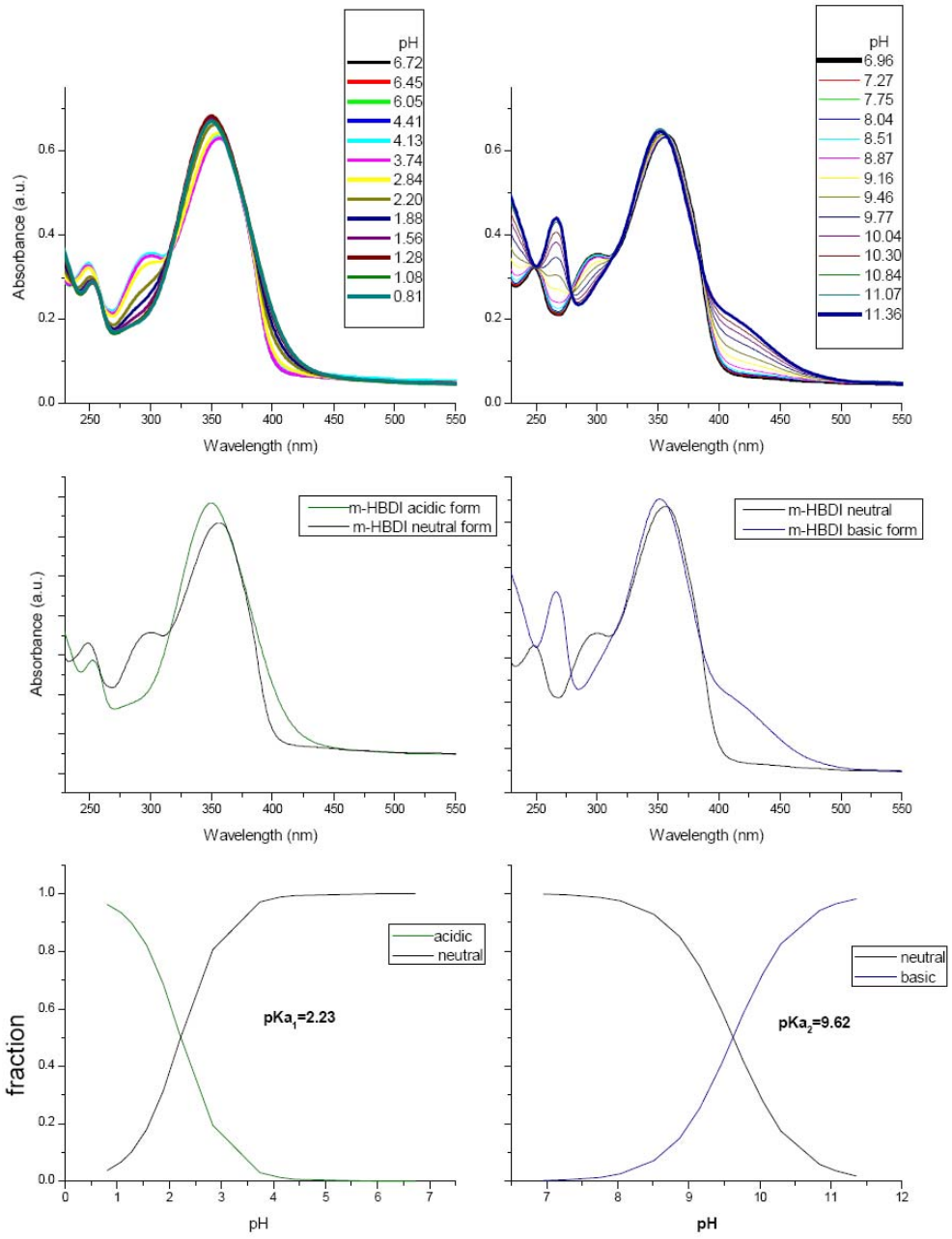

Figure 6.2. Top row: Spectrophotometric pH titration of *m*-**HOBDI** in MeOH/H_2O (1:1, v/v). Middle row: deconvoluted UV-vis spectra for the neutral, protonated, and deprotonated species. Bottom row: Calculated species distribution diagram. Real pH and p*K*a values are 0.1 unit lower than indicated.

Results and Discussion

A consequence of the para relationship between the incipient oxyanion center and the electron-withdrawing imidazolinone ring in GFP is that the ground-state acidity is increased. Substitution on the meta position provides no such possibility, while the excited state should show enhanced charge transfer. Thus the meta isomer should show diminished anion formation in the ground state but excellent excited-state acidity. This excited-state reversal of ortho, para directing effects, known as the "meta" effect, has been the subject of numerous theoretical and experimental observations[8] and is shown clearly by examining the corresponding frontier molecular orbitals (highest occupied molecular orbitals (HOMOs) and lowest unoccupied molecular orbitals (LUMOs)) for both conjugate bases at the AM1 level (see *Figure 6.3*), showing greater charge transfer for the meta isomer. The closest analogy in solution chemistry involves *m*- and *p*-hydroxystilbenes.[4] In this case, the para isomer undergoes rapid cis/trans isomerization and sluggish proton transfer, while the meta isomer exhibits the reverse behavior, reflecting the molecular orbital principles we outlined above. Thus the *m*-tyrosine GFP derivative may be much more photochemically robust than the wild-type GFP, and it should certainly exhibit an enhanced excited-state acidity.

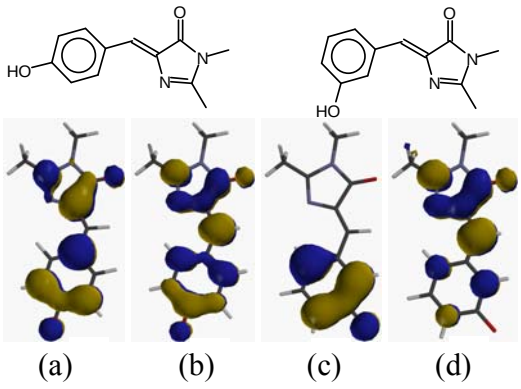

Figure 6.3. (a) HOMO and (b) LUMO for *p*-**HOBDI** (left structure); (c) HOMO and (d) LUMO for *m*-**HOBDI** (right structure).

m-**HOBDI** was synthesized using our modification[9] of Niwa's procedure.[10] The corresponding methyl ether *m*-**MeOBDI** was also prepared. It is noteworthy that, despite the previously unknown nature of *m*-**HOBDI** itself, several 2-methyl-substituted derivatives exhibiting various biological activities have been synthesized.[11]

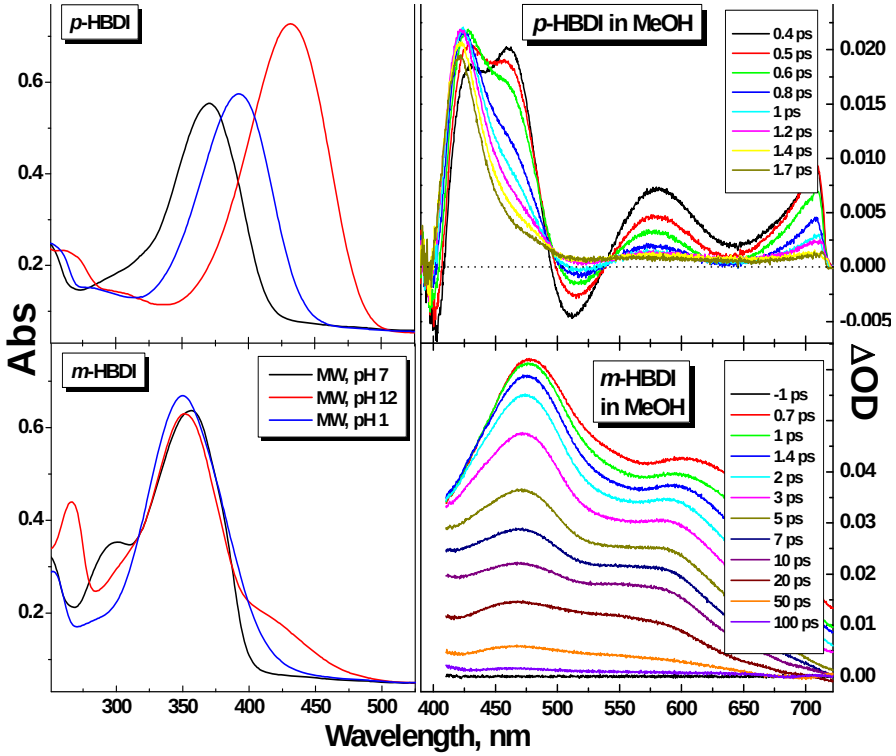

Figure 6.4. Left column: absorption spectra of *p*-**HOBDI** (top) and *m*-**HOBDI** (bottom) in methanol/water (MW) 1/1 vol. at various pH. Right column: transient absorption signal of *p*-**HOBDI** (top) and *m*-**HOBDI** (bottom) in methanol. Pumping occurred with 380 nm, 6 μJ, and 100 fs pulses.

While the basicity of the imidazolinone nitrogen (pK_a of 2.1) decreased by only 0.15 pK_a units as compared to *p*-**HOBDI**, the pK_a of the hydroxy group (9.5) increased by one pK_a unit, in keeping with the weaker ground-state acidity of the meta isomer and reflecting the localized conjugate base MOs of *Figure 6.3*. Moreover, in contrast to the very-well resolved absorbance bands of *p*-**HOBDI** in various protonation states (*Figure 6.4*), the absorbance of the *m*-**HOBDI** cation strongly overlaps with that of neutral

species, The anion of *m*-**HOBDI** is characterized by two bands, with the stronger one practically indistinguishable from that of the neutral. The analogous absorbance band splitting of *m*-hydroxystilbene anion is attributed to the mesomeric effect of the phenolate ion on two different charge-transfer transitions.[4b]

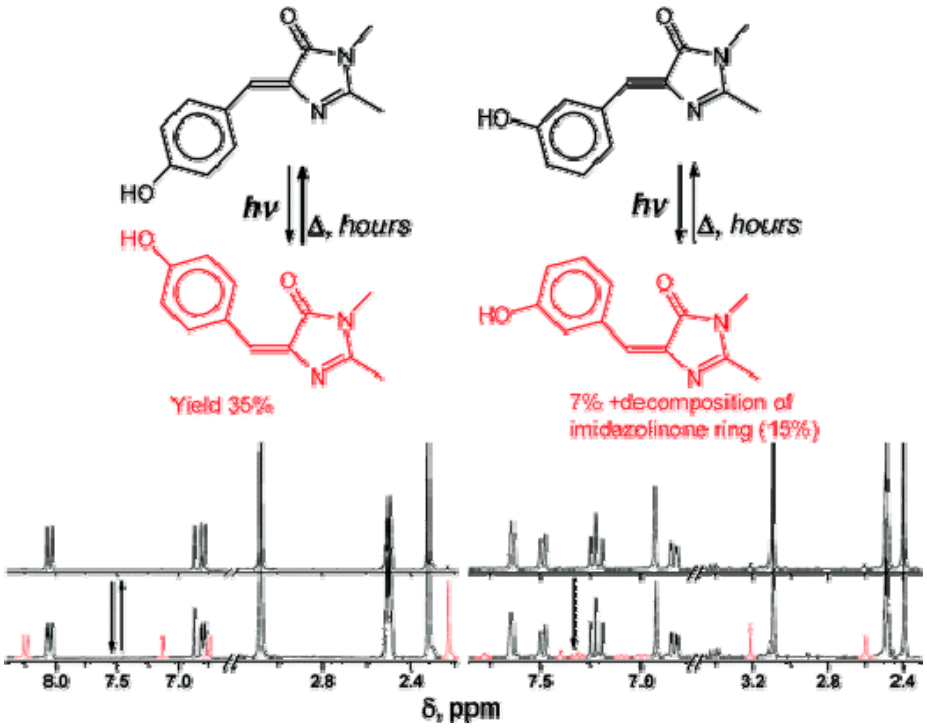

Figure 6.5. ^{1}NMR spectra of *p*-**HOBDI** (left) and *m*-**HOBDI** (right) in DMSO-d_6 before (top spectra) and after (bottom spectra) 2 h irradiation at 370 nm. The photolysis resulted in the new features shown in red.

The fluorescence lifetimes of *p*-**HOBDI** in various protonation states and in various solvents were less than 1.5 ps[12,13] and thus could not be determined by the time-correlated single-photon counting method. However the lifetimes of the meta isomer in some nonaqueous solvents were long enough to be measured. The highest fluorescent quantum yield (FQY 0.0023) and the longest fluorescence lifetimes (biexponential decay with 15 and 90 ps lifetimes, amplitude ratio 10) were detected in DMSO (λ_{max} = 440 nm). At the same conditions the FQY of *p*-**HOBDI** was 10 times smaller. The significantly longer fluorescence lifetime of *m*-**HOBDI** can be associated with slower cis/trans

photoisomerization, reminiscent of Lewis' observations with the corresponding hydroxystilbenes.[4] However, despite this slower kinetics, isomerization remains the major nonradiative decay pathway in nonaqueous solvents. ^{1}NMR measurements following irradiation of *p*-**HOBDI** revealed the photoconversion of the initial *Z*-isomer to the *E*-isomer to the extent of about 35% in DMSO (*Figure 6.5*), a result qualitatively similar to Tonge's observations in methanol;[14] however, in latter case the yields were not reported. This isomerization was thermally reversible. In contrast, under the same irradiation conditions *m*-**HOBDI** produced much less isomer (7%), and irreversible decomposition was also observed.

A dramatic difference between the meta and para isomers of **HOBDI** in methanol has been also demonstrated in preliminary fs pump-probe spectroscopic results: the meta isomer shows a much longer lived excited state (*Figure 6.4*), in agreement with fluorescence decay results. Very similar time-resolved spectra of *p*-**HOBDI** in water at various pH values were deconvoluted by Vengris et al.[13] into transient absorption and stimulated emission of excited- and ground-state intermediates, including photoionization products. In contrast, the transient absorption signal of *m*-**HOBDI** consisted of a very broad absorption signal best fit by a biexponential decay function with 5 and 31 ps components, and a $^{3}/_{2}$ amplitude ratio. In addition to slower photoisomerization, we have found that the quantum yields for solvated electrons and **HOBDI** radical-ions formed in the result of photolysis were much lower for the meta isomer. The formation of such radical cations, followed by electron transfer from a glutamate carboxylate, may account for the E222 decarboxylation observed for GFP[15] and thus provide for much less efficient decarboxylation in a protein having a *m*-hydroxyaromatic chromophore.

In solution, the decay rate of *p*-**HOBDI** is about 1 ps, and no excited-state proton transfer (ESPT) is observed for the free chromophore in all solvents. Nor is ESPT to methanol solvent observed for the meta chromophore (*Figure 6.4*). However, in mixed water-methanol solution, slower photoisomerization allows the excited-state protolytic

reaction of the free meta chromophore to compete. Our preliminary results demonstrate that, for *m*-**HOBDI**, an interesting sequential ESPT is observed, similar to that for hydroxyquinolines.[16] First, the hydroxyl group dissociates in 0.7 ps, and then the reprotonation of imidazolinone nitrogen occurs at 3.1 ps. Curiously, the second proton-transfer step is nonadiabatic and leads to fluorescence quenching. In water-rich solution *m*-**MeOBDI** shows ultrafast kinetics, probably associated with proton abstraction from water. This selective modulation of acid-base behavior in chromophores, together with solvent variation, including pH change, serves as a context for separation of elementary proton-transfer steps in these systems. Studies of such model unconventional *m*-GFP chromophores will help unravel the complex photochemistry and photophysics of fluorescent prototropic proteins.

Conclusions

m-Hydroxy isomer of the green fluorescent protein synthetic analogue (*m*-**HOBDI**) was synthesized. By analogy to hydroxystilbenes, longer singlet lifetimes and lower isomerization quantum yields were observed for the meta versus para isomer of the chromophore.

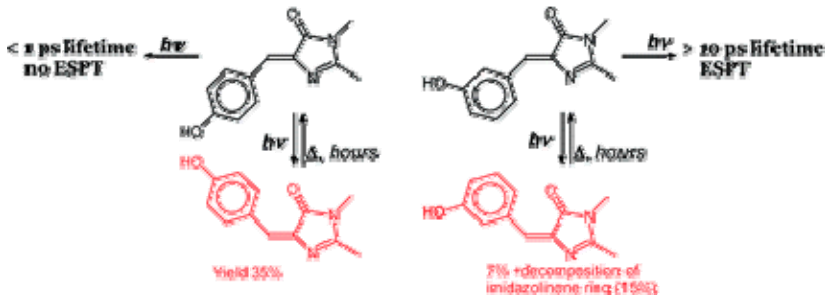

Figure 6.6 Table of contents for *Chapter 6*.

References

[1] Dong, J.; Solntsev, K. M.; Olivier, P.; Tolbert, L. M. *J. Am. Chem. Soc*. **2007**, *129*, 10084-10085.

[2] Chen, K.-Y.; Cheng, Y.-M.; Lai, C.-H.; Hsu, C.-C.; Ho, M.-L.; Lee, G.-H.; Chou, P.-T. *J. Am. Chem. Soc*. **2007**, *129*, 4534-4535.

[3] Tolbert, L. M.; Solntsev, K. M. "Design and Implementation of "Super" Photoacids." In *Handbook of Hydrogen Transfer*. Schowen, R. I., Ed.; Wiley-VCH, 2007; Vol. 1, pp 417-439.

[4] (a) Lewis, F. D.; Crompton, E. M. *J. Am. Chem. Soc.* **2003**, *125*, 4044-4045. (b) Crompton, E. M.; Lewis, F. D. *Photochem. Photobiol. Sci.* **2004**, *3*, 660-668. (c) Lewis, F. D.; Sinks, L. E.; Weigel, W.; Sajimon, M. C.; Crompton, E. M. *J. Phys. Chem. A* **2005**, *109*, 2443-2451.

[5] a) Bosch, E.; Bou, P.; Allemann, H.; Roses, M. *Anal. Chem*. **1996**, *68*, 3651-3657. (b) Avdeef, A.; Box, K. J.; Comer, J. E. A.; Gilges, M.; Hadley, M.; Hibbert, C.; Patterson, W.; Tam, K. Y. *J. Pharm. Biomed. Anal.* **1999**, *20*, 631-641. (c) Canals, I.; Portal, J. A.; Bosch, E.; Roses, M. *Anal. Chem*. **2000**, *72*, 1802-1809. (d) Canals, I.; Valko, K.; Bosch, E.; Hill, A. P.; Rose´s, M. *Anal. Chem*. **2001**, *73*, 4937-4945. (e) Canals, I.; Oumada, F. Z.; Rose´s, M.; Bosch, E. *J. Chromatogr., A* **2001**, *911*, 191-202.

[6] Binstead, R. A.; Zuberbühler, A. D.; *SPECFIT v. 3.0.27*; Spectrum Software Associates, Marlborough MA, 2001.

[7] Buntinx, G.; Naskrecki, R.; Poizat, O. *J. Phys. Chem.* **1996**, *100*, 19380.

[8] (a) Lewis, F. D.; Yang, J.-S. *J. Am. Chem. Soc.* **1997**, *119*, 3834-3835. (b) Zimmerman, H. E. *J. Am. Chem. Soc.* **1995**, *117*, 8988-8991. (c) DeCosta, D. P.; Howell, N.; Pincock, A. L.; Pincock, J. A.; Rifai, S. *J. Org. Chem.* **2000**, *65*, 4698-4705. (d) Sinha, H. K.; Yates, K. *J. Am. Chem. Soc.* **1991**, *113*, 6062-6067.

[9] Dong, J.; Solntsev, K. M.; Tolbert, L. M. *J. Am. Chem. Soc*. **2006**, *128*, 12038-12039.

[10] Kojima, S.; Ohkawa, H.; Hirano, T.; Maki, S.; Niwa, H.; Ohashi, M.; Inouye, S.; Tsuji, F. I. *Tetrahedron Lett.* **1998**, *39*, 5239-5242.

[11] (a) Pandey, B. R.; Parmar, S. S.; Kumar, S.; Brumleve, S. J. *Pharmacology* **1978**, *16*, 344-348. (b) Kumar, S.; Pandey, B. R.; Parmar, S. S.; Gallagher, J. R.; Mayer, G. G. *Res. Commun. Chem. Pathol. Pharmacol*. **1984**, *44*, 163-166.

[12] Mandal, D.; Tahara, T.; Meech, S. R. *J. Phys. Chem. A* **2004**, *108*, 1102-1108.

[13] Vengris, M.; Stokkum, I. H. M.; He, X.; Bell, A. F.; Tonge, P. J.; van Grondelle, R.; Larsen, D. S. *J. Phys. Chem. A.* **2004**, *108*, 4587-4598.

[14] He, X.; Bell, A. F.; Tonge, P. J. *FEBS Lett.* **2003**, *549*, 35-38.

[15] Bell, A. F.; Stoner-Ma, D.; Wachter, R. M.; Tonge, P. J. *J. Am. Chem. Soc.* **2003**, *125*, 6919-6926.

[16] Poizat, O.; Bardez, E.; Buntinx, G.; Alain, V. *J. Phys. Chem. A* **2004**, *108*, 1873-1880.

CHAPTER 7

META AND PARA EFFECTS IN THE ULTRAFAST EXCITED-STATE DYNAMICS OF THE GREEN FLUORESCENT PROTEIN CHROMOPHORE

Introduction

Continuing from last chapter, synthetic dimethyl derivative of the GFP chromophore *p*-**HOBDI** (see *Figure 7.1*) belongs to the hydroxystyryl aromatic family of compounds, for which two specific excited-state processes can be expected: internal conversion (IC) to the ground state induced by twisting around the exo-methylene double bond and, in protic solvents, intermolecular proton abstraction and/or release. The former process may happen because molecular relaxation on the excited-state potential surface toward a twisted (perpendicular) geometry minimum close to the ground state surface occurs with low barrier and leads to fast S_1 quenching, as in stilbene[2] and its para-substituted derivatives.[3-7] Conversely, proton exchange with aqueous solvents is favored by a drastic increase of the hydroxyl acidity and imidazolinone nitrogen-atom basicity upon excitation. For the free *p*-**HOBDI** molecule in solution, femtosecond upconversion, pump-dump-probe, and UV-pump-IR-probe[8] experiments have revealed that ultrafast S_1 state quenching occurs (<1 ps), but no excited state acid-base reaction was observed. It is assumed that the dominant radiationless decay pathway is isomerization-induced IC[9,10] that involves a conical intersection between the ground- and the excited-state potentials.[11] Indeed, the > 90° twist angle between the phenol and the imidazolinone moieties was determined by polarization-sensitive UV-pump-IR-probe measurements.[8] Such twisting

leads to accumulation of trans isomer upon photolysis.[12] However, the nature of the isomerization reaction coordinate that leads to IC is still being widely debated, and a very broad spectrum of cis-trans isomerization mechanisms[13] has been considered. Among them is the rotation along single[14,15] or double bond,[16] as well as concerted twist of the bridging C=C-C bonds ("hula twist").[11] Large conformational relaxation would be highly unfavorable in the rigid H-bonding environment of the chromophore in GFP, in agreement with the very different photophysical behavior. In contradistinction, for the recently synthesized *ortho* isomer of **HOBDI**, a ground-state hydrogen bond between hydroxyl group and imidazolinone nitrogen inhibits the twisting motion and results in ultrafast formation of the tautomer (zwitterion) with an increased fluorescence quantum yield.[17]

Interestingly, in stilbene derivatives,[3-5] strongly mesomeric substituents such as amine, methoxy, and hydroxy are found to markedly increase the excited state lifetime and fluorescence quantum yield when located in the meta, but not in the para position. [3-6] This "meta effect", as initially formulated by Zimmerman,[18,19] is attributed to stabilization of the planar singlet state versus the twisted geometry, resulting in an enhanced barrier for C=C torsion. In addition, in the case of the hydroxystilbene compounds, meta isomers are stronger photoacids than para isomers, an effect that has been explained from electron density considerations. [3-5] This excited-state reversal of ortho/para directing effects has been the subject of numerous theoretical and experimental observations.[18,20-22] In the meta isomers, the combination of greater photoacidity and longer singlet lifetime lead to the efficient excited state proton transfer (ESPT) in aqueous solution that competes with isomerization. Molecular orbital calculations at the AM1 level and picosecond spectroscopic measurements on the recently synthesized **HOBDI** meta isomer (*m*-**HOBDI**, see *Figure 7.1*) suggest that *meta*-hydroxy substitution in the **HOBDI** family has analogous effects on the photophysics to those reported for the hydroxystilbenes.[23] Thus, while we believe that the *m*-tyrosine

GFP derivative may be much more photochemically robust than the wild type GFP, it will certainly exhibit a greater difference in acidity between the ground and excited states.

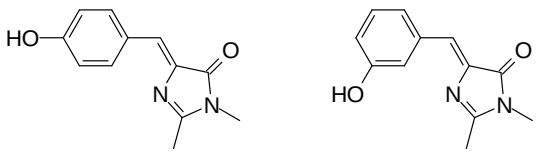

***p*-HBDI** ***m*-HBDI**

Figure 7.1 Structures of *p*-**HOBDI** and *m*-**HOBDI**.

We present here a comprehensive analysis by stationary and femtosecond time-resolved transient absorption and fluorescence spectroscopy of the excited-state dynamics of the synthetic m*eta*-green fluorescent protein chromophore (*m*-**HOBDI**) in the non-aqueous solvents methanol (MeOH) and acetonitrile (MeCN) and in various MeOH/water solutions at different pHs. We present in addition a similar analysis of the *O*-methylated derivative (*m*-**MeOBDI**) in which the replacement of the hydroxy group by a methoxy blocks one of the acid/base equilibria. Finally, we also present for comparison results obtained for the *para* analogue (*p*-**HOBDI**) and its *O*-methylated (*p*-**MeOBDI**) and *N*-methylated imidazolinone (*p*-**HOBDIMe**$^+$) derivatives.

Experimental

The GFP chromophore *(p*-hydroxybenzylideneimidazolinone, *p*-**HOBDI**) was synthesized according to ref. 24. The synthesis and characterization of its *O*-methylated derivative (*p*-**MeOBDI**) and *N*-methylated derivative (*p*-**HOBDIMe**$^+$) have been described previously.[25] The syntheses of the meta analogues, 4-(3-Hydroxybenzylidene)-1,2-dimethyl-imidazolinone (*m*-**HOBDI**) and 4-(3-Methoxybenzylidene)-2-methyl-oxazalone (*m*-**MeOBDI**), have also been reported recently.[23] Acetonitrile (MeCN) and methanol (MeOH) solvents (spectrophotometric grade) were purchased from Aldrich.

Acid and alkaline aqueous solutions were prepared from distilled and deionized water and redistilled perchloric acid (99.999%, Aldrich) and potassium hydroxide pellets (99.99%, Aldrich).

Ultraviolet-visible (UV-Vis) spectra were obtained on a Perkin Elmer Lambda 19 spectrophotometer. All emission data were collected on a SPEX Fluorolog spectrofluorometer at room temperature and corrected to the emission of a NIST tungsten lamp.

For fluorescence lifetime measurements, we have used a FOG-100 fluorescence up-conversion system from CDP Systems (Moscow, Russia) pumped by a Clark MXR CPA 2000 amplified laser system followed by a TOPAS optical parametric amplifier from Light Conversion (Lithuania). The FOG-100 is an up-conversion system for femtosecond and picosecond fluorescence lifetimes that has been adapted to match our femtosecond amplifier system operating at 1 kHz pulse repetition rate with laser output at 780 nm and 150 fs pulse width or for the tunable excitation wavelengths from the OPA. The time-resolution of the system was analyzed by the rise time of zinc porphyrin fluorescence and by crosscorrelation of the pump and gate pulse. Both methods revealed a 180-200 fs time resolution, depending on the day-to-day compression of the amplified laser pulses. The excitation wavelength was 390 nm.

The femtosecond transient absorption setup has been already described.[26] Briefly, it involves a 1 kHz Ti-sapphire laser system based upon a Coherent (MIRA 900D) oscillator and a BM Industries (ALPHA 1000) regenerative amplifier. Pump excitation at 380 nm was obtained by frequency doubling the Ti-sapphire fundamental tuned at 760 nm (0.3 mm BBO crystal). The pump pulse (~90 fs) power was limited to 2-6 μJ per pulse (0.2-0.6 mJ/cm^2). A white light continuum probe pulse was generated at 760 nm in a CaF_2 plate. The pump-probe polarization configuration was set at the magic angle. The probe pulse was delayed in time relative to the pump pulse using an optical delay line (Microcontrol Model MT160-250PP driven by an ITL09 controller, precision ±1 μm).

The overall time resolution (full-width at half maximum, fwhm, of the pump-probe intensity cross correlation) was estimated to be about 250 fs from the two-photon (pump + probe) absorption signal in pure hexane. The time dispersion of the continuum light over the 400-700 nm region of analysis was about 300 fs. The transmitted light was analyzed by a CCD optical multichannel analyzer (Princeton Instrument LN/CCD-1340/400-EB detector with ST-138 controller). Sample solutions (0.25-1.0 mM) were circulating in a flow cell with 2 mm optical path length. Data were accumulated over 3 min (~180000 pump-probe sequences). The characteristic times related to the spectral changes were obtained from exponential fit of the observed kinetics and convolution with the instrument response function.

Results

Acid/base and stationary optical properties

The parent **HOBDI** molecules have two protonation sites that are involved in ground-state acid-base interactions, the phenolic oxygen and the imidazolinone nitrogen. The former is replaced in the **MeOBDI** derivatives; the latter is replaced in the *p*-**HOBDIMe**$^+$ derivative. The pK_a measured by spectrophotometric titration for *m*-**MeOBDI** in MeOH-water (1/1 vol) is compared in *Table 7.1* with pK_a values reported previously[23,25] for the other compounds in the same solvent mixture.

Table 7.1. pK_a values in methanol/water (1/1 vol.) solution

	pK_a (NH^+/N)	pK_a (OH/O^-)
***m*-HOBDI**	2.1	9.5
***m*-MeOBDI**	1.7	-
***p*-HOBDI**	2.36	8.53
***p*-MeOBDI**	2.76	-
***p*-HOBDIMe$^+$**	-	6.48

The deconvoluted UV-vis absorption spectra of the corresponding neutral, protonated, and/or deprotonated species are shown in *Figure 7.2* for all molecules. UV-

vis spectra recorded in CH_3CN and CH_3OH are similar to those obtained for the neutral species in MeOH-water. The notable red shift of the lowest energy absorbance band of the para compounds upon *N*-protonation or hydroxyl deprotonation are indicative of enhanced electronic conjugation in the ionic states compared to the neutral molecules. As expected, the *p*-**HOBDIMe**$^+$ quaternized cation and the *N*-protonated cationic forms of *p*-**HOBDI** and *p*-**MeOBDI** (green trace in *Figures 7.2* E, C, D, respectively) have close absorption maxima. Also, the maximum shift is observed for the deprotonated, zwitterionic form of *p*-**HOBDIMe**$^+$ at basic pH (blue trace in *Figure 7.2*E). In contrast, for the meta compounds, the dominant absorbance of the neutral and ionic states closely overlap. The *m*-**HOBDI** anion shows an additional weaker band on the lowest energy side. Similar band splitting has been reported for the *meta*-hydroxystilbene anion and ascribed to the mesomeric effect of the phenolate ion on two different charge transfer transitions.[4]

The steady-state emission measured at room temperature for the neutral, cationic and anionic forms of the **HOBDI** and **MeOBDI** compounds are given in *Figure 7.3*. In all cases the fluorescence emission is extremely weak and obscured by Raman scattering. These spectra must be considered with caution. The λ_{max} observed for the neutral (~450 nm) and anionic (~500 nm) forms of *p*-**HOBDI** are consistent with the 450 ± 25 and 490 ± 25 nm values, respectively, reported from low temperature measurements.[27] Special attention must be paid to the *m*-**MeOBDI** compound (trace B) for which the fluorescence band of the neutral form in methanol (λ_{max} ~ 430 nm, dashed line), similar to that in MeCN, is strongly blue-shifted compared with the fluorescence in water at pH 7 (λ_{max} ~ 500 nm, black line). Spectra recorded for a series of methanol-water mixtures as a function of solvent composition (*Figure 7.4*) show the transition from one band to the other with an isoemissive point rather than a continuous frequency shift of the emission band maximum. This behavior indicates clearly that the different emission maxima observed in methanol and water do not result from a solvatochromic effect but reveal the

presence of two different emissive excited singlet states in these two solvents. No pH dependence of the emission properties has been found in the 3-11.5 pH range (*m*-**MeOBDI** decomposes at pH ≥ 12), the characteristic ~430 and ~500 nm emission bands being observed in methanol and water, respectively, in this whole pH domain. In contrast, at pH 0.6, the fluorescence spectrum of the protonated *m*-**MeOBDI** form (λ_{max} ~560 nm, green trace in *Figure 7.3*) is similar in MeOH, water, and MeOH-water solutions (*Figures 7.5* and *7.6*). It is nevertheless different from either of those obtained at neutral pH in methanol and in water. These results are discussed later in the light of the time-resolved spectroscopic data.

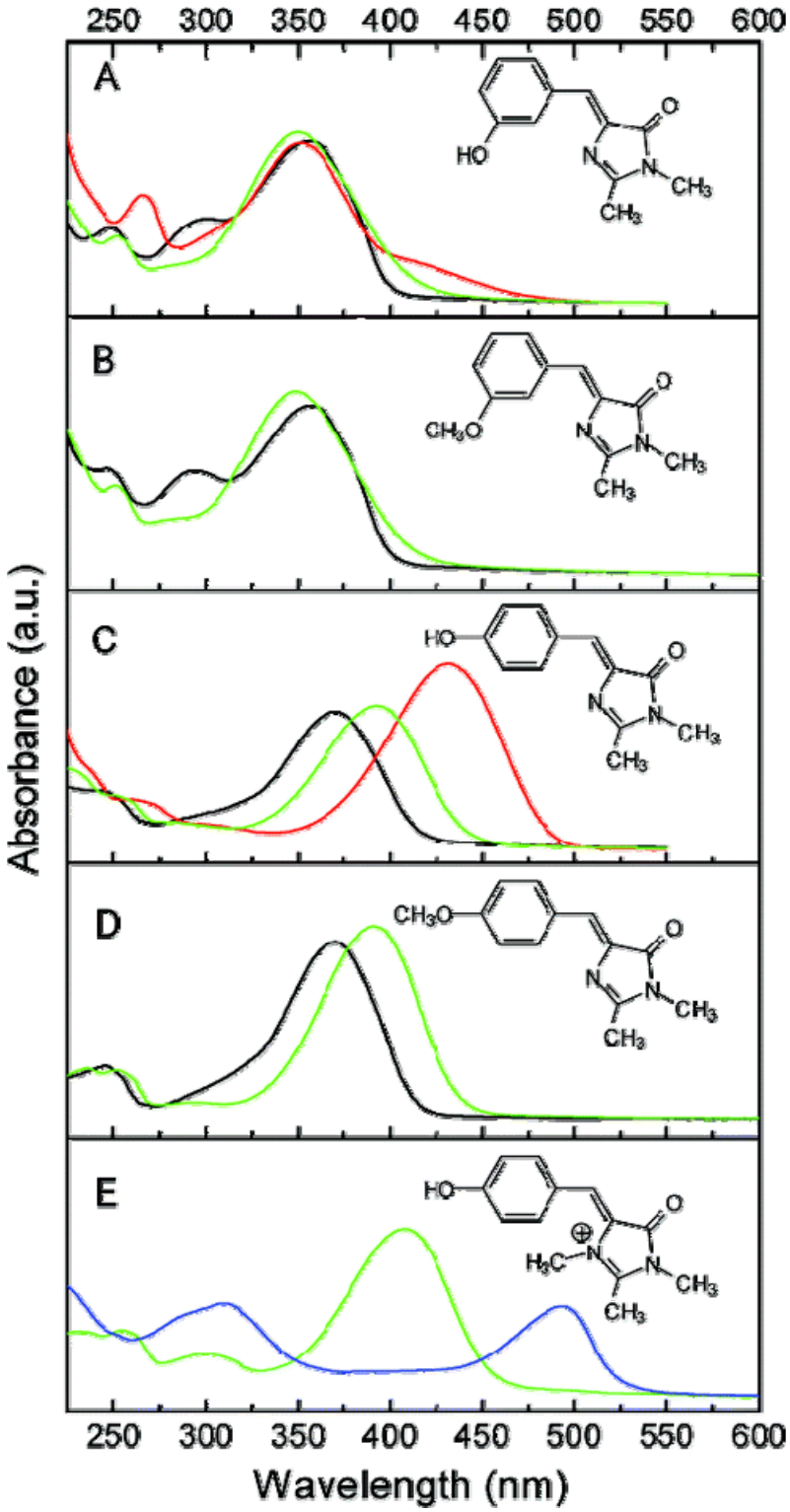

Figure 7.2. UV-vis absorption spectra of the acidic/basic forms of (A) *m*-**HOBDI**, (B) *m*-**MeOBDI**, (C) *p*-**HOBDI**, (D) *p*-**MeOBDI**, and (E) *p*-**HOBDIMe**$^{+}$ in MeOH-water (1/1 vol.). Black trace: neutral form; green trace: cationic form (*N*-protonated or *N*-quaternized species); red trace: anionic form (deprotonated hydroxyl); blue trace: zwitterionic form. Molecular structures of all compounds in their neutral form (p-**HOBDIMe**+) is an intrinsic cation) are presented.

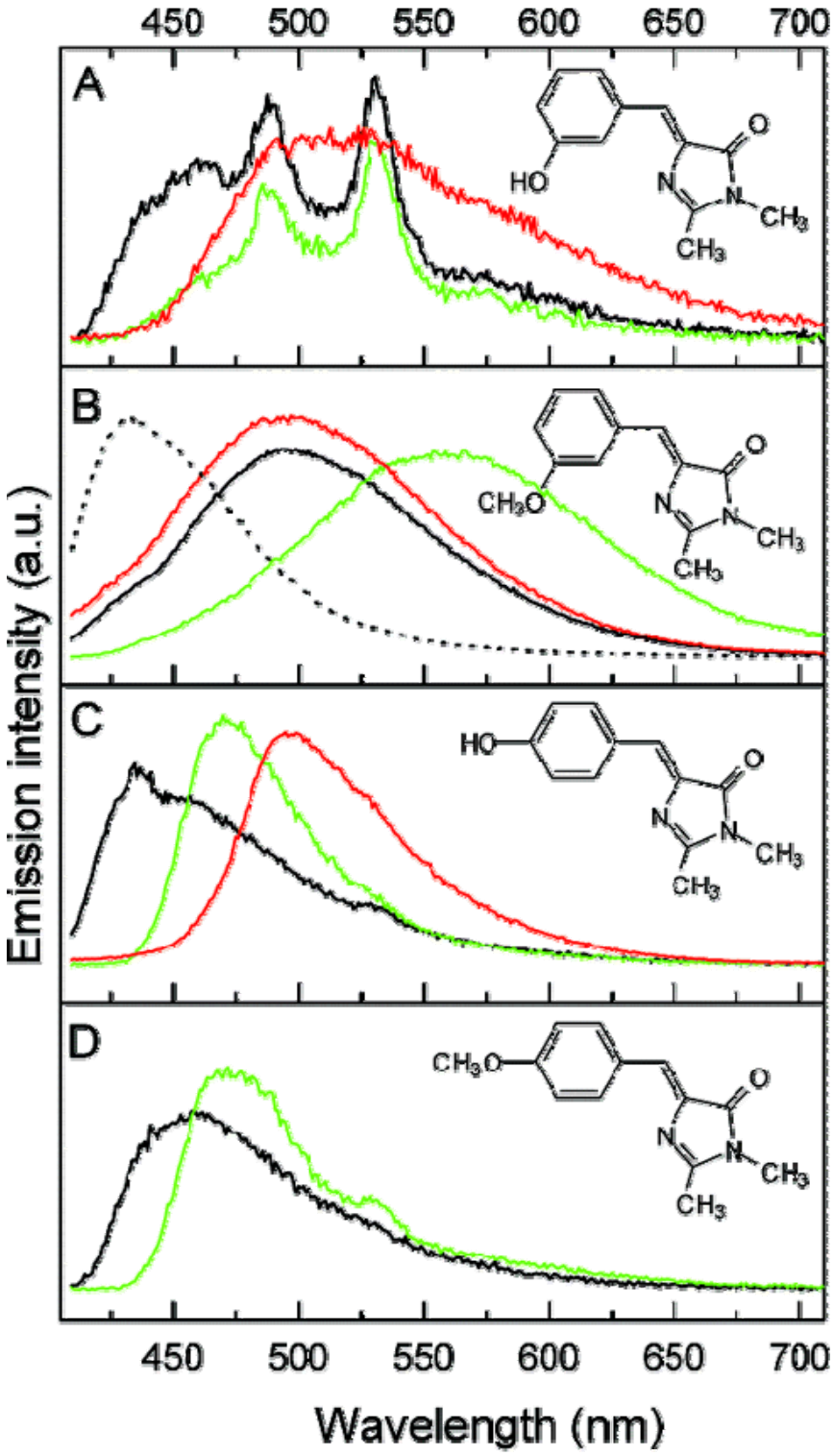

Figure 7.3. Emission spectra of (A) *m*-**HOBDI**, (B) *m*-**MeOBDI**, (C) *p*-**HOBDI**, and (D) *p*-**MeOBDI**. Black trace: MeOH-water (1/9 vol) solution at pH 7, except for *p*-**HOBDI**: MeCN solution; green trace: MeOH-water (1/9 vol) solution at pH 0.6; red trace: MeOH-water (1/9 vol) solution at pH 13 except for *p*-**MeOBDI**: pH 11.5; dashed trace: MeOH.

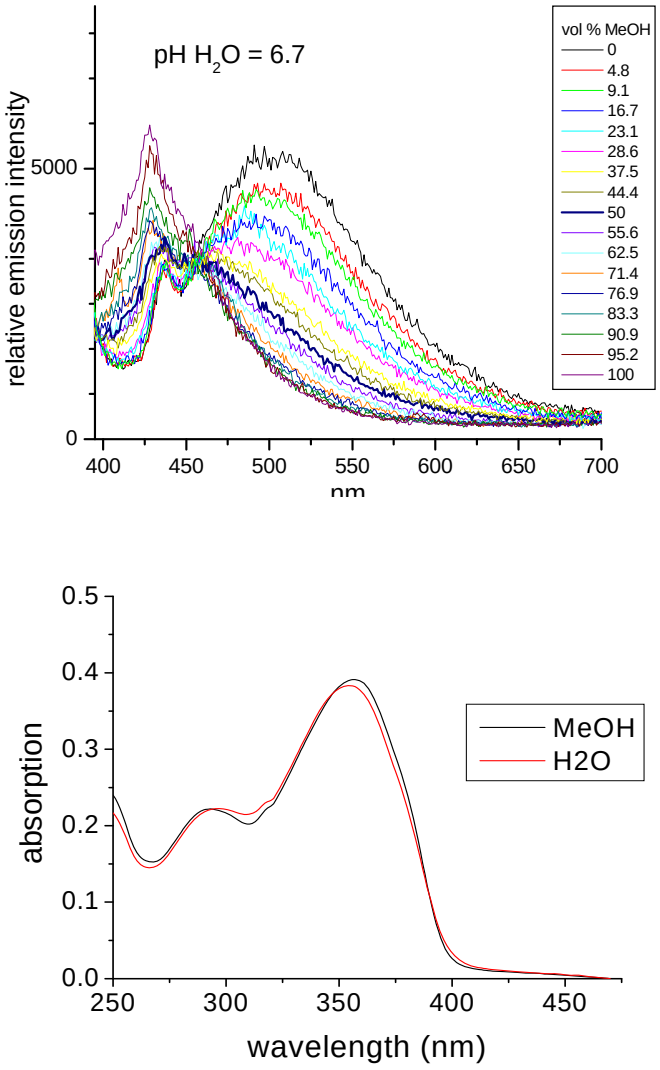

Figure 7.4. Top: Emission of *m*-**MeOBDI** in MeOH-water solution at pH 6.7 as a function of the MeOH content (% v/v); bottom: absorption of *m*-**MeOBDI** in neat MeOH and neat water at pH 6.7.

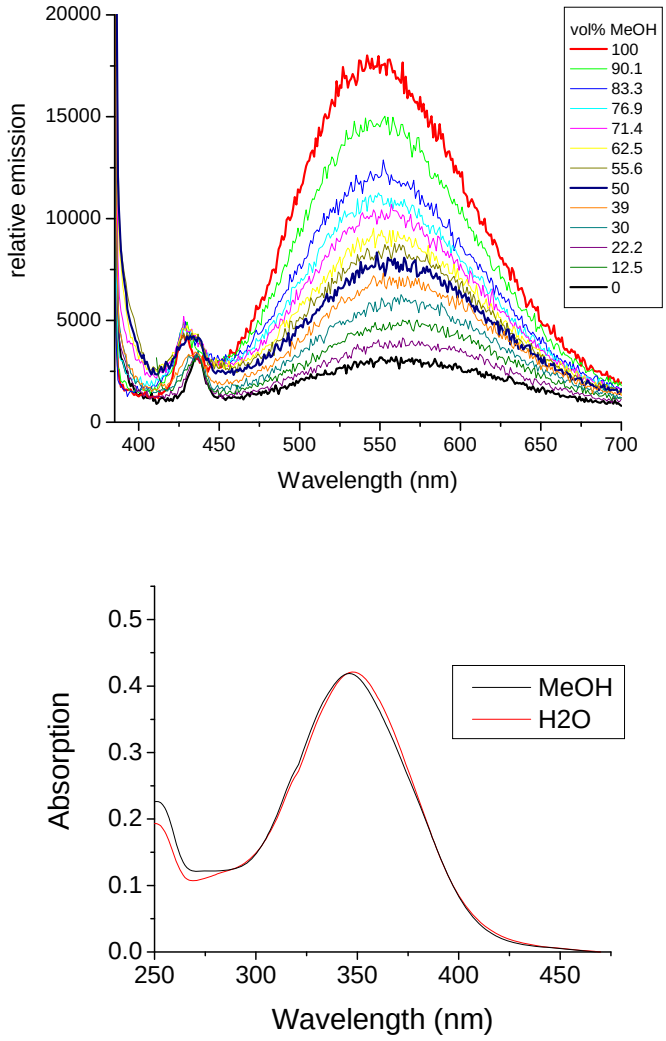

Figure 7.5. Top: Emission of *m*-**MeOBDI** in MeOH-water solution at pH 0.6 as a function of the MeOH content (% v/v); bottom: absorption of *m*-**MeOBDI** in neat MeOH and neat water at pH 0.6.

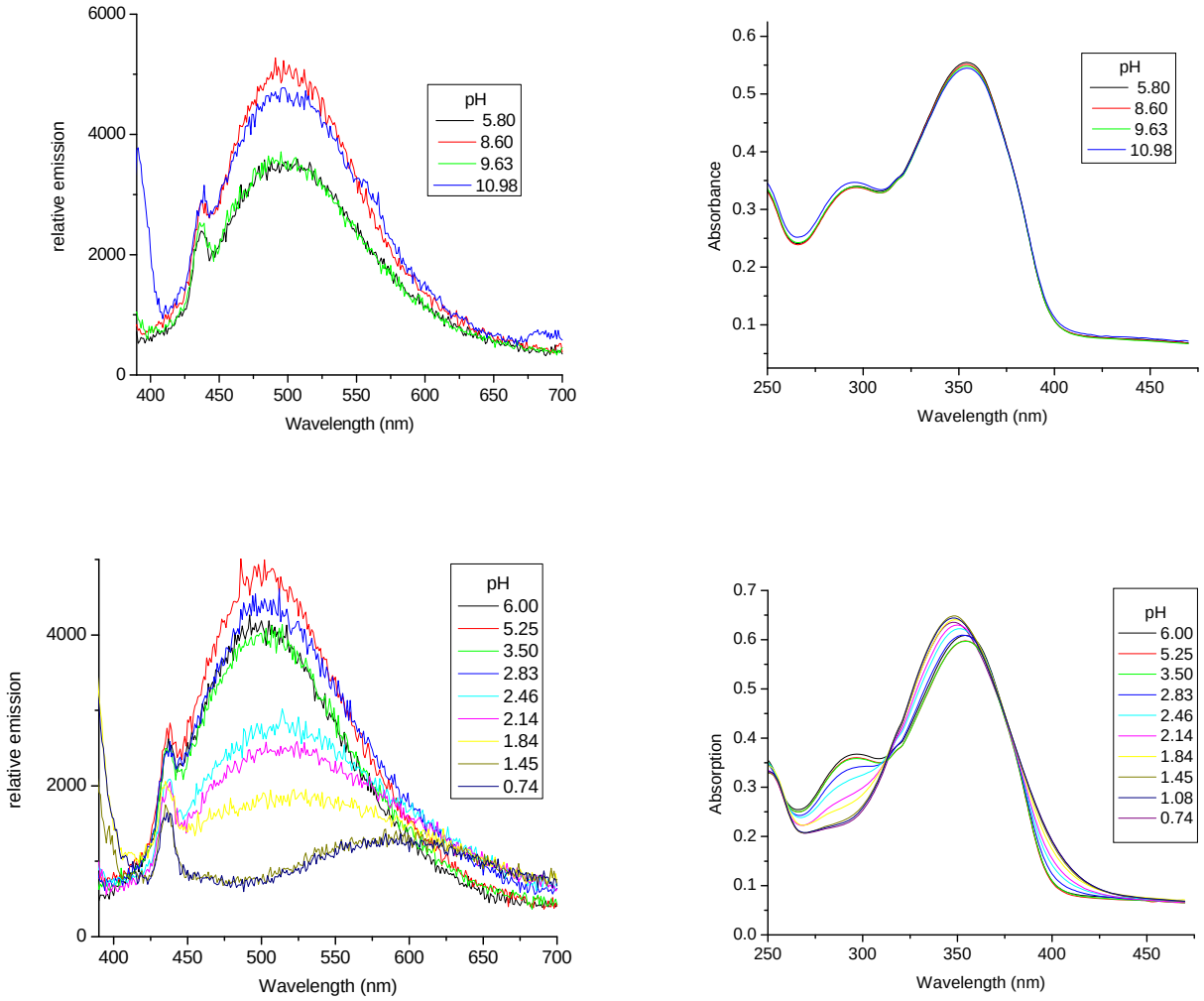

Figure 7.6. Emission (left column) and absorption (right column) of *m*-**MeOBDI** in water at various pH from >11.0 to 5.8 (top) and from 6.0 to 0.74 (bottom).

Transient spectroscopy of the *p*-HOBDI derivatives

Upconversion fluorescence and subpicosecond pump-probe measurements have been performed for ***p*-HOBDI**, ***p*-MeOBDI**, and ***p*-HOBDIMe$^+$** in MeOH, MeCN, and neutral (pH 5.5), acidic (pH 0.6) and basic (pH 11.5-13.0) MeOH-water (1/9 vol) solutions. The fluorescence kinetics, measured at four wavelengths (470, 510, 550, and 590 nm), have been fit to a sum of exponential components and convoluted with the instrument response function. They are characterized by an ultrafast decay in all solvents with time constants nearly independent on the probe wavelength. The decay shows a dominant subpicosecond component (see *Table 7.2*) but, in most cases, is not perfectly single-exponential and is better fit by adding a minor picosecond contribution (≤10%). These observations are in agreement with the results obtained by Mandal et al. for neutral and anionic ***p*-HOBDI** in alcohols and water.[28] In the latter case, from a detailed wavelength-dependent examination of the decay kinetics, the authors interpreted the observed ultrafast excited-state relaxation by a two-state two-coordinate dynamic model of internal conversion induced by isomerization. Our data lead us to generalize the ultrafast character of the excited-state radiationless relaxation to the methoxy and *N*-methyl derivatives. In the case of ***p*-HOBDIMe$^+$**, the measured kinetics have too low signal to noise to extract accurate decay time constants, but the signal has completely disappeared in less than 1 ps.

Pump-probe spectra recorded for ***p*-HOBDI**, ***p*-MeOBDI**, and ***p*-HOBDIMe$^+$** in the 380-700 nm range and in the 0-3 ns time domain following the pump excitation. The transient spectra recorded for the neutral, cationic, and anionic forms of ***p*-HOBDI** in MeOH-water (1/9 vol) solutions (at pH 5.5, 0.6, and 13.0, respectively) are similar to those reported by Vengris et al. in aqueous solutions.[29] The transient spectra measured for the neutral and cationic forms of ***p*-MeOBDI** in MeOH-water solutions appear quite comparable to those of the corresponding ***p*-HOBDI** forms, respectively. For example, *Figure 7.7* compares the spectral evolution observed for the two cations at pH 0.6. As

Table 7.2. Main time constants (ps) measured by upconversion (t_f) and pump-probe absorption (t_A) for *p*-**HOBDI**, *p*-**MeOBDI**, *p*-**HOBDIMe**$^+$, *m*-**MeOBDI** and *m*-**HOBDI** in MeCN, MeOH, and MeOH-water 1/9 vol at different pH.

	p-**MeOBDI**		*p*-**HOBDIMe**$^+$		*p*-**HOBDI**		*m*-**MeOBDI**		*m*-**HOBDI**	
	t_f	t_A	t_f	t_A	t_f [a]	t_A	t_f	t_A	t_f	t_A
MeCN	0.5±0.2	0.7±0.2 10.0±0.5	≤1	0.75±0.3 8.3±0.5	0.3±0.2	0.5±0.2 13.0±0.5	6.1±0.5 (0.85) 18±1	6.0±1.0 18±2	0.7±0.3 (0.3) 8.0±0.5 (0.50) 100±10 (0.2)	0.3±0.2 7.7±1.0 40±5 300±50
MeOH	0.4±0.2	0.5±0.2 5.0±0.5	≤1	[b]	0.3±0.2	0.4±0.2 4.8±0.5	1.5±0.5 (0.6) 6.8±1.0	1.8±0.6 8.5±1.0	0.5±0.2 (0.50) 5±1 (0.31) 33±5 (0.19)	0.7±0.3 5±1 35±5
MeOH-water 1/9(pH 0.6)	0.5±0.2	0.7±0.2 2.6±0.5	≤1	0.55±0.3 2.0±0.4	0.8±0.2	0.5±0.2 4.0±0.5	1.1±0.3 (0.7) 30±3	0.6-1.4 32±3	< 1	0.8±0.2 20±3
MeOH-water 1/9(pH 5.5)	0.3±0.2	0.5±0.2 5.0±0.5	≤1	0.65±0.3 2.0±0.5	0.3±0.2	0.65±0.2 1.8±0.3	0.9±0.3 (0.5) 25±3	1.1±0.3 4 ± 1 27 ± 5 (≥100)	0.5±0.2 (0.87) 2.8±0.4	0.6±0.2 3.2±0.4 (>100)
MeOH-water 1/9 (basic pH)[c]	0.3±0.2	0.5±0.2 5.5±0.5	≤1	0.50±0.3 4.0±1.0	0.8±0.2	0.6±0.2 2.8±0.5	0.8±0.2 (0.4) 25±5	1.2±0.3 4 ± 1 32 ± 5 (≥100)	< 1	0.8±0.3 2.8±0.3

[a] dominant contribution [b] not measured [c] pH =13.0 for *p*-**HOBDI**, *p*-**MeOBDI**, and *m*-**HOBDI**; pH =11.5 for *m*-**MeOBDI**; pH =7.3 for *p*-**HOBDIMe**$^+$

expected, there is no significant difference between spectra recorded in basic and neutral aqueous solution in the case of *p*-**MeOBDI** (*Figures 7.8* and *7.9*). A manifest analogy of *p*-**HOBDI** and *p*-**MeOBDI** is still visible in the pump-probe spectra recorded in MeCN (*Figure 7.10*) and MeOH (*Figure 7.11*). In contrast, the spectral evolution observed for *p*-**HOBDIMe**$^+$ in MeOH-water (1/9 vol.) at pH 5.5 (*Figure 7.12*) is nearly similar to that at pH 0.6 and in MeCN (*Figures 7.13* and *7.14*). It resembles notably that found for the cationic form of *p*-**HOBDI** and *p*-**MeOBDI** at pH 0.6 (*Figure 7.7*). At pH ≥ 8.0, *p*-**HOBDIMe**$^+$ decomposes irreversibly via hydrolysis of imidazolinone ring.[27] Transient spectra obtained at pH 7.0-7.4 (not shown) are extremely weak and noisy ($\Delta OD_{max} \sim 10^{-3}$) due to very inefficient sample excitation by the 380 nm pump light, as expected from the fact that the ground state absorption of the deprotonated, zwitterionic form (tautomer) is red-shifted to 500 nm (see *Figure 7.2*E). Despite this poor spectral quality, a qualitative

analysis of the time evolution is possible and shows first the decay in less than 1 ps of a broad negative band extending from 500 to 650 nm, which leads after complete decay to a weaker transient spectrum comprising a narrow negative component at 480 nm and a positive absorption at 520 nm. Both disappear in about 3 ps.

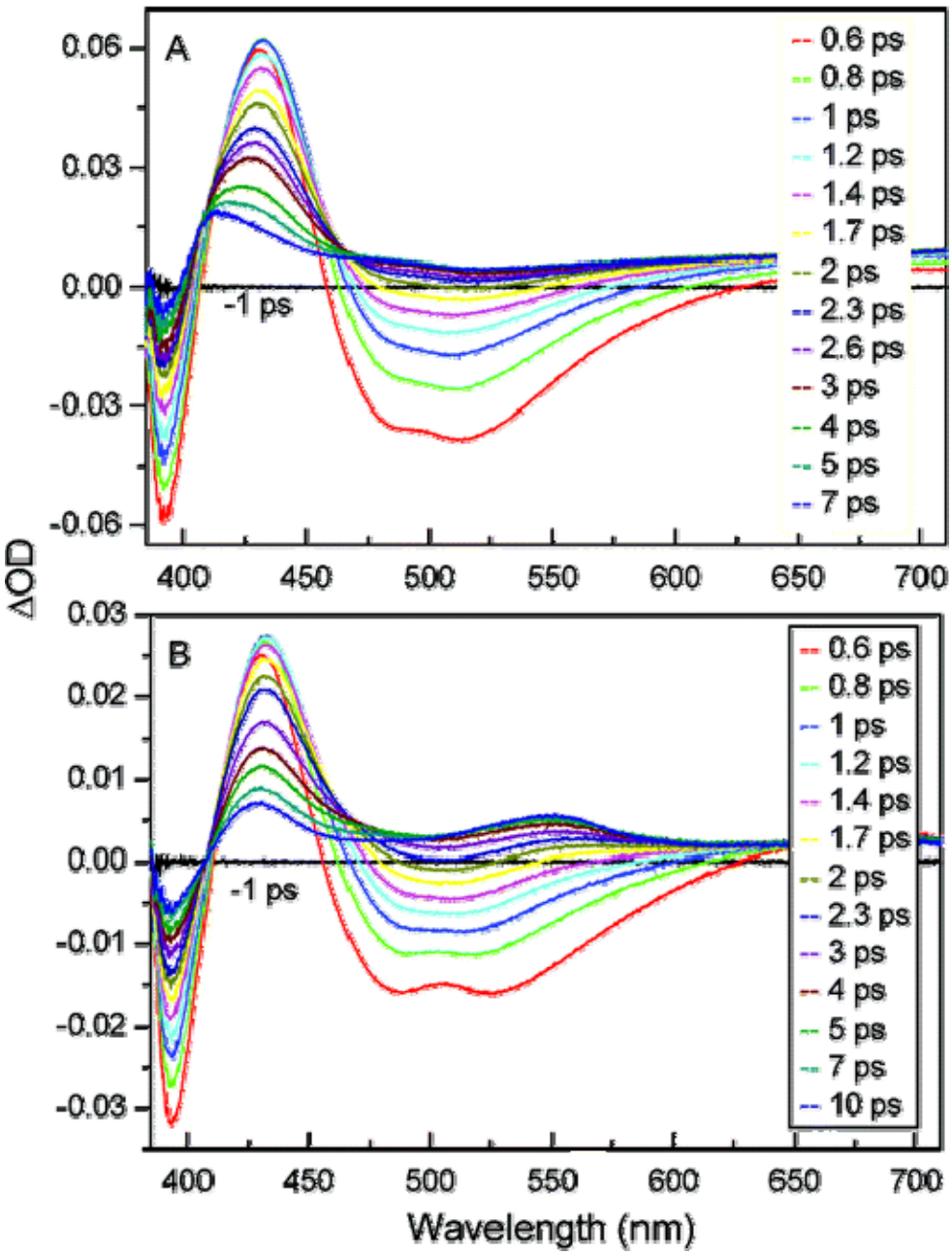

Figure 7.7. Transient absorption spectra of (A) *p*-**HOBDI** and (B) *p*-**MeOBDI** in MeOH-water (1/9 vol.) at pH 0.6 after excitation at 380 nm. The pump-probe time delays are given. The -1 ps trace corresponds to the spectral baseline in the absence of pump excitation.[1]

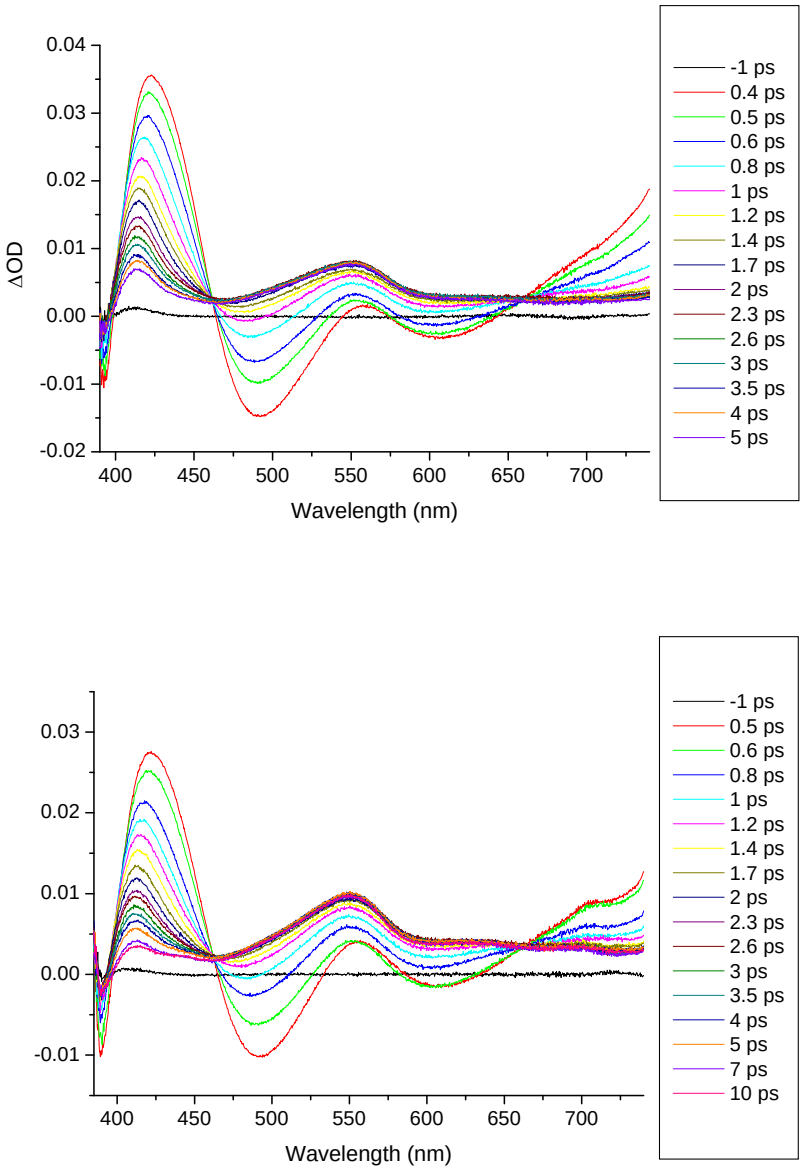

Figure 7.8. Transient absorption spectra of *p*-**MeOBDI** in MeOH-water (1/9 vol.) at pH 5.5 (top) and 13 (bottom) after excitation at 380 nm.[1]

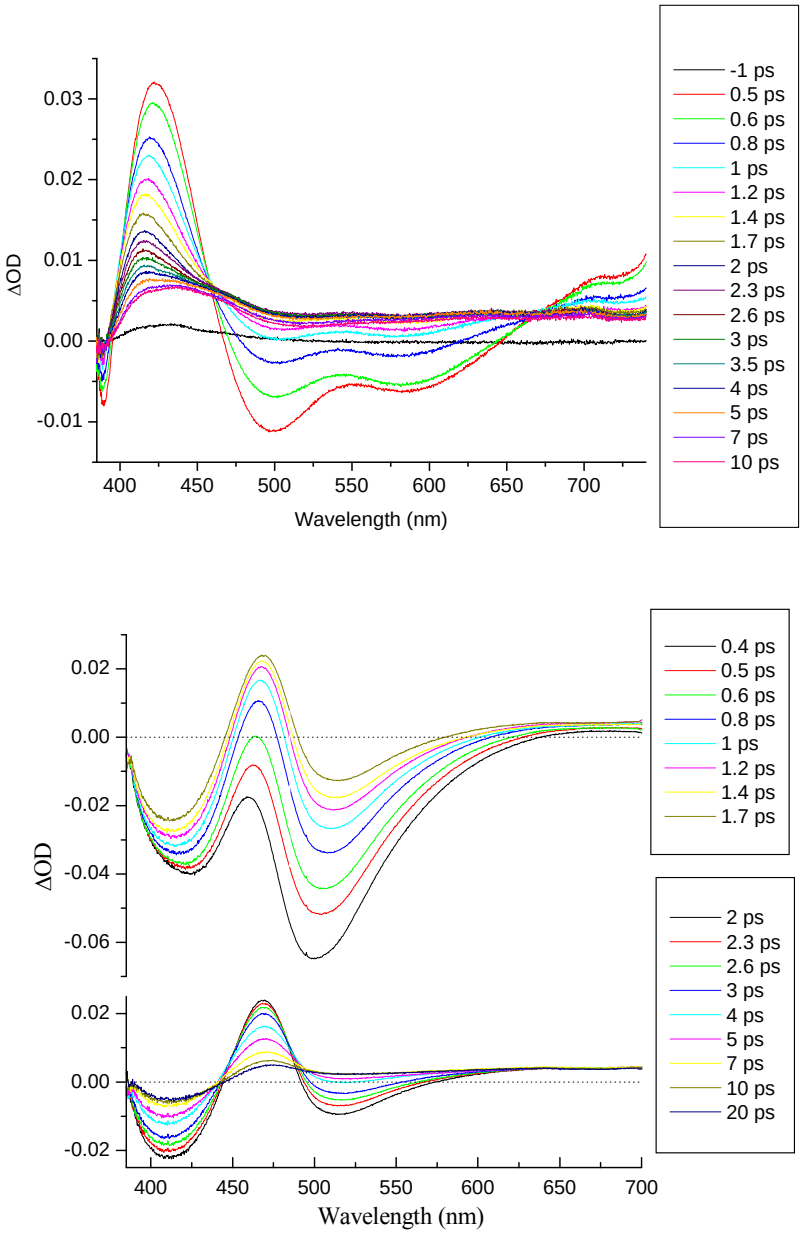

Figure 7.9. Transient absorption spectra of *p*-**HOBDI** in MeOH-water (1/9 vol.) at pH 5.5 (top) and 13 (bottom) after excitation at 380 nm.[1]

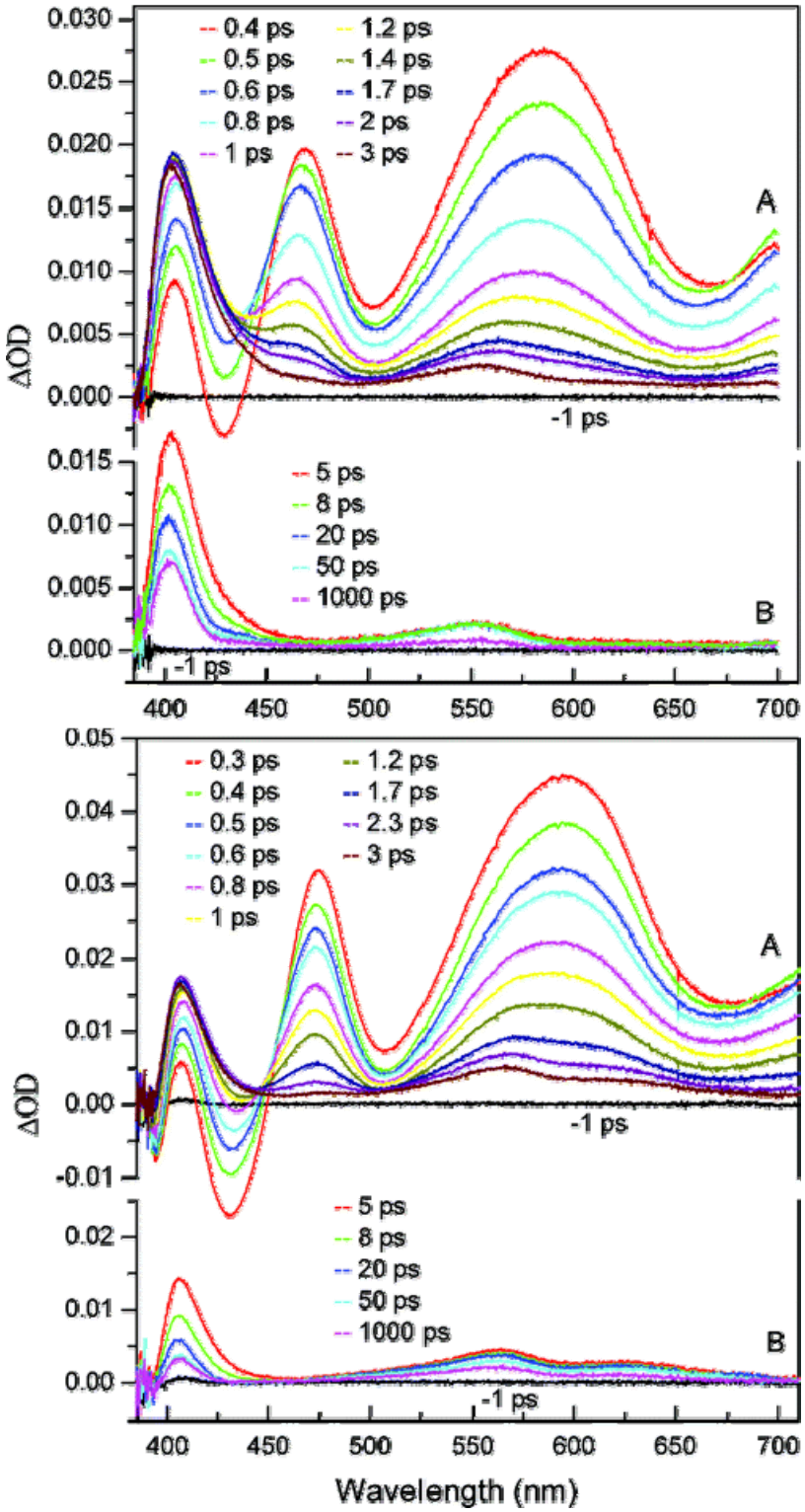

Figure 7.10. Transient absorption spectra of *p*-**HOBDI** (top) and *p*-**MeOBDI** (bottom) in MeCN after excitation at 380 nm. For clarity, the spectral evolution is separated in two time-domains 0-3 ps (A) and 5-1000 ps (B). The pump-probe time delays are given. The -1 ps trace corresponds to the spectral baseline in the absence of pump excitation.[1]

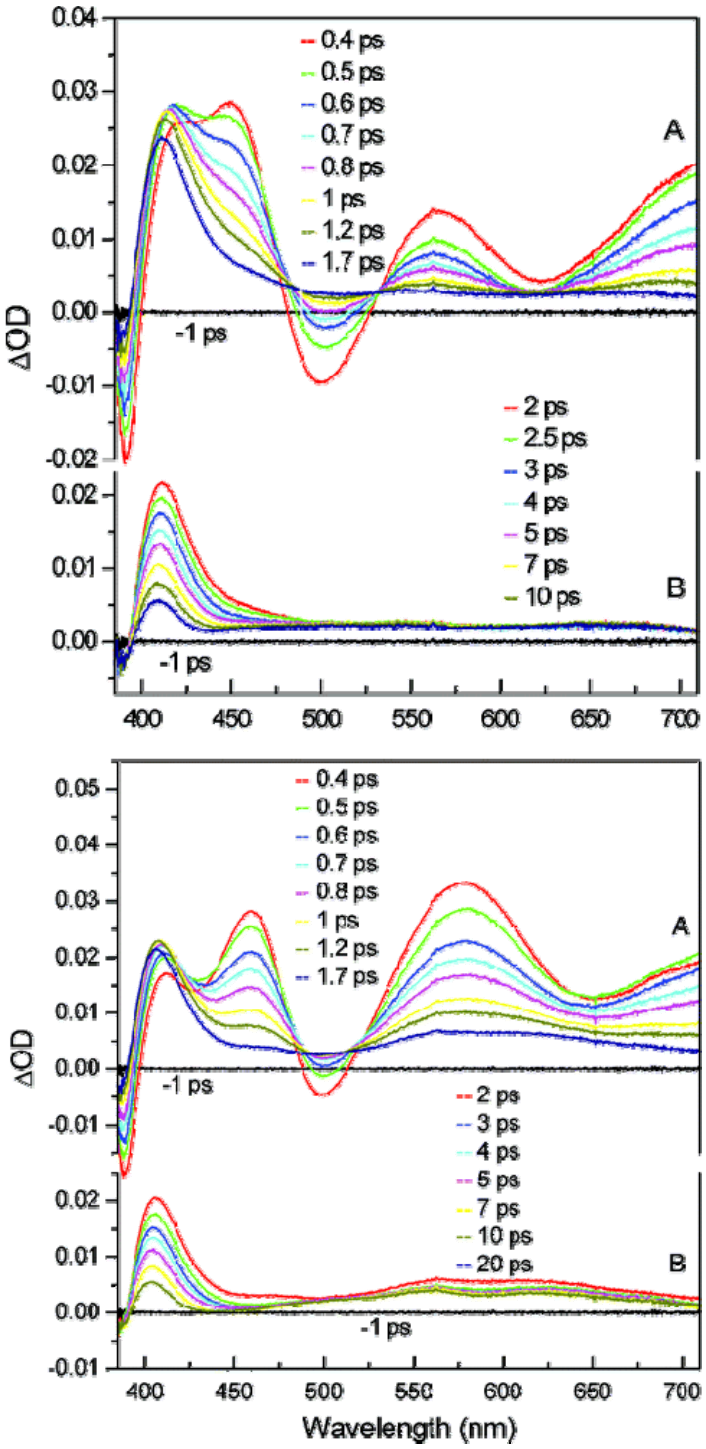

Figure 7.11. Transient absorption spectra of *p*-**HOBDI** (top) and *p*-**MeOBDI** (bottom) in MeOH after excitation at 380 nm. For clarity, the spectral evolution is separated in two time-domains 0-1.7 ps (A) and 2-20 ps (B). The pump-probe time delays are given. The -1 ps trace corresponds to the spectral baseline in the absence of pump excitation.[1]

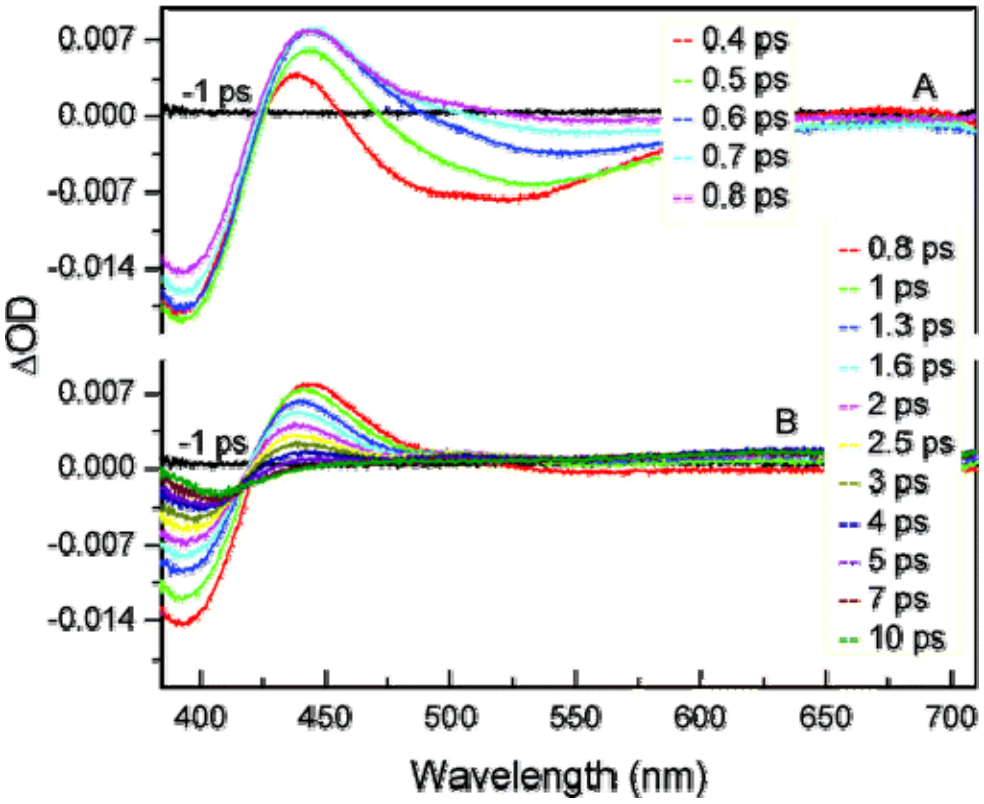

Figure 7.12. Transient absorption spectra of *p*-**HOBDIMe**$^{+}$ in MeOH-water (1/9 vol.) at pH 5.5 after excitation at 380 nm. For clarity, the spectral evolution is separated in two time-domains 0-0.8 ps (A) and 0.8-10 ps (B). The pump-probe time delays are given. The -1 ps trace corresponds to the spectral baseline in the absence of pump excitation.[1]

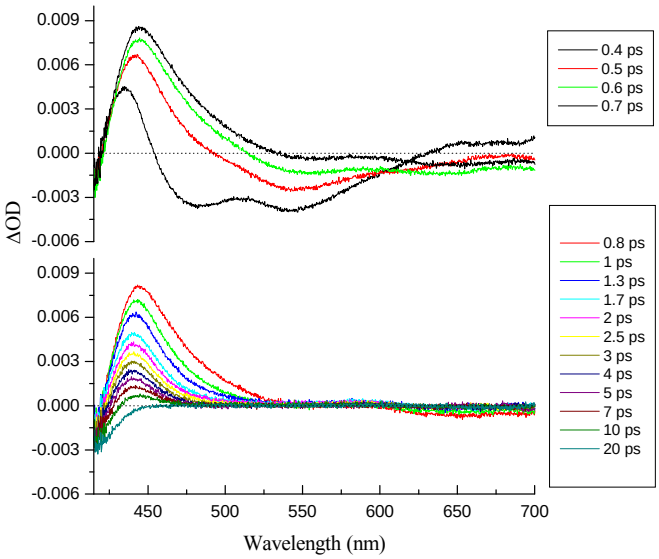

Figure 7.13. Transient absorption spectra of *p*-**HOBDIMe**$^+$ in MeCN after excitation at 380 nm (the probe light is entirely absorbed by the sample in the region below 420 nm).[1]

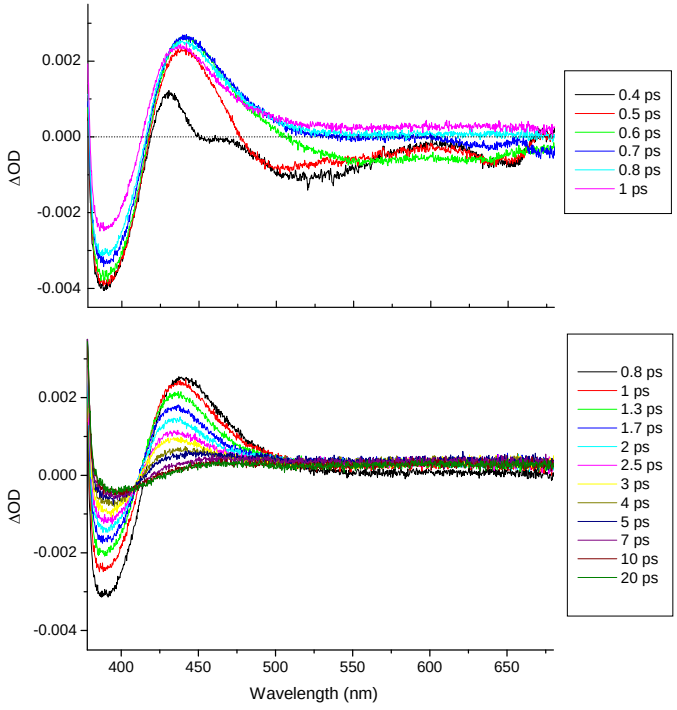

Figure 7.14. Transient absorption spectra of *p*-**HOBDIMe**$^+$ in MeOH-water (1/9 vol) at pH 0.6 after excitation at 380 nm (the probe light is entirely absorbed by the sample in the region below 420 nm).[1]

In all solutions, the pump-probe spectra can be analyzed as the superposition of positive bands due to photoinduced absorption (PA) and of two types of negative bands due to ground state bleaching (GSB) and stimulated emission (SE). The position of the GSB is determined by the ground-state absorption of the solute. According to the reference spectra in *Figure 7.2* (parts C-E), the highest energy negative band observed in almost all the transient spectra in the 385-440 nm domain can be systematically ascribed to GSB. Note that this component appears generally slightly shifted compared with the expected position because it is truncated on its high-energy side, on the one hand, by the presence of an optical filter used in the experimental setup to cut the 380 nm excitation light and, on the other hand, on its low-energy side by the partial overlap with a PA band situated in the vicinity. The transient negative signal observed in the 450-650 nm region is ascribable exclusively to SE, in agreement with the broad fluorescence spectra that extend far in the red region (*Figure 7.3*C, D). The apparent shape of the SE signal is markedly affected by the presence of overlapping PA bands. In the specific case of the zwitterionic form of *p*-**HOBDIMe**$^+$, the red-shift of the ground state absorption at 500 nm incites us to ascribe the above-mentioned narrow negative signal at 480 nm to the GSB and the shorter-lived broad negative band in the 500-650 nm region to the SE. The highly pH-dependent spectroscopic properties of *p*-**HOBDI**, *p*-**MeOBDI**, and *p*-**HOBDIMe**$^+$ [25] (*Figures 7.2* and *7.3*) can account for the notable changes in the general aspect of the pump-probe spectra in aqueous solution at different pHs. More surprising are the large spectral changes observed for the *p*-**HOBDI** and *p*-**MeOBDI** neutral species on changing the solvent from MeCN (*Figure 7.10*) to MeOH (*Figure 7.11*) then to water[29] or MeOH-water solution. Such changes cannot result from modification of the GSB component since only weak solvatochromism effects have been observed for both neutral species.[25] Important solvent dependent modulation of the PA and SE band position and/or relative intensity must probably take place.

Unfortunately, the extremely weak steady-state emission spectra measured in organic solvents are too imprecise to shed light on this problem.

Despite this apparent complexity, a common behavior can be found for all three compounds in all solvents and pHs, with essentially two characteristic times (t_A values in *Table 7.2*) in the spectral evolution that can be associated to two well-distinguished reaction steps. In a first step, a major spectral change occurs with a subpicosecond time constant that matches approximately the main fluorescence decay time (see *Table 7.2*). This change is characterized by the disappearance of the initial PA bands, the major part of the GSB signal, and the SE band. It is thus unambiguously ascribed to the decay of the excited S_1 state and partial repopulation of the ground state. All of the PA bands observed initially in the pump-probe spectra are thus characterizing the S_1 state absorption. In all cases, a new PA component is growing concomitantly with the decay of the S_1 spectrum with comparable subpicosecond time constant. It is positioned systematically to the red side of the GSB, with a λ_{max} that seems to shift together with the GSB on going from the neutral to the different ionic species (c.a. 410-420, 430-445, 470 and 520 nm for the neutral, cationic, anionic, and zwitterionic species, respectively). In a second step, the remaining GSB and new PA bands decay with a time constant of a few picoseconds that has no counterpart in the fluorescence kinetics. The decay of the PA band is accompanied by a notable narrowing of its red wing as if its disappearance were the result of a continuously better overlap with the negative GSB signal. Such behavior is typical of a cooling effect: immediately after the S_1 relaxation; the nascent ground state molecules are vibrationally excited and characterized by an absorption spectrum broader than the GSB spectrum that corresponds to the absorption of the cold ground state population before excitation. The PA component seen to the red edge of the GSB at the end of the S_1 state decay (1-2 ps spectra) is thus confidently ascribed to the broadened absorption of the hot S_0 population. As this population cools down, the PA spectrum narrows and progressively fills up the GSB hole. This assignment is consistent with the correlated PA

and GSB shift effect discussed above. Thus, the two kinetic contributions observed in the pump-probe data characterize the S_1 state decay and subsequent cooling of the hot ground state population, respectively. Finally, one observes that a spectrum persists after the cooling process ($t > 50$ ps) and does not evolve on the probed time window (3 ns). It consists of a weak residual GSB contribution, a PA band around 400 nm, and a very broad and flat absorption covering the whole visible region, with rough maxima around 650 nm in methanol and 700 nm in methanol/water solutions and at $\geq$ 700 nm in acetonitrile. These spectral characteristics are typical of the solvated electron,[30,31] which suggests that the ~400 nm residual PA band could be due to the cation radical produced from ionization.

Transient spectroscopy of *m*-MeOBDI

Upconversion fluorescence kinetics of ***m*-MeOBDI** were measured in MeOH, MeCN, and neutral (pH 5.5) and acidic (pH 0.6) MeOH-water (1:9 vol) solutions, at four wavelengths (480, 510, 550, and 590 nm). All decays are nonsingle exponential and can be satisfactorily fitted to a sum of two exponential components. The corresponding time constants t_f determined from this analysis are reported in *Table 7.2*.

The pump-probe absorption spectra of ***m*-MeOBDI** in MeOH and MeCN, displayed in *Figure 7.15* (parts A and B, respectively), are quite broad and cover the whole 400-725 nm region, with two overlapping PA bands at 460-470 and 640-645 nm. Such broadness contrasts with the well-structured pump-probe spectra that characterize the para compounds. Similar broadening effects on going from para to meta isomers have been observed within the family of hydroxystilbenes.[5] As suggested in the latter case, the broader PA spectrum of *meta*- vs. *para*-**MeOBDI** may be attributed to the presence of rotamers and/or to a symmetry lowering effect. The transient spectrum decays completely and uniformly with two-exponential kinetics characterized by time constants of 1.8 ± 0.6 and 8.5 ± 1 ps in MeOH and 6 ± 1 and 18 ± 2 ps in MeCN, close to the decay times

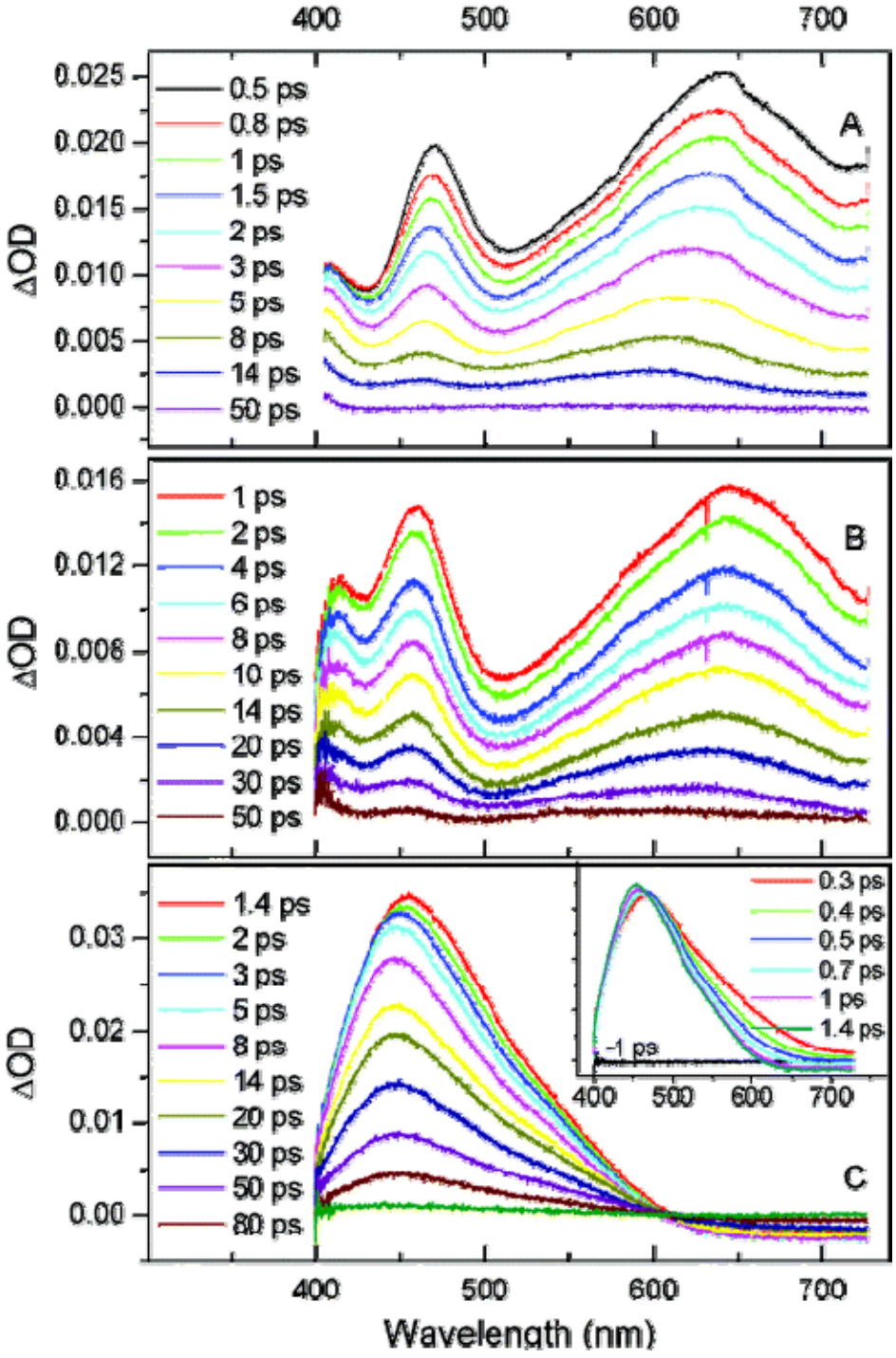

Figure 7.15. Transient absorption spectra of *m*-**MeOBDI** in MeOH (A), MeCN (B) and MeOH-water (1/9 vol) at pH 0.6 (C) after excitation at 380 nm. The pump-probe time delays are given. For clarity, the shortest time delay spectra in part C are shown in inset. The -1 ps trace corresponds to the spectral baseline in the absence of pump excitation.[1]

measured for the fluorescence emission (see *Table 7.2*). A narrow dip situated around 430 nm corresponds to the position of the fluorescence emission in nonaqueous solvents and is probably due to the SE. Therefore, in both solvents, the transient absorption signal is entirely ascribable to the excited S_1 state of the *m*-**MeOBDI** neutral form. As in the *p*-**HOBDI** derivatives, the S_1 state of *m*-**MeOBDI** disappears entirely without giving rise to the triplet state or any perceptible photoproduct. By analogy with the excited-state dynamics of the para derivatives, the S_1 decay can be assumed to be due to efficient IC promoted by the twisting motion around the exo-methylene double bond. Interestingly, the quenching dynamics is much slower than the <1 ps deactivation found for the *para* derivatives (time t_f, in *Table 7.1*). This observation reveals that, in the meta compound, a significant potential barrier must exist on the excited-state surface along the reaction coordinate toward the IC region, whereas no significant barrier was ascertained for the para molecules.[28,29] Finally, it can be seen that, simultaneously to the absorption decay, a 40 nm hypsochromic shift of the 640 nm PA band arises within the first 15 ps in MeOH but not in MeCN. This solvent-specific band shift probably reflects some effect of solvation dynamics of the S_1 state by H-bonding.

In part C of *Figure 7.15*, the pump-probe spectra of the cationic form of *m*-**MeOBDI** in MeOH-water (1/9 vol) at pH 0.6 are displayed. The measured kinetic characteristics are reported in *Table 7.2*. The short-time spectrum (0.3 ps) shows a broad PA band peaking at 468 nm that narrows and shifts to 448 nm in the first 5 ps, then decays with a single-exponential kinetics of time constant 32 ps consistent with the longer emission decay time (30 ps). A negative signal at wavelengths longer than 610 nm, that also decays with comparable kinetics (29.5 ps), corresponds to a SE contribution. In fact, the emission spectrum of the cationic form of *m*-**MeOBDI** shows a long tail that extends beyond 700 nm (see part B in *Figure 7.3*). At λ<610 nm, the SE signal is masked by the strong PA band. The initial narrowing and band shift kinetics can be fit to single exponentials of time constants 0.6 and 1.4 ps, respectively. These spectral rearrangements

can be accounted for to solvation and vibrational relaxation processes. They probably correspond to the shorter emission decay time (2 ps). Therefore, the data indicate clearly that the pump-probe evolution in acidic pH is essentially characterizing the S_1 state dynamics of the *m*-**MeOBDI** cationic form. The disappearance of S_1 does not lead to the growth of any perceptible photoproduct. As in nonaqueous solvents, the excited-state decay is thus likely due to radiationless quenching induced by isomerization, with a reaction barrier still higher than in the case of the neutral derivative.

The spectral evolution observed from pump-probe measurements in neutral 1/9 MeOH-water solution (*Figure 7.16*) is quite different from that in organic solvents. Yet, at short time (0.5 ps), the transient spectrum shows some resemblance with that obtained in MeOH and MeCN, with a broad PA band at about 600 nm and a second PA at 415 nm. The main difference is the absence of SE contribution at 430 nm, in agreement with the fact that the fluorescence band is shifted to 500 nm in water (see *Figure 7.3*). The initial transient spectrum in 1/9 MeOH-water can thus be reasonably ascribed to the excited S_1 state of the neutral form of *m*-**MeOBDI**, as in organic solvents. In contrast to what was observed in MeOH and MeCN, this spectrum decays with a time constant of 1.1 ± 0.3 ps to yield a new spectrum characterized by a broad and rather flat PA band extending from 400 to 600 nm and showing a slight maximum at 465 nm. Two approximate isosbestic points can be seen at 453 and 530 nm. This spectrum maximizes at 3 ps and disappears with multiexponential kinetics involving at least three time constants. The shorter one, 4 ± 1 ps, has significant contributions in the band edges kinetics, below 450 nm and above 600 nm, and characterizes a band narrowing effect. It is likely reflecting some solvation or vibrational relaxation dynamics. It is followed by a main decay component of 27 ± 5 ps and a weaker, very inaccurate component at ≥100 ps. The above 1.1 and 27 ps kinetics match the 0.9 and 25 ps fluorescence decay times. This correlation indicates that the transient species arising from the initial S_1 state is also an emitting species and must

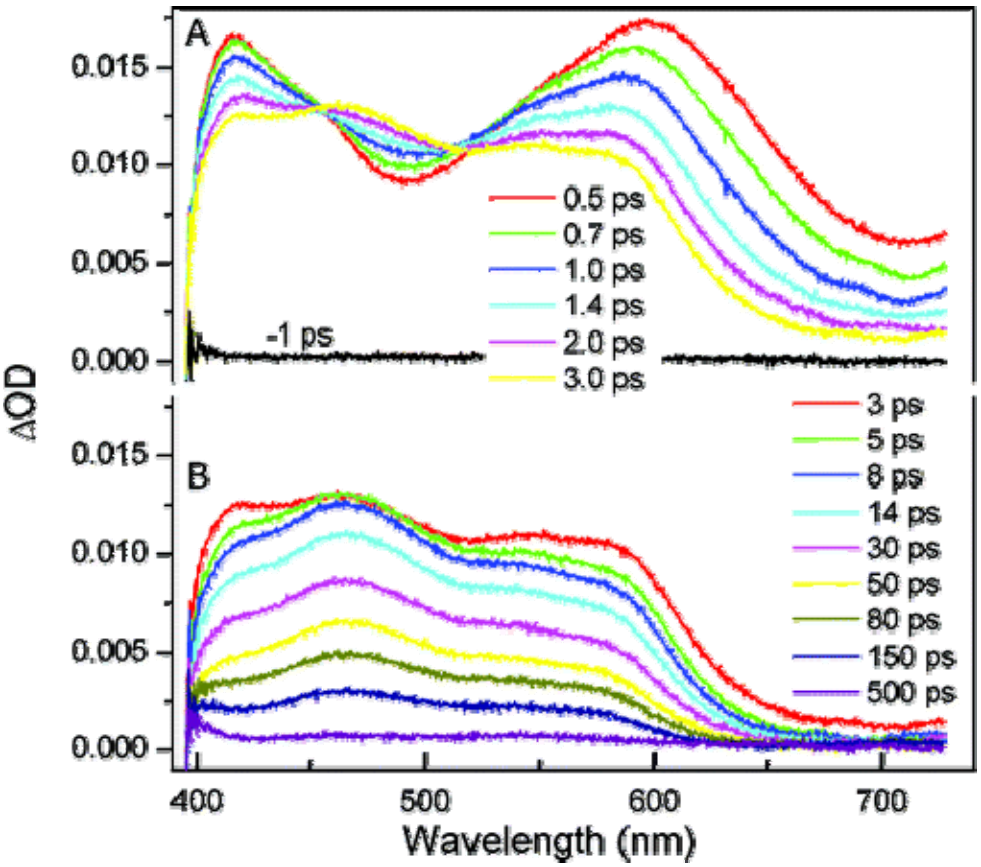

Figure 7.16. Transient absorption spectra of *m*-**MeOBDI** in MeOH-water (1/9 vol) at pH 5.5 after excitation at 380 nm. For clarity, the spectral evolution is separated in 2 time domains 0-3 ps (A) and 3-500 ps (B). The pump-probe time delays are given. The -1 ps trace corresponds to the spectral baseline in the absence of pump excitation.[1]

correspond to a second type of excited singlet state, S_1'. This excited state S_1' is thus produced specifically in the presence of water.

To get more information on this fast reaction process in aqueous solution, we have performed pump-probe measurements of *m*-**MeOBDI** in various MeOH-water solutions of 1/9, 1.5/8.5, 2/8, 2.5/7.5, 3.5/6.5, and 5/5 vol compositions, respectively, at a constant pH of 5.5. As an example, *Figure 7.17* presents some typical spectra recorded for the 3.5/6.5 MeOH-water mixture. We have also done measurements on 1/9 and 1.5/8.5 mixtures at pH 11.5 (*Figure 7.18*). The data obtained at pH 5.5 show that the short-time spectral evolution characterizing the $S_1 \rightarrow S_1$' reaction decreases gradually in amplitude upon increasing the MeOH content, though keeping a nearly constant kinetics of about 1 ps, and is progressively replaced by a second spectral evolution, close to that observed in pure MeOH, to which it is superimposed. At a MeOH-water composition of 3.5/6.5 (*Figure 7.17*), the initial transient spectrum (0.5 ps) shows clearly a superposition of the two PA bands at 415 and 450 nm characteristic of the S_1 state spectra in 1/9 MeOH-water and in neat MeOH, respectively. The dynamics of the $S_1 \rightarrow S_1$' process is so weak that the appearance of the S_1' spectrum is almost hidden and only perceived as a nearly flat plateau in the time evolution in the 0-6 ps time domain around 480 nm. However, at long time delay (in the 20-240 ps region), the spectral evolution is rather dominated by the decay of the S_1' spectrum, as in 1/9 MeOH-water solution, which is consistent with the fact that the S_1 decay in MeOH is almost completed (see *Figure 7.15*, part A). This trend is still more apparent in the spectra recorded for the 5/5 solvent mixture, where the $S_1 \rightarrow S_1$' process is barely discernible. Finally, no significant difference in the spectral features as well as the kinetics could be noticed when increasing the solution pH from 5.5 to 11.5.

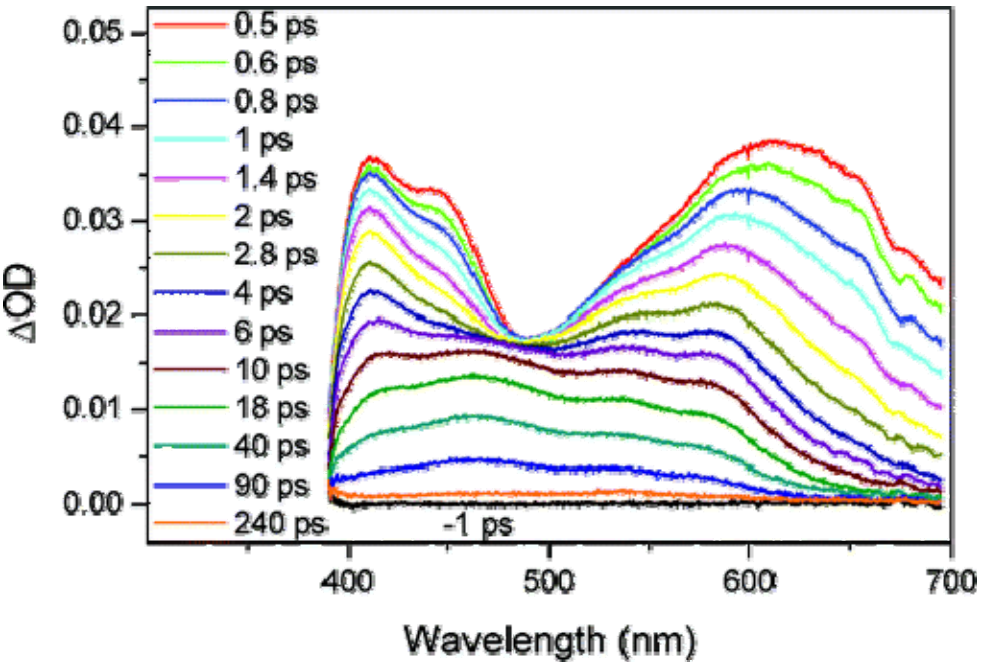

Figure 7.17. Transient absorption spectra of *m*-**MeOBDI** in MeOH-water (3.5/6.5 vol) at pH 5.5 after excitation at 380 nm. The pump-probe time delays are given. The -1 ps trace corresponds to the spectral baseline in the absence of pump excitation.[1]

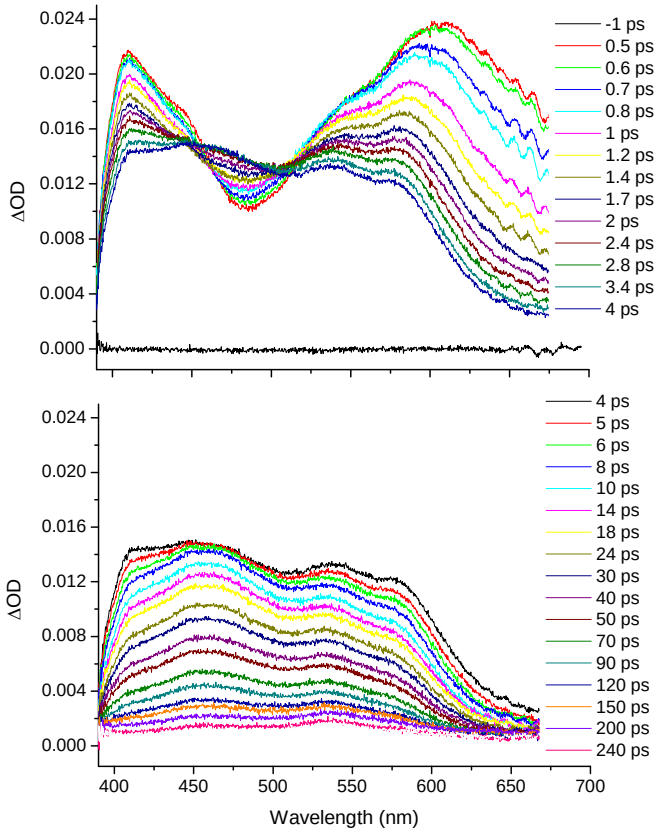

Figure 7.18. Transient absorption spectra of *m*-**MeOBDI** in MeOH-water (1/9 vol) at pH 11.5 after excitation at 380 nm.[1]

Transient spectroscopy of *m*-HOBDI

The fluorescence kinetics measured for ***m*-HOBDI** in MeOH, MeCN, and neutral (pH 5.5), acidic (pH 0.6) and basic (pH 13) MeOH-water (1/9 vol) solutions, at four wavelengths (480, 510, 550, and 590 nm). Typical examples of data for ***m*-HOBDI** in MeOH, MeCN, and MeOH-water at pH 5.5 are displayed in *Figure 7.19*. Decay kinetics in organic solvents can be approximately fit to a sum of two exponential components but the involvement of a third component improves slightly the fit in the 3-20 ps time domain. In aqueous solution, a two-exponential decay is observed at neutral pH. At acidic and basic pHs, the decay is ultrafast (< 1 ps), but no precise constant value can be extracted as the transient emission is very weak. The corresponding time constants are reported in *Table 7.2*.

The pump-probe absorption spectra of ***m*-HOBDI** show quite similar evolution in MeOH (*Figure 7.20*, part A) and MeCN. As for ***m*-MeOBDI**, the short-time spectrum is characterized by two broad PA bands that cover the whole 400-725 nm region (λ_{max} in the ~480 and 600-650 nm regions) and decay with multiexponential kinetics (see *Table 7.2*). Despite this complex kinetics and although slight band shifts are noticeable as the decay proceeds, this spectrum keeps a roughly unchanged global shape and is likely characterizing the same transient species during the whole decay. It is readily ascribed to the excited S_1 state of the neutral ***m*-HOBDI** molecule that decays without giving rise to any photoproduct. The kinetic fits involve the sum of three exponential components in MeOH and four components in MeCN with relative weights depending on the wavelength. This complex behavior may be a consequence of the presence of several relaxation processes such as solvation and vibrational relaxation concomitant to the S_1 state depopulation process, as evidenced by Vengris et al.[29] and by some of us[8] for ***p*-HOBDI**. It may also be partially accounted for to the presence of rotamers, suggested by the broadness of the PA spectrum, having slightly different decay characteristics. The

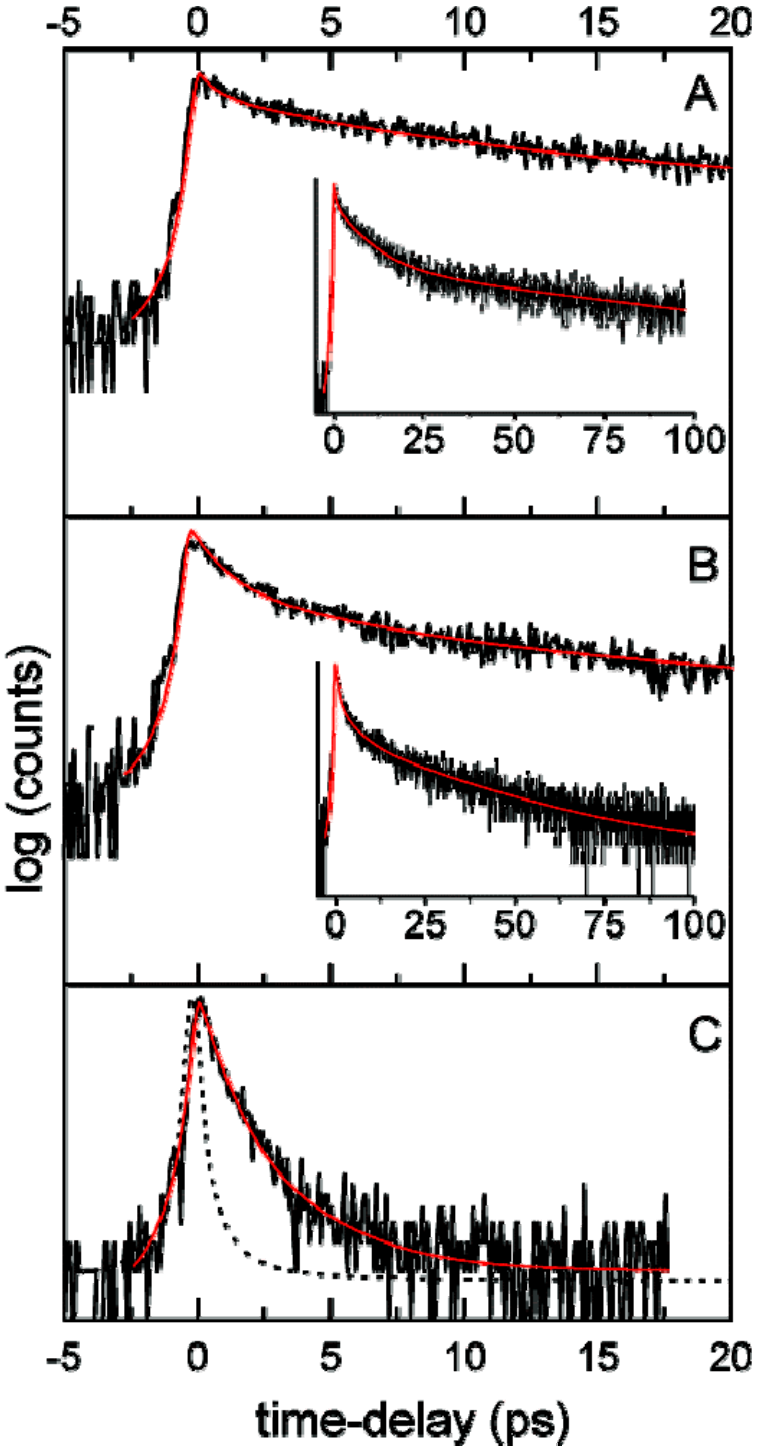

Figure 7.19. Up-conversion data for *m*-**HOBDI** in MeOH (A), MeCN (B), and MeOH-water (1/9 vol) at pH 5.5 (C) at 550 nm. The instrument response function (dashed line) and best fits to a sum of exponential components (red lines) are also shown. [1]

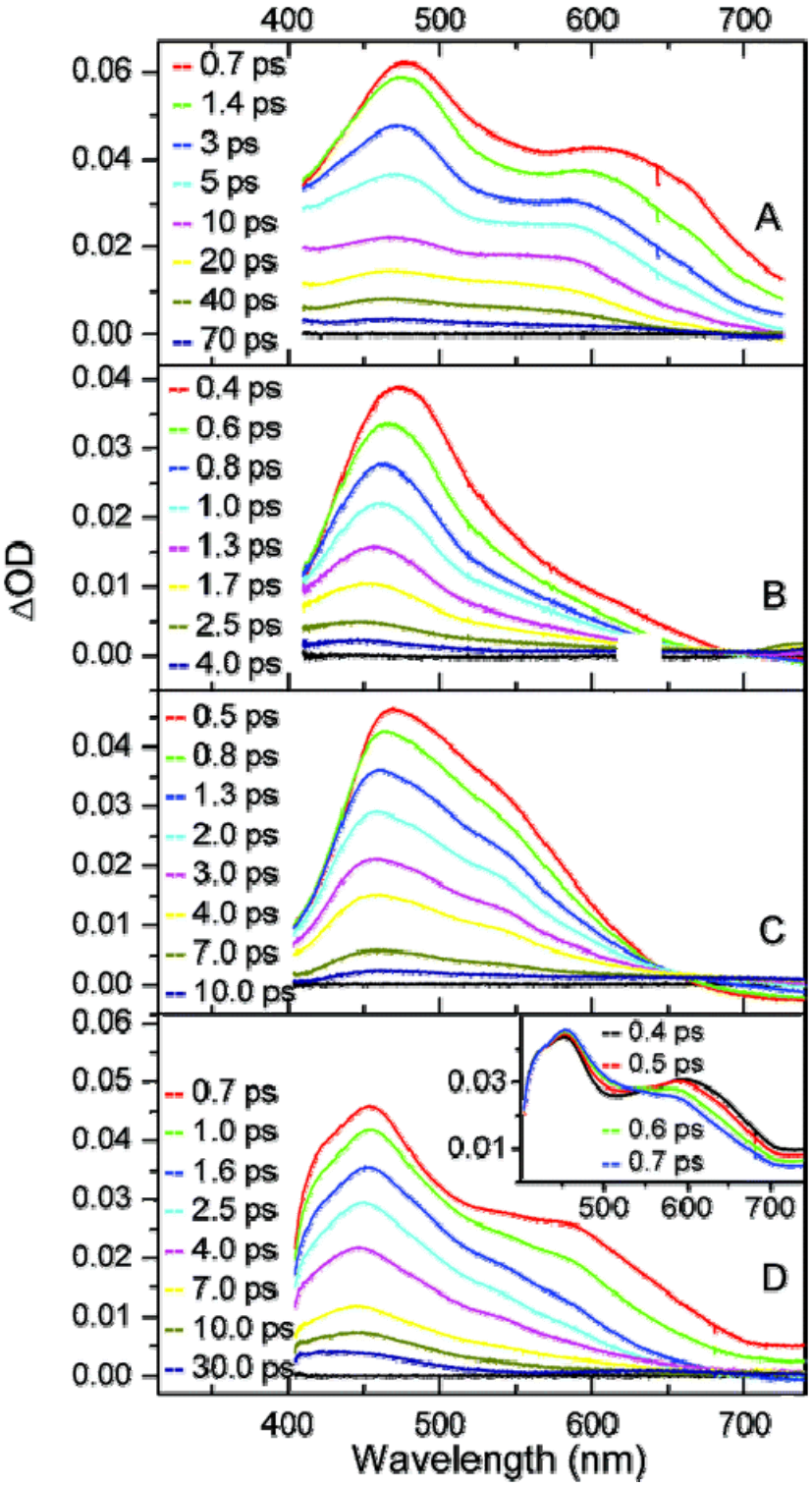

Figure 7.20. Transient absorption spectra of *m*-**HOBDI** in MeOH (A) and MeOH-water (1/9 vol) at pH 0.6 (B), 13.0 (C), and 5.5 (D) after excitation at 380 nm. The pump-probe time delays are given. For clarity, the shortest time delay spectra in part D are shown in inset. The horizontal black trace corresponds to the spectral baseline in the absence of pump excitation. [1]

shortest time constant (<1 ps) affects only the red band. In the case of MeOH, it is accompanied by a 15 nm hypsochromic shift. The three time constants measured in methanol match quite well the fluorescence decay times. In MeCN, good agreement between absorption and emission kinetics is also observed at short time (first two values) but two long time components (40 and 300 ps) are found in the pump-probe data for a single intermediate value (100 ps) in the emission data. This apparent disagreement is probably due to the inaccuracy of the fit of the weak long time kinetic tail. However, whatever the complexity of the relaxation processes, an unambiguous result is the fact that the mean S_1 state lifetime of *m*-**HOBDI** in organic solvents is much longer than that of *p*-**HOBDI** and even longer than that of *m*-**MeOBDI**. Obviously, the excited-state radiation-less decay pathway by internal conversion is much less efficient in the meta than in the para compounds.

The transient absorption spectra obtained upon excitation of the protonated cationic form of *m*-**HOBDI** in acidic 1/9 MeOH-water solution at pH 0.6 are displayed in *Figure 7.20*, part B. These spectra are characterized by a strong PA band at 474 nm that decays with an ultrafast single-exponential kinetics of time constant 0.8 ps, in agreement with the <1 ps fluorescence decay. A 25 nm hypsochromic shift of the PA peak position is observed simultaneously to the decay. After complete decay of this band (4 ps spectrum in *Figure 7.20*, part B), a weak residual transient absorption is observed at 450 nm which disappears with a time constant of 20 ps. The strong initial spectrum resembles clearly that obtained in the same conditions for *m*-**MeOBDI** (*Figure 7.15*, part C). In both cases, the PA band characterizes the excited S_1 state of the cationic form. However there is a remarkable difference between the two meta compounds concerning the excited-state lifetime, which is about 40 times shorter in the parent *m*-**HOBDI** molecule than in the methoxy derivative. Such a difference contrasts notably with the situation encountered in organic solvents where both molecules are characterized by S_1 state lifetimes much longer than 1 ps, the longest ones being observed for the *m*-**HOBDI** molecule. The

surprisingly fast S_1 decay observed specifically for the *m*-**HOBDI** cationic form in aqueous solution can be correlated to the presence of the acidic hydroxyl site that does not exist in the methoxy derivative. It suggests that ultrafast proton transfer from the hydroxyl group to water is the excited-state process that is responsible for quenching via IC to S_0. In this regard, the weak longer-lived component observed at 450 nm may characterize the ground state zwitterionic form resulting from the quenching reaction. Its 20 ps decay is likely due to return to the starting cationic form by fast ground state reprotonation of the hydroxy site (diffusional process) favored by the strong acidity of the solution.

The transient absorption spectra recorded for the anionic (deprotonated hydroxyl) form of *m*-**HOBDI** in basic 1/9 MeOH-water solution at pH 13 (*Figure 7.20*, part C) are mainly characterized by a strong PA band peaking at 471 nm and showing a rough shoulder around 550 nm, that we ascribe to the anion S_1 state. Beside this strong PA band, a slightly negative signal is noticed at wavelengths longer than 650 nm and can be assigned to a SE contribution corresponding to the long wavelength tail of the anion fluorescence spectrum (red trace in *Figure 7.3*, part A). A 25 nm hypsochromic shift of the PA band occurs at short time with a time constant of 0.8 ± 0.3 ps that might correspond to the <1 ps fluorescence decay. In contrast, the decay of the PA and SE components can be fit to a single exponential of time constant 2.8 ps, which has no apparent counterpart in the emission kinetics. However, because of the extreme weakness and very poor quality of the time-resolved fluorescence signal in basic aqueous solution, it is possible that a second, weaker and undetectable decay component can be present. In any case, the observation of a fast quenching of the S_1 state suggests that, as in acidic solution, internal conversion to the ground state is efficiently promoted by intermolecular proton transfer in aqueous solution. Excited-state protonation of the nitrogen atom by water is thus assumed to occur at pH 13. Spectral identification of the resulting zwitterionic form is less evident than at acidic pH. At 10 ps, the spectrum shows a weak

absorption peaking at about 450 nm similar to that ascribed to the zwitterion at pH 0.6, but no specific kinetic contribution can be associated to this absorption.

Finally, in 1/9 MeOH-water solution at pH 5.5 (*Figure 7.20*, part D), the initial spectrum (0.4 ps) resembles that in MeOH (*Figure 7.20*, trace A) or MeCN, with two broad PA bands peaking at 455 and 600 nm and extending beyond 730 nm. This spectrum is thus likely assignable to the S_1 state of the neutral *m*-**HOBDI** form. However, whereas in organic solvents the S_1 spectrum was found to decay within a few tenth picoseconds without exhibiting significant spectral change, in 1:9 MeOH-water the transient spectrum disappears much faster and shows important changes in the spectral shape. A first evolution, not observed in organic solvents nor at basic and acidic pHs, arises with a time constant of 0.6 ± 0.2 ps (inset of *Figure 7.20*, part D). It is characterized by fast intensity decay at the position of the 600 nm PA band and a growth of the 455 nm band. An isosbestic point is apparent at ~550 nm. This evolution leads to a spectrum that shows notable resemblance with that observed for the S_1 state of the deprotonated *m*-**HOBDI** anion produced by direct excitation of the ground state anionic form at pH 13 (part C in *Figure 7.20*). This analogy suggests that the 0.6 ps kinetics corresponds to an ultrafast excited-state proton release to water (hydroxyl dissociation). The transient spectrum decays almost entirely with a time constant of 3.2 ± 0.4 ps. This decay is still much faster than the lifetime found for *m*-**HOBDI** in organic solvents or for the *m*-**MeOBDI** cation in pH 0.6 aqueous solution. It is thus probable that this fast S_1 state depopulation is not induced by intramolecular isomerization, as in the latter cases, but rather by an intermolecular proton transfer from water to the imidazolinone nitrogen. Similar spectral evolution was observed in deuterated solvent (1/9 MeOD-D_2O solution at pH 5.5) with time constants of 0.6 ± 0.2 and 5.0 ± 0.5 ps. The notable isotopic effect found for the higher constant (k_H/k_D ~ 1.6) is consistent with the assumption that intermolecular proton motion is involved in the excited-state quenching process. In contrast, the insensitivity of the ultrafast hydroxyl deprotonation time constant upon

solvent deuteration is in accord with the generally very small kinetic isotopic effect expected for superstrong photoacids.[32]

After full decay of the excited-state of the anion, a residual spectrum is observed (30 ps spectrum in *Figure 7.20*, part D) that presents a rough maximum around 450 nm and a red tail extending up to 500 nm. Its decay is much longer than the experimental time window analyzed in this study (>100 ps). This weak residual spectrum seems quite similar to the spectra that have been found above following quenching of the excited state of the *m*-**HOBDI** cation and anion forms in acidic and basic solutions, respectively. This analogy is in favour of an assignment of the final transient species to the ground state zwitterionic form of *m*-**HOBDI** at neutral pH as well as at acidic and basic pHs, which supports the hypothesis of excited-state quenching via proton transfer in all cases. The long lifetime of this zwitterionic species in neutral solution contrasts with the very fast decay found at acid and basic pHs, as expected from the fact that the zwitterion lifetime is controlled by the diffusional processes of hydroxyl reprotonation and/or nitrogen deprotonation. In fact, the concentration of the H^+ and/or OH^- ions in the neutral aqueous solution is considerably lower than in strongly acidic and basic solutions. This pH-dependent kinetic behavior is thus also a point in agreement with the formation of *m*-**HOBDI** zwitterion at all pHs.

Discussion

Kinetics and Mechanism of Photoinduced Processes in *meta*- and *para*-GFP Synthetic Chromophores

para-**HOBDI** Derivatives

The time-resolved emission and absorption results described above can be summarized by *Figure 7.21* that recapitulates the overall photoinduced reactivity in the the *p*-**HOBDI** family:

$$S_0 + h\nu \rightarrow S_1 \xrightarrow{<1\,ps} \text{hot } S_0 \xrightarrow{2-30\,ps} \text{relaxed } S_0$$

$$S_0 + 2\,h\nu \rightarrow C^{+\cdot} + e^-_{solv}$$

Figure 7.21. Photoinduced reactivity in the *p*-**HOBDI** family.

The above interpretation of the time-resolved emission and absorption results is in agreement with that previously proposed by Vengris et al.[29] for *p*-**HOBDI** in aqueous solutions at different pHs. In particular, these authors have demonstrated from quantitative examination of the pump power effect that two-photon ionization of *p*-**HOBDI** occurs in water and leads to a cation radical absorbing in the 400-450 nm region. From a detailed global analysis of combined pump-probe and pump-dump-probe results, they also demonstrated that, in reality, each step of the above one-photon pathway is characterized by a sum of exponentials and involves a transition through a succession of states along a reaction coordinate that includes contributions from intramolecular twisting motion, solvation dynamics, and vibrational cooling. Accordingly, the experimental time constants in *Figure 7.21* can be considered as average values for a distribution of population in both the excited and ground states.[29] A similar mechanism was suggested by some of us[8] on the basis of femtosecond UV-pump-IR-probe results.

***m*-MeOBDI**

An excited-state intermediate S_1' was observed in transient absorption spectra of *m*-**MeOBDI** in aqueous solutions. Its yield decreased with the decrease of water content in solution, making this transient almost invisible in 1/1 vol MeOH/H_2O mixtures. This ensemble of results can be understood by considering the fact that the $S_1 \rightarrow S_1$' reaction is essentially nondiffusional; that is, it occurs only for those S_1-state molecules that are in direct contact with water. In fact, for the S_1 population that is preferentially solvated in MeOH domains, the reaction could in principle occur after diffusion, but its probability is rather negligible because the isomerization-induced deactivation of S_1 toward the ground state is so fast in MeOH (main decay time 1.8 ps) that diffusion has no chance to be

effective before quenching. Increasing the MeOH content in the solvent mixture leads to an increase in the population of *m*-**MeOBDI** molecules solvated by MeOH to the detriment of the population solvated by water and thus to decrease the ratio of S_1 state species able to react with water. This is consistent with the above observation that the yield of the $S_1 \rightarrow S_1$' process decreases upon increasing the MeOH content, but the reaction rate remains unchanged.

The nature of the S_1' state is now considered. The fact that the $S_1 \rightarrow S_1$' reaction arises exclusively in a water environment strongly suggests an excited-state intermolecular proton-transfer process. We thus ascribe the S_1' species to the lowest excited singlet state of a cationic form *m*-**MeOBDIH**$^+$ resulting from protonation by water of the initially produced neutral S_1 state. Surprisingly, the transient absorption spectrum observed for S_1' does not match the excited-state spectrum obtained from direct excitation of the protonated ground state molecule at acidic pH 0.6 (*Figure 7.15*, trace B). This unexpected result can be correlated to our above observation that the steady-state fluorescence spectrum of *m*-**MeOBDI** in neutral methanol/water solution differs from that in neat MeOH but also from that of the protonated molecule in acidic methanol/water at pH 0.6. The only plausible explanation of these results is that the site of protonation of *m*-**MeOBDI** is different in the ground state and in the excited state, leading to different cationic structures. Accordingly, the S_1 state of the neutral molecule in organic solvents, the S_1 state of the cation produced by direct excitation of the protonated ground state, and the cation formed indirectly by excited-state protonation of the neutral molecule in water emit at 430, 500, and 560 nm, respectively. We now consider two possible scenarios of the excited cation formation. The first one may involve the excited-state protonation of the carbonyl oxygen atom of imidazolinone ring, in contrast to the ground state protonation of the imidazolinone nitrogen. Ab initio [33,34] as well as semiempirical[35] studies predict that the latter is the ground state protonation site of the GFP chromophore in an acidic solution. This prevision was recently confirmed by us experimentally in the

case of *p*-**HOBDI**.[25] However, the stabilities of the cationic forms obtained by protonating the carbonyl oxygen and the nitrogen are found to be comparable.[34] It is probable that the pK_a of the two sites are reversed in the *m*-**MeOBDI** derivative. The second protonation scenario may not lead to the same conformer (rotamer) that is observed in the ground state. This may be influenced by the presence of water hydrogen bonded between the methoxy substituent or the carbonyl of the nigrogen in the meta derivative. We anticipate that time-resolved UV-pump-IR-probe measurements will distinguish between *O* and *N* protonation, since C=O stretch is known to shift upon H bonding/protonation.[36]

Excited-state protonation of *m*-**MeOBDI** is observed at pH 11.5 as well as at neutral pH, with similar ultrafast kinetics (~1 ps), which is indicative of an extremely strong photobasicity. Such photobasicity is confirmed by the above finding that the cationic emission at 500 nm is observed at all pHs from 3 to 11.5. The main decay kinetics of the excited singlet state of *m*-**MeOBDIH**$^+$ (~27 ps) is reasonably attributed to the relaxation to the ground state cationic species via IC induced by isomerization. Finally, the longest decay time observed in the pump-probe spectra (≥100 ps) can be tentatively related to a final ground state deprotonation step. Reaction *Figure 7.22* summarizes the photoinduced processes for *m*-**MeOBDI** in aqueous solution. Note that in MeOH-water mixtures those molecules that are preferentially solvated in alcoholic environment undergo direct IC to the ground state, as in neat MeOH.

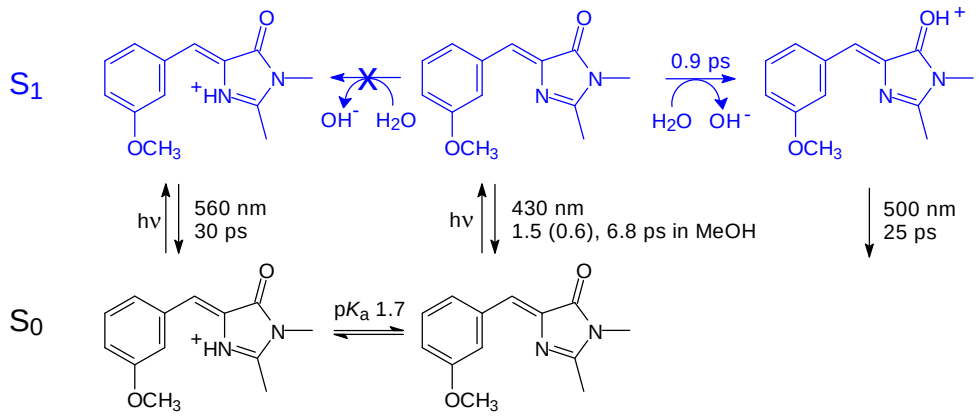

Figure 7.22. Photoinduced processes for *m*-**MeOBDI** in aqueous solution. [1]

m-HOBDI

By analogy with the kinetics analysis of *m*-**MeOBDI** time-resolved data, the overall reactivity of *m*-**HOBDI** in aqueous solution can be summarized by *Figure 7.23*.

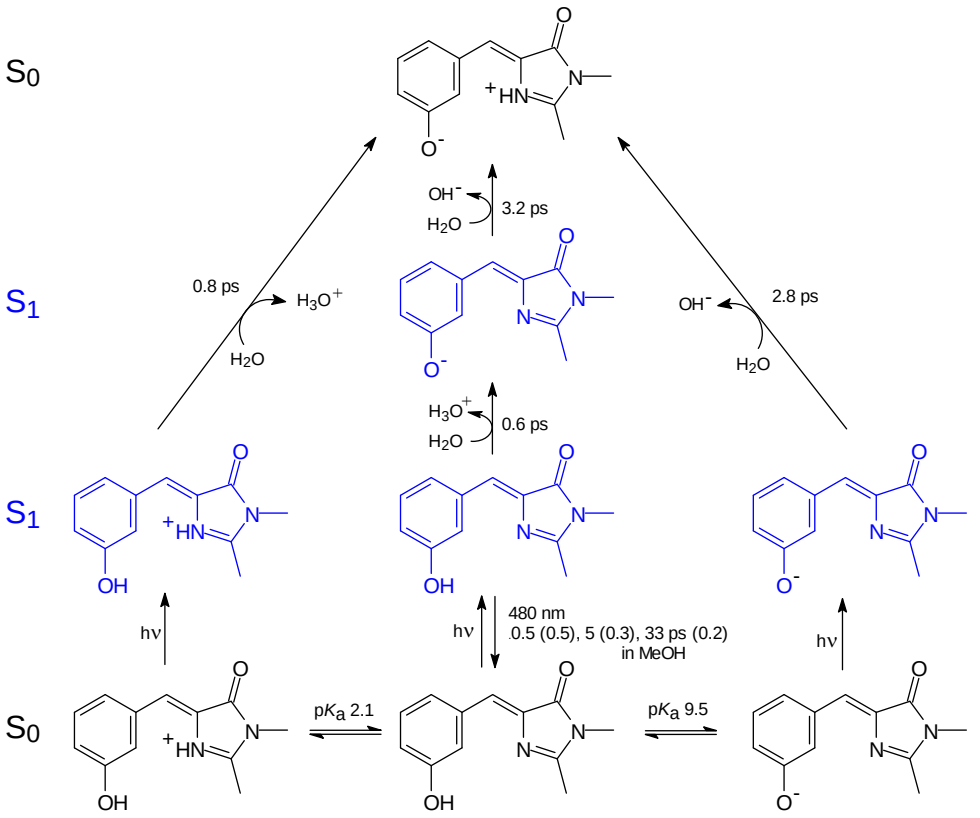

Figure 7.23. Photoinduced processes for *m*-**HOBDI** in aqueous solution (ESPT quenching mechanism). [1]

From comparing the photoinduced processes in *m*-**MeOBDI** (*Figure 7.22*) and *m*-**HOBDI** (*Figure 7.23*), it is interesting to remark that, as a general rule, the ESPT is diabatic and induces the $S_1 \rightarrow S_0$ deactivation when it leads to a zwitterion (protonation of the *m*-**HOBDI** anion, deprotonation of the *m*-**HOBDI** cation) but it is adiabatic when it leads to a single-charged form (deprotonation of *m*-**HOBDI** and *m*-**MeOBDI**). This behavior agrees perfectly with the previous assumption about the role of zwitterion as a quenching product.[37]

The excited-state hydroxyl dissoc iation and nitrogen protonation time constants measured in the pump-probe experiments correspond satisfactorily to the two fluorescence decay times found under the same conditions (see *Table 7.2*). They are also consistent with the time constants found for hydroxyl deprotonation of the cationic form at pH 0.6 (0.8 ps) and nitrogen protonation of the anionic form at pH 13 (2.8 ps), respectively. This correlation is an additional feature favoring reaction *Figure 7.23* that assumes that, at neutral pH, the first excited state reaction step is hydroxyl dissociation yielding the anionic *m*-**HOBDI** form. However, in regard to the resemblance of the excited-state spectra of the anionic and cationic species (Parts B and C, respectively, in *Figure 7.20*), an alternative assignment of the intermediate transient spectrum to the excited-state of the cationic form cannot be completely excluded. Therefore, the hypothesis that *N*-protonation occurs first and is followed by excited-state quenching via hydroxyl deprotonation cannot be definitely ruled out. Another possible digression from *Figure 7.23* is the consideration that the proton-transfer process responsible for the excited-state quenching in *m*-**HOBDI** is not effective. In fact, numerous examples of photoacids and photobases excited-state quenching promoted by inter- or intra-molecular proton transfer, designed as “aborted proton-transfer quenching mechanism”, have been reported.[38,39] In such cases, the system begins to evolve on the excited surface along the proton-transfer reaction coordinate and rapidly reaches a region where a conical intersection with the ground state surface leads to ultrafast internal conversion before the

ESPT reaction is completed. This reaction is aborted as the system comes back to the starting molecular structure on the ground state surface. According to this mechanism, one expects that the *m*-**HOBDI** molecule keeps the same tautomeric form before and after quenching, that is, the cationic form at acidic pH and the anionic form at neutral and basic pHs. The corresponding reaction mechanism can be summarized by *Figure 7.24*. In this hypothesis, the long-lived residual spectrum observed at neutral pH after quenching of the excited- state anion (30 ps spectrum in *Figure 7.20*, part D), tentatively ascribed to the ground state zwitterion in reaction *Figure 7.23*, should rather correspond in *Figure 6.24* to the ground state anion. Such assignment is plausible as this residual spectrum matches fairly well the long wavelength part of the ground state spectrum of the *m*-**HOBDI** anionic form that extends up to 500 nm (red trace in *Figure 7.2*, part A). An interesting variation of the mechanism discussed above was proposed by Vendrell et al.[40] and Manca.[41] Their calculations demonstrated a crossing between ππ* and πσ* states when the OH bond length is stretched leading to the excited-state H-atom transfer instead of the ESPT.

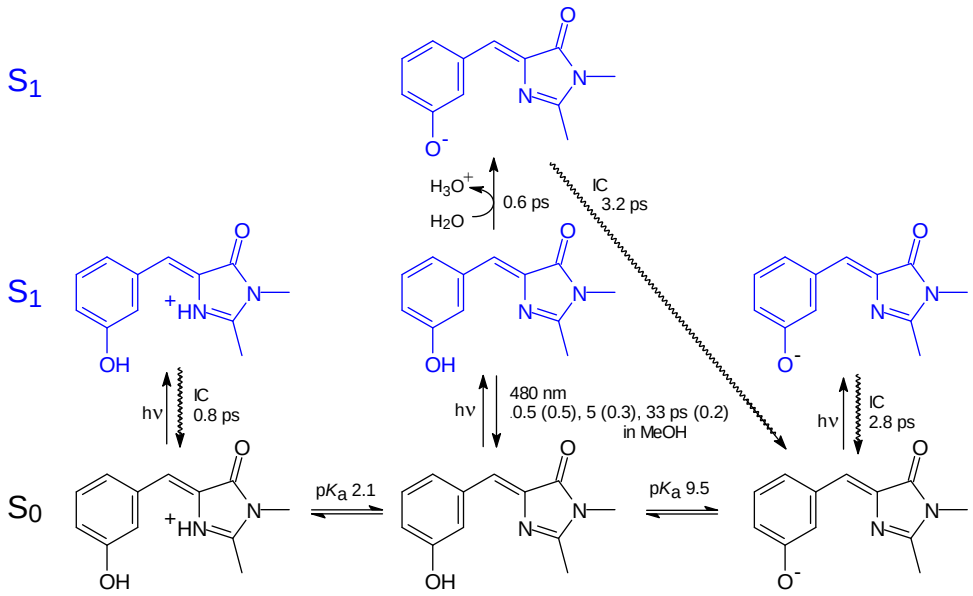

Figure 7.24. Photoinduced processes for *m*-**HOBDI** in aqueous solution (Aborted ESPT quenching mechanism). [1]

In any case, the essential result is that the overall photoinduced reactivity of the neutral form of *m*-**HOBDI** in aqueous solution, as well as of the anionic and cationic forms, appears dominated by the acid-base properties of the molecule, which are characterized by the drastic enhancement of both the basicity of the imidazolinone imine nitrogen and the acidity of the hydroxyl group in going from the ground state to the excited S_1 state. In this regard, *m*-**HOBDI** differs notably from *p*-**HOBDI** for which ultrafast isomerization is the main quenching process.

A final point is the observation that in all solvents the contribution from solvated electrons and **HOBDI** radical cations in the pump-probe transient spectra is much weaker for meta than for para compounds. Since the formation of such radical cations, followed by electron transfer from a glutamate carboxylate, may account for the E222 decarboxylation observed for GFP,[42] it can be assumed that a reduced quantum yield for two-photon ionization in the *meta* chromophore might provide for much less efficient decarboxylation in a protein having a *meta*-hydroxyaromatic chromophore, leading to more stable fluorophores.

Conclusions

From femtosecond transient absorption and fluorescence upconversion measurements, the photoinduced dynamics of the meta green fluorescent protein synthetic chromophore, *m*-**HOBDI**, were compared to that of the para isomer, *p*-**HOBDI**, and of the related *O*-methylated derivatives, *m*-**MeOBDI** and *p*-**MeOBDI**, and *N*-methylated cation, *p*-**HOBDIMe**$^+$. All of these compounds were investigated in MeOH, MeCN, and 1/9 vol MeOH-water mixtures at neutral, acidic and basic pH. In all cases, fast quenching of the excited S_1 state was observed, revealing that efficient internal conversion to the ground state occurs. However, a clear distinction can be made concerning the behavior of the meta and para families.

On one hand, in the para-substituted molecules, ultrafast (< 1 ps) S_1 state quenching is invariably observed in all solvents, regardless of the state of protonation of the hydroxyl group and imidazolinone nitrogen and independent of whether the acid-base sites of these groups are blocked by methylation or not. This common behavior provides strong evidence that the excited-state acid-base properties are not involved in the quenching process. So, as widely discussed in the literature, an ultrafast IC is resulted from a near barrierless twisting process within all three para chromophores. The mechanism of the twist is not proven yet.

On the other hand, the photoinduced reactivity of the meta isomers was found to present two main differences with respect to the reactivity of the para compounds. First, for *m*-**HOBDI** and *m*-**MeOBDI** in organic solvents as well as for the *N*-protonated cationic form of *m*-**MeOBDI** in 1/9 MeOH-water at pH 0.6, in all situations where intermolecular proton exchange with the solvent is unlikely, S_1 state quenching was found to be notably slower than for the para isomers. Obviously, the excited-state nonradiative decay pathway by IC is less efficient in the meta than in the para compounds, which can be associated with slower cis-trans photoisomerization. The presence of a significant barrier on the excited-state surface along the cis-trans isomerization coordinate inducing the IC can thus be inferred. The second major feature that characterizes the photoinduced reactivity of the meta-substituted derivatives is the observation of much faster quenching of S_1 in MeOH-water binary solvents, as clearly evidenced for *m*-**HOBDI** by the emission kinetics in *Figure 7.19*. This drastic solvent effect reveals that, in aqueous solutions, the S_1 state relaxation is essentially governed by the acid-base properties of the molecule. This situation is a consequence of the fact that, in the meta compounds, the rates of proton abstraction by the imidazolinone nitrogen from water and proton release by the hydroxyl group to water are both much higher than the isomerization-induced IC. For *m*-**HOBDI** at neutral pH, a sequential ESPT is observed, similar to that for hydroxyquinolines.[43] First, the hydroxyl group dissociates

adiabatically in 0.7 ps, and then the protonation of imidazolinone nitrogen occurs at 3.1 ps. The second proton transfer step is either a real, non-adiabatic ESPT that leads to fluorescence quenching and production of the ground state zwitterion form instead of the excited tautomer or an aborted proton-transfer that deactivates the excited-state without yielding the zwitterionic proton-transfer product. For *m*-**MeOBDI**, adiabatic excited-state nitrogen protonation by water arises in 1.1 ps and is followed by cis-trans isomerization induced IC to the ground state in about 27 ps.

The different photoinduced behavior of the meta versus para isomer of the GFP chromophore is reminiscent of Lewis' observations with the corresponding hydroxystilbenes,[3-5] or their derivatives.[44] This selective modulation of acid-base behavior in chromophores, together with solvent variation, including pH change, serves as a context for separation of elementary proton-transfer steps in these systems. Studies of such synthetic unconventional derivatives of the GFP chromophore will help elucidate the complex photochemistry and photophysics of fluorescent prototropic proteins and will shed more light on the problem of cis-trans isomerization in biochemistry.[45]

References

[1] Solntsev, K. M.; Poizat, O.; Dong, J.; Rehault, J.; Lou, Y.; Burda, C.; Tolbert, L. M. *J. Phys. Chem. B* **2008**, *112*, 2700-2711.

[2] Saltiel, J.; Waller, A. S.; Sears, D. F. *J. Am. Chem. Soc.* **1993**, *115*, 2453.

[3] Lewis, F. D.; Crompton, E. M. *J. Am. Chem. Soc.* **2003**, *125*, 4044.

[4] Crompton, E. M.; Lewis, F. D. *Photochem. Photobiol. Sci.* **2004**, *3*, 660.

[5] Lewis, F. D.; Sinks, L. E.; Weigel, W.; Sajimon, M. C.; Crompton, E. M. *J. Phys. Chem. A* **2005**, *109*, 2443.

[6] Lewis, F. D.; Kalgutkar, R. S.; Yang, J.-S. *J. Am. Chem. Soc.* **1999**, *121*, 12045.

[7] Lewis, F. D.; Weigel, W. *J. Phys. Chem. A* **2000**, *104*, 8146.

[8] Usman, A.; Mohammed, O. F.; Nibbering, E. T. J.; Dong, J.; Solntsev, K. M.; Tolbert, L. M. *J. Am. Chem. Soc*. **2005**, *127*, 11214.

[9] Litvinenko, K. L.; Webber, N. M.; Meech, S.R. *Bull. Chem. Soc. Jpn.* **2002**, *75*, 1065.

[10] Litvinenko, K. L.; Webber, N. M.; Meech, S.R. *J. Phys. Chem. A* **2003**, *107*, 2616.

[11] Toniolo, A.; Olsen, S.; Manohar, L.; Martı´nez, T. J. *FaradayDiscuss.* **2004**, *127*, 149.

[12] He, X.; Bell, A. F.; Tonge, P. J. *FEBS Lett.* **2003**, *549*, 35.

[13] Dugave, C.; Demange, L. *Chem. Re*V. **2003**, *103*, 2475.

[14] Martin, M. E.; Negri, F.; Olivucci, M. *J. Am. Chem. Soc.* **2004**, *126*, 5452.

[15] Gepshtein, R.; Huppert, D.; Agmon, N. *J. Phys. Chem. B* **2006**, *110*, 4434.

[16] Altoe, P.; Bernardi, F.; Garavelli, M.; Orlandi, G.; Negri, F. *J. Am. Chem. Soc*. **2005**, *127*, 3952.

[17] Chen, K.-Y.; Cheng, Y.-M.; Lai, C.-H.; Hsu, C.-C.; Ho, M.-L.; Lee, G.-H.; Chou, P.-T. *J. Am. Chem. Soc*. **2007**, *129*, 4534.

[18] Zimmerman, H. E. *J. Am. Chem. Soc.* **1995**, *117*, 8988.

[19] Zimmerman, H. E. *J. Phys. Chem. A* **1998**, *102*, 5616.

[20] Sinha, H. K.; Yates, K. *J. Am. Chem. Soc.* **1991**, *113*, 6062.

[21] Lewis, F. D.; Yang, J.-S. *J. Am. Chem. Soc.* **1997**, *119*, 3834.

[22] DeCosta, D. P.; Howell, N.; Pincock, A. L.; Pincock, J. A.; Rifai, S. *J. Org. Chem.* **2000**, *65*, 4698.

[23] Dong, J.; Solntsev, K. M.; Poizat, O.; Tolbert, L. M. *J. Am. Chem. Soc.* **2007**, *129*, 10084.

[24] Kojima, S.; Ohkawa, H.; Hirano, T.; Maki, S.; Niwa, H.; Ohashi, M.; Inouye, S.; Tsuji, F. I. *Tetrahedron Lett.* **1998**, *39*, 5239.

[25] Dong, J.; Solntsev, K. M.; Tolbert, L. M. *J. Am. Chem. Soc.* **2006**, *128*, 12038.

[26] Buntinx, G.; Naskrecki, R.; Poizat, O. *J. Phys. Chem.* **1996**, *100*, 19380.

[27] Kummer, A. D.; Kompa, C.; Niwa, H.; Hirano, T.; Kojima, S.; Michel-Beyerle, M. E. *J. Phys. Chem. B* **2002**, *106*, 7554.

[28] Mandal, D.; Tahara, T.; Meech, S. R. *J. Phys. Chem. B* **2004**, *108*, 1102.

[29] Vengris, M.; van Stokkum, I. H. M.; He, X.; Bell, A. F.; Tonge, P.T.; van Grondelle, R.; Larsen, D. S. *J. Phys. Chem. A* **2004**, *108*, 4587.

[30] Schindewolf, U. *Angew. Chem. Int. Ed. Engl.* **1978**, *17*, 887.

[31] Xia, C.; Peon, J.; Kohler, B. *J. Chem. Phys.* **2002**, *117*, 8855.

[32] Pines, E. In *Isotopic Effects in Chemistry and Biology*; Kohen, A.; Limbach, H. H., Eds.; Taylor & Francis; Boca Raton, 2006; p 451.

[33] El Yazal, J.; Prendergast, F. G.; Shaw, D. E.; Pang, Y.-P. *J. Am. Chem. Soc.* **2000**, *122*, 11411.

[34] Das, A. K.; Hasegawa, J.-Y.; Miyahara, T.; Ehara, M.; Nakatsuji, H. *J. Comput. Chem.* **2003**, *24*, 1421.

[35] Voityuk, A. A.; Kummer, A. D.; Michel-Beyerle, M.-E.; Rosch, N. *Chem. Phys.* **2001**, *269*, 83.

[36] Nibbering, E. T. J. ; Tschirschwitz, F. ; Chudoba, C.; Elsaesser, T. *J. Phys. Chem. A* **2000**, *104*, 4236.

[37] Weber, W.; Helms, V.; McCammon, J. A.; Langhoff, P. W. *Proc. Acad. Sci. U.S.A* . **1999**, *96*, 6177.

[38] Sinicropi, A.; Nau, W. M.; Olivucci, M. *Photochem. Photobiol. Sci.* **2002**, *1*, 537.

[39] Sobolewski, A.; Domcke, W. In *Ab-initio Reaction Paths and Potential Energy Functions*; Elsaesser, T.; Bakker, H. J., Eds.; Kluwer Academic Publishers; Amsterdam, 2002; p 93.

[40] Vendrell, O.; Gelabert, R.; Moreno, M.; Luch, J. M. J. *Am. Chem. Soc*. **2006**, *128*, 3564.

[41] Manca, C. *Chem. Phys. Lett.* **2007**, *443*, 173.

[42] Bell, A. F.; Stoner-Ma, D.; Wachter, R. M.; Tonge, P. J. *J. Am. Chem. Soc.* **2003**, *125*, 6919.

[43] Poizat, O.; Bardez, E.; Buntinx, G.; Alain, V. *J. Phys. Chem. A* **2004**, *108*, 1873.

[44] Burda, C.; Abdel-Kader, M. H.; Link, S.; El-Sayed, M. A. *J. Am. Chem. Soc*. **2000**, *122*, 6720.

[45] *cis-trans Isomerization in Biochemistry*; Dugave, C., Ed.; Wiley-VCH; Weinheim, 2006.

CHAPTER 8

CONCLUSIONS AND FUTURE WORK

Conclusions

The green fluorescent protein (GFP) from jellyfish *Aequorea victoria* has attracted great interest as a biological fluorescence marker.[1,2] The chromophore of this protein with 238 amino acid residues is a *p*-hydroxybenzylidene-imidazolidinone (**HBI**) derivative formed by an autocatalytic, posttranslational cyclization and oxidation of the Ser-65, Tyr-66, and Gly-67 residues.[3-5] The GFP crystal structure shows that the chromophore is embedded in the middle of an internal α-helix directed along a rigid β-barrel axis. However, the denatured protein, isolated fragments of protein containing the chromophore, and synthetic model compounds, are all essentially nonfluorescent in fluid solution at room temperature.[6-8]

In order to unveil the fluorescence mechanism details of *wt*GFP and the photophsical and photochemical behavior of its chromophore, we have synthesized an array of synthetic GFP chromophore (**HOBDI**) variants and studies their photoprocesses using various steady-state and time-resolved techniques, including *O*- and *N*-alkyl substituted **BDI**; *para*-chloro, methyl, acetyl, and H substituted **BDI**; *meta*- and *para*-**HOBDI**. Syntheses of these various **BDI** derivatives were carried out using either a condensation of the Erlenmeyer with a primary amine or imidate with an appropriate *N*-methylbenzylideneamine.

We consider the effect of the β-barrel on the optical properties of the GFP chromophore (*p*-**HOBDI**) experimentally by selective variation of the protonation state of the chromophore and different solvents. Each of these forms shows a complex solvatochromic behavior and is governed by both polar and acid/base properties of the

solvents. For neutral forms of *p*-**HOBDI**, an increase in all solvent parameters induced a bathochromic shift. The cationic form blue-shifts as solvent polarity and basicity are increased, while for anionic form the polarity and acidity of the solvent work in opposite directions. We also first experimentally observed the ground-state GFP chromophore zwitterion that allows the investigation of the long-debated *p*-**HOBDI** tautomer.[9]

In contrast to their behavior in solution, some *O*-alkyl GFP chromophore (alkoxy-**BDI**) derivatives exhibit large fluorescent enhancement in solid state. Our studies provide clear evidence for exciton splitting in the solid state resulting in red-shifted emission for the derivatives. The role of the alkyl chain length in controlling the nature of the molecular packing and consequently their fluorescence properties has been elucidated. In alkoxy-**BDI** derivatives, increasing the length of the alkyl chain results in a visual change in fluorescence from yellow to blue. On the basis of the analysis of the molecular packing in the single crystals, this difference is attributed to fluorescence arising from aggregates in the molecule possessing a short alkyl chain (methyl) to monomer fluorescence in the long alkyl chains (hexyl and docecyl) containing derivatives. The color of crystalline **BDI** is tuned by substituent-mediated crystal packing, showing their potential applications in optoelectronic devices.[10]

Using femtosecond polarization-sensitive infrared (IR) spectrosceopy of the C=O stretching mode of the **HOBDI**, we have discovered a near complete twisting around the ethylenic bridge between the phenolate and imidazolidinone groups upon electronic excitation, hinting at a decisive role of this motion in the efficient internal conversion process. [11]

Fluorescent proteins related to the GFP are thought to undergo *E/Z* photo-isomerization between dark and fluorescent states, which are also characterized by "blinking". Strong support for *cis*/*trans* isomerization is provided by the behavior of blinking fluorescent proteins, however, the mechanism of the thermal reverse isomerization is more problematic. Thus we synthesized **BDI** derivatives with decreasing

para-donating ability, HO, CH_3O, CH_3, H, and Cl, and used a Hammett plot for the rate study. With a positive ρ value, we conceived, for the first time, a novel nucleophile addition/elimination mechanism. We observed the rate of isomerization was proportional to the concentration of nucleophile, consistent with our proposed mechanism. Addition/elimination emerges as a compelling mechanism for isomerization of fluorescent protein chromophores. The presence of an internal nucleophile thus becomes an additional point of mutation of such chromophores that may mediate their photo-physical properties. Such mutations are currently being explored.[12]

The GFP chromophore falls into the general category of hydroxyarene photoacids, which exhibit high excited-state acidities but neutral ground states. A hydroxy substituent at the *meta* position shows enhanced charge transfer and greater acidity in the excited state, as is shown clearly by examining their corresponding frontier molecular orbitals (HOMOs and LUMOs). The *meta* **HOBDI** derivative was synthesized and the isomer exhibited fluorescence which was ca. 10 times more efficient than that for the *para* derivative. In non-aqueous solvents, a higher fluorescent quantum yield and longer fluorescence lifetimes were detected. The transient absorption signal of ***m*-HOBDI** consisted of a very broad absorption signal best fit by a biexponential decay function. In aqueous solutions, the *meta* compounds underwent ultrafast intermolecular excited state proton transfer that competed with isomerization. We believe that studies of such model unconventional *m*-GFP chromophores will help unravel the complex photochemistry and photophysics of fluorescent prototropic proteins.[13]

Femtosecond transient absorption and fluorescence upconversion measurements have been performed to investigate the photoinduced dynamics of the *meta* isomer of the GFP chromophore, ***m*-HOBDI**, and its *O*-methylated derivative, ***m*-MeOBDI,** in various solvent mixtures at neutral, acidic, and basic pH. The *para* isomer, ***p*-HOBDI,** and its *O*- and *N*-methylated derivatives, ***p*-MeOBDI** and ***p*-HOBDIMe+**, were also studied for comparison. In all cases, fast quenching of the excited S1 state by internal conversion

(IC) to the ground state was observed. In the *para* compounds, IC, presumably promoted by the internal twisting, arises in <1 ps. A similar process takes place in the *meta* compounds in nonaqueous solvents but with notably slower kinetics. In aqueous solutions, the *meta* compounds undergo ultrafast intermolecular excited-state proton transfer that competes with isomerization. [14]

Future Work

Based on the previous discussions, the fluorescence of synthetic **HOBDI** and its derivatives quench in solution at room temperature due to twisting about the exocyclic double bond resulting internal conversion. Thus, a straightforward and well-precedented solution for inhibition of twisting is to incorporate the exocyclic bond into a ring, an approach which has worked for yellow fluorescent protein (YFP).[15] Such an approach would prohibit the phenyl-twisting decay channel and thus "turn on" the fluorescence. The previous procedures used in syntheses of **HOBDI** and its derivatives can be applied in this approach. An alternative approach is using a Lewis acid, e.g., boron, to coordinate with synthetic GFP chromophore analogue. Such an approach has been reported by another research group very recently.[16]

The discovery of fluorescent enhancement in solid-state alkoxy-**BDI** chromophores provides broader impacts of synthetic GFP chromophore derivatives. Besides the mono-alkoxy substituent molecules, further investigations of di- and tri-alkoxy or *N*-alkyl substituted derivatives, including the effect of the length of alkyl chain, become necessary. It is also important to characterize their thermal properties and morphologies for better understanding the nature of noncovalent forces in the molecular packing and using them as key elements in optoelectronic devices.

References

[1] Tsien, R. Y. *Annu. Rev. Biochem*. **1998**, *67*, 509-544.

[2] Green Fluorescent Protein: Properties, Applications, and Protocols, 2nd edl; Chalfie, M., Kain, S. R., Eds.; *Methods of Biochemical Analysis* 47; Wiley-Intersciences: Hoboken, NJ, **2005.**

[3] Shimomura, O. *FEBS Lett.* **1979**, *104*, 220-222.

[4] Cody, C. W.; Prasher, D. C.; Westler, W.M.; Prendergast, F. G.; Ward, W. W. *Biochemistry,* **1993**, *32*, 1212-1218.

[5] Romoser, V. A.; Hinkle, P. M.; Persechini, A. *J. Biol. Chem*. **1997**, *272*, 13270-13274.

[6] Niwa, H.; Ionuye, S.; Horano, T.; Matsuno, T.; Kojima, S.; Kubota, M.; Ohashi, M.; Tsuji, F. I. *Proc. Natl. Acad. Sci. USA* **1996**, *93*, 13617.

[7] Kojima, S.; Ohkawa, H.; Hirano, T.; Maki, S.; Niwa, H.; Ohashi, M.; Inouye, S.; Tsuji, F. I.; *Tetrahedron Lett.* **1998**, *39*, 5239.

[8] Litvinenko, K. L.; Webber, N. M.; Meech, S. R. *J. Phys. Chem. A* **2003**, *107*, 2616-2623.

[9] Dong, J.; Solntsev, K. M.; Tolbert, L. M. *J. Am. Chem. Soc.* **2006**, *128*, 12038-12039.

[10] Dong, J.; Solntsev, K. M.; Tolbert, L. M. **2008**, in preparation.

[11] Usman, A.; Mohammed, O. F.; Nibbering, E. T. J.; Dong, J.; Solntsev, K. M.; Tolbert, L. M. *J. Am. Chem. Soc***. 2005**, *127*, 11214-11215.

[12] Dong J.; Abulwerdi, F.; Baldridge, A.; Kowalik, J.; Solntsev, K. M. Tolbert, L. M. **2008**, submitted.

[13] Dong, J.; Solntsev, K. M.; Poizat, O.; Tolbert, L. M. *J. Am. Chem.. Soc*. **2007**, *129*, 10084-10085.

[14] Solntsev, K. M.; Poizat, O.; Dong, J.; Rehault, J.; Lou, Y.; Burda, C.; Tolbert, L. M. *J. Phys. Chem. B* **2008**, *112*, 2700-2711.

[15] Vengris, M.; Larsen, D. S.; van der Horst, M. A.; Larsen, O. F. A.; Hellingwerf, K. J.; van Grondelle, R. *J. Phys. Chem. B* **2005**, *109*, 4197-4208.

[16] Wu, L.; Burgess, K, *J. Am. Chem. Soc*. **2008**, *130*, 4089-4096.